

Revista **ALCONPAT**

Latin American Journal of Quality Control, Pathology and Construction Recovery

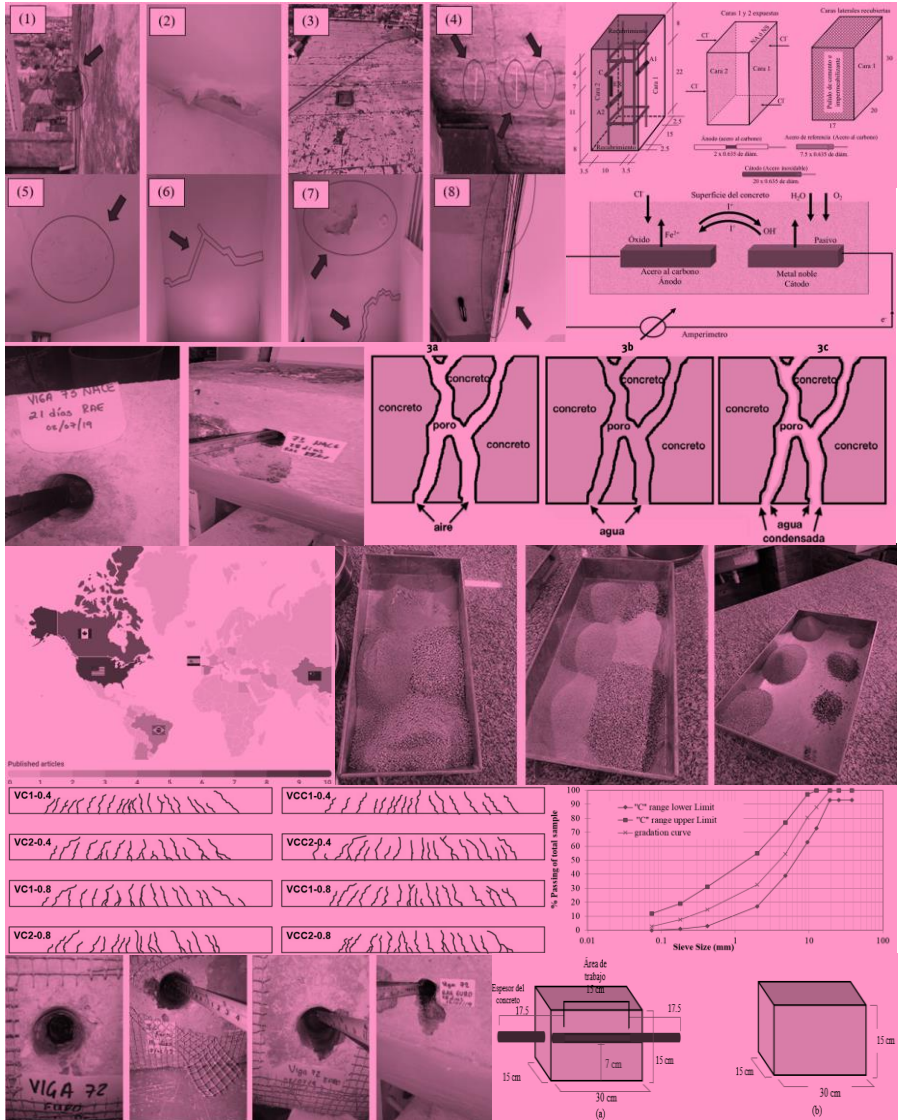
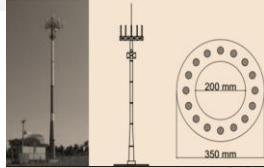
DOI: <http://dx.doi.org/10.21041/ra.v12i3>
editorial.revista.alconpat@gmail.com

eISSN: 2007-6835

Volume 12

September – December 2022

Issue 3



Latin American Journal of Quality Control, Pathology and Construction Recovery
<http://www.revistaalconpat.org>



ALCONPAT Internacional

Miembros Fundadores:

Liana Arrieta de Bustillos – **Venezuela**
Antonio Carmona Filho - **Brasil**
Dante Domene – **Argentina**
Manuel Fernández Cánovas – **España**
José Calavera Ruiz – **España**
Paulo Helene, **Brasil**

Junta Directiva Internacional:

Presidente de Honor

Carmen Andrade Perdrix, **España**

Presidente

Enio Pazini Figueiredo, **Brasil**

Director General

Pedro Castro Borges, **México**

Secretario Ejecutivo

César Juárez Alvarado, **México**

Vicepresidente Técnico

Pedro Garcés Terradillos, **España**

Vicepresidente Administrativo

Luis Álvarez Valencia, **Guatemala**

Tesorero

Jose Manuel Mendoza Rangel, **México**

Gestores

Enrique Cervera Aguilar, **México**
Paulo Helene, **Brasil**

Revista ALCONPAT

Editor en Jefe:

Dr. Pedro Castro Borges
Centro de Investigación y de Estudios Avanzados del
Instituto Politécnico Nacional, Unidad Mérida
(CINVESTAV IPN – Mérida)
Mérida, Yucatán, **México**

Co-Editor en Jefe (2022-2023):

Dra. Edna Possan
Universidade Tecnológica Federal do
Paraná, Curitiba, **Brasil**

Editor Ejecutivo:

Dr. José Manuel Mendoza Rangel
Universidad Autónoma de Nuevo León,
Facultad de Ingeniería Civil
Monterrey, Nuevo León, **México**

Editores Asociados:

Dr. Manuel Fernández Cánovas
Universidad Politécnica de Madrid.
Madrid, **España**

Ing. Raúl Husni

Facultad de Ingeniería - Universidad de Buenos Aires.
Buenos Aires, **Argentina**

Dr. Paulo Roberto do Lago Helene

Universidade de São Paulo.

São Paulo, **Brasil**

Dr. José Iván Escalante García

Centro de Investigación y de Estudios Avanzados del
Instituto Politécnico Nacional (Unidad Saltillo)
Saltillo, Coahuila, **México**.

Dra. Oladis Troconis de Rincón

Centro de Estudios de Corrosión

Universidad de Zulia

Maracaibo, **Venezuela**

Dr. Fernando Branco

Universidad Técnica de Lisboa

Lisboa, **Portugal**

Dr. Pedro Garcés Terradillos

Universidad de Alicante

San Vicente, **España**

Dr. Andrés Antonio Torres Acosta

Instituto Tecnológico y de Estudios Superiores de

Monterrey, Querétaro

Querétaro, **México**

Dr. Filippo Ubertini

Universidad de Perugia,

Perugia, **Italia**

Dr. Ravindra Gettu

Instituto Indio de Tecnología de Madrás,

Chennai, **India**

**JOURNAL OF THE LATIN-AMERICAN
ASSOCIATION OF QUALITY CONTROL,
PATHOLOGY AND RECOVERY OF
CONSTRUCTION**

<http://www.revistaalconpat.org>

With great satisfaction, we present the third issue of the twelfth year of the ALCONPAT Journal.

The objective of Revista ALCONPAT (RA) is the publication of citable production (basic or applied research, and reviews), documentary research and case studies, related to the topics of our association, that is, quality control, pathology, and recovery of the constructions.

This V12 N3 edition begins with a work from **Brazil**, where Joaquín Humberto Aquino Rocha and colleagues carry out a systematic review of the literature of the last five years on the use of cellulose nanofibers (NFC) in cement-based compounds. The main forms of production and dispersion are presented, with emphasis on the effect on the behavior of cement-based materials. The study considered the influence of NFC on properties in the fresh and hardened state: rheology, hydration, compressive strength, flexural strength, fracture energy, among others. NFCs have beneficial effects on mechanical properties; however, more research is still needed to optimize NFC production and pretreatment processes, establish relationships on the durability of compounds with NFC, and identify the possible environmental impacts of their use.

In the second paper, from **Brazil**, Marcus Luiz Alves dos Santos Costa and colleagues present and discuss the use of industrial solid waste in terms of how to improve the mechanical properties of cement composites. For this, the incorporation of "crushed" granite powder and marble powder in the manufacture of cement-based composites was evaluated, partially replacing the natural fine aggregate at levels of 50% and 100%. To achieve this, characterization tests of the aggregates were carried out, in addition to the evaluation of the axial compression resistance of the specimens. The results showed that the mixtures containing 50% recycled aggregate give the material a compressive strength of 29.09 MPa, that is, 4% higher than the reference mixtures, the results being satisfactory, demonstrating the viability of recycled aggregates on concrete pieces.

The third paper in this issue is from **Mexico**, where Josefa de los Angeles Paat Estrella and colleagues evaluate electrochemical realkalization at different times and current intensities in accordance with the provisions of the UNE-EN-1504, NACE-SP0107 and NMX- C-553-ONNCCE in previously carbonated reinforced concrete structures, determining the degree of realkalization, pH and half-cell potential every 7 days for 28 days. A pH recovery was achieved with respect to time and current intensity, obtaining E_{corr} values lower than -350 mV, which according to the ASTM C876-15 standard, correspond to a 90% probability of corrosion. However, it was the NMX-C-553-ONNCCE-

2018 that presented potential without reaching the region of overprotection, without the risk of producing hydrogen and brittleness in the steel.

In the fourth article from **Brazil**, Camila G. Luz Nunes and colleagues aimed to optimize the production of hot mix asphalt using asphalt rubber. For this, the mechanical performance of asphalt mixtures produced with different binders was evaluated: commercial rubber asphalt (AC08), rubber asphalt 10% (AC10) and 15% (AC15) of rubber residues and conventional asphalt (PEN 50-70). For the composition of these mixtures, the optimum asphalt content was defined by the Marshall method. To carry out the mechanical tests, specimens molded with Marshall and Superpave compactors were tested. From the results obtained, it was found that the mixtures with AR08 and AR10, compacted with Superpave, presented the best mechanical performance. However, the AR08 binder is already available on the market, which facilitates its use in paving works.

The fifth article, by José Luis Pérez-Díaz and colleagues, comes from **Mexico** and evaluated the corrosion risk of steel by using carbon steel/stainless steel internal galvanic sensors with an external Cu/CuSO₄ electrode. The sensors were used to monitor the macrocell potentials and currents of prismatic reinforced concrete specimens, with water-cement ratios of 0.4 and 0.6, immersed in a 5% NaCl solution for 18 months. The results of the potentials showed a good correlation between the two reference electrodes, being able to evaluate the corrosion of the system. Furthermore, the electrochemical noise technique supports the effect by chloride ions. Therefore, galvanic sensors can be considered for implementation in the monitoring and evaluation of the state of corrosion risk in reinforced concrete structures.

The sixth work in this issue is written by Danilo Pereira dos Santos and Maiara Feliciano dos Santos from **Brazil**. This work analyzes the impact of corrosion on the global stability of reinforced concrete columns, evaluating the effectiveness of the stiffness reduction criteria proposed by ABNT NBR 6118: 2014. With the analyses, using finite element models that reproduced the behavior of the materials, it was defined that corrosion causes the intensification of the second-order global stresses in the structure. However, in critical situations, loss of balance in the cross section resulted in structural failure even before loss of stability. The study was carried out both through a nonlinear geometric analysis and through the application of the γ_z coefficient, where it was concluded that the subsequent addition of rheological effects can lead to a configuration that goes beyond the limits proposed by the Brazilian standard.

In the seventh paper, from **Mexico**, Joel A. Moreno Herrera and colleagues evaluated the change in the flexural behavior of reinforced concrete beams. Beams without corrosion and beams with electrochemical parameters associated with a high level of corrosion were considered. The electrochemical parameters considered were corrosion rate, electrical resistivity and chloride concentration. The beams were tested under incremental vertical loads until failure. Cracking patterns, yield and maximum loads, yield stiffness and displacement ductility of the beams are presented. Based on the analysis of these structural parameters, it is concluded

that the bending behavior of the beams with and without corrosion was similar.

The article that closes the edition is by G. H. Teixeira from **Brazil** and colleagues, who show the application of the GDE (Degree of Deterioration of the Structure) and GUT (Gravity, Urgency and Trend) methodologies, quantifying the pathological manifestations and determining the points of greatest maintenance need. Thus, a quantitative perspective was applied with the application of the aforementioned methodologies and after the inspections of the building and a visual analysis with photographic records, annotations and mappings, the methodologies were applied and it was obtained that the majority of the pathological manifestations that occur in the the structure of the building is caused by humidity, giving rise to efflorescence, stains or infiltrations. In this way, this work defined the points that need priority, guiding the measures that can be taken later. The methodologies proved to be effective and important for decision making.

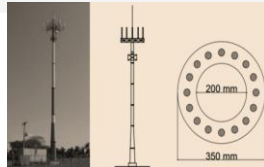
It is important to mention that the ONCyTS of Brazil and Mexico have kept Revista Alconpat in their indexes of Quality Scientific Journals. In particular, in Mexico, the Alconpat Journal has been consolidated at an international level and the National System of Researchers (SNI) already considers it as a valid product for the promotion and permanence of its members. This has been a great achievement, the product of everyone's efforts, authors, reviewers and editorial committee. Similarly, it is important to mention that Revista Alconpat already belongs to the Directory of Open Access Journals (DOAJ), which is a definitive step to apply to new indexes. Alconpat is also making a significant financial investment so that all its issues are being marked in XML-Jats so that it can be evaluated in more prestigious indexes. Congratulations and our thanks to all.

We are sure that the articles in this issue will constitute an important reference for those readers involved with questions of evaluation and characterization of materials, elements and structures. We thank the authors participating in this issue for their willingness and effort to present quality articles and meet the established deadlines.

On behalf of the Editorial Board

A handwritten signature in black ink, appearing to read 'Pedro Castro Borges', written over a circular stamp or seal.

Pedro Castro Borges
Editor in Chief



CONTENT

REVIEW

Rocha, J. H. A., Farias, L. do N., Siqueira, T. P. L.: Cellulose nanofibers (CNF) as reinforcement for cementitious matrices: a systematic literature review.

Página

311 - 327

BASIC RESEARCH

Costa, M. L. A. S., Valões, D. C. P., Nascimento, C. F. G., Silva, G. R., Lima, E. G. S., Silva, T. T. S., Santos, T. S.: Analysis of concrete characteristics with the replacement of natural fine aggregate by industrial solid waste.

328 – 346

Paat, J. A., Miam, J. A., Maldonado, E. E., Nieves, D., Pérez, T.: Electrochemical re-alkalinization applied to carbonated concrete beams samples under the criteria of three standards.

347 – 361

Nunes, C. G. L., Pereira, P. H. S., Melo, R. A., Rodrigues, J. F. K. G., Lucena, L. C. F. L.: Influence of unserviceable tires' rubber on the mechanical performance of hot mix asphalt.

362 – 377

Pérez, J. L., Cabrera, J. A., Hernández, D., Godínez, E. A., Mundo, M. D.: Comparison between galvanic sensors (steel/stainless steel) and half-cell potentials (E_{corr}) for monitoring the corrosion risk of steel reinforcement in concrete structures.

378 – 397

Santos, M. F., Santos, D. P.: Evaluation of the influence of corrosion on the global stability of reinforced concrete columns.

398 – 416

Moreno Herrera, J. A., Varela Rivera, J. L., Visairo Méndez, R., Castro Borges, P.: Flexural behavior of reinforced concrete beams with electrochemical parameters associated with high level of corrosion.

417 – 427

APPLIED RESEARCH

Teixeira, G. H., Silva, J. R. Alves, E.C.: Evaluation of the pathological manifestations of the Rio Negro Building in Anápolis-Goiás.

428 – 443

Cellulose nanofibers (CNF) as reinforcement for cementitious matrices: a systematic literature review

J. H. A. Rocha^{1*} , L. do N. Farias¹ , T. P. L. Siqueira¹ 

*Contact author: joaquin.rocha@coc.ufrj.br

DOI: <https://doi.org/10.21041/ra.v12i3.594>

Reception: 13/03/2022 | Acceptance: 08/07/2022 | Publication: 01/09/2022

ABSTRACT

The aim of this study is to conduct a systematic literature review of the last five years on the use of cellulose nanofibers (CNF) in cementitious composites. The main production and dispersion methods are presented with emphasis on their effect on the behavior of cement-based materials. The study considered the influence of CNF on the fresh and hardened state properties: rheology, hydration, compressive strength, flexural strength, fracture energy, among others. CNF show positive effects on mechanical properties. However, further research is still necessary to optimize the production and pretreatment processes of CNF, establishing relationships regarding the durability of composites with CNF, and identifying possible environmental impacts of their use.

Keywords: cellulose nanomaterials; cementitious composites; fresh state; hardened state; mechanical properties.

Cite as: Rocha, J. H. A., Farias, L. do N., Siqueira, T. P. L. (2022), “Cellulose nanofibers (CNF) as reinforcement for cementitious matrices: a systematic literature review”, Revista ALCONPAT, 12 (3), pp. 311-327., DOI: <https://doi.org/10.21041/ra.v12i3.594>

¹ Programa de Engenharia Civil, PEC/COPPE/UFRJ, Universidade Federal do Rio de Janeiro, Rio de Janeiro, Brasil.

Contribution of each author

In this work, the author J. H. A. Rocha, contributed with the original idea in 33%, data collection in 40%, choice and development of work methodology in 40%, writing and discussion of results in 40%; the author L. do N. Farias contributed with original idea in 33%, data collection in 30%, choice and development of work methodology in 30%, writing and discussion of results in 30%, and the author T. P. L. Siqueira contributed 34% original idea, 30% data collection, 30% choice and development of the work methodology, 30% writing and discussion of results in 30%.

Creative Commons License

Copyright 2022 by the authors. This work is an Open-Access article published under the terms and conditions of an International Creative Commons Attribution 4.0 International License ([CC BY 4.0](https://creativecommons.org/licenses/by/4.0/)).

Discussions and subsequent corrections to the publication

Any dispute, including the replies of the authors, will be published in the third issue of 2023 provided that the information is received before the closing of the second issue of 2023.

Nanofibras de celulose (NFC) como reforço de matrizes cimentícias: revisão sistemática da literatura

RESUMO

O objetivo deste estudo é realizar uma revisão sistemática da literatura dos últimos cinco anos sobre o uso de nanofibras de celulose (NFC) em compósitos cimentícios. São apresentadas as principais formas de produção e dispersão, com destaque para o efeito sobre o comportamento dos materiais à base de cimento. O estudo considerou a influência das NFC nas propriedades no estado fresco e endurecido: reologia, hidratação, resistência à compressão, resistência à flexão, energia de fratura, entre outras. As NFC têm efeitos benéficos nas propriedades mecânicas. No entanto, maior pesquisa ainda é necessária para otimizar a produção e os processos de pré-tratamento das NFC, estabelecer relações sobre a durabilidade dos compósitos com NFC, e identificar possíveis impactos ambientais da sua utilização.

Palavras-chave: nanomateriais de celulose; compósitos cimentícios; estado fresco; estado endurecido; propriedades mecânicas.

Nanofibras de celulosa (NFC) como refuerzo para matrices cementicias: revisión sistemática de la literatura

RESUMEN

El objetivo de este estudio es realizar una revisión sistemática de la literatura de los últimos cinco años sobre el uso de nanofibras de celulosa (NFC) en compuestos a base de cemento. Se presentan las principales formas de producción y dispersión, con énfasis en el efecto sobre el comportamiento de los materiales a base de cemento. El estudio consideró la influencia de las NFC en las propiedades en estado fresco y endurecido: reología, hidratación, resistencia a la compresión, resistencia a la flexión, energía de fractura, entre otras. Las NFC tienen efectos beneficiosos sobre las propiedades mecánicas; sin embargo, aún se necesita más investigación para optimizar la producción de NFC y los procesos de pretratamiento, establecer relaciones sobre la durabilidad de los compuestos con NFC, e identificar los posibles impactos ambientales de su uso.

Palabras clave: nanomateriales de celulosa; compuestos de cemento; estado fresco; estado endurecido; propiedades mecánicas.

Legal Information

Revista ALCONPAT is a quarterly publication by the Asociación Latinoamericana de Control de Calidad, Patología y Recuperación de la Construcción, Internacional, A.C., Km. 6 antigua carretera a Progreso, Mérida, Yucatán, 97310, Tel.5219997385893, alconpat.int@gmail.com, Website: www.alconpat.org

Reservation of rights for exclusive use No.04-2013-011717330300-203, and ISSN 2007-6835, both granted by the Instituto Nacional de Derecho de Autor. Responsible editor: Pedro Castro Borges, Ph.D. Responsible for the last update of this issue, Informatics Unit ALCONPAT, Elizabeth Sabido Maldonado.

The views of the authors do not necessarily reflect the position of the editor.

The total or partial reproduction of the contents and images of the publication is carried out in accordance with the COPE code and the CC BY 4.0 license of the Revista ALCONPAT.

1. INTRODUCTION

The search for more sustainable building materials with reduced CO₂ emissions has been growing significantly over the last decades, mainly due to global warming and the fact that the construction industry is considered one of the most polluting industries in the world (UN Environment *et al.*, 2018; CAO *et al.*, 2020). In this pursuit for materials with lower environmental impact there is the use of the so-called biomaterials, that is, materials that incorporate in their formulation plant derived products (Barnat-Hunek *et al.*, 2019; Nishimura *et al.*, 2019; Abdellaoui; Bouhfid, 2020; Barría *et al.*, 2021). According to Hoyos *et al.* (2019) the sustainability of a material is defined by its capacity and regeneration rate and the possibility of being reassimilated to the environment after its use.

Moreover, the potential use of nanoscale materials, called nanomaterials, in construction materials has also been growing over the last few years. Through nanomodification it is possible to alter the nano- and microstructure of cementitious matrices in order to modify several properties of the material (Santos *et al.*, 2021; Tang *et al.*, 2019; Zhang *et al.*, 2021). These changes impact the macro behavior of the matrices, and can increase the strength, deformability, and thermal conductivity of the materials. Therefore, cellulose nanofibers (CNFs) are presented as a promising material to be incorporated into building materials (Hisseine *et al.*, 2019; Claramunt *et al.*, 2019). CNFs are a biopolymer class that can be synthesized by plants, bacteria, and algae (Hoyos *et al.*, 2019; Ogura *et al.*, 2020) and exhibit high strength, stiffness, and elastic modulus, being able to improve several characteristics of traditional cementitious matrices (Mejdoub *et al.*, 2016; Dongre; Suryawanshi, 2021). In addition, CNFs show high biodegradability, low toxicity and minimal environmental and health risks as one of the main environmental advantages (Hisseine *et al.*, 2019). Studies show that the incorporation of cellulose nanofibers can increase the viscosity of the matrices, acting in a similar way to a viscosity modifier admixture, and have the ability to retain water which, consequently, reduces the exudation of the mixtures (Hisseine *et al.*, 2018a; Bakkari *et al.*, 2019). Analyzing the mechanical performance of the matrices with CNF incorporation, a tendency to increase the compressive and flexural strength of the matrices is noticed when compared to the reference mixtures (Cengiz *et al.*, 2017; Kolour *et al.*, 2020). However, when the addition is done in very high levels, the effects can be negative due to the increased porosity of the mixtures (Sun *et al.*, 2016; Correia *et al.*, 2018; Alzoubi *et al.*, 2020).

Therefore, the present study aims to perform a systematic literature review (SLR) to collect existing data on the use of cellulose nanofibers (CNF) in cementitious matrices and identify unexplored knowledge gaps. To this end, both a survey of the most recent works published on the subject, and an analysis of the data found were performed. So that this work can serve as a basis for future studies.

2. METHODOLOGY

To conduct this study some questions were set that were the basis for the selection and analysis of the studies found. The formulated questions were:

1. - What are the dimensions of the most commonly used fibers and the incorporation percentage currently employed in the literature?
2. - What are the most commonly used CNF treatment/dispersal methods observed in the studies?
3. - What are the most analyzed properties of CNF-reinforced composites and, consequently, what are the most performed tests?

In addition to these questions, a mapping of the studies found was performed by analyzing the countries, institutions, and authors that most published on the subject and the most used keywords.

To answer these questions, two databases were chosen to collect the articles: *ScienceDirect* and *Google Scholar*. The first database encompasses several journals indexed in Scopus and *Web of Science*. In addition, using the method known as “snowballing”, we added relevant and highly cited articles from Google Scholar that were not present in the first database and that were published in journals with an impact factor (*Scopus* and *Web of Science*).

This study analyzed all research articles related to the topic published between the years 2016 and 2021 that were written in English. The search string used to collect the articles was: "CELLULOSE NANOFIBERS" AND ("CEMENT MATRICES" OR "MORTAR" OR "CONCRETE") resulting in a total of 163 articles for analysis.

After excluding the book chapters and literature review articles and adding the relevant articles using the "snowball method", the titles and abstracts of the articles were analyzed. Those that did not answer the proposed questions or did not incorporate fibers into cementitious matrices were excluded. Finally, all 29 papers considered relevant were analyzed in their entirety.

The *VOSViewer* program (version 1.6.17) was used for further bibliometric analysis of the selected articles.

3. RESULTS AND DISCUSSIONS

3.1 Mapping of the studies

The map in Figure 1 shows that the countries that have published the most on this subject are the United States with 10 articles, Canada with 7 articles, China with 4 articles, and Spain and Brazil with 3 articles each. All the other countries represented in a lighter shade of green contributed with one publication each. With these results we can see a predominance of the Northern Hemisphere countries in publishing on the theme, being present in 43% of the publications. Despite this, it can be seen that this is a subject that is being studied around the world, with the involvement of 16 different countries in the articles found.

The authors who have published the most on the theme are presented in Figure 2, where the light colors (yellow) indicate a greater number of published papers, differentiated by groups of authors. It was noted that some authors were involved in more than one publication on the topic. While 70% of the studies presented different authors. This analysis shows that there is a high interest in the incorporation of CNF in cementitious matrices since several institutions and several authors are involved in this research.

Figure 3 shows the most used words in the titles and keywords of the articles studied. According to the data collected, it is possible to notice a predominance of the words "cellulose nanofibers". Furthermore, it is possible to note the presence of the properties that the articles analyzed, among them, "mechanical properties" and "compressive strength". Through the results found it is clear that there is a wide variety of approaches being currently employed regarding the use of CNF, indicating the range of advantages that this material can offer when incorporated into various types of matrices.

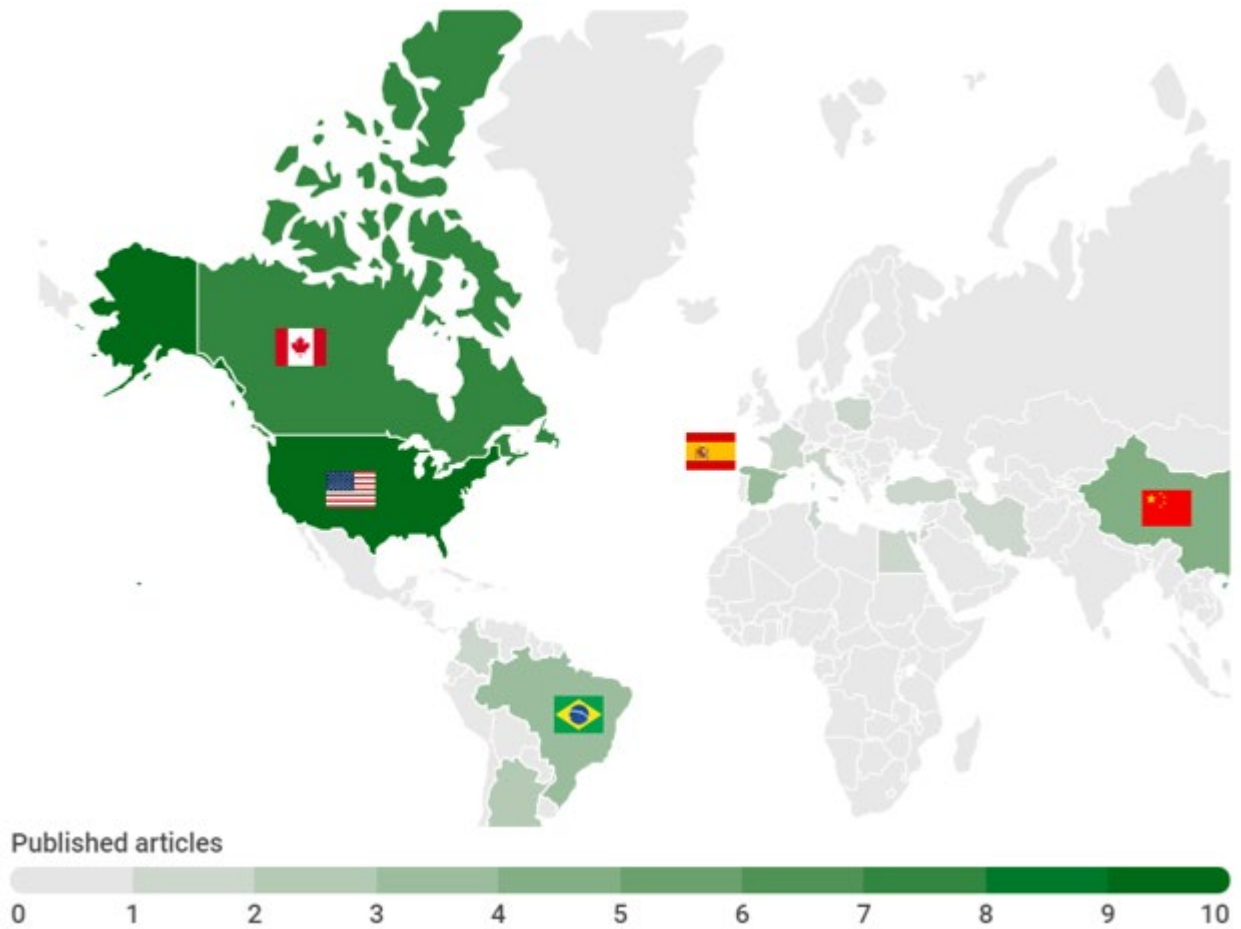


Figure 1. Countries that have most published on the subject.

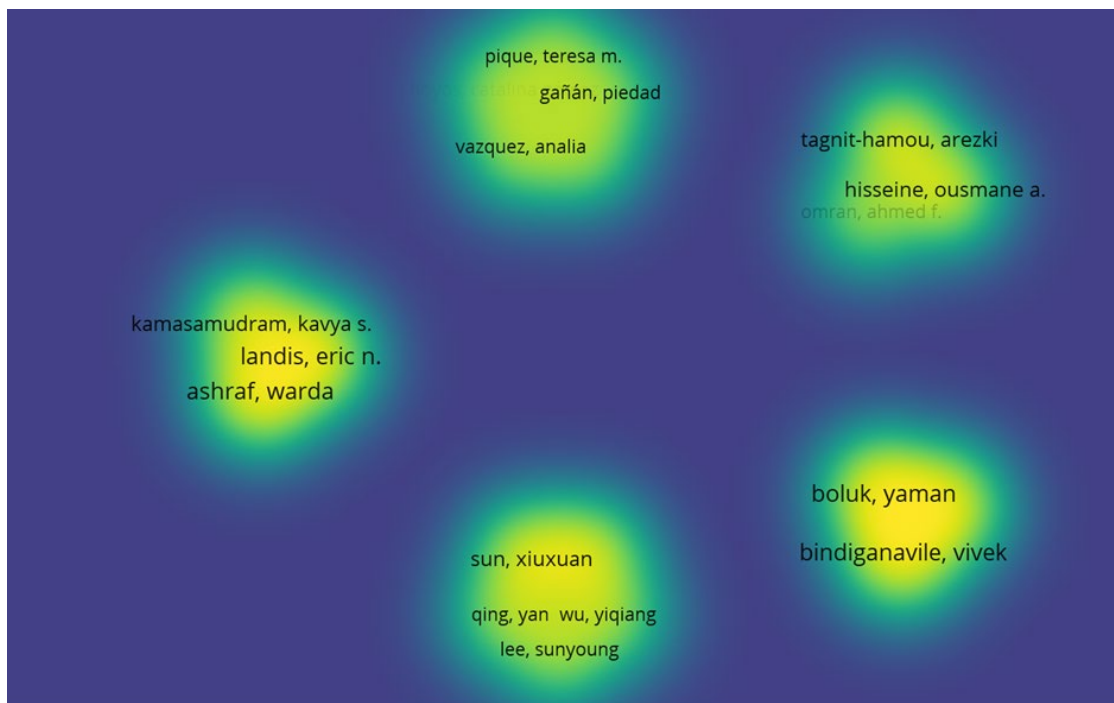


Figure 2: Density map of the authors who have most published on the subject.

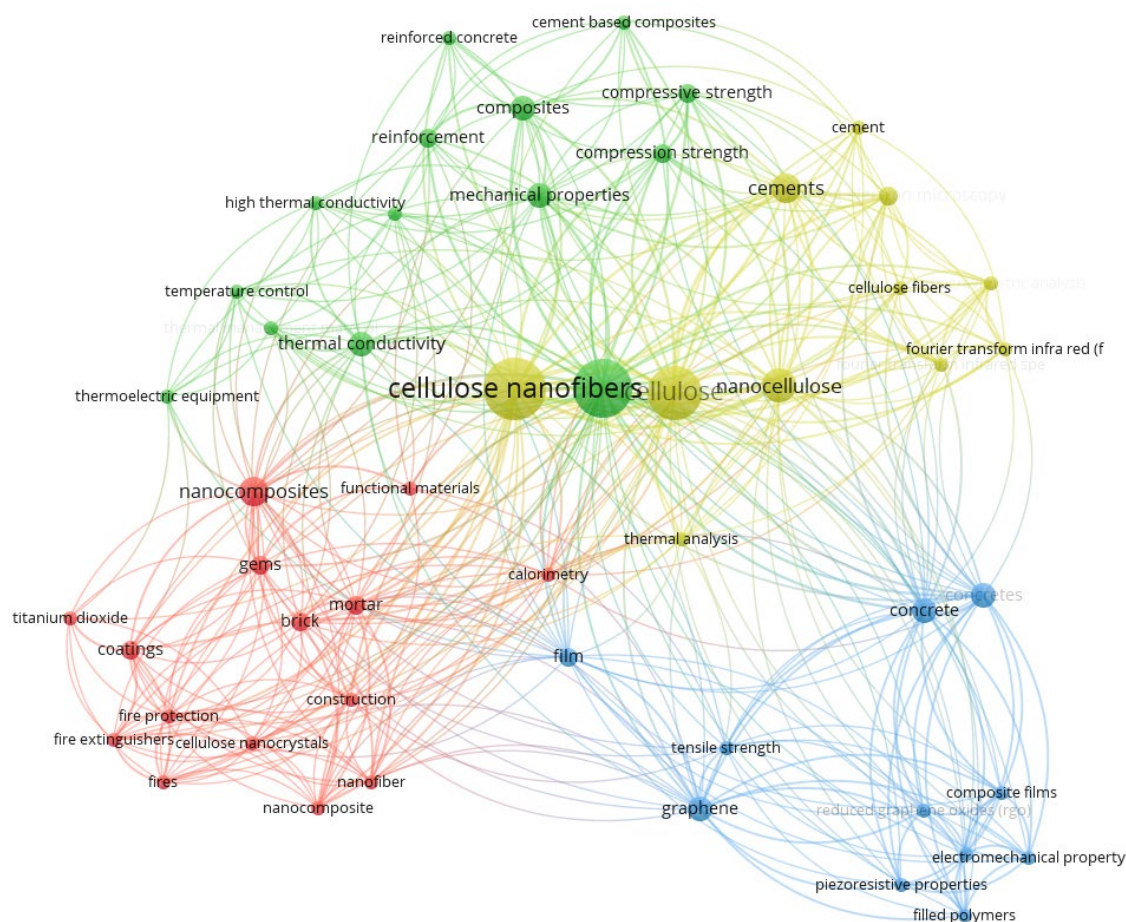


Figure 3: Main words in titles and keywords of articles.

3.2 Cellulose nanofibers (CNF)

Cellulose undergoes several chemical or physical treatments until it results in nanocellulose. Depending on the extraction method employed, nanocellulose can also be divided into a few groups, such as nanofiber cellulose (CNF) and nanocrystals of cellulose (NCC). NCC are commonly known as nanocrystalline cellulose, nanowhiskers, nanocrystals and the monocrystals, while CNF are much finer as they are extracted from the cellulose microfibrils present in the biomass, they are usually cited as cellulose microfibrils, nanofibrils or nanofibrillated cellulose and basically consist of long flexible nanoparticles/nanofibrils with interchanged crystalline and amorphous domains (Abdul Khalil *et al.*, 2012; Guo *et al.*, 2020; Dhali *et al.*, 2021).

CNFs have dimensions ranging from 5-50 nm in width and 1-5 μm in length, have 50-70% crystallinity and an extremely high surface area (Goncalves *et al.*, 2021). CNFs exhibit a hydrophilic nature, so a low content, between 0.1% and 5% by weight, is generally used as reinforcement in cementitious matrices. However, even in small amounts, CNF diluted in water can create a stable and uniform gel (Zhang; Scherer, 2020).

Some studies report the use of CNF as reinforcement in cementitious composites, and this has been seen in the present literature review. Appendix 1 summarizes the general characteristics of the nanofibers used by the authors, it is observed among the studies that the CNF dimensions used ranged from 10-500 nm in diameter, 2-20 nm in width and reached up to several microns in length. However, it is important to note that in the literature the cross-sectional dimension of CNFs is designated as both diameter and width. As for the percentage of CNF used as reinforcement in the

cementitious matrix, they varied between 0.02% and 3%. In addition to the so-called CNF, studies have designated other names/types of cellulosic nanofibers, such as hydrophilic cellulose nanofibrils (Zhang; Scherer, 2020), nanofibrillated cellulose (Correia *et al.*, 2018) and the bacterial CNFs (Akhlaghi *et al.*, 2020; Barría *et al.*, 2021). Studies such as Cengiz *et al.* (2017) conducted comparisons between natural and commercial nanofibers. The natural nanofibers were derived from *Cladophora* sp (algae) which has a residual form in a river. In general, the CNFs studied by the authors were used in cementitious matrices of pastes (62%); pastes and concretes (17%); pastes and mortars (13.7%) - some studies simultaneously linked two types of matrices. An exception to this is the work of Panesar *et al.* (2017) who only conducted a study of alkali treatment in CNFs. The crystallinity of the nanofibrils is reduced due to the amorphous characteristic of the lignin and hemicellulose present in cellulose, which also affects the mechanical properties provided to the cementitious composites. In this way, chemical or enzymatic treatment methods are also performed (Dhali *et al.*, 2021).

The alkaline pretreatment, also known as mercerization, performed by the authors Panesar *et al.* (2017) and Fonseca *et al.* (2019), consists of exposing the nanofibers to a solution such as sodium hydroxide. Fonseca *et al.* (2019) explain that the alkaline treatment was performed in order to improve the defibrillation of the jute fibers into nanofibrils. According to Abdul Khalil *et al.* (2012), alkaline pretreatment also has the function of completely removing lignin and hemicellulose from CNFs. However, alkaline treatment is not sufficient for removing cellulosic constituents, in this case, further removal of a residual lignin can be done by the bleaching method. The homogenization method has been performed by authors such as Hoyos *et al.* (2019), Tang *et al.* (2019), Sun *et al.* (2017), Mejdoub *et al.* (2016), and Jiao *et al.* (2016), and is a type of mechanical treatment for cellulose fibers that consists of high-pressure refining and homogenization processes. The fibers are generally subjected to repeated cyclic stress. According to Abdul Khalil *et al.* (2012), this treatment increases the utilization potential of the fibers because it modifies part of their morphology.

The TEMPO-mediated oxidation system was also mentioned and employed by Jiao *et al.* (2016). Oxidation performed in the presence of TEMPO is a method used to modify the hydrophilic characteristic of the nanocellulose surface. However, the efficiency of this type of method has been proven in NCC as they show better dispersibility due to the introduction of dense carboxylate groups on their surfaces (Hassan *et al.*, 2021).

Sonication is considered one of the most widely used methods for CNF dispersion and was also found in the present review, in the studies by Sun *et al.* (2017), Claramunt *et al.* (2019), Barnat-Hunek *et al.* (2019), Nassiri *et al.* (2021) and Ez-zaki *et al.* (2021). Yet, although sonication can be effective in dispersing nanocellulose, Guo *et al.* (2020) reported challenges for this treatment, such as the difficulty of converting the adsorbed nanocellulose on cement particles into free nanocellulose that enables the formation of fiber clusters in cementitious matrices.

3.3 CNF in cementitious composites

Appendix 2 presents the detailed properties evaluated in the literature of pastes, mortars and concrete with CNF. This section presents a brief summary on the influence of CNF addition on hydration, rheology, shrinkage, mechanical properties (compressive and flexural strength), among others.

3.3.1 Hydration

Several studies indicate that the degree of cement hydration increases with the presence of CNF, as it promotes hydration to produce more calcium silicate hydrate (C-S-H) and calcium hydroxide (CH); therefore, an improvement in mechanical properties is presented (Mejdoub *et al.*, 2016; Sun

et al., 2017; Hoyos *et al.*, 2019; Hisseine *et al.*, 2019). Although no adverse effect is reported on the degree of hydration, there is an influence on its kinetics (Hisseine *et al.*, 2018a).

Jiao *et al.* (2016) point out that cement paste samples with and without CNF show no differences in hydration at early ages (10 hours), since the exposed surface of the cement particles dominates heat release and there is enough water around the particles for hydration (Lootens; Bentz, 2016). The addition of CNF prolongs induction periods and delays the peak heat flow rates. The hydroxyl and carboxyl groups of cellulose molecules are hydrophilic (Klemm *et al.*, 2011), the oxygen atom found in these groups has unpaired electrons that can react with the Calcium ion (Ca^{2+}) and form a hydrophilic compound that delays the induction period of hydration and hardening. Therefore, fewer contact sites are generated between cement particles and water, decreasing the rates of C-S-H and CH formation (Sedan *et al.*, 2008).

Due to this same phenomenon, Goncalves *et al.* (2019) and Kamasamudram *et al.* (2020) reported there is also a reduction in ettringite formation. Kamasamudram *et al.* (2021a) found that lignocellulose nanofibers (LCNF) and delignified cellulose nanofibers (DCNF) reduce the amounts of ettringite and CH in the hydrated cement paste. However, CNF with silica nanoparticles was shown to increase the amount of CH, around 4%, due to the enhanced cement reaction speed (filler effect); whereas, for the CNF-only samples, a reduction in CH was observed (Kamasamudram *et al.*, 2020).

On the other hand, at long times, CNFs release water in the surrounding regions and contribute to the hydration of unhydrated cement particles, improving the microstructure and mechanical properties of cement pastes (Jiao *et al.*, 2016). In this regard, Ez-zaki *et al.* (2021) pointed out the same trend when using alkali activated ground granulated blast furnace slag with CNF. Kolour *et al.* (2020) suggest that the degree of hydration increases with the presence of CNF after 3 days. Zhang and Scherer (2020) also mention that CNFs improve cement hydration in the long term; however, this may vary depending on the CNF source.

In contrast, Mejdoub *et al.* (2016), Kamasamudram *et al.* (2020) and Kamasamudram *et al.* (2021b) indicate that CNF accelerate early-stage cement hydration as a result of the nucleation effect and that this effect is greater for CNF with silica nanoparticles. After 80 h of hydration, CNF additions showed no significant effects on the hydration degree (Kamasamudram *et al.*, 2021a). Kamasamudram *et al.* (2021b) conclude that the influence of CNF on hydration depends on the w/c ratio (the concentration of alkali ions in the pores depends on the w/c ratio), where for a w/c ratio of 0.35 there is accelerated hydration at early ages; whereas, for a w/c ratio of 0.45, hydration was not as prominent.

Although no adverse effects on hydration are reported, further studies of hydration kinetics at early ages are needed in order to define possible applications in construction, in addition to analyzing other variables such as cement type, different w/c ratios, etc.

3.3.2 Rheology

Every study that analyzed the rheology of cement paste and concrete with CNF reported improvements, such as yield strength and viscosity (Hisseine *et al.*, 2018a; Bakkari *et al.*, 2019; Ez-zaki *et al.*, 2021). In general, CNFs act as a modifying agent on the viscosity of cement pastes, increasing their yield strength at small additions of CNFs, this is due to two main reasons: a) water retention capacity, since hydrophilicity is an intrinsic characteristic of CNFs (Hisseine *et al.*, 2018a; Hisseine *et al.*, 2018b; Ez-zaki *et al.*, 2021), and b) the formation of CNF networks, which are prominent in longer and more flexible CNF (Hoyos *et al.*, 2019; Nassiri *et al.*, 2021).

Hisseine *et al.* (2018a) and Hisseine *et al.* (2019) indicate that CNF incorporation requires the use of high-range water-reducing admixtures (HRWRA), due to the viscosity modification produced by CNFs. This is associated with the hydrophilicity of CNFs, increasing water retention and also it is associated with a high surface area and high aspect ratio of CNFs, increasing the formation of

CNF chains. On this last point, Hisseine *et al.* (2018a) found that CNF chains increase the viscosity of the mixture at low shear rates; however, for high shear rates, CNF chains led to a lower viscosity, due to the streamlining of CNFs in the flow direction, exhibiting a shear thinning behavior.

The CNF addition increased the elastic limit of oil well cement (OWC) suspension, improving its rheological properties (Sun *et al.*, 2016). Tang *et al.* (2019) found that the gel strength, elastic limit, and viscosity of CNF and OWC suspensions were higher when compared to cellulose nanocrystal (NCC) suspensions, this is because CNF are more likely to form the interlocking grid. In another study of CNF with OWC, it was found that the addition of graphene nanoplates (GNP) leads to higher yield stresses in the fresh state (Sun *et al.*, 2019). It is observed that CNFs have an important influence on the rheological behavior of cementitious materials; however, few authors have considered this aspect, and it is an important topic for future research.

3.3.3 Shrinkage

Zhang and Scherer (2020) demonstrated the use of CNF to investigate the chemical shrinkage of high w/c ratio cementitious pastes at early ages (3 days), since there is no chemical effect on short-term hydration. The CNFs created a stable structure to support the cement particles and allowed them to hydrate without sedimentation.

Kolour *et al.* (2020) found that adding an amount of 0.06% CNF (by weight of cement) leads to a reduction in autogenous shrinkage by up to 49% in cement pastes with a w/c ratio of 0.30. For self-compacting concretes, Hisseine *et al.* (2018b) reported that the use of CNF reduced autogenous shrinkage deformations by up to 31% in 7 days.

The use of CNF with higher levels of carboxyl groups in Portland cement systems mitigates dimensional shrinkage-related changes and cracking in cement pastes (Bakkari *et al.*, 2019).

Studies show that CNFs mainly reduce chemical and autogenous shrinkage. However, there are no long-term studies, such as drying shrinkage and creep, as well as relating these properties to the materials, dosage, humidity, temperature, curing, among others.

3.3.4 Mechanical properties

As mentioned earlier, the mechanical properties of cementitious pastes improve with CNF addition, due to the water retention of CNF and the increased degree of hydration (internal curing), as well as the increased adhesion of CNF and the cementitious matrix. However, high CNF contents are detrimental as they increase porosity and other factors must be taken into consideration for the development of mechanical properties (Sun *et al.*, 2016; Correia *et al.*, 2018; Hisseine *et al.*, 2018a; Hisseine *et al.*, 2019; Kolour *et al.*, 2020; Alzoubi *et al.*, 2020).

a) Compressive strength: Most studies report an increase in compressive strength with the addition of CNF (Hisseine *et al.*, 2019; Sun *et al.*, 2017). Mejdoub *et al.* (2016) found more than 50% increase in compressive strength with 0.3% CNF. In the results of Kolour *et al.* (2020) for a mixture with 0.15% CNF, there was an increase of up to 31% after 7 days, and for a mixture with 0.09% CNF, there was an increase of up to 16% after 28 days. In self-compacting concrete, Hisseine *et al.* (2018b) indicate a positive tendency in the addition of CNF, as compressive strength increased by up to 16%.

Kamasamudram *et al.* (2020) showed that by adding 0.1% CNF with silica nanoparticles the compressive strength increased by 13% (at 90 days) over the control batch and by 10% over the batch without silica nanoparticles.

The addition of DCNF showed a maximum 15% increase in compressive strength for 0.05% and 0.1% DCNF after 90 days of curing. The maximum increase in compressive strength of cement paste cured for 90 days with the addition of 0.1% LCNF was approximately 16% (Kamasamudram *et al.*, 2021a).

The addition of CNF and phase change material led to an increase in the compressive strength of cement mortar, where the best result is achieved with the addition of 0.5% CNF, due to the reduction in the mortar porosity (Alzoubi *et al.*, 2020).

On the other hand, some studies have reported that CNF addition does not have a considerable effect on the compressive strength of cement pastes (Kamasamudram *et al.*, 2021b), partly because it can be adversely affected by air entrainment and CNF agglomeration (Hisseine *et al.*, 2018b). Although Nasiri *et al.* (2019) report an increase in compressive strength (17-18%) with the addition of CNF, concentrations above 0.065% resulted in small improvements in strength at 7 days and decreased strength at 28 days when compared to the reference mixtures.

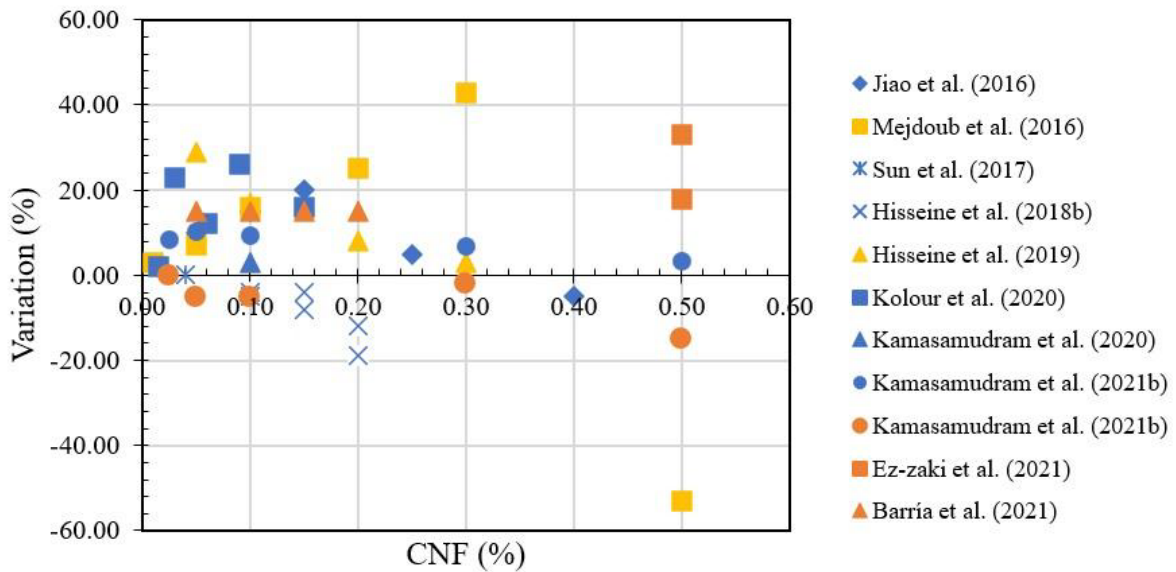
Figure 4a shows the summary of the variation rate of the compressive strength at 28 days as a function of the added content of CNF. It is important to note that only the studies that provided data were considered. When the variation results are classified by w/c ratio (Figure 4b), it is observed that the lower the w/c ratio, the higher the positive variation (9.80% for a w/c ratio from 0.26 to 0.30), presenting a single atypical data. Additionally, it is observed that for this w/c ratio there are only positive rates and a smaller data dispersion (3-43%). For other w/c ratios, the dispersion of the data is higher and the reduction in compression strength results are reported.

b) Flexural strength: For flexural strength, a generally positive effect is reported (Hisseine *et al.*, 2018a; Hisseine *et al.*, 2018b; Hisseine *et al.*, 2019). Hisseine *et al.* (2019) described an increase of up to 25%. Kamasamudram *et al.* (2020) found that with the addition of 0.1% CNF, flexural strength increased by 70%, a rate close to that reported by Kamasamudram *et al.* (2021b), 75%. Even higher percentages were presented by Kolour *et al.* (2020), 116% and Cengiz *et al.* (2017), 169.7%.

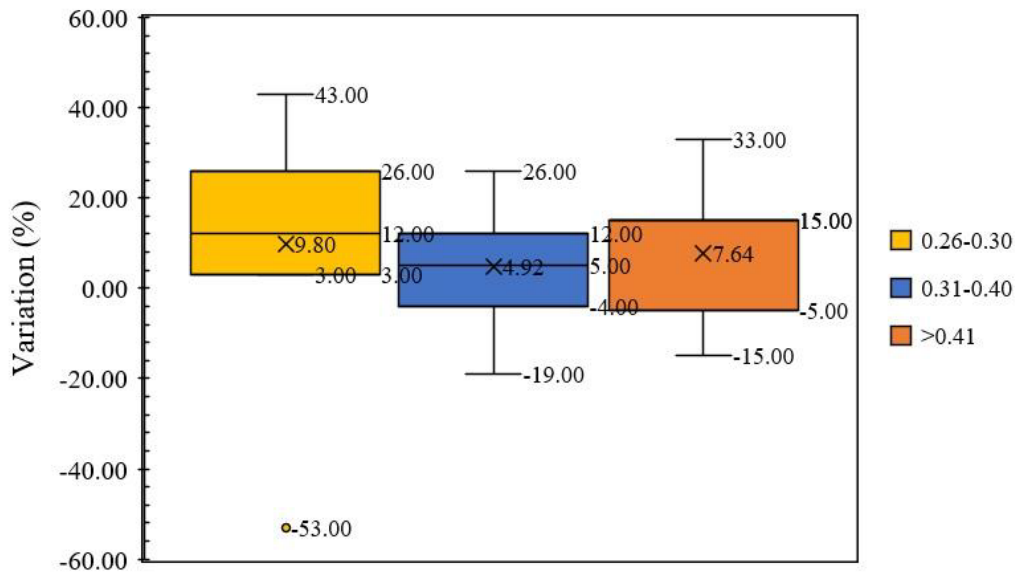
Sun *et al.* (2016) found that flexural strength increased by 20.7% for a CNF/CPM ratio of 0.04, attributed to increased hydration and the binding effect of CNF, but they also noted that excessive addition of CNF is damaging due to nanoparticles agglomeration. In more recent work from the same authors, it was indicated that both compressive and flexural strength increased with the addition of CNF (2017).

In the study by Cengiz *et al.* (2017) it is reported that the flexural strength in mortars increased 2.7 times with the addition of algal CNF, due to the high aspect ratio of CNF, which improves the bonding interface between the CNF and cement paste. However, the use of commercial CNF has a negative effect on the bending stress due to its low aspect ratio and insolubility.

Hisseine *et al.* (2018a) indicated positive effects of CNF on the mechanical performance of cementitious pastes, due to greater homogeneity and stability. As for self-compacting concrete, the authors demonstrated that bending capacity and tensile strength at rupture increased by up to 21 and 26%, respectively. Hisseine *et al.* (2018b) also reported the same trend in self-compacting concrete, where all measured mechanical properties were improved, only in flexural 22%, as a result of nanoreinforcement and internal curing.



(a)

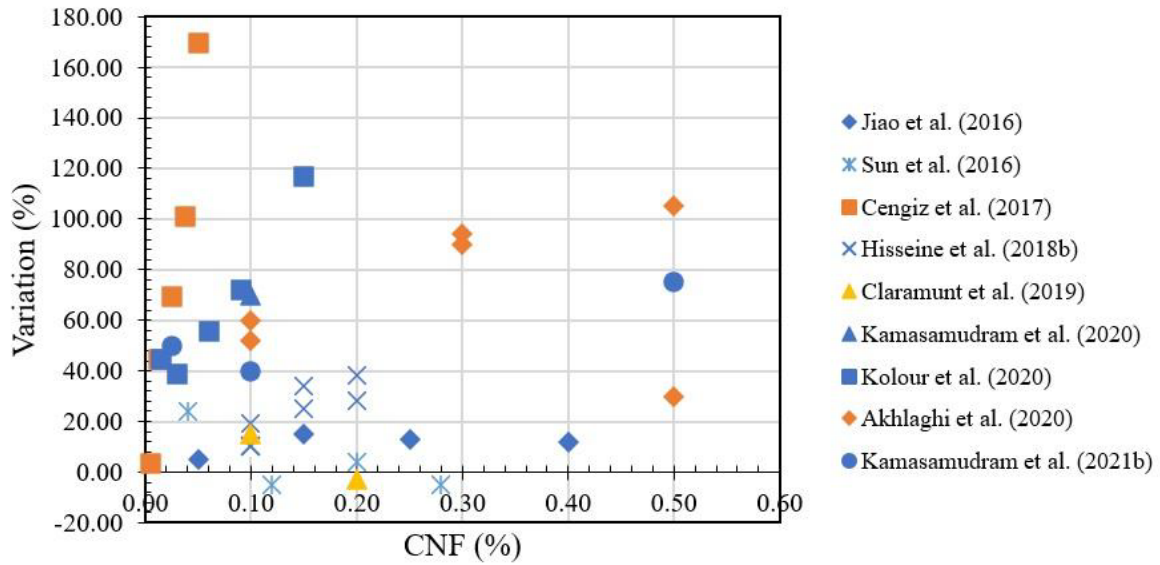


(b)

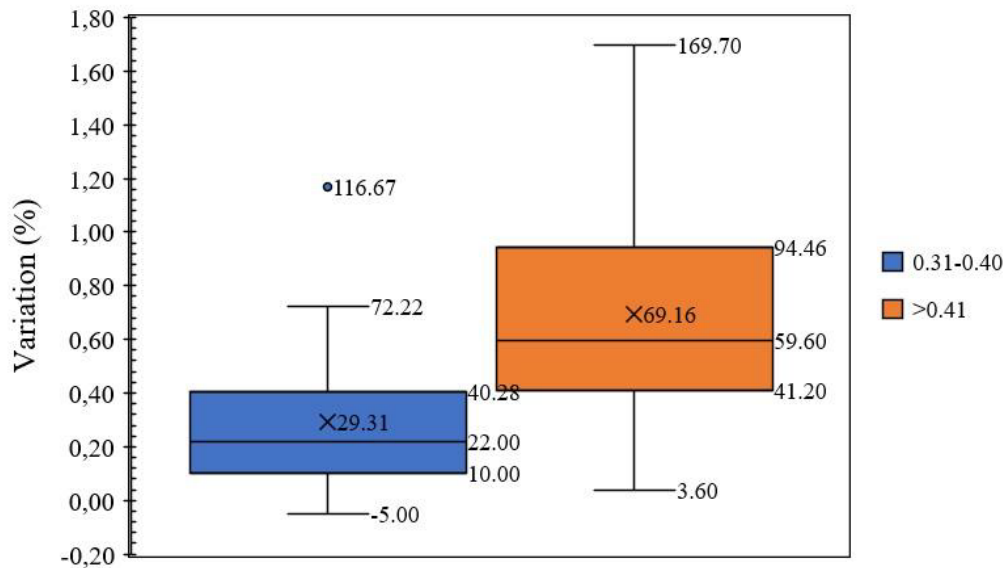
Figure 4. a) Variation of compressive strength at 28 days, and b) data dispersion considering the w/c ratio.

The flexural strength of cement pastes can increase from 20% up to 111% with CNF addition, this last value for 0.1% of CNF, both for DCNF and LCNF (Kamasamudram *et al.*, 2021a).

Figure 5a shows a detailed breakdown of the results reported in the literature for flexural strength at 28 days, showing that most are positive and with higher percentages compared to compressive strength. Figure 5b presents that the results reported for a w/c ratio from 0.31 to 0.40, are less scattered, with an average of 29.3% and a single atypical data (116.67%). For a w/c greater than 0.41 there is an average of 69.16%, but a greater data dispersion. The dispersion for an w/c ratio of 0.26 to 0.30 is not presented because there is only one study within this range (Claramunt *et al.*, 2019).



(a)



(b)

Figure 5. a) Flexural strength variation at 28 days, and b) data dispersion considering the w/c ratio.

Finally, Figure 6 summarizes all the results reported in the literature for both compressive strength (green) and flexural strength (red) of concretes and mortars, showing the positive effects of CNF addition, mainly for flexural strength.

c) Fracture mechanics: Hisseine *et al.* (2019) indicate that the maximum flexural capacity occurs at a low CNF content (0.05-0.10%), but the energy absorption capacity increases at higher CNF contents, up to 74%. Similarly, Hisseine *et al.* (2018b) point out that CNF improves energy absorption (96%) which is reflected in an increase in maximum displacement, up to 43%, a behavior that is required for both impact- and blast-resistant structures. Significant increases in fracture energy, up 60% in the study by Kolour *et al.* (2020), suggest that CNFs are an effective hardening mechanism, acting as bridges that increase the energy required for crack propagation.

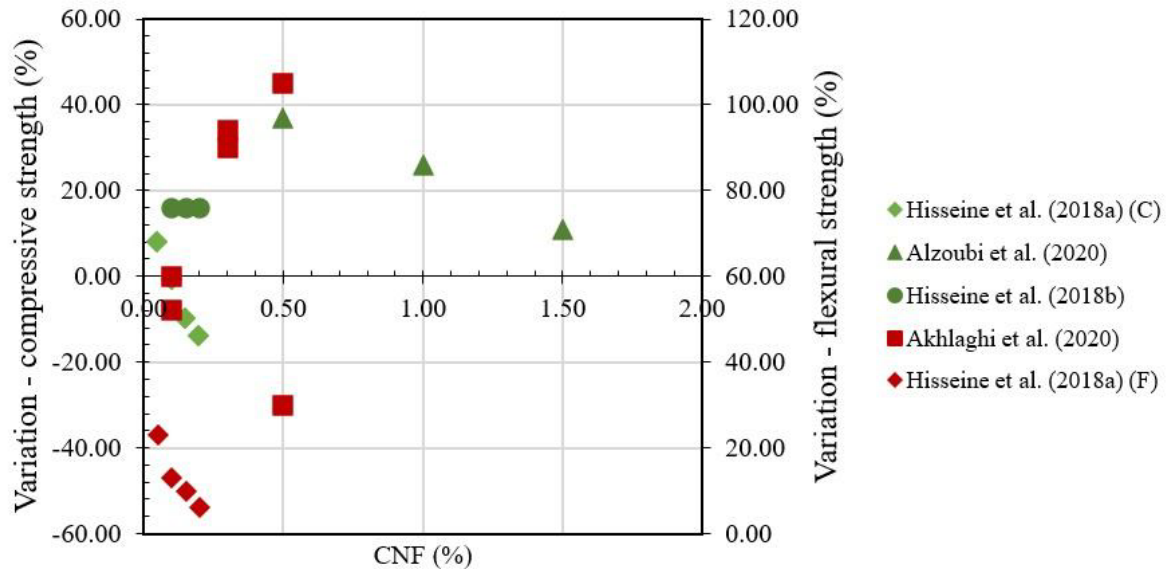


Figure 6. Compressive and flexural strength of concrete and mortar.

Hisseine *et al.* (2018b) also report the same trend in self-compacting concrete, where all measured mechanical properties were improved. Improvements of up to 16% in compression, 34% in splitting stress, 22% in bending, and 96% in energy absorption were obtained. These improvements were attributed to two effects imparted by CNF: nano-strength and internal curing.

The content of 1% CNF with 8% cellulosic pulp contributes to the formation of stress transfer bridges in nano- and micro-cracks, improving the mechanical performance of the composites before and after accelerated aging tests: modulus of rupture (MOR), fracture toughness (KIC) and fracture energy (FE), results attributed to the adhesion between CNF and the cement matrix (Correia *et al.*, 2018).

Composites reinforced with 2% cellulose micro/nanofibers showed higher limit of proportionality (LOP), MOR, and toughness than control composites after 28 days of curing (Fonseca *et al.*, 2019). Ez-zaki *et al.* (2021) indicate that CNFs have the ability to swell, creating internal water deposits and can behave as stress concentrators, leading to the initiation of microcracks.

The addition of low CNF and NCC contents (between 0.1 and 0.2% by weight), in calcium aluminate cement (CAC) systems, led to an overall increase in MOR values in unaged samples, in contrast to Portland cement systems (Claramunt *et al.*, 2019).

In the literature, it is observed that mechanical properties have been extensively investigated, which makes it possible to identify trends and better understand the effect of CNFs on the mechanical behavior of cementitious materials. However, most studies have only reported compressive and flexural strength results for pastes. The mechanical behavior in other specific and long-term applications still needs to be further investigated.

3.3.5 Other properties

This topic presents other properties that have been investigated in some published works, highlighting that the durability of cementitious materials with CNF is the least researched aspect, but with growing interest in recent years.

a) Sulfate ion penetration: CNF reduce the penetration of sulfate ions into a cementitious system. It was observed that the addition of CNF (0.3-0.4%) to GU Type Portland Cement provided the same or greater resistance to sulfate attack than a specially formulated HS Type Portland Cement (Goncalves *et al.*, 2019).

b) Chloride ion penetration: The use of CNF prevents the penetration of chloride ions. This is attributed to the amount of carboxyl groups, which leads to the restriction of chloride entrance, besides improving workability (Goncalves *et al.*, 2020).

c) Modulus of elasticity: Kamasamudram *et al.* (2021b) observed that 0.025% and 0.5% CNF increased the modulus of elasticity of cement paste by about 200% and 250%. Hisseine *et al.* (2019) reported an increase of 18% and Fonseca *et al.* (2019) indicate that in general, composites with CNF show better mechanical performance and that the dynamic modulus of elasticity increases with time even when exposed to weathering. CNFs with calcium aluminate cement (CAC) show an increase in modulus of elasticity compared to mixtures with Portland cement (Claramunt *et al.*, 2019).

d) Porosity: Mejdoub *et al.* (2016) indicated that the porosity in cement pastes was reduced with the addition of CNF, the best result being with 0.3% of CNF. On the other hand, Goncalves *et al.* (2019) point out that CNF refines the pore size, showing an increase in the total volume of micro and nanopores; however, there was a reduction in porosity for sizes larger than 10 nm.

e) Coefficient of thermal expansion and thermal conductivity: The use of CNF increased both the coefficient of thermal expansion and thermal conductivity of cementitious pastes, mainly due to the potential of CNF to reduce porosity and improve the microstructure of the cementitious matrix (Mejdoub *et al.*, 2016). Alzoubi *et al.* (2020) also reported an increase in the thermal conductivity of PCM/CNF composites.

f) Exudation: CNF act as a water retention agent and water reservoir to prevent segregation and exudation (Ez-zaki *et al.*, 2021). Goncalves *et al.* (2021) showed that the addition of CNF significantly reduces the volume of the exudation water. CNF makes it difficult for cement grains to settle and obstructs the upward migration of free water. However, in the presence of superplasticizers, CNF are less effective in reducing exudation. The authors consider that the effect of CNF on exudation reduces both the plastic shrinkage and the autogenous shrinkage during the initial stages of hydration.

Finally, the lack of studies evaluating the environmental impacts of cementitious composites with CNF was noted; and, in this sense, Life Cycle Analysis (LCA) studies could be carried out in a complementary way.

4. CONCLUSIONS

Although the use of cellulose nanofibers (CNF) in the construction industry is a recent field, not yet widely explored, studies of CNF as reinforcement in cementitious matrices show that its use can improve their performance.

Recent studies on CNF application in cementitious matrices have focused on cement pastes, accounting for 62% of the research analyzed (for pastes exclusively).

Small percentages of CNF are added to cement-based composites, reinforcement contents usually range between 0.02% and 3%. However, there are challenges in using this material as to its dispersion in the cement matrix, thus pre-treatments on the nanofibers are of great importance because they increase their potential use. The most commonly used treatments/dispersions are sonication, homogenization, TEMPO-mediated oxidation, and alkaline pretreatment of the fibers. As for the CNF dimensions used most in the research, the most commonly used CNFs were reported to range from 10-500 nm and 2-20 nm as diameter and width, respectively.

The addition of CNF usually increases the degree of hydration of cement, improving rheological properties, such as viscosity and elastic limit, as well as favoring the water retention capacity of the mixture with indications for reducing segregation and exudation, and improving the shrinkage performance of cementitious composites.

Most studies indicate a tendency to improve mechanical properties such as compressive strength, flexural strength, fracture mechanics, and modulus of elasticity. With an emphasis on the flexural strength property, with even more positive improvements when compared to the compressive strength.

It is important to emphasize that the good dispersion of the fibers, homogeneity of the matrix and the content of CNF used have a great influence on these results; however, a greater incorporation tends to be associated with the formation of fiber agglomerates, causing reductions or being detrimental to the results.

5. REFERENCES

- Abdellaoui, H., Bouhfid, R. (2020), *Review of nanocellulose and nanohydrogel matrices for the development of sustainable future materials*. In Sustainable Nanocellulose and Nanohydrogels from Natural Sources, 155-176. <https://doi.org/10.1016/B978-0-12-816789-2.00007-9>
- Abdul Khalil, H. P. S., et al. (2012), *Green composites from sustainable cellulose nanofibrils: A review*. Carbohydrate Polymers. 87(2):963–979. <https://doi.org/10.1016/j.carbpol.2011.08.078>
- Akhlaghi, M. A., et al. (2020), *Application of bacterial nanocellulose fibers as reinforcement in cement composites*. Construction and Building Materials. 241:118061. <https://doi.org/10.1016/j.conbuildmat.2020.118061>
- Alzoubi, H. H., et al. (2020), *Performance of cementitious composites with nano PCMs and cellulose nanofibers*. Construction and Building Materials. 236:117483. <https://doi.org/10.1016/j.conbuildmat.2019.117483>
- Bakkari, M., et al. (2019), *Preparation of cellulose nanofibers by TEMPO-oxidation of bleached chemi-thermomechanical pulp for cement applications*. Carbohydrate Polymers. 203:238–245. <https://doi.org/10.1016/j.carbpol.2018.09.036>
- Barnat-Hunek, D., et al. (2019), *Effect of cellulose nanofibrils and nanocrystals on physical properties of concrete*. Construction and Building Materials. 223:1–11. <https://doi.org/10.1016/j.conbuildmat.2019.06.145>
- Barriá, J. C., et al. (2021), *Effect of bacterial nanocellulose on the fresh and hardened states of oil well cement*. Journal of Petroleum Science and Engineering. 199. <https://doi.org/10.1016/j.petrol.2020.108259>
- Cao, Z., et al. (2020), *The sponge effect and carbon emission mitigation potentials of the global cement cycle*. Nature communications. 11(1): 1-9. <https://doi.org/10.1038/s41467-020-17583-w>
- Cengiz, A., et al (2017), *Flexural stress enhancement of concrete by incorporation of algal cellulose nanofibers*. Construction and Building Materials. 149:289–295. <https://doi.org/10.1016/j.conbuildmat.2017.05.104>
- Claramunt, J., et al. (2019), *Effect of nanocelluloses on the microstructure and mechanical performance of CAC cementitious matrices*. Cement and Concrete Research. 119:64–76, 2019. Disponível em: <https://doi.org/10.1016/j.cemconres.2019.02.006>
- Correia, V. C., et al., (2018), *Nanofibrillated cellulose and cellulosic pulp for reinforcement of the extruded cement based materials*. Construction and Building Materials. 160:376–384. <https://doi.org/10.1016/j.conbuildmat.2017.11.066>
- Dhali, K., et al. (2021), *A review of nanocellulose as a new material towards environmental sustainability*. Science of the Total Environment. 775:145871. <https://doi.org/10.1016/j.scitotenv.2021.145871>
- Dongre, M., Suryawanshi, V. B. (2021), *Analysis of cellulose based nanocomposites & potential applications*. Materials Today: Proceedings. 45:3476–3482. <https://doi.org/10.1016/j.matpr.2020.12.943>

- UN Environment, *et al.*, (2018), *Eco-efficient cements: Potential economically viable solutions for a low-CO₂ cement-based materials industry*. Cement and Concrete Research. 114:2-26. <https://doi.org/10.1016/j.cemconres.2018.03.015>
- Ez-zaki, H., *et al.* (2021), *Correction to: Influence of cellulose nanofibrils on the rheology, microstructure and strength of alkali activated ground granulated blast-furnace slag: a comparison with ordinary Portland cement*. Materials and Structures/Materiaux et Constructions. 54(2). <https://doi.org/10.1617/s11527-021-01665-2>
- Fonseca, C. S., *et al.* (2019), *Jute fibers and micro/nanofibrils as reinforcement in extruded fiber-cement composites*. Construction and Building Materials. 211:517–527. <https://doi.org/10.1016/j.conbuildmat.2019.03.236>
- Goncalves, J., *et al.* (2019), *Cellulose nanofibres (CNF) for sulphate resistance in cement based systems*. Cement and Concrete Composites. 99:100–111. <https://doi.org/10.1016/j.cemconcomp.2019.03.005>
- Goncalves, J., *et al.* (2021), *Turbidity-based measurement of bleeding in fresh cement paste as affected by cellulose nanofibres*. Cement and Concrete Composites. 123:104197. <https://doi.org/10.1016/j.cemconcomp.2021.104197>
- Goncalves, J., *et al.* (2020), *Cellulose nanofibres mitigate chloride ion ingress in cement-based systems*. Cement and Concrete Composites. 114. <https://doi.org/10.1016/j.cemconcomp.2020.103780>
- Guo, A., *et al.* (2020), *A Review on the Application of Nanocellulose in Cementitious Materials*. Nanomaterials. 10(12):2476. <https://doi.org/10.3390/nano10122476>
- Hassan, S. H., *et al.* (2021), *TEMPO-oxidized nanocellulose films derived from coconut residues: Physicochemical, mechanical and electrical properties*. International Journal of Biological Macromolecules. 180:392–402. <https://doi.org/10.1016/j.ijbiomac.2021.03.066>
- Hisseine, O. A., *et al.* (2018a) *Feasibility of using cellulose filaments as a viscosity modifying agent in self-consolidating concrete*. Cement and Concrete Composites, 94:327–340. <https://doi.org/10.1016/j.cemconcomp.2018.09.009>
- Hisseine, O. A., *et al.* (2018b), *Influence of cellulose filaments on cement paste and concrete*. Journal of materials in civil engineering. 30(6):04018109. [https://doi.org/10.1061/\(ASCE\)MT.1943-5533.0002287](https://doi.org/10.1061/(ASCE)MT.1943-5533.0002287)
- Hisseine, O. A., *et al.* (2019), *Nanocellulose for improved concrete performance: A macro-to-micro investigation for disclosing the effects of cellulose filaments on strength of cement systems*. Construction and Building Materials. 206:84–96. <https://doi.org/10.1016/j.conbuildmat.2019.02.042>
- Hoyos, C. G., *et al.* (2019), *Cellulose nanofibrils extracted from fique fibers as bio-based cement additive*. Journal of Cleaner Production. 235:1540–1548. <https://doi.org/10.1016/j.jclepro.2019.06.292>
- Jiao, L., *et al.* (2016), *Natural Cellulose Nanofibers As Sustainable Enhancers in Construction Cement*. PLoS ONE. 11(12):e0168422. <https://doi.org/10.1371/journal.pone.0168422>
- Kamasamudram, K. S., *et al.* (2021), *Cellulose Nanocomposites for Performance Enhancement of Ordinary Portland Cement-Based Materials*. Transportation Research Record. <https://doi.org/10.1177/0361198120958421>
- Kamasamudram, K. S., *et al.* (2021a), *Effects of ligno- and delignified- cellulose nanofibrils on the performance of cement-based materials*. Journal of Materials Research and Technology. 13: 321–335. <https://doi.org/10.1016/j.jmrt.2021.04.090>
- Kamasamudram, K. S., *et al.* (2021b), *Cellulose nanofibrils with and without nanosilica for the performance enhancement of Portland cement systems*. Construction and Building Materials. 285:121547. <https://doi.org/10.1016/j.conbuildmat.2020.121547>

- Klemm, D., *et al.* (2011), *Nanocelluloses: a new family of nature-based materials*. *Angewandte Chemie International Edition*. 50(24):5438-5466. <https://doi.org/10.1002/anie.201001273>
- Kolour, H., *et al.* (2020), *Hydration and early age properties of cement pastes modified with cellulose nanofibrils*. *Transportation Research Record*. 0361198120945993. <https://doi.org/10.1177/0361198120945993>
- Lootens, D., Bentz, D. P. (2016), *On the relation of setting and early-age strength development to porosity and hydration in cement-based materials*. *Cement and Concrete Composites*. 68:9-14. <https://doi.org/10.1016/j.cemconcomp.2016.02.010>
- Mejdoub, R., *et al.* (2016), *Nanofibrillated cellulose as nanoreinforcement in Portland cement: Thermal, mechanical and microstructural properties*. *Journal of Composite Materials*. 51(17):2491-2503. <https://doi.org/10.1177/0021998316672090>
- Nassiri, S., *et al.* (2021), *Comparison of unique effects of two contrasting types of cellulose nanomaterials on setting time, rheology, and compressive strength of cement paste*. *Cement and Concrete Composites*. 123:104201. <https://doi.org/10.1016/j.cemconcomp.2021.104201>
- Nishimura, T., *et al.* (2019), *Effects of powdery cellulose nanofiber addition on the properties of glass ionomer cement*. *Materials*. 12(19):3077. <https://doi.org/10.3390/ma12193077>
- Ogura, I., *et al.* (2020), *Measurements of cellulose nanofiber emissions and potential exposures at a production facility*. *NanoImpact*. 20:100273. <https://doi.org/10.1016/j.impact.2020.100273>
- Panesar, D., *et al.* (2017), *The effect of sodium hydroxide surface treatment on the tensile strength and elastic modulus of cellulose nanofiber*. *Sustainable and Nonconventional Construction Materials using Inorganic Bonded Fiber Composites*. 17–26. <https://doi.org/10.1016/B978-0-08-102001-2.00002-4>
- Santos, R. F., *et al.* (2021), *Nanofibrillated cellulose and its applications in cement-based composites: A review*. *Construction and Building Materials*. 288:123122. <https://doi.org/10.1016/j.conbuildmat.2021.123122>
- Sedan, D., *et al.* (2008), *Mechanical properties of hemp fibre reinforced cement: Influence of the fibre/matrix interaction*. *Journal of the European Ceramic Society*. 28(1):183-192. <https://doi.org/10.1016/j.jeurceramsoc.2007.05.019>
- Sun, X., *et al.* (2017), *Rheology, curing temperature and mechanical performance of oil well cement: Combined effect of cellulose nanofibers and graphene nano-platelets*. *Materials & Design*. 114:92-101. <https://doi.org/10.1016/j.matdes.2016.10.050>
- Sun, X., *et al.* (2016), *Cellulose nanofibers as a modifier for rheology, curing and mechanical performance of oil well cement*. *Scientific reports*. 6(1):1-9. <https://doi.org/10.1038/srep31654>
- Tang, Z., *et al.* (2019), *Influence of cellulose nanoparticles on rheological behavior of oil well cement-water slurries*. *Materials*. 12(2):291. <https://doi.org/10.3390/ma12020291>
- Zhang, S., *et al.* (2021), *High-flexural-strength of geopolymer composites with self-assembled nanofiber networks*. *Ceramics International*. 47(22):31389–31398. <https://doi.org/10.1016/j.ceramint.2021.08.014>
- Zhang, Z., Scherer, G. W. (2020), *Measuring chemical shrinkage of ordinary Portland cement pastes with high water-to-cement ratios by adding cellulose nanofibrils*. *Cement and Concrete Composites*. 111:103625. <https://doi.org/10.1016/j.cemconcomp.2020.103625>

Analysis of concrete characteristics with the replacement of natural fine aggregate by industrial solid waste

M. L. A. S. Costa^{1*} , D. C. P. Valões² , C. F. G. Nascimento³ ,
E. G. S. Lima¹ , G. R. Silva¹ , T. T. S. Silva¹ , T. S. Santos¹ 

*Contact author: luizmarcus3@gmail.com

DOI: <https://doi.org/10.21041/ra.v12i3.573>

Reception: 17/12/2021 | Acceptance: 08/07/2022 | Publication: 01/09/2022

ABSTRACT

The objective of this study comprises the use of industrial solid waste in terms of improving the mechanical properties of cement composites. Therefore, the incorporation of granitic “crushed” powder and marble powder in the manufacture of cement-based composites was evaluated, partially replacing the natural fine aggregate at levels of 50% and 100%. For that, tests were carried out to characterize the aggregates, in addition to the evaluation of the axial compressive strength of the specimens. The results showed that the mixtures containing 50% of recycled aggregate give the material a compressive strength of 29.09 MPa, that is, 4% higher when compared to the reference mixtures, making the results satisfactory, demonstrating the viability of recycled aggregates on concrete pieces.

Keywords: concrete; solid waste; mechanical properties; sustainability.

Cite as: Costa, M. L. A. S., Valões, D. C. P., Nascimento, C. F. G., Silva, G. R., Lima, E. G. S., Silva, T. T. S., Santos, T. S., (2022), “*Analysis of the characteristics of concrete with the replacement of natural fine aggregate by industrial solid waste*”, Revista ALCONPAT, 12 (3), pp. 328 – 346, DOI: <https://doi.org/10.21041/ra.v12i3.573>

¹ Laboratory of Civil Construction Materials, Faculty of Integration of the Sertao, Serra Talhada/PE, Brazil.

² Advanced Laboratory of Civil Construction Materials, University of Pernambuco, Recife/PE, Brazil.

³ Laboratory of Civil Construction Materials, Catholic University of Pernambuco, Recife/PE, Brazil.

Contribution of each author

In this work, the authors M. L. A. S. Costa and D. C. P. Valões contributed to the original idea of the study, development and results analysis, supervision and guidelines for the paper. The authors E. G. S. Lima, G. R. Silva and T. T. Silva contributed with 40%, 30% and 30% of the data collection, respectively. The authors C. F. G. Nascimento and T. S. Santos, were responsible for the research content improvement, discussions and conclusions.

Creative Commons License

This work is published under the terms of an International Creative Commons Attribution 4.0 International License ([CC BY 4.0](https://creativecommons.org/licenses/by/4.0/)).

Discussions and subsequent corrections to the publication

Any dispute, including the replies of the authors, will be published in the third issue of 2023 provided that the information is received before the closing of the second issue of 2023.

Análise das características do concreto com a substituição do agregado miúdo natural por resíduos sólidos industriais

RESUMO

O objetivo deste estudo compreende na utilização de resíduos sólidos industriais quanto à melhoria das propriedades mecânicas dos compósitos cimentícios. Para tanto, foi avaliado a incorporação do pó de “brita” granítica e pó de mármore na confecção de compósitos à base de cimento, substituindo parcialmente o agregado miúdo natural em teores de 50% e 100%. Para isso, foram realizados ensaios de caracterização dos agregados, além da avaliação da resistência à compressão axial dos corpos-de-prova. Os resultados evidenciaram que as misturas contendo 50% de agregado reciclado confere ao material uma resistência à compressão de 29,09 MPa, ou seja, 4% superior quando comparado com as misturas de referência, tornando os resultados satisfatórios, demonstrando a viabilidade dos agregados reciclados em peças de concreto.

Palavras-chave: concreto; resíduos sólidos; propriedades mecânicas; sustentabilidade.

Análisis de las características del hormigón con la sustitución del árido fino natural por residuos sólidos industriales

RESUMEN

El objetivo de este estudio incluye el uso de residuos industriales sólidos para mejorar las propiedades mecánicas de los composites cementicios. Para ello, se evaluó la incorporación de polvo de grava de granito y polvo de mármol en la fabricación de composites cementosos, sustituyendo parcialmente el árido fino natural en niveles del 50% y del 100%. Para ello, se realizaron ensayos de caracterización de los áridos, además de la evaluación de la resistencia a compresión axial de las probetas. Los resultados mostraron que las mezclas que contenían 50% de agregado reciclado dieron al material una resistencia a la compresión de 29,09 MPa, es decir, un 4% mayor en comparación con las mezclas de referencia, por lo que los resultados fueron satisfactorios, demostrando la viabilidad de los agregados reciclados en las piezas de hormigón.

Palabras clave: hormigón; residuos sólidos; propiedades mecánicas; sostenibilidad.

Legal Information

ALCONPAT Magazine is a quarterly publication by the Asociación Latinoamericana de Control de Calidad, Patología y Recuperación de la Construcción, Internacional, AC, Km. 6 antigua carretera a Progreso, Mérida, Yucatan, 97310, Tel.5219997385893, alconpat.int@gmail.com, Web site: www.alconpat.org

Responsible editor: Pedro Castro Borges, Ph.D. Reservation of rights for exclusive use No.04-2013-011717330300-203, and ISSN 2007-6835, both granted by the Instituto Nacional de Derecho de Autor. Responsible for the last update of this issue, Informatics Unit ALCONPAT, Elizabeth Sabido Maldonado, Km. 6, old road to Progreso, Mérida, Yucatan, CP 97310.

The views of the authors do not necessarily reflect the position of the editor.

The total or partial reproduction of the contents and images of the publication is carried out in accordance with the COPE code and the CC BY 4.0 license of the Revista ALCONPAT.

1. INTRODUCTION

Cementitious composites are the most used and widespread materials in the world due to their physical and mechanical properties, which includes questions about durability. Factors such as these stimulate interest in the discovery of new technologies and new compounds as proposals for the improvement of some properties (Mechtcherine et al., 2020; Nguyen; Castel, 2020).

The durability of concrete is an essential issue, as it allows understanding the performance of the material during the entire life of a structure (Kashani et al., 2017). In addition, it can be affected by the action of external aggressive agents, such as chloride ions and (CO₂) – carbon dioxide (Nascimento et al., 2021).

According to Azevedo et al., (2020) civil construction, despite having great importance in the economy, is the largest consumer in the world of natural raw materials among industrial sectors. This consumption is estimated at 40% to 75% of the raw material produced on the planet. Oliveira et al., (2020), emphasize that the impact of the industry on the environment involves, from the exploitation of raw material, to its use, which can generate solid waste.

As a way of reducing the negative impact on the environment generated by this disposal and the use of natural raw material in the manufacture of cement composites, granitic crushed stone and marble dust have been materials with great potential to be reinserted as aggregates in the cycle. production in the construction industry.

Despite the large generation of solid waste, civil construction is the industry that can most absorb this waste in the form of aggregates in cementitious composites. Both in Brazil and in other countries, most of the aggregates market is used in concrete and mortar. These residues can be recycled and reused in the construction itself, or they can also be sent to recycling plants and, later, be acquired as aggregates, in different granulometries, for a reduced cost (Brandão et al., 2021).

Despite research demonstrating the feasibility of using these residues, achieving quite significant results for physical and mechanical properties, national standards allow the use of recycled aggregates only in low-strength composites, that is, in non-structural cement-based materials (Mohajerani et al., 2020).

Generally, concrete residues are used in cement composites as a material, partially or totally replacing natural aggregates. After being discarded, the material goes through the beneficiation process, consisting of reducing the size of the material in granulometries similar to those of natural aggregates, which are used as substitute materials for the production of cement composites (Klepa et al., 2019).

The replacement percentage used in research is quite heterogeneous, ranging from 10% to 100%. The water/cement ratio used by the researchers varies according to the percentage of replacement adopted. The highest ratio (w/c) observed was 1.2 and the lowest was 0.35 (Andrade et al., 2018). According to Cipriano et al., (2021) and Silva et al., (2021) the increase in the ratio (w/c) is due to the need to maintain the workability of the material, and this fact may be attributed to the greater absorption of water from the recycled aggregates, which implies the migration of water to the aggregates, reducing the amount of water that contributes to the workability of the concrete. One way to give concrete with recycled aggregate greater workability, keeping the ratio (w/c) constant and equal to that of conventional concrete, is through the use of superplasticizing additives.

Varadharajan, Jaiswal and Verma (2020) analyzed the durability and strength of concrete with 5%, 10%, 15% of marble powder in place of fine aggregate, in addition to a water/cement (w/c) ratio of 0.43. The study revealed an improvement in compressive strength of approximately 35 MPa at 28 days, that is, 15% greater when compared to reference composites.

Zhen and Liu (2021) analyzed the behavior of cementitious composites using percentages of 10%, 20% and 30% of granitic crushed stone in partial replacement of the fine aggregate. The researchers observed that mixtures containing 30% crushed stone powder had an improvement in axial

compressive strength at 28 days of 20%, resulting in 50 MPa when compared to the reference composites.

Research carried out by Thapa and Waldmann (2021) showed the effectiveness of cement composites using 10%, 20% and 30% of granitic crushed stone. The authors noticed that the use of 30% of the recycled material made it possible to improve the axial compressive strength in the concrete mixtures, being observed at 90 days, 58.1 MPa.

Aliabdo, Elmoaty and Auda (2014) performed mechanical tests on concrete using 0%, 5%, 7.5%, 10% and 15% of marble powder in cement-based composites at different curing times. For a water/cement (w/c) ratio of 0.50, an increase in flexural tensile strength in the mixture containing marble powder of approximately 10% compared to the reference mixture was reported. For all curing times, maximum flexural tensile strength was reached at 7.5% and minimum at 15% replacement. The data obtained in this study did not corroborate those obtained by Rodrigues, Brito and Sardinha (2015), where they report a decrease in the results of axial compressive strength due to the increase in the percentage of marble dust residues. The authors reported a maximum loss of 31% at 28 days of healing.

Aiming at mitigating the environmental impacts resulting from the generation of waste, there is currently a great search for alternative materials that can be used as partial or total substitutes for natural aggregates. According to Meena et al., (2021), the amount of solid waste generated by the construction industries will increase from 12.7 billion tons to 27 billion tons by 2050. With this, it confirms that the generation and disorderly disposal of waste solids in civil construction need to be mitigated, reintroducing these wastes into the production cycle of the generating industry itself (Meena et al., 2021; Paiva et al., 2021).

In view of this problem, the objective of this work is to study the feasibility of using marble powder and granitic crushed stone, replacing the natural fine aggregate in the production of cement composites, aiming at the search and definition of an alternative for a correct disposition of these residues and the reduction of the use of the natural fine aggregate, aiming at mitigating the environmental impacts caused by the extraction process.

2. EXPERIMENTAL PROCEDURE

This topic aims to present the experimental schedule performed and the respective methodologies carried out to achieve the objectives of this work, being divided into 8 subtopics, considering from the initial characterization tests of the fine aggregates to the final tests of workability and resistance to axial compression. The tests were carried out in the Civil Engineering laboratories of the Faculty of Integration of the Sertao – FIS, located in the municipality of Serra Talhada – PE. The marble dust was collected in a company (Pedra Bonita Mármore e Granitos) and the others (granitic gravel dust and natural fine aggregate) were acquired through a local enterprise, and later, they were transported to the Engineering Laboratory Complex. Institution's Civil Service.

2.1 Materials

The cement used was type CP-II-F-32 RS (Sulphate Resistant). This type of binder was chosen due to its rapid strength gain and absence of additives. The content of mineral additions contained in other types of cement could contribute to the refining and filling of the pores inside the concrete, which makes it difficult for aggressive agents to enter and improves durability.

Marble powder and granitic gravel powder were used, where the fractions of the materials can be seen in (Figure 1 (a) and (b)). Natural fine aggregate (sand), of quartz origin, used in the region was used (Figure 1 (c)). The sand was acquired by a company taking into account its physical characteristics. The material was in a wet state and therefore it was necessary to correct its water content by natural drying.

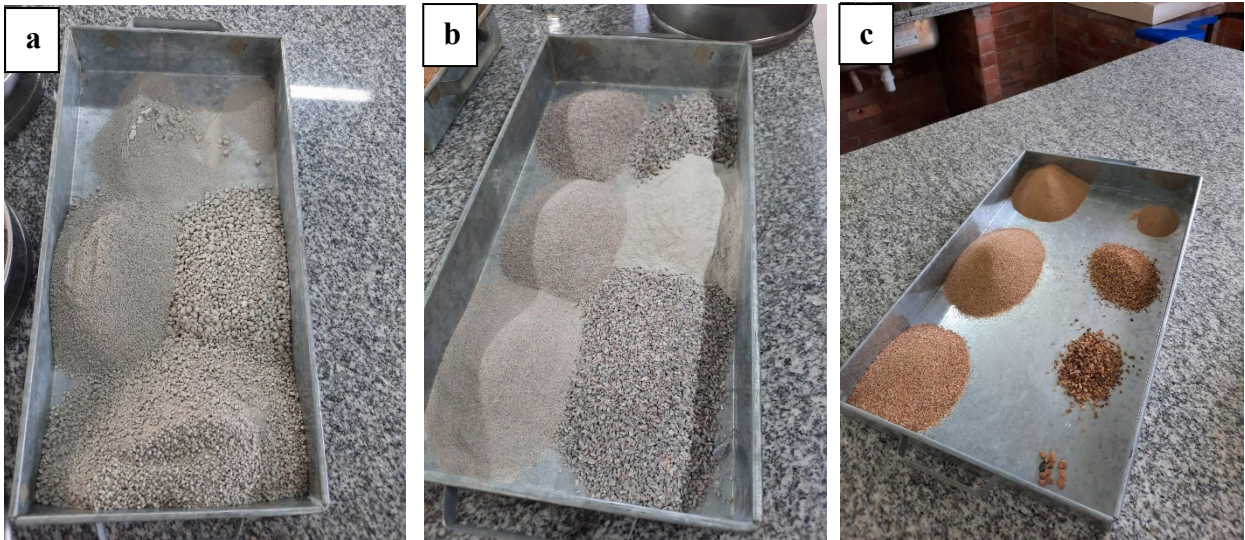


Figure 1. Fractions of marble dust particles (a) granitic crushed stone dust (b) natural fine aggregate (c).

The additive used was Techniflow 520, by MC Baushemie. This plasticizing additive was used in the matrix dosage of concrete with a mass density of 1.08 kg/L.

The coarse natural aggregates used had a maximum diameter of 19 mm and a fineness modulus of 6.48 mm. The granulometric curve of the material was not exposed in this research, but the type of aggregate used was classified as gravel 1.

2.2 Methods

2.2.1 Correction of fine aggregate moisture (sand)

To ensure the moisture content, 600 g of material were placed in an oven for about 24 hours at a temperature of $100^{\circ}\text{C} \pm 2^{\circ}\text{C}$ and, after this procedure, 300 g were used for the granulometric characterization test taking into account the granulometry of the fine aggregate according to the NBR NM 248 standard (ABNT, 2003), using the set of sieves in a normal series and the sieve shaker at a frequency of 8 hertz, for 2 minutes. The sieves used were #6.3mm, #4.8mm, #2.4mm, #1.2mm, #0.60mm, #0.30mm and #0.15mm. In view of the mass retained in each sieve, the Maximum Characteristic Dimension - (DMC) was obtained, which corresponds to the nominal opening, in mm (millimeters), of the sieve as to the normal or intermediate series in which the aggregate has an accumulated retained percentage equal to or less than 5% by mass – of the fine natural aggregates. In addition, the fineness modulus, which according to NBR NM 248 (ABNT, 2003) is the “sum of the retained percentages accumulated in the mass of an aggregate, in the normal series sieves, divided by 100” – of the fine aggregates were obtained with the use of (Equation 1).

$$\omega = \frac{\Sigma\% \text{cumulative retained}}{100} \quad (1)$$

where:

ω = fineness modulus of the fine aggregate;

$\Sigma\% \text{ cumulative retained}$ = sum of retained percentages accumulated in mass of an aggregate, in the normal series sieves.

2.2.2 Characterization of the natural fine aggregate

For crystallographic analysis, the fine aggregate was dried to mass consistency in an oven at a temperature of 105 °C and in the appropriate minimum granulometry passing through #200/0.075 mm. The X-ray diffraction technique used for the characterization of the aggregates was performed using a D8 Advance diffuser, Bruker, which contains a $K\alpha$ tube of copper radiation with a wavelength (λ) of 1,541 Å, a current of 10 mA and 30 kV voltage. The tests were performed with the scanning range (STEP) (2θ) ranging from 10° to 60°, time of 1 second and increment of 1° (degree), speed (Scan-Speed) angular step of 0.02°/second and divergent slit. of 1st degree. The phases present in the samples were later identified with the computer program X'Pert HighScore, through the PDF system (Powder Diffraction).

2.2.3 Specific mass

Due to the lack of the type of flask required to perform the test according to NBR NM 52 (ABNT, 2009), as an alternative means to analyze the specific masses of fine aggregates, the Chapman flask was used, according to NBR 9776 (ABNT, 1987), with the specific mass: “the ratio between the mass of the oven-dried aggregate (100 °C to 110 °C) until mass constancy and the equal volume of the solid, including impermeable pores”. The materials were submitted to the test after 24 hours in the oven at 110 °C. After reading the results, the formula (Equation 2) that the standard governs was applied to obtain the specific masses.

$$y = \frac{500}{L - 200} \quad (2)$$

where:

y = density of the fine aggregate in g/cm³;

L = bottle reading (volume occupied by the water-fine aggregate set).

2.2.4 Unit mass in loose state

The unit mass tests in the loose state of the fine aggregates were carried out according to the parameters established by NBR 7251 (ABNT, 1982). According to NBR 7251 (ABNT, 1982): “the unit mass of loose aggregate is the average of the individual results obtained in at least three determinations, dividing the aggregate mass by the volume of the container used”. Therefore, the test was performed 3 times for each type of fine aggregate. The test consisted of weighing the dry container first, then filling it up to its top with fine aggregate and smoothing the surface with a rod and weighing it, then the necessary calculations were performed using (Equation 3).

$$\mu = \frac{M_{r+a} - M_r}{V_r} \quad (3)$$

where:

μ = unit mass of the aggregate in the loose state in kg/dm³;

M_{r+a} = mass of container plus mass of sample in kg;

M_r = mass of container in kg;

V_r = Volume of container in dm³.

2.2.5 Dosage of mixtures of cementitious composites (concrete)

Taking into account that the municipality of Serra Talhada - PE falls into the environmental aggressiveness class (CAA) II of NBR 6118 (ABNT, 2014), the strength established for the concrete traces of the present work was 25MPa at 28 days of age. (curing), with a water/cement factor of 0.55. In addition, for the execution of the different types of mixtures, a mass volume ratio (TMV) of 1 : 2 : 3 ratio (mix/weight), M% = 55% (mortar content) and A% = 10.5% was established. (ratio of water-dry material. For the preparation of the different types of concrete mix, National cement CP II-F-32 RS, crushed stone 1 and the plasticizer additive MC-TechniFlow 520 from MC-Bauchemie (also used by local concrete plant) in 0.65% of the cement mass.

After the granulometry, specific mass and unit mass tests were carried out, the data obtained were used to establish the defined amount of each type of material to be incorporated into the concrete, to make different types of mix. Obtaining, for example, the amount of materials for the production of 1m³ of concrete from the reference trace, being: 352.36 kg of cement/binder; 740.66 kg of fine aggregate; 1133.89 kg of coarse aggregate; and 193.79 liters of water (w/c = 0.55). The same process was carried out with the other traces using the values obtained for the unit mass in the loose state and the specific mass.

To carry out the research, 3 different types of concrete mixtures were performed, as shown in (Table 1), where: mixture 1, being the conventional mix using 100% natural sand as fine aggregate; mixture 2, with the mix replacing 50% of the sand volume with marble powder (10%) and granitic crushed stone powder (40%); and mixture 3, being the line with the total replacement (100%) of the sand by solid industrial residues, marble dust (15%) and granitic gravel dust (85%).

The percentages of marble dust and granitic gravel dust used in the research were defined in order to understand the mechanical behavior of a cementitious compound (concrete) when using 100% industrial recycled aggregates. The main focus of the study was not to analyze the optimal percentage to be used in composites with different cementitious matrices, but the properties of these materials that are not defined by national regulations.

Table 1. Mixtures and amounts of specimens analyzed at different curing times.

MIXTURES	Total specimens that were produced to be ruptured by curing time			
	7 days	14 days	21 days	28 days
Mixture 1: reference trace, using completely (100%) natural sand as fine aggregate.	10 SP	10 SP	10 SP	10 SP
Mixture 2: partially replacing (50%) the natural sand with granitic crushed stone powder (40%) and marble powder (10%).	10 SP	10 SP	10 SP	10 SP
Mixture 3: completely replacing (100%) the natural sand with granitic crushed stone powder (85%) and marble powder (15%).	10 SP	10 SP	10 SP	10 SP
Total of 120 specimens				

2.2.6 Procedure for execution of concrete specimens

The production of specimens was developed according to the procedures and parameters established by NBR 5738 (ABNT, 2015). The cylindrical molds used had dimensions of (10 cm x 20 cm) of diameter and height respectively. All the (SP's) produced were used to carry out the analyzes through complementary tests which, in turn, were of paramount importance to understand the physical-mechanical behavior of the material studied. Before starting the separation of the percussive materials for the production of different types of concrete, it was necessary to use a type of liquid release agent in all the forms, where it was left to rest for 15 minutes, to facilitate the removal of the hydrated material. After that, it was necessary to carry out the moisture correction of the fine aggregate (sand), as it directly influences the quality and fluidity of the material under study. This correction implies a reduction in the amount of water used in the production process of the specimens. For this purpose, the matrix materials such as: cement, fine aggregate (sand), coarse aggregate (gravel) and solvent (water), were duly weighed and directed to the mixer according to the corresponding order: the coarse aggregate was taken to the mixer and, after that, approximately 2/3 of the water was used, where the mixing process took about 1 minute. Then, the binder (cement), the fine aggregate (sand) and 1/3 of the remaining water were added. All materials underwent a homogenization process for approximately 5 minutes and, after this process, the consistency test (Slump test) was performed, also known as truncated cone slump according to the procedures established by NBR NM 67 (ABNT, 1998).

After these procedures, the specimens were molded according to the parameters established by NBR 5738 (ABNT, 2015). Firstly, the concretes were introduced in two layers in the molds, each one being densified from the application of 15 blows evenly distributed with a metal rod, without affecting the base. In addition, the external face of the molds was lightly tapped in order to minimize the voids caused by densification. Finally, the last layer was molded with a certain amount of material, in order to exceed the volume of the mold, to facilitate flattening with a metal ruler, without adding material after consolidation. After completing the molding of the concrete, the specimens were taken to a room with an ambient temperature of $25\text{ }^{\circ}\text{C} \pm 2\text{ }^{\circ}\text{C}$, where they remained for 24 hours for the hydration process to be successfully completed and, after this period, were demolded, identified and subjected to wet curing in a container with the presence of water in a static state with relative humidity above 95% until the time of the tests.

2.2.7 Consistency test (slump test)

The consistency test (slump test) was performed for each trait, characterized as slump of the trunk of a cone according to the procedures established by NBR NM 67 (ABNT, 1998). The purpose of this test was to evaluate the workability of the concrete, with regard to the mobility of the binder against the cohesion of the constituent materials in its matrix. The slump test is composed of a metal plate with dimensions (50 cm x 50 cm) and thickness of 3 mm, a truncated cone with a maximum height of 300 mm, a metal rod with dimensions of 600 mm and a diameter equivalent to 16 mm

To carry out the procedures, first the plate and the trunk of the cone were moistened and placed in a flat region free from vibrations. After that, a sample of the concrete to be analyzed was collected and directed to the trunk of the cone in three layers. The material was compacted with the rod, exerting 25 blows evenly distributed over each layer. This procedure was repeated two more times until the top of the mold.

At the end of the procedure, it was necessary to even out the surface using the compaction rod, and to clean the base. After that, the mold was carefully removed vertically, where the standard informs that this time varies between 5 to 10 seconds. After removal, it is necessary to measure the slump of the material given by the difference in height between the top of the mold (inverted) and the axis of the demolded material.

2.2.8 Axial compressive strength test

The axial compressive strength test was performed according to the established parameters prescribed by NBR 7239 (ABNT, 2018) which comprises the determination of the mechanical behavior of the material. After molding the specimens and after 7, 14, 21 and 28 days of wet curing, the materials were submitted to analysis. All specimens were rectified and taken to a SOLOTEST model DL 200 hydraulic press with load application speed of 0.50 ± 0.15 MPa/second, maximum load of 1000 kN, which is related to 30% applied at end of charge. The equipment used was a hydraulic press with a capacity of 200 tons, which provides the results of the axial compressive strength (F_{ck}) in MegaPascals (MPa) and their respective rupture curves.

3. RESULTS

3.1 Particle size analysis of aggregates

From the granulometric analysis of the aggregates, it was verified that the fine natural aggregate (sand) presented a fineness modulus of 2.15 and a maximum diameter of 4.8 mm, being classified as an aggregate of medium granulometry. The recycled aggregates called crushed stone and marble powder showed, respectively, a fineness modulus of 2.73 and 3.88, both higher when compared to the fine natural aggregate. The maximum diameter of the particles of the recycled aggregate was 4.8 mm, which can be classified as a medium granulometry material. Each sieve used presented a retained fraction of aggregates, where they were weighed and served to project the granulometric curve. In the #6.3 mm sieve, no material was retained; #4.8 mm, 0.29 g; #2.4 mm, 3.03 g; #1.2 mm, 10.88 g; #0.60 mm, 32.26 g; #0.30 mm, 71.38 g; #0.15 mm, 97.32 g.

As for marble powder, the quantity of particles retained on each sieve was: #4.8 mm, 0.42 g; #2.4 mm, 22.35 g; #1.2 mm, 70.83 g; #0.60 mm, 95.05 g; #0.30 mm, 99.51 g; #0.15 mm, 99.96 g. Regarding the granitic crushed stone powder, the quantity of particles retained on each sieve was: #4.8 mm, 0.16 g; #2.4 mm, 15.77 g; #1.2 mm, 42.70 g; #0.60 mm, 58.78 g; #0.30 mm, 72.17 g; #0.15mm, 99.96 g. For both, the total amount tested was 300 g. Figure 2 shows the granulometric distribution curves of natural fine aggregate, marble dust and granitic crushed stone. It is possible to observe that the curves of the natural fine aggregate and of the granitic crushed stone behave in a similar way, both being able to be used within the limits established by the Brazilian standard NBR 7211 (ABNT, 2019), as also observed by Barros e Fucale (2016), who used recycled aggregates in the concrete production. However, the curve referring to marble dust does not fit within the limits established by the standard, presenting particles with dimensions of 1.18; 0.6 and 0.3 mm in excess.

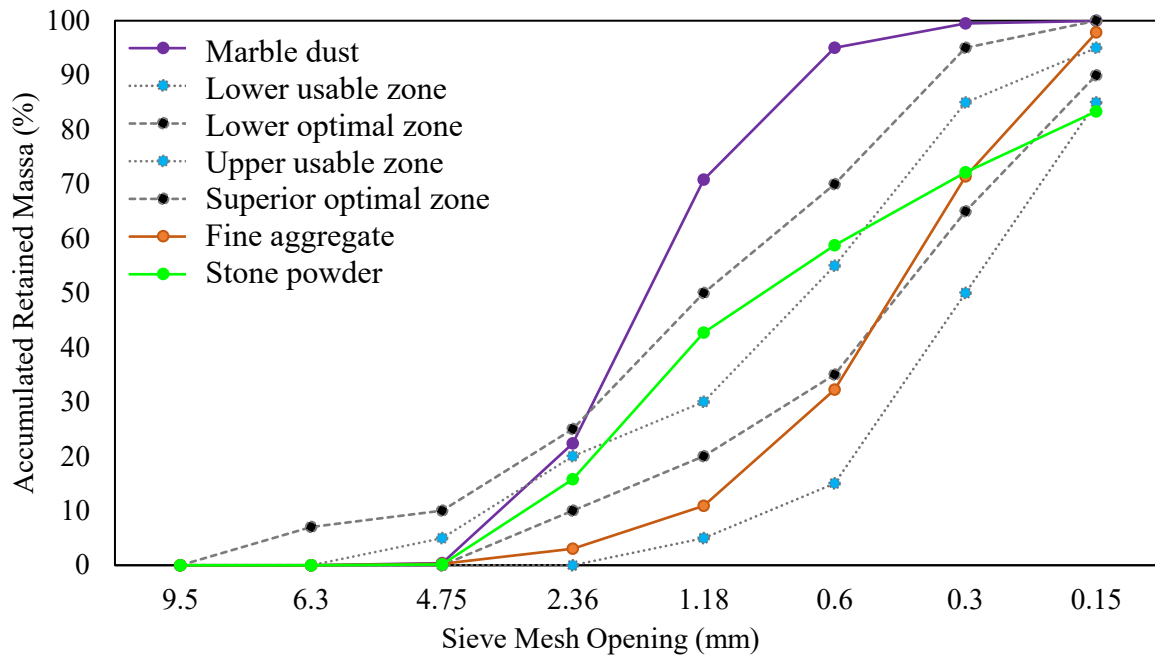


Figure 2. Size distribution of aggregates.

The powdery material content test was carried out. Natural sand presented a fine material content of 7%, while marble powder and granitic crushed stone powder presented a rate of 12.5% and 10.3%, respectively, showing an increase of more than 50% compared to the natural aggregate. However, despite the fact that recycled aggregates have a high content of powdery material, this result allows this increase to remain within the limit established by the standard for recycled aggregates of solid waste according to NBR 15116 (ABNT, 2004), not exceeding 20%.

According to Souza (2019), continuous granulometry aggregates, which do not present excess or deficiencies of particles of any dimension, produce the most workable and economical concrete mixtures, however, the other characteristics of the aggregates, such as the dimension maximum characteristic and the fineness modulus. In (Table 2), the results of the other characterization tests of the fine aggregates are presented.

Table 2. Fineness modulus, maximum characteristic dimension, specific mass and unitary mass in loose state of the fine aggregates used in the work.

Feature	natural sand	Granite crushed stone dust	marble dust
Fineness module:	2.15	2.73	3.88
Maximum characteristic dimension (DMC):	4.8	4.8	4.8
Specific mass (g/cm ³):	2.63	2.65	2.74
Unit mass in loose state (g/cm ³):	1.46	1.62	0.94
The aggregate fineness modulus limit values according to NBR 7211 (ABNT, 2009) are:			
NOTE 1: The fineness modulus of the optimal zone varies from 2.20 to 2.90.			
NOTE 2: The fineness modulus of the lower usable zone ranges from 1.55 to 2.20.			
NOTE 3: The fineness modulus of the upper usable zone ranges from 2.90 to 3.50.			

According to the data presented in (Table 2), comparing the values of fineness modulus of the aggregates with the limits established by NBR 7211 (ABNT, 2009), both natural sand and granitic gravel powder present fineness modulus within the usable zones, mainly the granitic stone dust that fits in the optimal zone. However, marble dust does not fall within the usable zone.

The granulometric curves of the recycled aggregates were evaluated separately in order to understand how their particles behave, which helps for a better distribution of the percentages used. Even used together, an individual analysis is necessary as proposed in the research, because the characteristics of these materials are different. A similar feature is the specific area, as both have high levels of fine materials which, in turn, require a higher percentage of water or a higher water/cement ratio (w/c).

According to Souza (2019), the higher the fineness modulus, the larger the dimensions of the aggregate (which was the case with marble powder), in addition, aggregates with similar fineness modulus tend to produce cementitious composites with similar characteristics, but this depends of other factors such as the maximum size of each aggregate and the presence of powdery materials. Also according to the same author, the greater the maximum characteristic dimension, the smaller the surface area to be covered by the cement paste, which can influence the reduction of costs in the manufacture of concrete, but this depends on other factors, such as the presence of powdery materials.

3.2 Analysis of consistency (*slump test*)

All mixtures were evaluated according to their physical characteristics, which cover the behavior of cementitious materials in terms of workability. In (Figure 3), the mixtures were analyzed separately and the results of the slump of the “trunk cone” were obtained in cm. It can be seen that the mixtures containing 50% of industrial solid waste, have similar behavior to the reference composites. The mixtures containing 100% had a “trunk cone” slump of 4 cm, which indicates that the material has a greater specific surface, which consumes a greater amount of water.

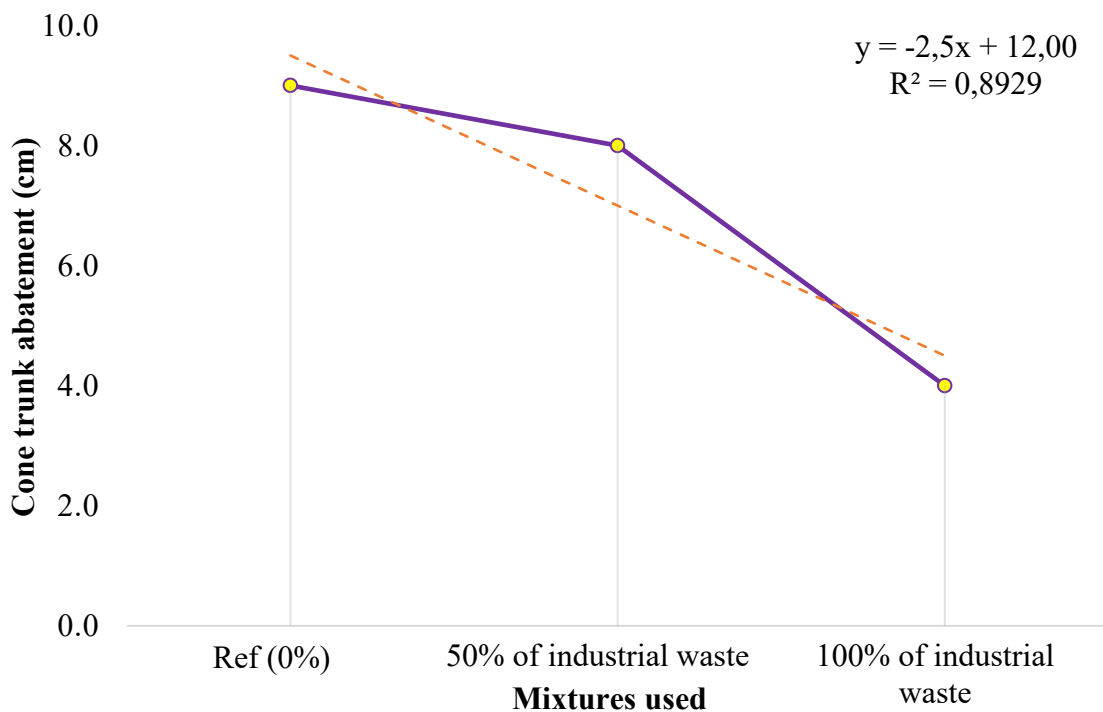


Figure 3. Representation of the workability (obtained through the Slump Test) of the different types of strokes.

Although the natural fine aggregate and crushed stone powder present their granulometric ranges within the limits established by the standard, none of the 3 (three) mixtures presented slumps between 10 cm and 16 cm, which, according to NBR 8953 (ABNT, 2015) would be ideal. for the execution of the structural elements.

Observing (Figure 3), it can be seen that the mixtures containing 50% of industrial solid waste showed a workability around 11.11% lower when compared to the reference mixtures, which demonstrates their feasibility for the development of new cementitious composites for structural purposes. However, the mixtures containing 100% of industrial solid aggregates showed a 55.56% lower slump when compared to the reference mixtures.

The marble powder showed unfavorable characteristics when mixed with water, where its grains were deposited, forming a powdery material. In addition, the material had a viscous characteristic when saturated, which negatively influenced the workability of cementitious composites (concrete).

3.3 Analysis of axial compressive strength

The use of industrial solid waste in the matrix structure of cementitious materials (concrete) provides a better physical-mechanical behavior which, in turn, fills the voids/interstices due to the specific surface area of these materials, according to the results obtained through the granulometric classification. All analyzes were performed at 7, 14, 21 and 28 days and the results were expressed in the graph shown in (Figure 4).

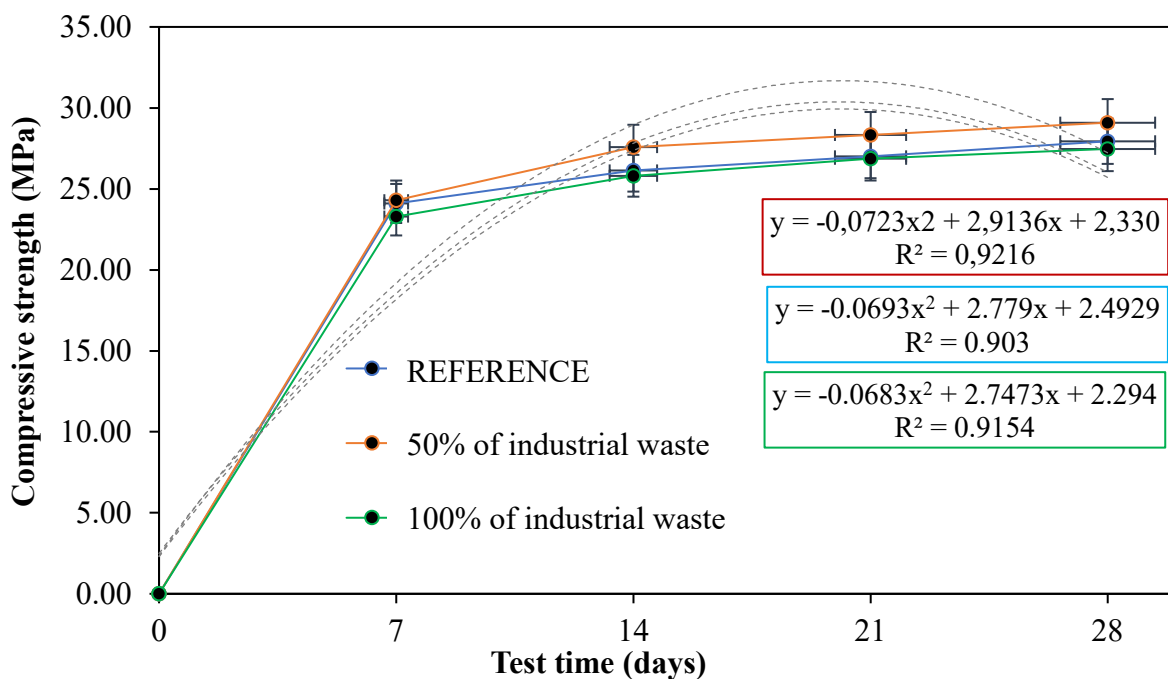


Figure 4. Average axial compressive strength of cementitious composites.

The mixtures containing 50% of industrial solid waste in their composition provided the material with greater mechanical efficiency when compared to the reference (SP's), which were greater than 20 MPa at 7 days. However, the results of the reference mixtures and with 100% recycled aggregates have similar behavior at the 28 days of analysis, where the values obtained were 27.94 MPa and 27.47 MPa, respectively. It is possible to notice that all mixtures have a significant sample correlation, that is, the (R^2) vary around 0.900 and 0.920.

Considering the analyzes carried out, it was observed that the mixtures containing 50% of industrial solid waste provided an increase in the compressive strength at 28 days of approximately 4% when compared to mixtures of (REF), which is considered an adequate value in the face of the presentation of the physical characteristics of the materials under study. These composites gave more significant values, however, at 7 days, they resulted in a slightly higher behavior when compared to the reference mixtures.

As for the mixtures containing 100% of industrial solid waste, it was noticed that at 28 days of analysis, it obtained axial compressive strength values of 27.47 MPa, that is, 2% lower when compared to the reference mixtures. This behavior will be due to the percentage of fine materials present in the material and the water/cement ratio (w/c). The higher the content of powdery materials, the greater the absorption of water, making it difficult for all particles to become wet. This process implies the absence of better cohesion and, above all, the formation of voids inside the cement matrix, leading to the loss of mechanical properties.

The growth of the compressive strength occurs linearly, as the increase in the content of particles of residual materials dispersed in the cement matrix of the mixtures with 100% does not coincide with the good mechanical behavior of the material. Furthermore, it is known that the increase in the void ratio can cause pressures inside the hydrated compound, forming microcracks that, when a force is applied, contract in the regions close to the transition zone of the aggregate/binder.

In order to better represent the data obtained, and from the values of the axial compressive strength at 7, 14, 21 and 28 days, a statistical analysis was performed using histogram and ANOVA (single factor method). It can be seen, therefore, that the analyzed mixtures have statistically different results according to the representative P-value less than 5%, the $F > F_{critical}$ and by the dispersion of the data circled in red (Figure 5). When there is this behavior, it is verified that the data are significant at a confidence level of 95%, as can be seen in (Table 3).

Table 3. Analysis of variance of the axial compressive strength of cementitious composites at 7, 14, 21 and 28 days of curing.

Analysis time	source of variation	SQ	gl	MQ	F	p-value	F-critical
7 days	between groups	82.079557	5	16.41591	2.6582498	3.00E-02	2.353808958
14 days		340.7330211		68.14660	7.1096072	2.26E-05	2.589189854
21 days		159.0295567		31.80591	5.7705620	1.77E-04	2.848108839
28 days		380.5367882		76.10736	39.3874620	1.54E-18	3.132919723

SQ: Sum of squares;

gl: Degree of freedom;

MQ: Mean of squares;

F: Test F, calculated value;

P: Significance level associated with the calculated value F.

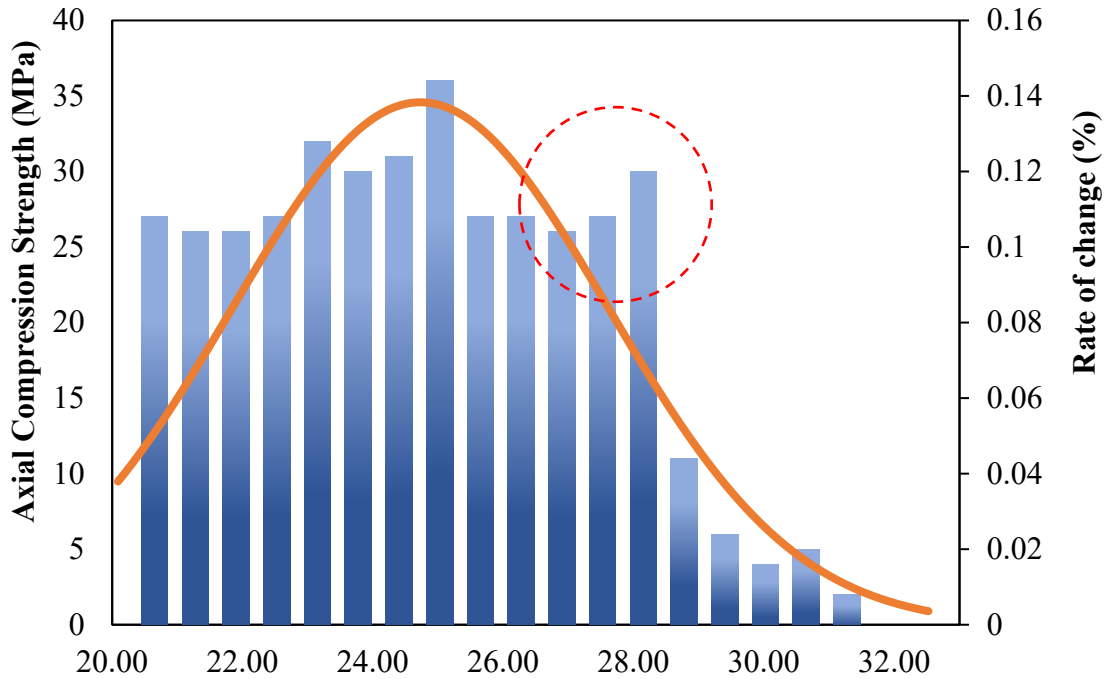


Figure 5. Analysis of the normal distribution of the data.

Some analyzes were carried out corresponding to the data obtained in the result of simple compressive strength, which, in turn, made it possible to understand the behavior of each mixture. The evaluated samples went through a quantitative statistical process (Table 4), where it was noticed that the reference composites had an average standard deviation of 1.699 and a coefficient of variation of 6.081 compared to the other mixtures. Mixtures with 50% of industrial waste had a standard deviation of 0.804 and a coefficient of variation of 2.765, that is, 11% and 15% lower compared to the reference composites, respectively.

Table 4. Statistical analysis of axial compressive strength data at 28 days of curing.

Data	REF	50% industrial waste	100% industrial waste
No. of samples	30	30	30
Average	27.94	29.09	27.47
Standard deviation (mean)	0.906	0.804	0.768
Standard deviation (sample)	1,156	1.073	1.019
Standard deviation (population)	1,156	1,027	0.975
Coefficient of variation (%)	3,243	2,765	2,794
standard error	0.143	0.127	0.121
95% confidence interval	28.30	29.41	27.77
	27.58	28.77	27.17
	0.358	0.318	0.302

3.5 Microstructural analysis

To understand the microstructural behavior of cementitious composites, using different percentages of industrial waste, it was necessary to perform diffractometric analyses. All samples were analyzed after 28 days using the X-ray diffraction test, in order to identify the crystalline phases present in the material in the hydration process, as well as to understand the portlandite reactions in the hydration states. XRD patterns can be seen in (Figure 6 (a) and (b)).

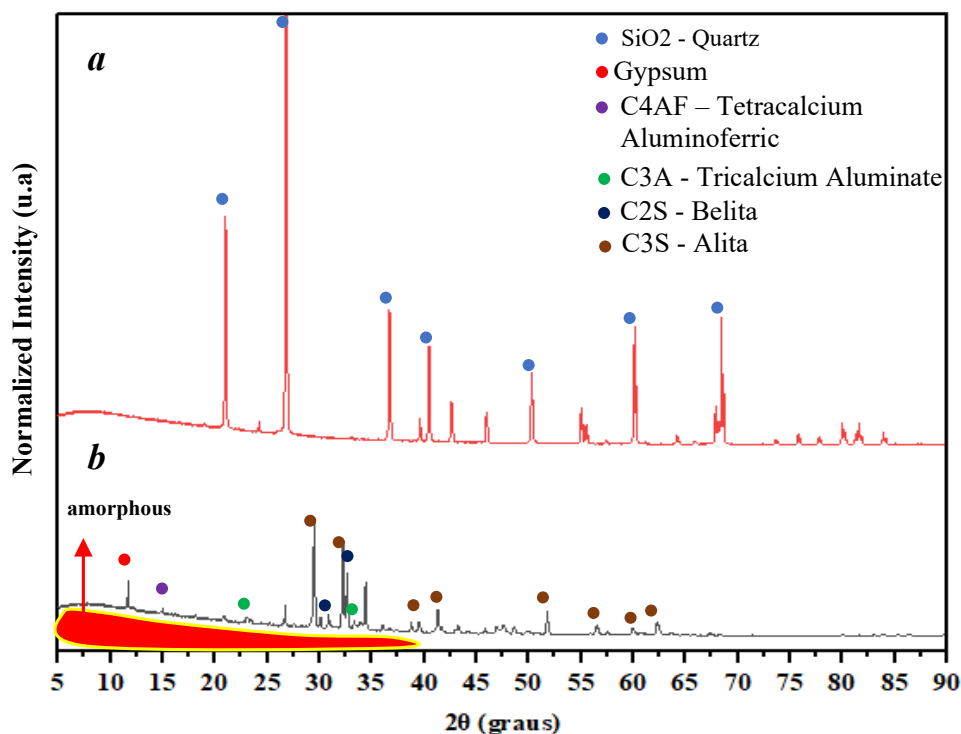


Figure 6. X-ray diffraction of natural fine aggregate (a) Portland cement/binder (b).

Regarding the behavior of the percussive materials, it can be seen that the fine aggregate and Portland cement have a crystalline structure with well-defined intensity peaks, as can be seen in ((Figure 6) (a)). The detection of the fine aggregate peaks is indicated in the 2θ positions: 21.2° , 26.8° , 36.7° , 40.4° , 50.3° , 60.0° and 68.6° , where they refer to the crystalline phases of quartz.

As for the Portland cement aliquot, one can see the formation of diffraction spectra peaks, where some phases were identified. Positions $2\theta = 29.5^\circ$ and 32.2° are formed by the decomposition of alite ($3\text{CaO} \cdot \text{SiO}_2$) and at position $2\theta = 62.3^\circ$ there is the presence of tricalcium silicate – (C_3S). Furthermore, at positions $2\theta = 27.6^\circ$ and 32.8° , the crystalline phase composed of belite ($2\text{CaO} \cdot \text{SiO}_2$) is observed and in the regions $2\theta = 30.2^\circ$ and 31.1° , the formation of dicalcium silicate can be seen – (C_2S).

The formation of tricalcium aluminate – (C_3A) defined by the chemical correlation ($3\text{CaO} \cdot \text{Al}_2\text{O}_3$), can be seen at positions $2\theta = 23.2^\circ$ and 33.4° . Note that tetracalcium ferric aluminate defined by the chemical correlation ($4\text{CaO} \cdot \text{Al}_2\text{O}_3 \cdot \text{Fe}_2\text{O}_3$) abbreviated as (C_4AF), can be seen at position $2\theta = 14.7^\circ$ and gypsum, in turn, can be seen at position $2\theta = 11.8^\circ$.

In this context, it is noticeable that the content of (C_3S), (C_2S), (C_3A), (C_4AF) and gypsum in Portland cement aliquots is well defined. All the crystalline phases identified in the material, as well as the chemical composition present in the hydration phase of the binder, are correlated with the studies carried out by Geng et al., (2018).

All results, in turn, directly influence the behavior of the hydrated cementitious compound. As they are very thin materials with a high specific area, some particles are often agglomerated, which

directly influence the physical-mechanical behavior of the material under study (concrete).

4. DISCUSSIONS

Current research aims to evaluate the use of marble powder and granitic crushed stone as an alternative material that aims to reduce environmental impacts. In terms of the mechanical performance of cementitious composites modified with marble powder, Arshad et al., (2014) concluded that the replacement of 15% of fine aggregate by marble powder residues in the presence of plasticizing additives, evidenced a maximum compressive strength, similar to the reference mixture, after 28 days of curing.

Shukla, Gupta and Gupta (2020) when producing cementitious composites containing marble powder in the proportion of 100%, it was observed values of average axial compressive strength at 28 days of approximately 40 MPa, which was 6.5% higher when compared to the reference mixtures. Likewise, Barros and Fucale (2016) verified the possibility of using the total replacement of natural aggregate by recycled and concluded that the concrete was able to withstand 22% higher compressive forces when compared to the reference mixture.

Studies carried out by Aliabdo et al., (2014) showed that the use of a water/cement ratio (w/c) of 0.40 enabled a significant increase in the axial compressive strength of cementitious composites containing industrial waste in their matrix. In addition, they observed that the mechanical compaction of concrete affects the filling of voids.

Ali and Hashmi (2014) evaluated the mechanical behavior of cementitious composites using different percentages of marble dust and stone dust individually. The authors found that the use of 20% stone powder improves the mechanical properties of cement-based materials by approximately 17% at 7 days and 16% at 28 days of analysis.

Studies by Hebhoub et al. (2011) reported an increase in axial compressive strength using 75% recycled aggregates. In addition, the authors performed a comparative behavioral analysis, where they realized that the use of 100% recycled aggregates affects the loss of axial compressive strength determined by the filling of micropores in the cement matrix, improving the properties in the transition zone. All analyzes corroborated the results obtained in this study.

Rodrigues, Brito and Sardinha (2015), evaluated the behavior of cement composites containing industrial solid materials, where they realized that the use of plasticizers improves the axial compression strength and workability. In addition, it is necessary to use industrial waste properly, because when used incorrectly, it can lead to the decomposition of dicalcium silicate (C_2S) and tricalcium silicate (C_3S), constituents that are responsible for the increase in compressive strength of cement-based composites.

5. CONCLUSIONS

In this article, the behavior of cement composites, more specifically concrete, was analyzed in terms of the use of industrial aggregates composed of marble dust and granitic crushed stone as a partial replacement for natural fine aggregate, as an alternative to minimize environmental impacts. The main conclusions are described below:

- Cementitious composites (concrete) containing 50% of industrial waste resulted in an increase in axial compressive strength of 29.09 MPa, that is, 4% higher when compared to the reference mixtures;
- The use of plasticizers improves the behavior of cementitious materials, especially with low water/cement ratios. In addition, the mixtures containing 100% recycled aggregates had a lower truncated cone slump, even though they contained plasticizer in their composition;

- The results of the reference mixtures and with 100% recycled aggregates have similar behavior when analyzed at 28 days, where the values obtained were 27.94 MPa and 27.47 MPa, respectively.
- The use of components with higher contents of powdery materials can affect the workability due to the high specific surface. On the other hand, the proper use of percentages can promote the filling of voids inside the cement matrix, as well as contributing to the cohesion process and improvement of the mechanical properties of cement-based materials;
- It was possible to notice that all mixtures have a significant sample correlation, that is, they vary between 0.900 and 0.920.

6. ACKNOWLEDGMENTS

This research is of great relevance to the scientific/academic community and would not have been possible without the collaboration of all participants. We also thank the Faculty de Integration of the Sertao – FIS, Polytechnic School of Pernambuco – POLI/UPE, the Catholic University of Pernambuco and, above all, the research funding agencies of the CNPq “*Conselho Nacional de Desenvolvimento Científico e Tecnológico*” and CAPES “*Coordenação de Aperfeiçoamento de Pessoal de Nível Superior*”.

7. BIBLIOGRAPHIC REFERENCES

ABNT – Associação Brasileira de Normas Técnicas. (1998). *NBR NM 67: Concreto – Determinação da consistência pelo abatimento do tronco de cone*. Rio de Janeiro.

ABNT – Associação Brasileira de Normas Técnicas. (2003), *NBR NM 248: Agregados – Determinação da composição granulométrica*. Rio de Janeiro, 2003.

ABNT – (2015), *NBR 5738: Procedimento para moldagem e cura de corpos de prova*. Rio de Janeiro.

ABNT – (2018), *NBR 5739: Concreto – Ensaio de compressão de corpos de prova cilíndricos*. Rio de Janeiro.

ABNT – Associação Brasileira de Normas Técnicas. (2014), *NBR 6118: Projeto de estruturas de concreto – Procedimento*. Rio de Janeiro.

ABNT – Associação Brasileira de Normas Técnicas. (2009), *NBR 7211: Agregados para concreto Especificação*. Rio de Janeiro.

ABNT – Associação Brasileira de Normas Técnicas. (1982), *NBR 7251: Agregado em estado solto – Determinação da massa unitária*. Rio de Janeiro.

ABNT – Associação Brasileira de Normas Técnicas. (2015), *NBR 8953: Concreto para fins estruturais – Classificação pela massa específica, por grupos de resistência e consistência*. Rio de Janeiro.

ABNT – Associação Brasileira de Normas Técnicas. (1987), *NBR 9776: Agregados – Determinação da massa específica de agregados miúdos por meio do frasco Chapman*. Rio de Janeiro.

ABNT – Associação Brasileira De Normas Técnicas. (2004), *NBR 15116: Agregados reciclados de resíduos sólidos da construção civil: Utilização em pavimentação e preparo de concreto sem função estrutural – Requisitos*. Rio de Janeiro.

Aliabdo, A. A., Elmoaty, A. E. M. A., Auda, E. M. (2014), *Re-use of waste marble dust in the production of cement and concrete*. Construction and Building Materials. 50(1):28-41. <http://dx.doi.org/10.1016/j.conbuildmat.2013.09.005>

- Ali, M. M., Hashmi, S. M. (2014), *An Experimental investigation on strengths characteristics of concrete with the partial replacement of Cement by Marble Powder dust and Sand by Stone dust*. IJSRD – International Journal for Scientific Research & Development. 2(7):360-368.
- Andrade, J. J. O., Possan, E., Squiavon, J. Z., Ortolan, T. L. P. (2018), *Evaluation of mechanical properties and carbonation of mortars produced with construction and demolition waste*. Construction and Building Materials. 161(1):70-83. <http://dx.doi.org/10.1016/j.conbuildmat.2017.11.089>
- Arshad, A., Shahid, I., Anwar, U. H. C., Baig, M. N., Khan, S., Shakir, K. (2014), *The Wastes Utility in Concrete*. International Journal of Environmental Research. 8(4):1-20. <http://dx.doi.org/10.22059/ijer.2014.825>
- Azevedo, A. R. G., Vieira, C. M. F., Ferreira, W. M., Faria, K. C. P., Pedroti, L. G., Mendes, B. C. (2020), *Potential use of ceramic waste as precursor in the geopolymerization reaction for the production of ceramic roof tiles*. Journal of Building Engineering, 29(1). <http://dx.doi.org/10.1016/j.jobe.2019.101156>
- Barros, E., Fucale, S. (2016), *O uso de resíduos da construção civil como agregados na produção de concreto*. Revista de Engenharia e Pesquisa Aplicada. 2(1). <http://dx.doi.org/10.25286/rep.v2i1.343>
- Brandão, R., Edwards, D. J., Hosseini, M. R., Melo, A. C. S., Macêdo, A. N. (2021), *Reverse supply chain conceptual model for construction and demolition waste*. Waste Management & Research: The Journal for a Sustainable Circular Economy. 39(11):1341-1355. <http://dx.doi.org/10.1177/0734242x21998730>
- Cipriano, P. B., Galdino, T. S. G., Sá, C. S., Ferraz, A. V. (2021), *Avaliação dos parâmetros de calcinação do resíduo de gesso nas propriedades do gesso reciclado*. Matéria (Rio de Janeiro). 26(3). <http://dx.doi.org/10.1590/s1517-707620210003.13026>
- Geng, G., Li, J., Zhou, Y., Liu, L., Yan, J., Kunz, M., Monteiro, P. J. M. (2018), *A high-pressure X-ray diffraction study of the crystalline phases in calcium aluminate cement paste*. Cement and Concrete Research. 108(1):38-45. <http://dx.doi.org/10.1016/j.cemconres.2018.03.004>
- Hebhoub, H., Aoun, H., Belachia, M., Houari, H., Ghorbel, E. (2011), *Use of waste marble aggregates in concrete*. Construction and Building Materials. 25(3):1167-1171. <http://dx.doi.org/10.1016/j.conbuildmat.2010.09.037>
- Kashani, A., Ngo, T. D., Mendis, P., Black, K. R., Hajimohammadi, A. (2017), *A sustainable application of recycled tyre crumbs as insulator in lightweight cellular concrete*. Journal of Cleaner Production. 17(3):1-32. <https://doi.org/10.1016/j.jclepro.2017.02.154>
- Klepa, R. B., Medeiros, M. F., Franco, M. A. C., Tamberg, E. T., Farias, T. H. B., Paschoalin Filho, J. A., Berssaneti, F. T., Santana, J. C. C. (2019), *Reuse of construction waste to produce thermoluminescent sensor for use in highway traffic control*. Journal of Cleaner Production. 209(1):250-258. <http://dx.doi.org/10.1016/j.jclepro.2018.10.225>
- Mechtcherine, V., Michel, A., Liebscher, M., Schneider, K., Großmann, C. (2020), *Mineral-impregnated carbon fiber composites as novel reinforcement for concrete construction: material and automation perspectives*. Automation in Construction. 110(1):1-8. <http://dx.doi.org/10.1016/j.autcon.2019.103002>
- Meena, R. V., Chouhan, H. S., Jain, J. K., Satankar, R. K. (2021), *Construction and Demolition Waste as an Alternative of Rigid Pavement Material: a review*. Iop Conference Series: Earth and Environmental Science. 795(1). <http://dx.doi.org/10.1088/1755-1315/795/1/012019>
- Mohajerani, A., Burnett, L., Smith, J. V., Markovski, S., Rodwell, G., Rahman, M. T., Kurmus, H., Mirzababaei, M., Arulrajah, A., Horpibulsuk, S. (2020), *Recycling waste rubber tyres in construction materials and associated environmental considerations: a review*. Resources, Conservation and Recycling. 155(1). <http://dx.doi.org/10.1016/j.resconrec.2020.104679>

- Nascimento, C. F. G., Monteiro, E. C. B., Silva e Souza, M. G., Teixeira, I. A. R., Vale, L. J. S., Valões, D. C. P., Cavalcanti, L. R., Figueira, A. M. A., Pedrosa, P. G. V. (2020), *Viabilidade da substituição parcial do resíduo de construção civil pelo agregado miúdo nas propriedades físicas e mecânicas do concreto*. Brazilian Journal of Development. 6(8):62073-62081. <http://doi.org/10.34117/bjdv6n8-581>
- Nascimento, C. F. G., Silva, T. M., Teixeira, I. A. R., Silva, F. G. A., Neves, D. C. M., Pedrosa, P. G. V., Valões, D. C. P., Monteiro, E. C. B. (2021), *Influência do agregado reciclado na durabilidade do concreto armado frente a corrosão de armadura desencadeada por carbonatação acelerada*. Conjecturas. 21(4):569-599. <http://dx.doi.org/10.53660/conj-237-801>
- Nguyen, Q. D., Castel, A. (2020), *Reinforcement corrosion in limestone flash calcined clay cement-based concrete*. Cement And Concrete Research. 132(1):1-15. <http://dx.doi.org/10.1016/j.cemconres.2020.106051>
- Oliveira, P. S., Antunes, M. L. P., Cruz, N. C., Rangel, E.C., Azevedo, A. R. G., Durrant, S. F. (2020), *Use of waste collected from wind turbine blade production as an eco-friendly ingredient in mortars for civil construction*. Journal of Cleaner Production. 274(1). <http://dx.doi.org/10.1016/j.jclepro.2020.122948>
- Paiva, F. F. G., Tamashiro, J. R., Silva, L. H. P., Kinoshita, A. (2021), *Utilization of inorganic solid wastes in cementitious materials – A systematic literature review*. Construction and Building Materials. <http://dx.doi.org/10.1016/j.conbuildmat.2021.122833>
- Rodrigues, R., Brito, J., Sardinha, M. (2015), *Mechanical properties of structural concrete containing very fine aggregates from marble cutting sludge*. Construction and Building Materials. 77(1):349-356. <http://dx.doi.org/10.1016/j.conbuildmat.2014.12.104>
- Shukla, A., Gupta, N., Gupta, A. (2020), *Development of green concrete using waste marble dust*. Materials Today: Proceedings. 26(1):2590-2594. <http://dx.doi.org/10.1016/j.matpr.2020.02.548>
- Silva, J. A., Piva, J. H., Wanderlind, A., Savi, A. E., Antunes, E. G. P. (2021), *Análise das características físicas e propriedades mecânicas de argamassa com inserção de resíduos de madeira*. Matéria (Rio de Janeiro). 26(3). <http://dx.doi.org/10.1590/s1517-707620210003.13008>
- Thapa, V., Waldmann, D. (2021), *Binary blended cement pastes and concrete using gravel wash mud (GWM) powders*. Construction and Building Materials. 302(1). <http://dx.doi.org/10.1016/j.conbuildmat.2021.124225>
- Souza, F. C. (2019), *Avaliação de propriedades mecânicas e físicas do concreto com a adição de pó de brita*. Trabalho apresentado como requisito para obtenção do título de bacharel no Curso de Graduação em Engenharia Civil de Infraestrutura do Centro Tecnológico de Joinville da Universidade Federal de Santa Catarina. Joinville.
- Varadharajan, S., Jaiswal, A., Verma, S. (2020), *Assessment of mechanical properties and environmental benefits of using rice husk ash and marble dust in concrete*. Structures. 28(1):389-406. <http://dx.doi.org/10.1016/j.istruc.2020.09.005>
- Zhen, Y., Liu, B. (2021), *Experimental Study on the Performance of Improved Collapsible Loess Mixture with Concrete Crushed Gravel*. Iop Conference Series: Earth and Environmental Science. 781(2). <http://dx.doi.org/10.1088/1755-1315/781/2/022068>

Electrochemical re-alkalinization applied to carbonated concrete beams samples under the criteria of three standards

J. A. Paat Estrella^{1*}, J. A. Miam Cuevas², E. E. Maldonado Bandala³,

T. Pérez López⁴, D. Nieves Mendoza³

*Contact author: josapaac@uacam.mx

DOI: <https://doi.org/10.21041/ra.v12i3.619>

Reception: 15/06/2022 | Acceptance: 30/08/2022 | Publication: 01/09/2022

ABSTRACT

The effect of electrochemical re-alkalinization was evaluated by applying the standards UNE-EN-1504, NACE-SP0107-2007 and NMX-C-553-ONNCCE-2018, on previously carbonated reinforced concrete samples. With the monitoring of the degree of re-alkalinization, through pH and half-cell potential measurements at 7, 14, 21 and 28 days, pH recovery is observed in all cases, obtaining characteristic half-cell potential values in each current application, which confirms the polarization of the steel modifying the thermodynamic condition of the concrete-steel interface and causing chemical changes in the concrete paste. With the NMX-C-553-ONNCCE-2018 standard, the steel was polarized without reaching the overprotection region, avoiding the risk of producing hydrogen and brittleness in the steel.

Keywords: electrochemical re-alkalinization; pH; half-cell potential; current intensity.

Cite as: Paat Estrella, J. A., Miam Cuevas, J. A., Maldonado Bandala, E. E., Pérez López, T., Nieves Mendoza, D. (2022), “*Electrochemical re-alkalinization applied to carbonated concrete beams samples under the criteria of three standards*”, Revista ALCONPAT, 12 (3), pp. 347 – 361, DOI: <https://doi.org/10.21041/ra.v12i3.619>

¹ Doctorado en Ingeniería, Facultad de Ingeniería Mecánica y Eléctrica, Universidad Veracruzana, campus Xalapa, Veracruz, México.

² Facultad de Ciencias Químico Biológicas, Universidad Autónoma de Campeche, Campeche, México.

³ Facultad de Ingeniería, Universidad Veracruzana, campus Xalapa, Veracruz, México.

⁴ Centro de Investigación en Corrosión, Universidad Autónoma de Campeche, Campeche, México

Contribution of each author

Conceptualization, Pérez, T. (50%), Paat, J. A. (50%); Experimental development, Paat, J. A. (70%), Miam, J. A. (30%); Methodology, Maldonado, E. E. (40%), Nieves, D. (40%), Paat, J. A. (20%); Research, Paat, J.A. (100%); Organization and Analysis of results, Pérez, T. (50%), Nieves, D. (50%); Writing, Paat, J. A. (60%), Pérez, T. (40%); Review and edition, Pérez, T. (60%), Nieves, D. (40%).

Creative Commons License

Copyright 2022 by the authors. This work is an Open-Access article published under the terms and conditions of an International Creative Commons Attribution 4.0 International License ([CC BY 4.0](https://creativecommons.org/licenses/by/4.0/)).

Discussions and subsequent corrections to the publication

Any dispute, including the replies of the authors, will be published in the second issue of 2023 provided that the information is received before the closing of the third issue of 2023.

Realcalinización electroquímica aplicada a muestras de concreto carbonatadas bajo criterios de tres normatividades

RESUMEN

Fue evaluado el efecto de realcalinización electroquímica aplicando las normas UNE-EN-1504, NACE-SP0107 2007 y NMX-C-553-ONNCCE-2018, en muestras de concreto reforzado previamente carbonatadas. Con el seguimiento del grado de realcalinización, mediante mediciones de pH y potencial de media celda a 7, 14, 21 y 28 días, se observa la recuperación del pH en todos los casos, obteniendo valores de potencial de media celda característicos en cada aplicación de corriente, que confirma la polarización del acero modificando la condición termodinámica de la intercara concreto-acero y ocasionando cambios químicos en la pasta de concreto. Con la norma NMX-C-553-ONNCCE-2018 se polarizó el acero sin llegar a la región de sobreprotección, evitando el riesgo de producir hidrógeno y fragilidad en el acero.

Palabras clave: realcalinización electroquímica; pH; potencial de media celda; intensidad de corriente.

Realcalização eletroquímica de mostrars de concreto carbonatado aplicado sob os critérios de três regulamentações

RESUMO

O efeito da realcalização eletroquímica foi avaliado pela aplicação das normas UNE-EN-1504, NACE-SP0107 2007 e NMX-C-553-ONNCCE-2018, em amostras de concreto armado previamente carbonatadas. Com o acompanhamento do grau de realcalização, através de medidas de pH e potencial de meia célula aos 7, 14, 21 e 28 dias, observa-se a recuperação do pH em todos os casos, obtendo valores característicos de potencial de meia célula em cada aplicação de corrente, o que confirma a polarização do aço, modificando a condição termodinâmica da interface concreto-aço e provocando alterações químicas na pasta de concreto. Com a norma NMX-C-553-ONNCCE-2018 o aço foi polarizado sem atingir a região de sobreproteção, evitando o risco de produção de hidrogênio e fragilidade no aço.

Palavras-chave: realcalização eletroquímica; pH; potencial de meia célula; amperagem.

Legal Information

Revista ALCONPAT is a quarterly publication by the Asociación Latinoamericana de Control de Calidad, Patología y Recuperación de la Construcción, Internacional, A.C., Km. 6 antigua carretera a Progreso, Mérida, Yucatán, 97310, Tel.5219997385893, alconpat.int@gmail.com, Website: www.alconpat.org

Reservation of rights for exclusive use No.04-2013-011717330300-203, and ISSN 2007-6835, both granted by the Instituto Nacional de Derecho de Autor. Responsible editor: Pedro Castro Borges, Ph.D. Responsible for the last update of this issue, Informatics Unit ALCONPAT, Elizabeth Sabido Maldonado.

The views of the authors do not necessarily reflect the position of the editor.

The total or partial reproduction of the contents and images of the publication is carried out in accordance with the COPE code and the CC BY 4.0 license of the Revista ALCONPAT.

1. INTRODUCTION

The durability of reinforced concrete structures is considered as their ability to keep their physical and chemical conditions unchanged during their useful life when they are subjected to material degradation, so the structural design of a reinforced concrete building, must stipulate the appropriate measures so that it reaches the useful life established in the project, taking into account the environmental and climatic conditions and the type of building to be built.

The deterioration of infrastructure such as bridges, pipelines, tanks, buildings, canals, ports, storage plants, historical monuments, airports, railways, etc., is a serious problem that currently affects not only the agencies responsible for them, but also it indirectly affects society because these structures are rendered unusable for some time before reaching the end of their established useful life. Therefore, within the priorities in Mexico, are the safety of people, real estate and the protection of the environment.

Techniques such as Electrochemical Re-alkalinization (ERA) and Electrochemical Chloride Removal (ECR), have shown to be promising according to the experiences obtained both in the laboratory and *in situ* (Weichung, Y., Jiang, JC, 2005).

Electrochemical re-alkalinization has been used on numerous occasions in practical and laboratory applications, however, there is currently no consensus on what the parameters are related to the structure and the technique that allow evaluating its effectiveness over time (Gonzalez, F., 2010). Although this technique has shown its effectiveness on real structures, it cannot yet be considered a routine technique due to the lack of detailed information on some aspects such as the side effects it causes and that in the long term it could affect the durability of concrete (Mietz, J., 1998; Rincón, T., 1994).

The application of these electrochemical techniques (ET) as unconventional intervention and maintenance methods have aroused great interest in the field of Civil Engineering. In some of the industrialized countries there are experiences of implementation of the techniques, however, the number of reported works explaining the application conditions is not abundant (Rincón, T. 1994; Helene, P. 1994; Pollet, V. 2000; Bize, B. 2001; Raharinaivo 1992; Chatterji, S. 1994; Fajardo, G., et al. 2006).

As a rehabilitation method or as a preventive treatment, ERA method has been used to recover the alkalinity of concrete near the reinforcement region (Mietz, J., 1998). The advantage of this method is that, when the treatment is finished, the system can be disassembled and the structure of concrete can continue its function without major destructive interventions such as it happens in conventional patch repair treatment (Redaelli, E., & Bertolini, L. 2011).

Studies on the re-alkalinization treatment that focused on understanding the characteristics of the phenomenon, such as the transport mechanisms involved (Aguirre, A., and Gutiérrez, R., 2018; Castellote, M., et al., 2003; González, F., 2010), the re-passivation efficiency of the reinforcement (Redaelli, E., and Bertolini, L. 2011; Yeih, W., and Chang, J., 2005), the efficiency of different electrolytes in re-alkalinization (Mietz, J. 1995), the effects on the properties of concrete and the side effects (González, F., 2010; Ribeiro, P., et al., 2013; Tong Y., et al., 2012), have been carried out in recent years.

In situ applications were introduced in the late 1980s and a significant number of structures have been treated with this technique. Some documents report on these experiences and show the ability of the technique to recover protective pH levels.

These studies also show that, even after a few years, the alkalinity remains at high levels, which would be sufficient to protect the reinforcement (Yeih, W., Chang, J., 2005). Some of these advances have only been included in local and regional regulations and standards.

As is known, application of an intensity of electric current induces the polarization of the concrete-steel interface with variation in the value of the half-cell potential (HCP), as well as changes in the

chemical composition of the concrete paste, mainly reflected by the pH, it was considered convenient to compare 3 re-alkalinization conditions established in the UNE EN 1504, NACE SP0107 2007 and NMX-C-553-ONNCCE-2018 standards, in which the experimental set-up is practically the same, the variation is the application time, being 7 days for the NACE, 14 for the UNE and 28 for the NMX and the applied current intensity, being 4 A/cm² in the first case, 2 A/m² for the second and 1 A/m² for the third, considering the surface of the steel rod.

It is to be expected that the most intense polarization was reached for the NACE conditions, followed by the UNE (EURO) and finally the least for the NMX. Similarly, the rate of re-alkalinization was expected in the same order. However, it was decided to take the polarization up to 28 days in all cases, with the interruption for measurement of carbonation recovery and half-cell potential at 7, 14, 21 and 28 days, to observe the alkalinity recovery capacity and the condition of the concrete-steel interface. At the same time, was recorded the range of HCP values that exceed overprotection values that reach the hydrogen embrittlement zone, a very harmful phenomenon, especially for post-stressed and pre-stressed steel. Results obtained show that, for the NACE and UNE standards, re-alkalinization is achieved in less time, but the HCP values polarize the steel-concrete interface up to the hydrogen generation region, which can lead to the fragility of the metallic element, being a negative factor in the re-alkalinization treatment. With the NMX-C-553-ONNCCE-2018 standard, re-alkalinization occurs more slowly, but it does not reach half-cell potentials in the hydrogen generation zone, so its application under this criterion is more recommended.

2. EXPERIMENTAL PROCEDURE

2.1 Materials

Materials used for the manufacture of the concrete specimens complied with current regulations. Aggregates were selected in compliance with NMX-C-111-ONNCCE-2018. Washed sea sand was used as fine aggregate, and crushed stone with a maximum size of 19 mm as coarse aggregate. Materials used are characteristics of the southeastern region of Mexico, whose properties are presented in Table 1.

Table 1. Characteristics of the components used in the mixtures.

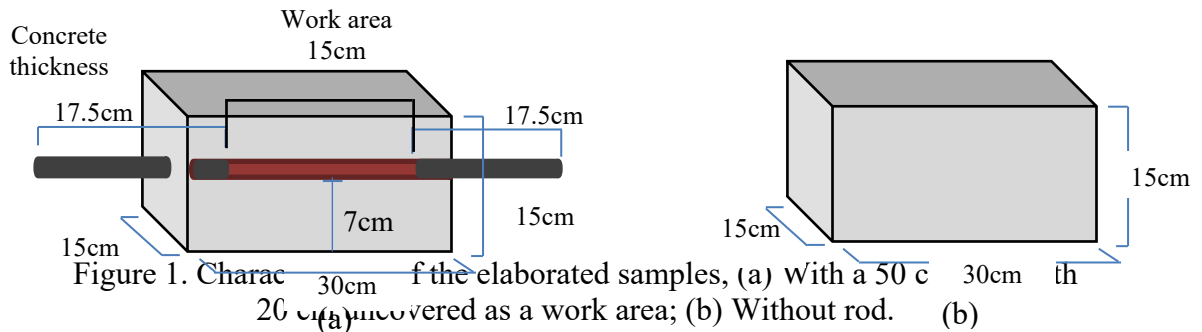
Tests	Coarse Aggregate	Fine Aggregate	Cement
PSSS (Kg/m ³)	1241	1335	1400
PLWHA (Kg/m ³)	1417	1514	
Density or specific weight (gr/cm ³)	2.26	2.56	3.2
% Absorption	2.5	2.56	---
TMNA (mm)	12.5	2.5	---

For the manufacture of the specimens, Portland Cement Compound of Rapid Resistance (CPC 30R) was used, with a specific weight of 3200 kg/m³ (NMX-C-414-ONNCCE-2017). Commercial purified water was supplied with, in order to avoid sample contamination.

2.2 Specimen design and preparation

66 concrete specimens were made with reinforcing steel A615 (ASTM), of 0.95 cm (3/8") and 18 without steel (Figure 1), with a w/c ratio of 0.6, in order to obtain concrete specimens with high porosity to be able to control the diffusion of ions and CO₂.

Rods were cut to a length of 50 cm, later they were cleaned with a 1:1 HCl solution, and 17.5 cm from each end were covered with insulating tape, leaving a central work area of 15 cm, as is shown in Figure 1(a).



Mix design was carried out as established of ACI (American Concrete Institute) 211.1 for an average compressive strength of 250 kg/cm².

To improve the plasticity of the mixture, 35 mL/L of a water-reducing fluidizer were used. Amounts of the materials for the mix design are presented in Table 2.

Table 2. Material weights per cubic meter of concrete mix.

Materials	Amount used (kg)
Water	115.82
Cement	288.43
Coarse aggregate	500.15
Fine aggregate	511.51

After 24 hours, the samples were removed from the mold and subjected to curing by immersion with a saturated solution of Ca(OH)₂ for 28 days. After this time, the samples reached an average compressive strength of 204 kg/cm².

Samples were divided in three series (I, II and III), to which current intensities were applied regarding the steel area in accordance with regulations NMX-C-553-ONNCCE-2018 (1 A/m²), UNE EN 1504 (2 A/m²) and NACE SP0107 2007 (4 A/m²), respectively.

2.3 Accelerated Test

In order to achieve greater carbonation in less time, the specimens were placed in an accelerated carbonation chamber, because carbonation under natural conditions is a slow phenomenon from a technical point of view. During the accelerated tests, the concrete samples were subjected to an environment with a concentration of CO₂ of 4 + 0.5%, according to experimental conditions carried out by Turcry, Oksri-Nelfia, Younsi, & Ait-Mok in 2014, and with a relative humidity of 60 + 5%. It has been proposed that with accelerated tests at CO₂ concentrations of 4%, the same depth of carbonation than normal concentrations (0.03%) in one year (Moreno, M., et al, 2004).

2.4 Electrochemical Re-alkalinization (ERA)

Electrochemical re-alkalinization is a technique used to recover the alkaline pH from concrete, allowing the re-passivation of the reinforcing steel. The operation of the ERA is very similar to the impressed current cathodic protection, since a continuous electric current is applied from the anode, closing the circuit using the reinforcing steel as the cathode. This technique was carried out based

on the criteria established in the NACE SP0107-2007, UNE-EN-1504 and NMX-C-553-ONNCCE-2018 standards, considering the specifications presented in Table 3.

Table 3. Experimental conditions.

Parameters	Mexican Standard	European Standard	Nace
Current density	1 A/m ²	2 A/m ²	4 A/m ²
Voltage range	15 – 30 V DC		
Anodic system	Galvanized steel mesh		
Electrolyte	Sodium Carbonate		
Time	7 - 28 days		
pH	Re-alkalinization depth measurement		

After the accelerated carbonation to which the concrete samples were exposed, they were subjected to the electrochemical re-alkalinization process, requiring the implementation of re-alkalinization device, as described below.

To submit to ERA, 27 samples were selected. Were painted the cross sections of samples for the sodium carbonate penetrated only through the sides of the beam. Subsequently, each of the samples was covered with a galvanized steel mesh, which served as an anode during the RAE, they were arranged vertically in a plastic container with enough capacity, to which a hole was drilled in the base, to expose one side of the rod and not be affected by the immersion electrolyte (sodium carbonate 1M) (see Figure 2).



Figure 2. Experimental setup used for electrochemical re-alkalinization.

2.4.1 Measurement of re-alkalinization depth and re-alkalinization current intensity

A parallel connection was made at 3 different currents: 1 A/m², 2 A/m² and 4 A/m², making the connections in triplicate. To carry out this connection, it was necessary to design an electrical distribution device that would maintain a constant electrical flow connected to two power sources to reach the required voltage.

ERA was carried out for 28 days, the samples being divided into three series (serie I, serie II and serie III), of 9 samples each, with the aim of comparing the possible side effects that could occur. During this time, the pH at the concrete-steel interface and the concrete paste was monitored by the indicator method. These measurements were made every seven days, from the day the ERA began until completing 28 days, as mentioned by several authors (Ton, Y., et al 2012, Yeih, W.,

and Chang, J., 2005). The extraction of nuclei and the dust samples were carried out on the 15 cm of uncovered rod, using a 1.5" diameter and 7 cm long hollow drill coupled to a drill. (Figure 3). During extraction, depth and pH of each beam exposed to re-alkalinization were determined by the wet method using phenolphthalein (vary between 8.2 -10) and thymolphthalein (vary between 9 - 10.5) as indicators. Measurement was made by obtaining an average of the carbonation front from the surface of the sample. Additionally, pH was determined at the depth of the surface of the rod in samples extracted from the samples, by means of the potentiometric method, which determines the level of alkalinity of the concrete, by means of an extraction with distilled water, established in ASTM D4262 –05 (2018) Standard Test Method for pH of Chemically Cleaned or Etched Concrete Surfaces.



Figure 3. Extraction of cylinders and dust samples.

2.4.2 Half-cell potential (HCP)

The monitoring of the thermodynamic surface condition of the reinforcement is mainly based on measurements of the HCP, which is related to the active or passive state of the reinforcing steel. The measurement consisted in the determination of the electrical potential difference between the reinforcing steel and a reference electrode (Cu/CuSO₄) placed on the concrete surface (American Society for Testing and Materials, 2016), ASTM C-876-15, NMX-C-495-ONNCCE-2015.

3. RESULTS

Next, the experimental results of the electrochemical re-alkalinization of reinforced specimens are presented with a depth of carbonation of 6.7 cm. Results of pH and carbonation coefficient are presented. In the ERA, the behavior of the HCP of the reinforcing steel (cathode) for 28 days, with measurement intervals of 24 hours is shown. Measurements without interrupting the electrical current were made.

3.1 Carbonation

3.1.1 Accelerated carbonation chamber test (ACC)

Chemical degradation process or deterioration of concrete by CO₂ was carried out over a period of six months. Figure 4 shows the measurement of carbonation progress with respect to time, using the acid-base indicators in accordance with the NMX-C-515-ONNCCE-2016 standard. A linear trend can be seen in the advance of carbonation over the course of the exposure time because there is a great difference between the rate of diffusion of CO₂ in air and water, the latter being approximately 10⁴ times lower than in air, so that in the conditions of relative humidity of the ACC (60%) , concrete pores are partially filled, which allows CO₂ to diffuse easily. In contrast, if the

pores were filled with water (Figure 5) there is hardly any carbonation because there is very little CO₂ diffusion in the water (Del Valle *et al* 2001).

Hydrated cement paste with a pH of 11.5 to 12.5 acquired a red-violet coloration; however, when it was subjected to the action of CO₂, a decrease in pH was caused until reaching values of the order of 8 due to the neutralization, to a greater or lesser degree, of the hydroxyl ions, producing, among others, reaction (1):



Calcium carbonate is formed, incorporating CO₂ from the environment.

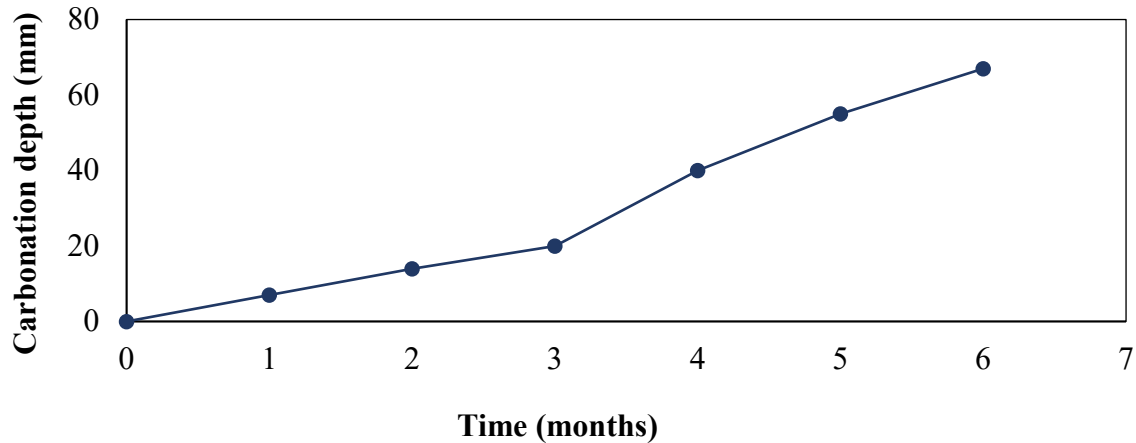


Figure 4. Carbonation depth with respect to exposure time in CCA.

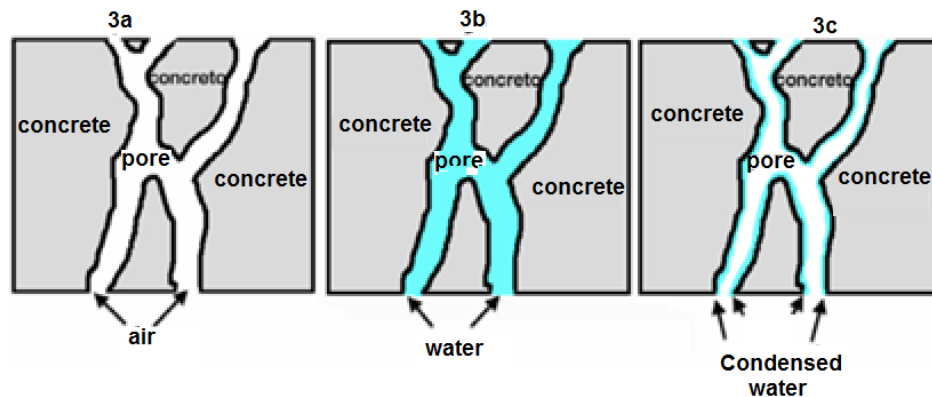


Figure 5. Filling of the pores. a) Dry pore, b) Water saturated pore, c) Partially filled pore. Images modified from Del Valle *et al* 2001.

3.1.2 pH measurement at the concrete-steel interface.

Objective of carbonating the specimens prior to the ERA process was to lower the pH and be able to recover it through re-alkalinization to observe the effects caused by this recovery. The average pH value obtained was 8 with a standard deviation of +0.8, which coincided with what was established by Aguirre, AM, *et al* (2016) and Ribeiro, PHLC, *et al* (2013) who determined that the pH of the pore solution in practically carbonated areas ranged between 11.5 and values below 9 (Figure 4). This indicates that from the third month of carbonation, the concrete samples were already carbonated, however, to achieve greater pH recovery, it was decided to obtain pH values below 9.

Figure 6 shows the graphs of pH at the level of reinforcing steel and HCP, showing that during the

carbonation process the pH gradually decreased, from a pH of approximately 13 to a pH of 9 in the vicinity of the rod, coinciding with the value of the HCP that shifted its initial value of -120 mV to approximately -700 mV, which according to the standard ASTM C-876-15, these values are below the established value of -350 mV, with a 90% risk of corrosion. Raja and Tetsuya (2010), report a similar follow-up, in which the HCP decreases with the advance of carbonation, starting from -180 to -475 mV vs ECS. They propose that the critical carbonation depth is 80% of the total concrete cover.

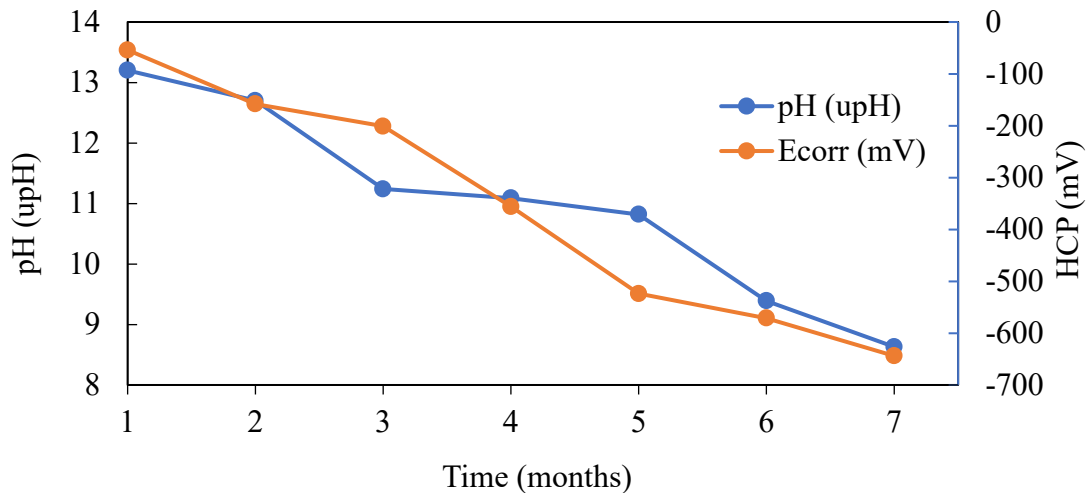


Figure 6. pH and HCP monitoring during carbonation.

3.2.1 Electrochemical Re-alkalinization

The electrochemical re-alkalinization technique is an alternative method based on the application of an electric field to a system formed by steel-concrete within an alkaline solution that functions as an electrolyte. It is considered a temporary technique because it is applied between a few days to a few weeks (Gonzalez, F., et al. 2011).

To start the re-alkalinization process, specimens were selected whose corrosion potentials were between -350 mV and -650 mV, with an average carbonation depth of 6.5 cm and a pH below 9. During the duration of the ERA process, a progressive increase in the depth of re-alkalinization was obtained, which meant a recovery in the alkalinity of the concrete from the contact surface between the electrolyte and the sample.

Below are the results obtained from the ERA in the concrete specimens at three current intensities used.

3.2.1.1 Reinforced samples re-alkalized at 1 A/m² in accordance with NMX-C-553-ONNCCE-2018

During this treatment, indicator technique was used to follow the progress of the re-alkalinization of the concrete in each structure. This evolution was monitored every 7 days during the 28 days of current application.

In the first 7, 14 and 21 days of re-alkalinization (Figures 7, 8 and 9), the samples showed a slight color change to pink and violet in the first three centimeters of depth, due to the phenolphthalein indicators (it changes to pink at pH 8.2 with color intensifying at > pH) and thymolphthalein (turns violet at pH 9.2 with color intensifying at > pH), respectively. At 28 days of re-alkalinization (Figure 10), an increase greater than 11 was obtained, reaching the objective of electrochemical re-alkalinization. As of day 21, both the internal and external RAE are observed overlapping along the 7 cm depth.

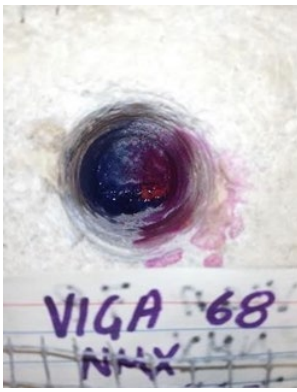


Figure 7. 7 days.



Figure 8. 14days.

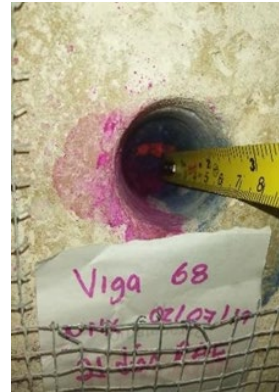


Figure 9. 21 days.



Figure 10. 28 days.

3.2.1.2 Reinforced samples re-alkalized at 2 A/m² in accordance with the UNE-EN-1504 standard

In Figure 11, a sample is observed after 7 days of re-alkalinization, in which the color change can be observed at the end of the 7 cm depth, however, after 14 days of this process the coloration intensifies, remaining constant on days 21 (Figure 12) and 28 (Figure 13), which, according to the results obtained from the determination of pH by the electrode method, reaches values close to 12.



Figure 11. 7 days.



Figure 12. 14 days.



Figure 13. 21 days.



Figure 14. 28 days.

3.2.1.3 Reinforced samples re-alkalized at 4 A/m² according to the NACE SP0107-2007 standard

Finally, the samples that were subjected to a current intensity of 4 A/m², which presented an increased coloration from the first 7 days of the re-alkalinization process in a homogeneous way throughout the 7 centimeters of thickness of the concrete (Figure 15), escalating over time and remaining constant until 28 days after re-alkalinization (Figure 16, 17 and 18), reaching pH values above 11 (see Figure 19).



Figure 15. 7 days.



Figure 16. 14 days.



Figure 17. 21 days.



Figure 18. 28 days.

In the case of these specimens, an improvement in the propagation of both alkalinities is observed, one produced by the cathodic reaction and the other due to the penetration of the alkaline electrolyte, allowing the effects of the treatment to be extended throughout the depth of the concrete. This coincides with that published by Mietz (1995) and by Redaelli & Bertolini (2011). According to the intensity of the color, and comparing them with the EURO and NACE standards, the samples under the criteria of the NMX-C-553-ONNCCE-2018 corresponding to 1 A/m² did not present a considerable increase in pH during the first 7 days of re-alkalinization (see Figure 19), which, according to Aguirre-Guerrero, A., and Mejía de Gutiérrez, R., 2018, makes it less effective in the first 7 days. However, regardless of the regulations used, all the samples at 28 days of re-alkalinization obtained pH greater than 11 (see Figure 19).

As can be seen in Figures 6-9, the coloration of the indicators is presented with greater intensity in two directions, which represents a recovery of pH in the same way, 1) from the reinforcing steel towards the internal surface (internal ERA), due to the production of alkalinity induced by the application of the cathodic current and 2) from the concrete surface towards the reinforcing steel (external ERA) due to the penetration of the alkaline solution in contact with the anodic system (Redaelli, E. & Bertolini, L., 2011), being observed more slowly in the samples subjected to 1 A/m² (Figure 7).

pH recovery behavior in both directions confirms a production of OH ions induced by the application of a cathodic current (Redaelli, E. & Bertolini, L., 2011, Castellote, M., et al., 2006), and a penetration of the alkaline electrolyte through the concrete (Castellote, M., et al., 2006), confirming that important mechanisms are carried out during the ERA process, such as migration of ions between the magnetic field, negative ions migrate towards the anode (steel mesh), positive ions migrate towards the cathode (reinforcing steel); absorption due to the capillarity effects of alkaline solutions; diffusion of alkaline compounds due to the different concentrations; and electroosmosis of the electrolyte on the concrete surface moving towards the cathode (Redaelli, E. & Bertolini, L., 2011, Castellote, M., et al., 2003, Mietz, 1998 and González, F., et al. 2011).

Regarding the pH results obtained in the three current intensities used (Figure 19), the highest values were presented at higher electrochemical re-alkalinization time.

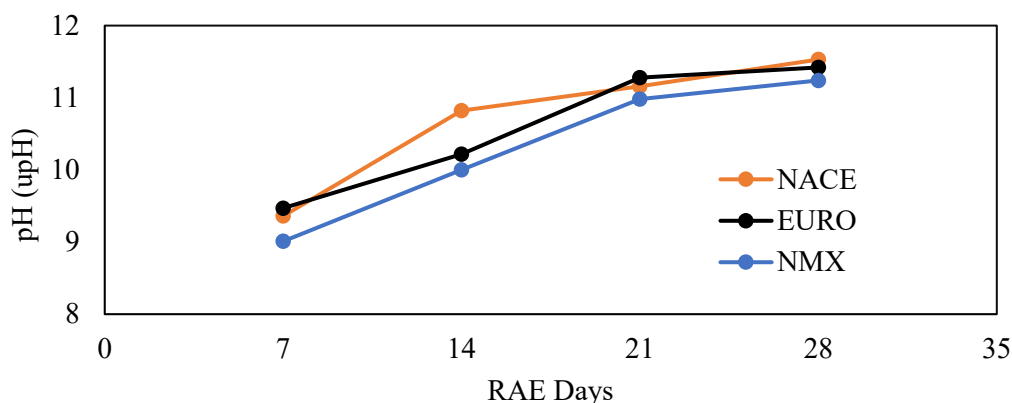


Figure 19. pH values during the 28 days of RAE treatment.

3.3 Half-cell potential (HCP)

It has been seen that in reinforced concrete structures, the concrete acts as an electrolyte, in this way the reinforcing steel immersed in the cementitious matrix will develop a potential that will depend on the physical and chemical characteristics of the concrete.

Average results of the electrical potentials measured daily during the 28 days of application of the RAE are presented below. Measurements were made in order to obtain a relative value of the probability of corrosion that could have occurred in the reinforcing steel during this electrochemical process.

Samples were subjected to current intensities of 1 A/m^2 (NMX), 2 A/m^2 (EURO) and 4 A/m^2 (NACE) for a period of 28 days, in which the galvanized steel mesh coating was used as the anode and the reinforcing steel rod as the cathode. During this period, it was observed that the embedded steel maintained half-cell potentials very negative (less than -350 mV), regardless of the applied current intensity, which, according to the provisions of the ASTM C876-15 standard, corresponds to a 90% probability of corrosion. These values indicate that the reinforcing steel remained in an active state throughout the electrochemical re-alkalinization period.

In Figure 20 the behavior of the electrochemical potential that the specimens presented at different intensities of applied current is observed, it can be seen that the HCP values presented a behavior directly proportional to the current intensity that was used, that is, the higher the current intensity, the greater corrosion potential value and vice versa. This current intensity reached values $> -900 \text{ mV}$, due to the strong cathodic polarization (Redaelli, E., & Bertolini, L., 2011). Of the three regulations used, it was the test samples under NMX conditions that presented less negative values of HCP. However, in the three cases of current intensities, the steels embedded in the concrete remained active throughout the electrochemical re-alkalinization process. After treatment, the HCP reached values greater than -200 mV , which represents a decrease in the probability of corrosion in accordance with what is established in the standard ASTM C876-15, which, according to Redaelli, & Bertolini, (2011), represents effectiveness in the treatment and suggests that the reinforcing steel reached re-passivation.

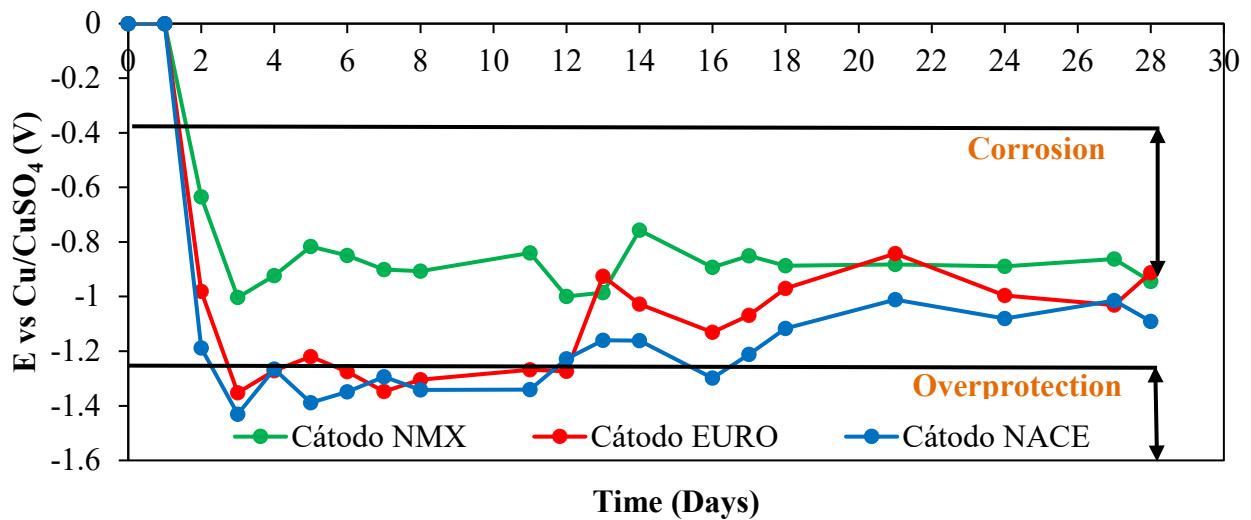


Figure 20. Average values of half cell potentials (V) during the 28 days of RAE subjected to three different current intensities.

It is observed that with the application of the NMX-C-553-ONNCCE-2018 standard, the overprotection region is not reached, which is why it does not represent a risk of producing hydrogen and brittleness in the steel. For the European standard (UNE-EN-1504), the polarization reaches the range of overprotection during the first 12 days, subsequently it increases its HCP values outside the risk zone of hydrogen embrittlement. In these cases, it is convenient to carry out tensile tests to verify if the steel was affected by the generation of hydrogen. It is particularly important to consider in concrete with post-stressed or prestressed steel.

4. CONCLUSIONS

The action of CO_2 on the hydrated compounds of Portland cement produces a decrease in pH, modifying the chemical composition of compounds and forming various carbonated compounds. In the application of the electrochemical re-alkalinization technique, the recovery of the pH (re-alkalinization) of the concrete is obtained mainly during the first 7 days at 4 A/m^2 , allowing a complete recovery of the thickness of the concrete.

However, the stable value or the slight increase in pH together with the increase in the alkali content in the steel-concrete interface would support the conditions that promote the formation of the passive layer of steel that will serve as protection after applying the ERA. Therefore, electrochemical re-alkalinization can be applied as a preventive technique in partially carbonated concrete structures.

A recovery of the pH of the concrete directly proportional to time was achieved, so that of the three regulations used, the specimens under conditions established in the NMX-C-553-ONNCCE-2018 were the ones that presented less negative values of E_{mc} without reaching the overprotection region, which does not represent a risk of producing hydrogen and brittleness in the steel.

5. ACKNOWLEDGEMENTS

The authors thank the Universidad Veracruzana, Xalapa campus, the Autonomous University of Campeche, the Program for the Development of Teaching Personnel (PRODEP) and the Pablo

García Foundation for the facilities provided to carry out this project.

To Dr. Victor Moo, for his valuable support in the design and development of the electrical device used during electrochemical re-alkalinization.

6. REFERENCES

- Aguirre-Guerrero, A. M., & de Gutiérrez, R. M. (2018), *Efficiency of electrochemical realkalisation treatment on reinforced blended concrete using FTIR and TGA*. *Construction and Building Materials*, 193, 518-528. DOI: [10.1016/j.conbuildmat.2018.10.195](https://doi.org/10.1016/j.conbuildmat.2018.10.195)
- Aguirre-Guerrero, A. M., Mejía-de-Gutiérrez, R., Montês-Correia, M. J. R. (2016), *Corrosion performance of blended concretes exposed to different aggressive environments*. *Construction and Building Materials*, 121, 704-716. DOI: [10.1016/j.conbuildmat.2016.06.038](https://doi.org/10.1016/j.conbuildmat.2016.06.038)
- Annual Book of ASTM Standards (2016), *Construction. Chemical-resistant materials; vitrified clay, concrete, fiber-cement products; mortars; masonry*. Section 4. Vol. 04.05.
- Andrade, C., Alonso, C., Rodríguez, J. (1989), *Remaining service life of corroding structures*. IABSE Symposium on Durability, Lisbon, Sep., pp. 359-363.
- ASTM C876-15. Standard Test Method for Corrosion Potentials of Uncoated Reinforcing Steel in Concrete.
- Bize, B. (2001), *Béton armé corrode: Les traitement électrochimiques*. In: CSTB Magazine, No. 136. juillet - août 2001.
- Castellote, M., Llorente, I., Andrade, C. (2003), *Influence of the external solution in the electroosmotic flux induced by realkalisation*. in: *Mater. Construcc.*, vol. 53, no 271– 272. pp. 101– 111. DOI: <https://doi.org/10.3989/mc.2003.v53.i271-272.294>
- Castellote, M., Llorente, I., Andrade, C., Turrillas, X., Alonso, C., Campo, J. (2006), *In-situ monitoring the realkalisation process by neutron diffraction: electro-osmotic flux and portlandite formation*. *Cem Concr Res*. 36:791–800. <https://doi.org/10.1016/j.cemconres.2005.11.014>
- Castellote M., Llorente, I., Andrade C., Turrillas, X., Alonso, C., Campo, J. (2006), *Neutron diffraction as a tool to monitor the establishment of the electro-osmotic flux during realkalisation of carbonated concrete*. *Physica B*. 385– 386:26–528. <https://doi.org/10.1016/j.physb.2006.05.263>
- Chatterji, S. (1994), *Simultaneous chloride removal and realcalisation of old concrete structures*. *Cement and Concrete Research* 24. No. 6. pp. 1051 -1054. DOI: [10.1016/0008-8846\(94\)90028-0](https://doi.org/10.1016/0008-8846(94)90028-0)
- CYTED – DURAR. *Manual de Inspección, Evaluación y Diagnóstico de Corrosión en Estructuras de Hormigón Armado*. Reporte Final, Red Durar, CYTED, Maracaibo, (1997).
- Fajardo, G., Escadeillas G., Arliguie, G. (2006), *Electrochemical chloride extraction (ECE) from steel reinforced concrete specimens contaminated from artificial seawater*. *Corrosion Science* 48, pp: 110-125. <https://doi.org/10.1016/j.corsci.2004.11.015>
- Del Valle Moreno, A., Pérez-López T., Martínez Madrid, M. (2001), *El fenómeno de la corrosión en estructuras de concreto reforzado*. Publicación Técnica No. 182, Secretaría de Comunicaciones y Transportes, Instituto Mexicano del Transporte, Sanfandila, Querétaro.
- González Díaz, F. (2010), *Realcalinización electroquímica del concreto reforzado carbonatado: una opción de prevención contra la corrosión*. Doctorado thesis, Universidad Autónoma de Nuevo León.
- González, F., Fajardo, G., Arliguie, G., Juárez, C. A., Escadeillas, G. (2011), *Electrochemical Realkalisation of Carbonated Concrete: An Alternative Approach to Prevention of Reinforcing Steel Corrosion*. *International Journal of Electrochemical Science*. 6. pp 6332 – 6349.
- Helene, P., Monteiro, J. (1994), *Can local repairs be durable solutions for steel corrosion in concrete structures*. *Annals of international Conference on Corrosion and Corrosion Protection of Steel in Concrete*, Vol. 2.
- Linares, D., Sánchez, M. (2003), *Construction, operation and performance of a chamber for tests*

- of accelerated carbonation. *Rev. Tec Ing. Univ Zulia*, 26, 34-44.
- Mietz, J. (1995), *Electrochemical realkalisation for rehabilitation of reinforced concrete structures*. *Materials and corrosion*. 46(9), 527-533. <https://doi.org/10.1002/maco.19950460904>
- Mietz, J. (1998), *Electrochemical rehabilitation methods for reinforced concrete structures a state of the art report*. EFC N°24, IOM Communications Ltd, London.
- NACE (2007), *SP0107-2007 Electrochemical Realkalization and Chloride Extraction for Reinforced Concrete*
- Normas mexicanas del ONNCCE (2018), *NMX-C-111-ONNCCE-2018 Industria de la Construcción-Agregados para concreto hidráulico-Especificaciones y métodos de ensayo*.
- Normas mexicanas del ONNCCE (2017), *NMX-C-414-ONNCCE-2017 Industria de la Construcción - Cementantes Hidráulicos - Especificaciones y Métodos de Ensayo*.
- Normas mexicanas del ONNCCE (2015), *NMX-C-495-ONNCCE-2015 Industria de la Construcción - Durabilidad de Estructuras de Concreto Reforzado - Medición de Potenciales de Corrosión del Acero de Refuerzo sin Revestir, Embebido en Concreto - Especificaciones y Método de Ensayo*.
- Normas mexicanas del ONNCCE (2018), *NMX-C-553-ONNCCE-2018 Industria de la construcción - Concreto - Durabilidad - Métodos Electroquímicos de Rehabilitación (Intervención) Especializados (Recalcinización y Remoción de Cloruros) - Especificaciones y Métodos de Ensayo*
- Norma ACI 211.1. *Diseño de mezcla de concreto patrón*.
- Pollet, V., Dieryck, V. (2000), *Re - alkalization: specification for the treatment application and acceptance criteria*. Annual Progress Report, 1999 - 2000, COST 521, Workshop, Belfast, p. 271.
- Raharinaivo and Carpio, J. (1992). *The stepping down the current method: a new corrosion control for cathodic protection of steel*. Paper No. 228, NACE Conference Corrosion 92, Nashville USA, p. 9.
- Hussain, R. R., Tetsuya, I. (2011), *Enhanced electro-chemical corrosion model for reinforced concrete under severe coupled actions of chloride and temperature*. *Construction and Building Materials Journal*. Vol. 25, Issue 3. pp. 1305-1315, Elsevier, ISI. <https://doi.org/10.1016/j.conbuildmat.2010.09.014>
- Redaelli, E., Bertolini, L. (2011), *Electrochemical repair techniques in carbonated concrete. Part I: electrochemical realkalisation*. *J Appl Electrochem* 41, 817–827. DOI:[10.1007/s10800-011-0301-4](https://doi.org/10.1007/s10800-011-0301-4)
- Ribeiro, P. H. L. C., Meira, G. R., Ferreira, P. R. R., Perazzo, N. (2013), *Electrochemical Realkalisation of Carbonated Concretes – Influence of Material Characteristics and Thickness of Concrete Reinforcement Cover*. Elsevier. *Construction and Building Materials* 40. 280-290. <https://doi.org/10.1016/j.conbuildmat.2012.09.076>
- Rincón, T., Rincón, O. (1994), *Electrochemical evolution of mortar based on acrylic and epoxy resins used to repair concrete structures*. 1st Mexican Symposium and 2nd International Workshop on Metallic Corrosion, Mérida, México.
- Tong, Y., Bouteiller, V., Marie-Victoire, E. Joiret, S. (2012). *Efficiency Investigations of Electrochemical Realkalisation Treatment Applied to Carbonated Reinforced Concret. Part I: sacrificial anode process*. *Cem. Concr. Res.* 42 (1), 84-94. DOI:[10.1016/j.cemconres.2011.08.008](https://doi.org/10.1016/j.cemconres.2011.08.008)
- Tuutti, K. (1982). *Corrosion of steel in concrete*. Report 4.82, The Swedish Cement and Concrete Association, Stockholm.
- UNE-EN 1504 Norma de productos y sistemas para la protección y reparación de estructuras de hormigón.
- Yeih, W., Chang, J. J. (2005), *A study on the efficiency of electrochemical realkalisation of carbonated concrete*. *Construction and Building Materials* 19. 516-524 p. <https://doi.org/10.1016/j.conbuildmat.2005.01.006>

Influence of unserviceable tires' rubber on the mechanical performance of hot mix asphalt

C. G. L. Nunes^{1*} , P. H. S. Pereira² , R. A. Melo³ ,
J. K. G. Rodrigues⁴ , L. C. F. L. Lucena⁴ 

*Contact author: camilagluznunes@gmail.com

DOI: <https://doi.org/10.21041/ra.v12i3.575>

Reception: 23/12/2021 | Acceptance: 08/07/2022 | Publication: 01/09/2022

ABSTRACT

This work aimed to optimize the production of hot mix asphalt (HMA) from the use of asphalt-rubber. For that, the mechanical performance of asphalt mixtures produced with different binders was evaluated: commercial asphalt-rubber (AR08), asphalt crumb rubber 10% (AR10) and 15% (AR15), and conventional asphalt (PEN 50-70). For the composition of these mixtures, the optimum asphalt contents were defined by the Marshall design. To carry out the mechanical tests, specimens molded with Marshall and Superpave compactors were tested. From the results obtained, it was verified that AR08 and AR10 asphaltic mixtures, compacted with Superpave, carried out the best mechanical performance. However, the AR08 binder is already available on the market, which facilitates its usage in paving works.

Keywords: hot mix asphalt; asphalt-rubber; *Marshall*; *Superpave*.

Cite as: Nunes, C. G. L., Pereira, P. H. S., Melo, R. A., Rodrigues, J. F. K. G., Lucena, L. C. F. L. (2022), "Influence of unserviceable tires' rubber on the mechanical performance of hot mix asphalt", Revista ALCONPAT, 12 (3), pp. 362 – 37, DOI: <https://doi.org/10.21041/ra.v12i3.575>

¹ Ph.D. student of the Graduate Program in Civil and Environmental Engineering, Federal University of Paraíba, João Pessoa, Brazil.

² Master's student of the Graduate Program in Civil and Environmental Engineering, Federal University of Paraíba, João Pessoa, Brazil.

³ Department of Civil Engineering, Federal University of Paraíba, João Pessoa, Brazil.

⁴ Department of Civil Engineering, Federal University of Campina Grande, Campina Grande, Brazil.

Contribution of each author

In this work, the 1st author contributed to the conceptualization (50%), experimentation (60%), analysis (100%) and writing of the original draft (100%). The 2nd author contributed to the experimentation activity by 40%. The 3rd author contributed to the conceptualization (50%), orientation (100%) and writing - review and editing (70%). The 4th author contributed resources for the experiments (50%). The 5th author contributed to the writing - review and editing (30%) and resources for the experiments (50%).

Creative Commons License

Copyright 2022 by the authors. This work is an Open-Access article published under the terms and conditions of an International Creative Commons Attribution 4.0 International License ([CC BY 4.0](https://creativecommons.org/licenses/by/4.0/)).

Discussions and subsequent corrections to the publication

Any dispute, including the replies of the authors, will be published in the third issue of 2023 provided that the information is received before the closing of the second issue of 2023.

Influencia del caucho de desecho de neumáticos en el rendimiento mecánico de mezclas asfálticas en caliente

RESUMEN

Este trabajo tuvo como objetivo optimizar la producción de mezclas asfálticas en caliente utilizando caucho asfáltico. Para ello, se evaluó el desempeño mecánico de mezclas asfálticas producidas con diferentes aglutinantes: asfalto caucho comercial (AC08), asfalto caucho 10% (AC10) y 15% (AC15) de residuos de caucho y asfalto convencional (PEN 50-70). Para la composición de estas mezclas, el contenido óptimo de asfalto fue definido por el método Marshall. Para la realización de las pruebas mecánicas se ensayaron probetas moldeadas con compactadores Marshall y Superpave. De los resultados obtenidos se encontró que las mezclas con AC08 y AC10, compactadas con Superpave, presentaron el mejor desempeño mecánico. Sin embargo, el ligante AC08 ya está disponible en el mercado, lo que facilita su uso en trabajos de pavimentación.

Palabras clave: mezcla asfáltica en caliente; asfalto de caucho; *Marshall*; *Superpave*.

Influência da borracha de pneus inservíveis no desempenho mecânico de misturas asfálticas a quente

RESUMO

Este trabalho teve como objetivo otimizar a produção de misturas asfálticas a quente a partir da utilização de asfalto-borracha. Para isso, avaliou-se o desempenho mecânico de misturas asfálticas produzidas com diferentes ligantes: asfalto-borracha comercial (AB08), asfalto-borracha 10% (AB10) e 15% (AB15) de resíduos de borracha e asfalto convencional (PEN 50-70). Para a composição dessas misturas, os teores ótimos de asfalto foram definidos pela dosagem Marshall. Já para a realização dos ensaios mecânicos, foram ensaiados corpos de prova moldados com compactadores Marshall e Superpave. Pelos resultados obtidos, constatou-se que as misturas com AB08 e AB10, compactadas com o Superpave, apresentaram o melhor desempenho mecânico. Porém, o ligante AB08 já está disponível no mercado, o que facilita seu uso em obras de pavimentação.

Palavras-chave: mistura asfáltica a quente; asfalto-borracha; *Marshall*; *Superpave*.

Legal Information

Revista ALCONPAT is a quarterly publication by the Asociación Latinoamericana de Control de Calidad, Patología y Recuperación de la Construcción, Internacional, A.C., Km. 6 antigua carretera a Progreso, Mérida, Yucatán, 97310, Tel.5219997385893, alconpat.int@gmail.com, Website: www.alconpat.org

Reservation of rights for exclusive use No.04-2013-011717330300-203, and ISSN 2007-6835, both granted by the Instituto Nacional de Derecho de Autor. Responsible editor: Pedro Castro Borges, Ph.D. Responsible for the last update of this issue, Informatics Unit ALCONPAT, Elizabeth Sabido Maldonado.

The views of the authors do not necessarily reflect the position of the editor.

The total or partial reproduction of the contents and images of the publication is carried out in accordance with the COPE code and the CC BY 4.0 license of the Revista ALCONPAT.

1. INTRODUCTION

Unserviceable tires are used tires that cannot be reused after retread because they present irreparable structural damages. These tires are related to one of the biggest and most problematic sources of waste. A great volume of tires is produced every year and it takes tires a long time to decompose. In addition, unserviceable tires become threats to human health and the environment when they are inadequately disposed of (Lo Presti, 2013).

In Brazil, there is a high reliance on highways for transporting freight and people. It boosts the tire market and, consequently, the generation of tire waste. Furthermore, this dependency increases the operating costs of transportation, accelerates pavement wear and the need for preservation and maintenance. Based on this, the utilization of asphalt-rubber in paving is a practicable alternative not only to protect the environment but also to reduce the transportation operational costs in the country.

The asphalt-rubber presents numerous advantages in comparison to the standard asphalt, such as lower penetration index, flexibility and ductility under low temperatures, greater resistance to permanent deformation, greater resistance to the appearance of cracks under low temperatures, and greater resistance to fatigue (Yetkin, 2007; Palit et al., 2004; Xiang et al., 2009). Other advantages include greater lifespan, lower conservation and maintenance costs, reduction of the asphalt mixture aging, and reduction of traffic noise (Sol-Sánchez et al., 2020; Lee et al., 2008; Navarro et al., 2004; Chiu and Lu, 2007; Bueno et al., 2014; Ding et al., 2017).

Despite the benefits, asphalt-rubber is not widely accepted and used yet. This occurs due to two reasons. First, there is a lack of professional training in terms of mastering the various techniques and fully understanding some variables (e.g., rubber content, dimensions of the rubber particles, rubber surface and storage). Second, there are no local public policies that encourage the usage of asphalt-rubber (Lo Presti, 2013; Picado-Santos et al., 2020).

The use of asphalt-rubber is still low at Brazil. In the country, there is a lack of specialized labor (Thives, 2009) and public policies that encourage the use of this material. Thus, one of the objectives of this study was to evaluate the mechanical performance of hot mix asphalt (HMA). The mixtures were produced with four types of binder: (i) commercial asphalt-rubber (AR08), (ii) asphalt-rubber 10% (AR10), and (iii) 15% (AR15) both produced in a laboratory from crumb rubber, and (iv) conventional asphalt, i.e., asphalt binder penetration grade of 50-70 (PEN 50-70), which is usual for paving in Brazil. In addition, it was also aimed to analyze the effectiveness of the dominant aggregate size range (DASR), method for predicting permanent deformation on asphalt mixtures, as well as analyzing the influence of the compaction method (Marshall or Superpave) on the mechanical performance of the mixtures.

The Brazilian way to select the grain size of asphalt mixtures follows the standard guidelines from National Department of Transportation Infrastructure (DNIT, in Portuguese) that recommend a procedure to fit the aggregates in one of the granulometric ranges. This method consists of a trial-and-error procedure in which the proportions of the aggregates that make up the mixture are adjusted so that the limits are within these ranges. Therefore, this method does not take into account the effects of aggregate distribution on the mechanical behavior of asphalt mixtures. This may result in mixtures with lower stability and lower resistance to permanent deformation. Therefore, the concept of DASR porosity was used in this study to evaluate the permanent deformation of asphalt mixtures.

The DASR is a rational method to select the granulometric composition of the asphalt mixtures. The method is simple to apply and only uses a single parameter, the DASR porosity, which does not depend on the asphalt mixture's maximum nominal size. Under this method, mixtures with porosity greater than 50% do not provide good interaction between the aggregates, which would make these mixtures less resistant to permanent deformation. Previous studies show the efficiency

of applying this method to obtain proper dosage design with a lower propensity to developing permanent deformation (Greene et al., 2014; Kim et al., 2009). Therefore, the DASR method was used to verify the efficiency of choosing the composition of the aggregates' matrix.

In this work, the optimum asphalt content was determined using the Marshall design, since this method is still the most commonly used in Brazil. Later on, to carry out the mechanical tests, specimens were molded with Marshall and Superpave compactors. In previous studies with other materials, which also used these two compactations, it was found that specimens compacted with Superpave tend to present better results in mechanical tests. These better results are usually attributed to the greater efficiency of the crushing compaction used by the Superpave, than the impact compaction used in the Marshall (Assis et al., 2017). Thus, in this work, the results obtained with the two forms of compaction were compared.

2. PROCEDURE

2.1 Materials

This study followed an experimental procedure that began with the collection of materials: PEN 50-70, AR08, granite aggregate, and crumbled tire rubber. These materials were donated by companies in the Northeast and Southeast. The rubber had a density of 0.99 g/cm³. A preliminary screening was performed to remove coarse particles that could affect the homogeneity of the mixture with the conventional binder. ASTM D6114/D6114M-19 recommends not using very coarse rubber particles. Therefore, in this study, the particle sizes varied between 0.15 and 0.59 mm.

2.2 Production of asphalt-rubber

In the production of the asphalt-rubber in a laboratory, 10% and 15% of the conventional asphalt content were replaced by rubber, so carried out AR10 and AR15 binders. For these binders, rubber was added to the conventional asphalt in a mechanical mixer at a constant rotation of 2,000 rpm and a temperature of 170 °C for one hour. The AR10, AR15, PEN 50-70, and AR08 binders were tested to determine their physical properties. These tests included penetration, softening point, rotational viscosity, elastic recovery, and storage stability. In addition, aggregate properties tests were performed, including particle size, absorption, density, durability, Los Angeles abrasion, and sodium sulfate soundness. The tests were performed in accordance with DNIT standards.

2.3 Asphalt mixture design

2.3.1 Granulometric composition selection

To determine the granulometric composition of the aggregate, the experimental method was used to fit the mixture into the "C" range of DNIT. The DASR porosity was also calculated to estimate whether the selected aggregate size would give the mixture good resistance to permanent deformation. Before calculating the DASR porosity, the aggregates that make up the DASR mixture were selected. The DASR method suggests the use of an interaction diagram to select the aggregates. Two types of aggregates should be selected: (i) with a particle size greater than 1.18 mm and (ii) with a ratio of percent retained material between successive sieves of 0.43 and 2.33 mm. The porosity was calculated according to equation (1).

$$\eta_{DASR} = \frac{VIC_{ag} + VMA}{VTM - V_{ag>DASR}} \quad (1)$$

Where η_{DASR} is the DASR porosity (%), VIC_{ag} is the volume of aggregate below the DASR; VMA is the voids in the mineral aggregate; VTM is the total volume of the mixture; $V_{ag>DASR}$ is the volume of aggregate above the DASR.

2.3.2 Selection of the Optimum Asphalt Content

The Marshall mix design was used to determine the optimum asphalt content. Cylindrical specimens were shaped and compacted with 75 blows on each side (DNER ME-043/95 Brazilian standard). Three parameters were selected to determine the optimum asphalt content: volume of voids, maximum bulk density, and maximum stability. Four dosages (i.e., one for each binder) were performed in total.

To produce the asphalt mixture with PEN 50-70, the aggregates were heated at 165 °C for 24 hours and mixed with the binder at 155 °C. To mix the three asphalt-rubber types, the aggregates were heated at 175 °C for 24 hours and mixed with the binder at 165 °C. These temperatures were determined by the rotational viscosity Brookfield test, which were determined to four binder types.

2.3.3 Mechanical Tests

To evaluate the mechanical performance, the asphalt mixtures were tested by the indirect tensile strength test (ITS), the resilient modulus test (RM), the moisture susceptibility, and the flow number (FN). The tests were performed with specimens produced by Marshall and Superpave compactors. Each test was conducted three times to analyze the accuracy of the results. Table 1 shows the standards that were followed to perform the tests.

Table 1. Standards for the mechanical tests

Test	Standard
Indirect tensile strength test	DNIT ME 136/2010
Resilient modulus	DNIT 135/2018-ME
Moisture susceptibility	AASHTO T 283/2002
Flow number	NBR 16505/2016

3. RESULTS AND DISCUSSIONS

3.1 Physical Properties

Table 2 shows the results for the physical properties of the aggregates. The acceptance criteria are based on the DNIT ES 031/2006 standard for flexible pavements.

Table 2. Physical properties of natural aggregates.

Properties	Test values	Criteria
Los Angeles abrasion (%)	27.53	Max. 50
Sodium sulfate soundness (%)	1	Max. 12
Absorption (%)		-
3/4" crushed stone	0.51	
3/8" crushed stone	0.79	
Crushed dust Bulk specific gravity (g/cm ³)		-
3/8" crushed stone	2.67	
3/4" crushed stone	2.63	
Crushed dust	2.64	

According with the Table 2, the physical properties of the granite aggregate meet the criteria of the Brazilian standards. Therefore, the aggregate can be used to construct flexible pavements.

Table 3 shows the physical properties of the binders. For the PEN 50-70, the DNIT standards were followed for each test, except for the viscosity test. For this test, the criteria established in ASTM D4402 were followed. For the asphalt-rubber binders, the specifications in DNIT ES 111/2009 were followed.

Table 3. Physical properties of asphalt binders.

Tests	Asphalt Binders				Standard Conventional Asphalt	Standard Asphalt-Rubber
	PEN 50-70	AR10	AR15	AR08		
Penetration (10^{-1} mm)	69	44	36	45	50 – 70	30-70
Softening point ($^{\circ}$ C)	51	62	64	62	Min. 46	Min. 55
Brookfield Viscosity 135GC-SP21 (cP)	395	2,106	3,667	2,085	Min. 274	-
Brookfield Viscosity 150GC-SP21 (cP)	203	1,132	1,735	1,096	Min. 112	-
Brookfield Viscosity 177GC-SP21 (cP)	79	578	819	562	57 – 285	-
Elastic Recovery (%)	0	57	39	61	-	Min. 50
Storage Stability ($^{\circ}$ C)	0.5	5.0	8.5	5.5	-	Max. 9

According with the Table 3, PEN 50-70, AR08 and AR10 binders meet the Brazilian standards. Then, the binders can be used in the production of hot mix asphalt. The AR15 binder cannot be used because it does not meet the minimum requirements for elastic recovery testing. However, in this study, the test procedure using AR15 was retained in order to evaluate the mechanical performance of asphalt mixtures produced with this binder.

3.2 Granulometric composition of the mixtures

Figure 1 shows the results of the granulometric composition of the asphalt mixture. The gradation curve is composed of: (1) 21% crushed stone 3/4", (2) 30% crushed stone 3/8", and 49% crushed dust. This composition was used for the four asphalt mixtures. A trial procedure was used so that the gradation curve could fit into the limits of the "C" range, which is specified at DNIT ES 031/2006.

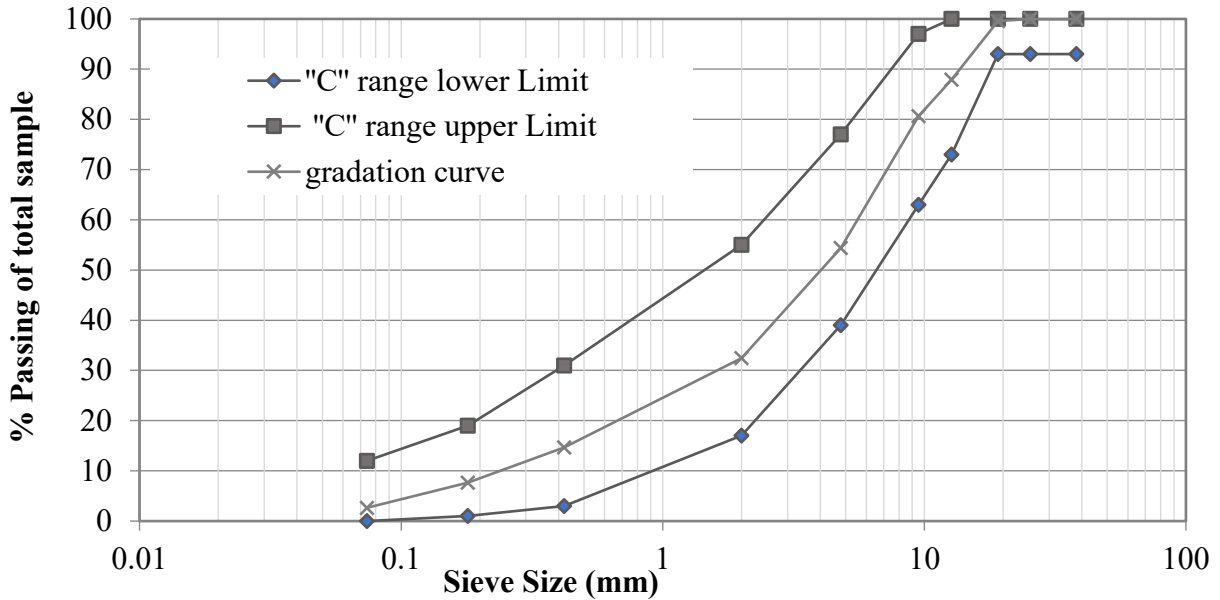


Figure 1. Gradation curve of mixtures.

The granulometric composition was tested by the DASR method to evaluate whether the asphalt mixtures had great resistance to permanent deformation. The interaction diagram was built to apply the DASR method, which is exhibited in Figure 2. This diagram enabled the definition of the coarse aggregate ranges that would compose the DASR.

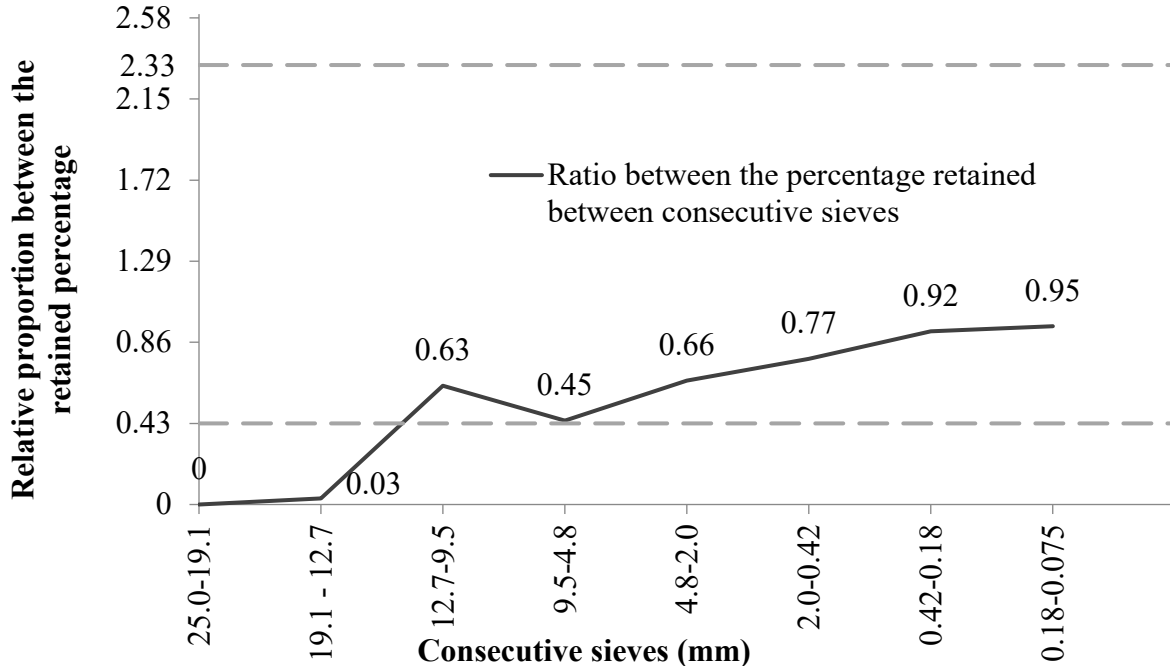


Figure 2. Diagram of interaction between aggregates

In accordance with the Figure 2, the 12.7-9.5, 9.5-4.8, and 4.8-2.0 mm ranges have aggregate with grain sizes greater than 1.18 mm. In addition, the ratio between the percent retained between consecutive sieves ranges from 0.43 to 2.33. The range of 9.5-4.8 mm had a ratio between the percent retained between consecutive sieves that was very close to the minimum estimated value

for good interaction between aggregates. Therefore, this value was not considered in the DASR selection. To select the ranges of 12.7-9.5 and 4.8-2.0 mm, the DASR porosity was calculated for each range using equation (1).

To calculate the VMA in Eq. (1), values for air voids (AV) and voids filled with asphalt (VFA) were assumed based on the limits required for these parameters in the standard DNIT ES 031/2006. According to this standard, asphalt mixtures to be used for wearing course must have an AV between 3 and 5% and a VFA between 75 and 82%. In this work, the average values of these limits (AV of 4% and VFA of 79%) were used to calculate the VMA. An approximate value VMA of 19% was obtained.

For the η_{DASR} , the following results were obtained: 53% for the range of 12.7-9.5 and 39% for the range of 4.8-2.0 mm. Therefore, only the range of 4.8-2.0 mm had a η_{DASR} of less than 50%. This is considered to be the minimum porosity for mixes that exhibit high resistance to permanent deformation. Therefore, this range was used to calculate the DASR. Since the particle size distribution curve provided by the DNIT methods showed a η_{DASR} value of less than 50%, the aggregate composition did not need to be adjusted.

3.3 Marshall Mix Design

Table 4 shows the results by Marshall mix design for the four binder types.

Table 4. Parameters obtained by the Marshall mix design.

Properties	Asphalt Binders				Standard Conventional Asphalt	Standard Asphalt Rubber
	PEN 50-70	AR10	AR15	AR08	DNIT ES 031/2006	DNIT ES 112/2009
Optimum asphalt content (%)	5.2	6.8	7.0	6.2	-	-
Marshall Stability (kgf)	1,163	1,374	806	1,351	> 500	> 800
Bulk Density (g/cm ³)	2.31	2.27	2.21	2.26	-	-
AV (%)	3.86	4.99	4.87	4.92	3-5	3-5
VMA (%)	17	20	23	20	Min.16	Min.13
VFA (%)	77	74	78	75	75-82	65-78

Table 4 shows that the majority of mixtures with asphalt-rubber have higher Marshall stability than the conventional binder. According to Setyawan et al. (2017), rubber provides better interlocking and bonding between the aggregates and the asphalt binder, which increases the stability of the mixes. Therefore, it was expected that the asphalt-rubber mixtures would give better results. For the mixture with the AR15 binder, it was also expected that the mixtures with this type of binder would not have as good mechanical performance as the other asphalt-rubber mixtures. This binder does not meet all of the required physical criteria. The lower Marshall stability and density of the AR15 mix are related to the higher rubber content and lower homogeneity of this binder. These factors led to a volumetric expansion of the specimens. Consequently, they promoted the reduction of density and stability in this mixture.

Despite the reduction in stability with the AR15 binder, Table 4 shows that all the mixes met the standard Brazilian criteria in terms of Marshall mix design. The DASR porosity was calculated for each mixture after the volumetric parameters were determined. The results are exhibited in Table 5.

Table 5. η_{FAD} after Marshal dosage.

Binder Designation	VMA (%)	η_{FAD} (%)	Criteria
PEN 50-70	17	36	<50%
AR10	20	40	
AR15	23	44	
AR08	20	40	

Table 5 shows that the mixtures with AR10 and AR08 binders had η_{DASR} close to the estimated value of 39% (before dosage). The other mixtures showed greater variability for the estimated η_{DASR} value. This was due to greater variability between the post-dosage VMA values and the estimated VMA value of 19%. Despite the differences, the estimates were acceptable with respect to the DASR method, as all mixtures had a η_{DASR} value of less than 50%.

3.4 Mechanical Tests

3.4.1 Indirect Tensile Strength (ITS)

Figure 3 shows the results of the indirect tensile strength test for Marshall and Superpave methods.

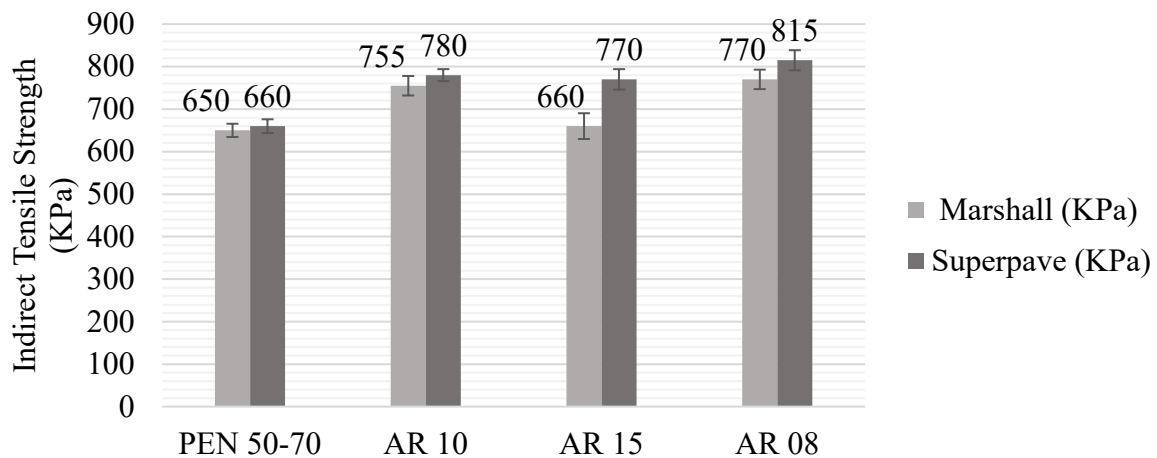


Figure 3. ITS results of mixtures.

Figure 3 shows that the mixtures exhibited greater ITS when compacted by the Superpave method. This result was expected since the Superpave method better replicates field conditions and has a lower risk of altering the granulometric composition of the aggregates.

The mixture with the PEN 50-70 binder met the minimum tensile strength of 650 kPa (i.e., according to the standard DNIT ES 031/2006), for both the Marshall and Superpave methods. For asphalt-rubber mixtures, DNIT ES 112/2009 requires a minimum tensile strength of 750 kPa. This limit was met by all mixes, except for the AR15 mix, which was compacted using the Marshall method.

For the AR15 mix, the results of the indirect tensile strength test and the Marshall stability may have been influenced by the higher rubber content. The storage stability gave a result close to the maximum value allowed by the standards. This indicates that the higher rubber content leads to lower adhesion between the rubber and the binder, which reduces the cohesion and homogeneity of the mixture (Navarro et al., 2004; Navarro et al., 2005; Shen et al., 2009; Dantas Neto et al., 2006; Navarro and Gámez, 2012). This leads to lower values in tensile strength and stability (Navarro and Gámez, 2012).

3.4.2 Resilient Modulus Test (RM)

Figure 4 shows the results for the Resilient Modulus Test using Marshall and Superpave methods.

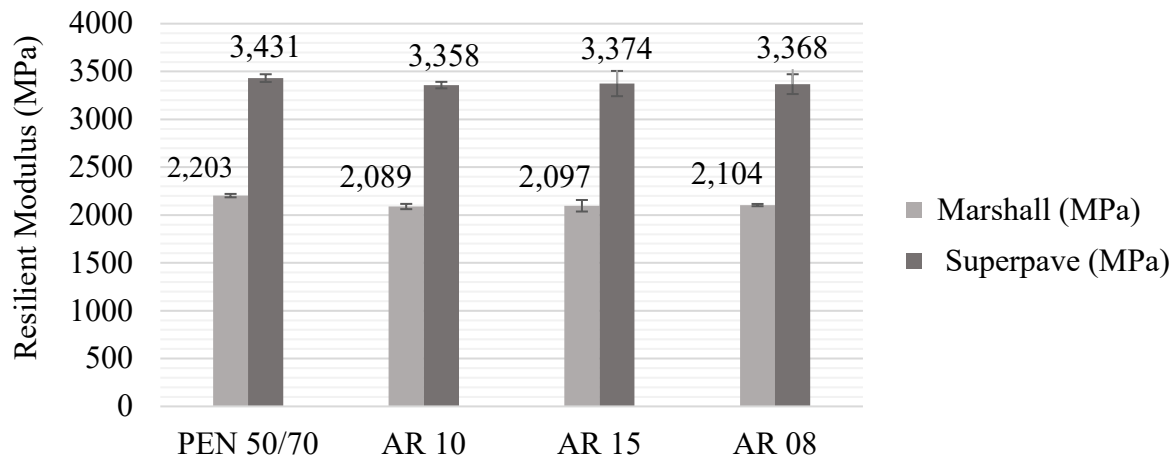


Figure 4. RM results of mixtures.

Figure 4 shows that the asphalt-rubber mixtures have lower RM values when both methods are considered. The reduction of RM is related to the greater elasticity of the asphalt-rubber mixtures. At low temperatures, these mixtures generally exhibit a decrease in resilient modulus than conventional mixtures. On the other hand, as the temperature increases, the value of the modulus tends to become higher. This results in the mixtures being less susceptible to brittle fracture and more flexible at low temperatures and exhibiting higher stiffness than conventional mixtures at higher temperatures (Palit et al., 2004). Therefore, the reduction in resilient modulus with asphalt-rubber does not mean that these mixtures have lower mechanical performance (than the mixture with PEN 50-70).

3.4.3 Moisture Susceptibility

Figure 5 shows the results of the moisture susceptibility test.

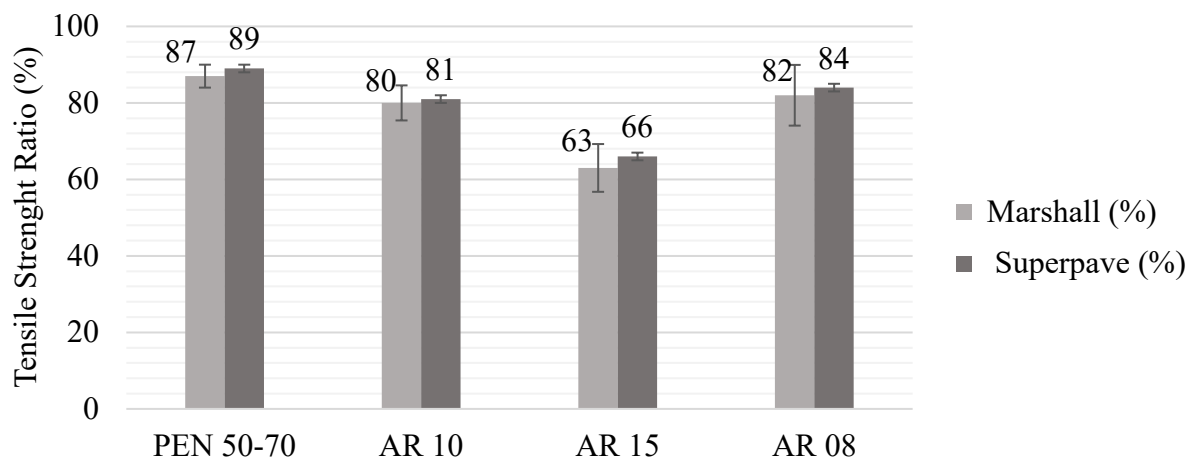


Figure 5. Moisture susceptibility results of mixtures.

Figure 5 shows that all of the mixtures, with the exception of the AR15 mixture, met the minimum TSR requirement of 80% as specified in AASHTO T 283/2002. Lower TSR values were obtained for the mixtures containing the asphalt-rubber binder. The California Department of Transportation

noted that dense mixtures with the asphalt-rubber binder are more susceptible to moisture effects than conventional mixtures. Therefore, the use of anti-stripping additives in these mixtures is recommended (Shatnawi, 2001).

In this study, an anti-stripping additive was used in all mixtures. The AR10 and AR08 mixtures were highly moisture susceptible, although the results were lower than those of the PEN 50-70 mixture, and the use of the additive in the AR15 mixture was not sufficient to achieve the minimum 80% recommended by the standards. This indicates a greater susceptibility to moisture damage in this mixture.

3.4.4 Flow Number (FN)

Figure 6 shows the results of the FN tests for the mixtures using the Superpave method.

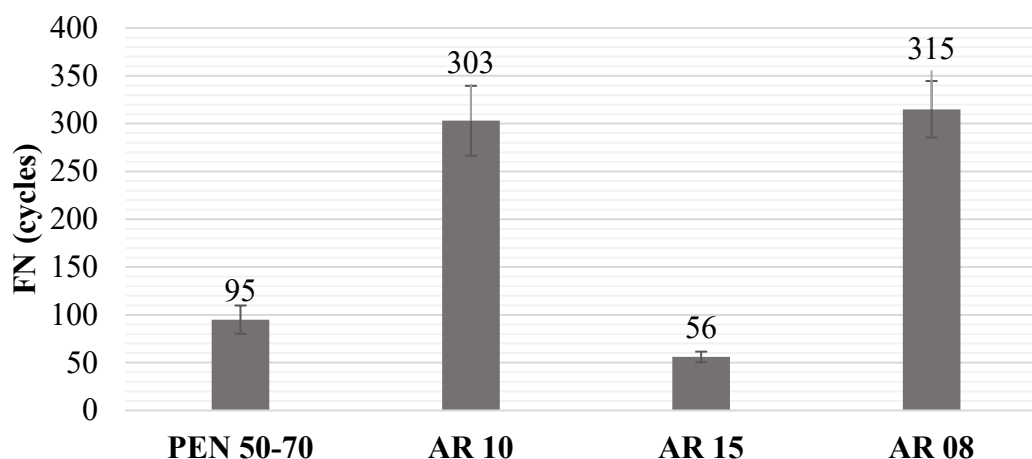


Figure 6. FN results of mixtures.

Figure 6 shows that the mixes with the AR10 and AR08 binders have better results than mix with the conventional binder. This indicates greater resistance to permanent deformation for these mixes. The lower values for the AR15 mix were to be expected given the results of the other tests. They showed that the higher rubber content and lower homogeneity negatively affected the mechanical performance of this mix.

4. STATISTICAL ANALYSIS

Analysis of variance (ANOVA) is a statistical method that allows comparisons between means of different populations. Therefore, it was used in this study to compare the performance of the different mixtures for each of the tests. For ANOVA, mixture type (or binder type in the case of the physical tests) was the explanatory variable. Four levels (treatments) were considered: PEN 50-70, AR08, AR10, and AR15. In addition, a significance level of 5% was assumed to test two hypotheses:

H_0 : The mean values of the treatments are equal;

H_1 : At least one of the mean values of the treatments is different from the others.

The null hypothesis is rejected if the p-value is less than or equal to the significance level. After this test, Tukey's test was applied to determine whether the pairs of treatments were significantly different or not. The results of the Tukey test are shown in Tables 6, 7, and 8 for the physical tests, the mechanical tests using the Marshall method, and the mechanical tests using the Superpave method, respectively.

Table 6. Tukey test results for physical tests.

Treatment		p-value - comparing pairs of means (ij)				
(i)	(j)	Penetration	Softening Point	Brookfield Viscosity	Elastic Recovery	Storage Stability
PEN 50-70	AR08	0.00000	0.00033	0.00000	0.00000	0.00171
	AR10	0.00000	0.00033	0.00000	0.00000	0.00336
	AR15	0.00000	0.00000	0.00000	0.00000	0.00006
AR08	AR10	0.91770	1.00000	0.28040	0.39200	0.93380
	AR15	0.00010	0.55530	0.00000	0.00000	0.03246
AR10	AR15	0.00018	0.55530	0.00000	0.00030	0.01464

* The mean difference is significant at the .05 level.

Table 7. Tukey test results for mechanical tests with the Marshall method

Treatment		p-value - comparing pairs of means (ij)		
(i)	(j)	ITS	RM	Moisture Susceptibility
PEN 50-70	AR08	0.00114	0.03360	0.71820
	AR10	0.00272	0.01633	0.48400
	AR15	0.95610	0.02392	0.00401
AR08	AR10	0.86120	0.94980	0.97230
	AR15	0.00198	0.99430	0.01556
AR10	AR15	0.00495	0.99160	0.02776

* The mean difference is significant at the .05 level.

Table 8. Tukey test results for mechanical tests with the Superpave method

Treatment		p-value - comparing pairs of means (ij)			
(i)	(j)	ITS	RM	Moisture Susceptibility	FN
PEN 50-70	AR08	0.00006	0.81640	0.42600	0.00002
	AR10	0.00036	0.74480	0.12140	0.00003
	AR15	0.00066	0.85530	0.00035	0.28970
AR08	AR10	0.21800	0.99900	0.77230	0.93140
	AR15	0.09347	0.99980	0.00184	0.00000
AR10	AR15	0.92500	0.99580	0.00539	0.00000

* The mean difference is significant at the .05 level.

Tables 6, 7, and 8 show that the null hypothesis was rejected for all tests, except the Resilient Modulus using the Superpave method (i.e., there were significant differences between the means of the treatments). Also, the AR08 and the AR10 binders, as well as the mixtures with these binders did not have significantly different mean values (i.e., p-values greater than 0.05). This indicates that there are no statistically significant differences between the physical and mechanical properties of the two binders.

Table 6 shows that there were significant differences between the conventional binder (i.e., PEN 50-70) and the asphalt-rubber binders in all tests. This indicates that the asphalt-rubber binders have different physical properties than PEN 50-70, and it shows that the rubber changes the physical properties of the mixtures. No significant difference was expected in the performance of AR08, AR10, and AR15 binders. The AR15 binder did not meet the minimum requirements in the physical tests.

For the mechanical tests using the Marshall method, the results in Table 7 show that there were no significant differences in the tensile strength capacities for the mixes with the binders PEN 50-70 and AR15. Similarly, no differences were found between the results for moisture susceptibility of mixes with PEN 50-70, AR08, and AR10. Therefore, it can be said that the reduction of TSR in mixtures with AR08 and AR10 did not affect the moisture susceptibility of these mixtures. The opposite effect was observed in the resilient modulus test. In this test, the reduction in RM of asphalt-rubber mixtures than the PEN 50-70 mixture can be considered significant.

Table 8 shows that the results obtained with the Superpave method do not show significant differences in the RM test. Since this method simulates field conditions more efficiently than the Marshall method, it is assumed that asphalt-rubber mixtures at RM do not show large variations than the PEN 50-70 mixture. In the ITS and FN tests, it was found that there were significant differences between the PEN 50-70, AR08, and AR10 mixtures. Thus, it can be said that the increase in ITS and FN observed in the AR08 and AR10 mixes, was indeed relevant than the PEN 50-70 mix. When moisture susceptibility was tested, significant differences were only observed with the AR15 mixture. This was to be expected as this blend showed a greater reduction in moisture susceptibility.

5. CONCLUSIONS

The main objective of this study was to evaluate the mechanical performance of asphalt-rubber mixtures through laboratory tests used for the construction of flexible pavements. In this sense, after the statistical analysis carried out, it can be said that asphalt-rubber mixtures have better performances than the mixture PEN 50-70, which makes their use practicable. A greater elastic recovery, a lower thermal susceptibility, a greater tensile strength and the occurrence of permanent deformations can be cited mentioned as advantages of the mixtures AR08 and AR10 than the mixture PEN 50-70.

The AR15 binder could not be used in asphalt mixtures because it did not meet the elastic recovery requirements. However, in some tests, it performed similarly to conventional asphalt (i.e., PEN 50-70). Similar results were also obtained when testing the resilient modulus than the other asphalt-rubber types. Therefore, the performance of this mixture in all tests could be acceptable if an additive were used. An agent compatible with the AR15 binder could increase its homogeneity.

In all the tests, the AR10 and AR08 mixtures showed no significant differences. This means that no significant differences in the mechanical performance of these mixtures were found in this study. However, the AR08 is already produced on large scale, which makes it more attractive than the AR10 binder. The AR10 was produced in the laboratory for this study. Therefore, the use of the AR08 binder would be more suitable for road construction.

For granulometric selection, the DASR method estimates good mechanical performance for porosity values below 50%, but this estimate was not valid for the AR15 mix. However, the lower performance of this mix is most likely due to the lower quality of the AR15 binder (than the granulometric selection). Therefore, the use of the DASR method to predict the mechanical performance of mixtures in this study cannot be considered unacceptable. For the compaction method, the trend of previous studies was confirmed (Jitsangiam et al., 2013; Swami et al., 2004; Asi, 2007): the results for the Superpave method were better than the results for the Marshall method in all tests. Therefore, the Superpave method should be preferred for the compaction of asphalt mixtures.

6. ACKNOWLEDGEMENTS

The authors would like to thank the *Coordenação de Aperfeiçoamento de Pessoal de Nível Superior* (CAPES) and the *Conselho Nacional de Desenvolvimento Científico e Tecnológico* (CNPq) for the financial support, the company Greca Asfaltos, for the donation of asphalt rubber, and the company DAFONTE Pneus, for the donation of crushed rubber from tires. The authors also wish to express their appreciation to the laboratory technicians and colleagues who helped in the development of the research.

7. REFERENCES

- American Association of State Highway and Transportation Officials. (2002). *AASHTO T 283 Resistance of compacted asphalt mixtures to moisture induced damage*. Washington, D.C.
- Asi, I. M. (2007), *Performance evaluation of Superpave and Marshall asphalt mix designs to suite Jordan climatic and traffic conditions*. *Construction and Building Materials*. 21:1732–1740. <https://doi.org/10.1016/j.conbuildmat.2006.05.036>.
- Assis, S. R. H., Queiroz, B. O., Araújo, C. C., Nunes, K. K. F., Melo, R. A., Lucena L. C. F. L. (2017), *Evaluation of limestone crushed dust aggregates in hot mix asphalt*. *Construction and Building Materials*. 148: 659-665. <https://doi.org/10.1016/j.conbuildmat.2017.05.107>.
- Associação Brasileira de Normas Técnicas. (2016). *NBR 16505: Misturas asfálticas-Resistência à deformação permanente utilizando o ensaio uniaxial de carga repetida*. Rio de Janeiro.
- ASTM International. (2012). *ASTM 4402/D4402M Standard test method for viscosity determination of asphalt at elevated temperatures using a rotational viscometer*.
- ASTM International. (2019). *ASTM D6114/D6114M-19 Standard Specification for Asphalt-Rubber Binder*.
- Bueno, M., Luong, J., Terán, F., Viñuela, U., Paje, S.E. (2014), *Macrotecture influence on vibrational mechanisms of the tyre-road noise of an asphalt rubber pavement*. *International Journal of Pavement Engineering*. 15:606-613. <http://dx.doi.org/10.1080/10298436.2013.790547>.
- Chiu C., Lu, L. (2007), *A laboratory study on stone matrix asphalt using ground tire rubber*. *Construction and Building Materials*. 21:1027–1033. doi: 10.1016/j.conbuildmat.2006.02.005.
- Dantas Neto, S. A., Farias, M. M, Pais, J. C., Pereira, P. A. A., Sousa, J. B. (2006), *Influence of crumb rubber and digestion time on the asphalt rubber binders*. *Road Materials and Pavement Design*. 7:131–148. <https://doi.org/10.1080/14680629.2006.9690030>.
- Departamento Nacional de Infraestrutura de Transportes. (2009). *DNIT 112:2009-EM: Pavimentos flexíveis – Concreto asfáltico com asfalto borracha, via úmida, do tipo “Terminal Blending” - Especificação de serviço*. Rio de Janeiro.
- Departamento Nacional de Infraestrutura de Transportes. (2009). *DNIT 111:2009-EM: Pavimentação flexível-Cimento asfáltico modificado por borracha de pneus inservíveis pelo processo via úmida, do tipo “Terminal Blending” – Especificação de material*. Rio de Janeiro.
- Departamento Nacional de Infraestrutura de Transportes. (2006), *DNIT 031/2006 – ME– Método de ensaio. Pavimentos flexíveis - concreto asfáltico - especificação de serviço*. Rio de Janeiro.
- Departamento Nacional de Infraestrutura de Transportes. (1995). *DNER 043/1995–ME: Misturas Betuminosas a Quente. Ensaio Marshall – Método de Ensaio*. Rio de Janeiro.
- Departamento Nacional de Infraestrutura de Transportes. (2010). *DNIT 136/2010–ME: Método de Ensaio. Pavimentos flexíveis- Misturas asfálticas–Determinação da resistência à tração por compressão diametral*. Rio de Janeiro.
- Departamento Nacional de Infraestrutura de Transportes. (2018). *DNIT135/2018–ME: Pavimentação asfáltica – Misturas Asfálticas – Determinação do Módulo de Resiliência – Método de Ensaio*. Rio de Janeiro.

- Ding, X., Ma, T., Zhang, W., Zhang, D. (2017), *Experimental study of stable crumb rubber asphalt and asphalt mixture*. Construction and Building Materials. 157:975–981. <https://doi.org/10.1016/j.conbuildmat.2017.09.164>.
- Greene, J., Chun, S., Choubane, B. (2014), *Enhanced Gradation Guidelines to Improve Asphalt Mixture Performance*. Transportation Research Record: Journal of the Transportation Research Board. 2456: 3–10. <https://doi.org/10.3141/2456-01>.
- Jitsangiam, P., Chindapasirt, P., Nikraz, H. (2013), *An evaluation of the suitability of Superpave and Marshall asphalt mix designs as they relate to Thailand's climatic conditions*. Construction and Building Materials. 40:961–970. <https://doi.org/10.1016/j.conbuildmat.2012.11.011>.
- Kim, S., Roque, R., Birgisson, B., Guarin, A. (2009), *Porosity of the Dominant Aggregate Size Range to Evaluate Coarse Aggregate Structure of Asphalt Mixtures*. Journal of Materials in Civil Engineering. 21: 32–39. [https://doi.org/10.1061/\(asce\)0899-1561\(2009\)21:1\(32\)](https://doi.org/10.1061/(asce)0899-1561(2009)21:1(32))
- Lee, S., Akisetv, C.K., Amirkhanian, S. N. (2008), *Recycling of laboratory-prepared long-term aged binders containing crumb rubber modifier*. Construction and Building Materials. 22:1906–1913. <https://doi.org/10.1016/j.conbuildmat.2007.07.012>.
- Lo Presti, D. (2013), *Recycled Tyre Rubber Modified Bitumens for road asphalt mixtures: A literature review*. Construction and Building Materials. 49 863-881. <http://dx.doi.org/10.1016/j.conbuildmat.2013.09.007>.
- Navarro, F.J., Partal, P., Martínez-Boza F., Gallegos C. (2004), *Thermo-rheological behaviour and storage stability of ground tire rubber-modified bitumens*. Fuel. 83:2041–2049. <https://doi.org/10.1016/j.fuel.2004.04.003>.
- Navarro, F.J., Partal, P., Martínez-Boza F., Gallegos C. (2005), *Influence of crumb rubber concentration on the rheological behavior of a crumb rubber modified bitumen*. Energy & Fuels. 19:1984-1990. <https://doi.org/10.1021/ef049699a>
- Navarro, F. M., Gámez, M. C. R. (2012). *Influence of Crumb Rubber on the Indirect Tensile Strength and Stiffness Modulus of Hot Bituminous Mixes*. Journal of materials in civil engineering. 24(6):715–724. [https://doi.org/10.1061/\(ASCE\)MT.1943-5533.0000436](https://doi.org/10.1061/(ASCE)MT.1943-5533.0000436).
- Palit, S. K., Reddy, K. S., Pandey, B. B. (2004), *Laboratory Evaluation of Crumb Rubber Modified Asphalt Mixes*. Journal of Materials in Civil Engineering, 16(1): 45–53. [https://doi.org/10.1061/\(asce\)0899-1561\(2004\)16:1\(45\)](https://doi.org/10.1061/(asce)0899-1561(2004)16:1(45)).
- Picado-Santos, L.G., Capitão, S. D., Neves, J. M.C. (2020), *Crumb rubber asphalt mixtures: A literature review*. Construction and Building Materials. 247:118577. <https://doi.org/10.1016/j.conbuildmat.2020.118577>.
- Setyawan, A., Febrianto, N., Sarwono, D. (2017), *Design and Properties of Thin Surfacing Hot Mix Asphalt Containing Crumb Rubber as Partial Aggregate Replacement*. IOP Conf. Series: Earth and Environmental Science 75: 1-6. <https://doi.org/10.1088/1755-1315/75/1/012016>.
- Shatnawi, S. (2001), *Performance of Asphalt Rubber Mixes in California*. International Journal of Pavement Engineering. 2(1): 1-16. <http://dx.doi.org/10.1080/10298430108901713>.
- Shen, J., Amirkhanian, S., Xiao, F., Tang, B. (2009), *Influence of surface area and size of crumb rubber on high temperature properties of crumb rubber modified binders*. Construction and Building Materials. 23: 304–310. <https://doi.org/10.1016/j.conbuildmat.2007.12.005>.
- Sol-Sánchez, M., Jiménez del Barco Carrión, A., Hidalgo-Arroyo, A., Moreno-Navarro, F., Saiz, L., Rubio-Gámez, M. del C. (2020), *Viability of producing sustainable asphalt mixtures with crumb rubber bitumen at reduced temperatures*. Construction and Building Materials. 265:120154. <https://doi.org/10.1016/j.conbuildmat.2020.120154>.
- Swami, B.L.; Mehta, Y.A.; Bose, S. (2004), *A Comparison of the Marshall and Superpave Design Procedure for Materials Sourced in India*. International Journal of Pavement Engineering. 5(3):163-173. <http://dx.doi.org/10.1080/10298430412331309115>.

- Thives, L. P. (2009), “*Optimizing the performance of bituminous mixtures with rubber modified bitumen for pavement rehabilitation*”. Phd Thesis. University of Minho/ Federal University of Santa Catarina, p.581.
- Xiang, L., Cheng, J., Que, G. (2009), *Microstructure and performance of crumb rubber modified asphalt*. Construction and Building Materials. 23:3586–3590, <https://doi.org/10.1016/j.conbuildmat.2009.06.038>.
- Yetkin, Y. (2007), *Polymer modified asphalt binders*. Construction and Building Materials. 21: 66–72. <https://doi.org/10.1016/j.conbuildmat.2005.07.007>.

Comparison between galvanic sensors (steel/stainless steel) and half-cell potentials (E_{corr}) for monitoring the corrosion risk of steel reinforcement in concrete structures

J. L. Pérez-Díaz^{1*} , J. A. Cabrera-Madrid¹ , D. Hernández Cruz¹ ,
E. A. Godínez-Domínguez¹ , M. D. Mundo Molina¹

*Contact author: jose.perez@unach.mx

DOI: <https://doi.org/10.21041/ra.v12i3.620>

Reception: 24/06/2022 | Acceptance: 29/08/2022 | Publication: 01/09/2022

ABSTRACT

The corrosion risk of steel in concrete was assessed using internal galvanic carbon/stainless steel sensors and the external Cu/CuSO₄ electrode. The sensors were used to monitor the macrocell potentials and currents of reinforced concrete prismatic specimens, with water to cement ratios of 0.4 and 0.6, immersed in 5% NaCl solution, for 18 months. The results of the potentials showed a good correlation between the two reference electrodes, being able to evaluate the corrosion of the system. In addition, the electrochemical noise technique supports observations of the effect of chloride ions. Therefore, galvanic sensors can be considered for implementation in the monitoring and evaluation of corrosion risk of reinforced concrete structures.

Keywords: steel reinforcement; reinforced concrete; corrosion potential; microcell; galvanic sensor.

Cite as: Pérez, J. L., Cabrera, J. A., Hernández, D., Godínez, E. A., Mundo, M. D. (2022), "Comparison between galvanic sensors (steel/stainless steel) and half-cell potentials (E_{corr}) for monitoring the corrosion risk of steel reinforcement in concrete structures", Revista ALCONPAT, 12 (3), pp. 378 – 400, DOI: <https://doi.org/10.21041/ra.v12i3.620>

¹ Facultad de Ingeniería, Universidad Autónoma de Chiapas, Tuxtla Gutiérrez, Chiapas, México.

Contribution of each author

In this work, the author J. L. Pérez-Díaz contributed with the design of the research and the performance of laboratory tests (100%), the writing of the text (70%), analysis and discussion of the results (60%) and review (50%). The author J.A. Cabrera-Madrid contributed with the writing of the text (15%), analysis and discussion of the results (15%) and revision (15%). The author D. Hernández Cruz contributed with the writing of the text (15%), analysis and discussion of the results (15%) and revision (15%). The author E. A. Godínez-Domínguez contributed with the analysis and discussion of the results (10%) and review (10%). The author M. D. Mundo Molina with the revision 10%.

Creative Commons License

Copyright 2022 by the authors. This work is an Open-Access article published under the terms and conditions of an International Creative Commons Attribution 4.0 International License ([CC BY 4.0](https://creativecommons.org/licenses/by/4.0/)).

Discussions and subsequent corrections to the publication

Any dispute, including the replies of the authors, will be published in the second issue of 2023 provided that the information is received before the closing of the third issue of 2023.

Comparativa entre sensores galvánicos y potenciales de corrosión para el monitoreo del riesgo por corrosión del acero de refuerzo en estructuras de concreto

RESUMEN

Se evaluó el riesgo por corrosión del acero en concreto, utilizando sensores galvánicos internos de acero al carbono/acero inoxidable y un electrodo externo de Cu/CuSO₄. Los sensores se utilizaron para monitorear los potenciales y corrientes de macrocelda de probetas prismáticas de concreto reforzado con relaciones agua-cemento de 0.4 y 0.6, inmersas en solución de NaCl al 5% durante 18 meses. Los resultados de los potenciales mostraron buena correlación entre los dos electrodos de referencia, pudiendo evaluar la corrosión del sistema. Además, la técnica de ruido electroquímico respalda el efecto por iones cloruro. Por lo tanto, los sensores galvánicos pueden considerarse para su implementación en el monitoreo y evaluación del estado de riesgo por corrosión en estructuras de concreto reforzado.

Palabras clave: acero de refuerzo; concreto reforzado; potencial de corrosión; macrocelda; sensor galvánico.

Comparação entre sensores galvânicos e potenciais de corrosão para monitoramento do risco de corrosão de armaduras de aço em estruturas de concreto

RESUMO

O risco devido à corrosão do aço em particular foi avaliado, utilizando sensores galvânicos internos de aço carbono/aço inoxidável e o eletrodo externo de Cu/CuSO₄. Os sensores foram utilizados para monitorar os potenciais e correntes de macrocélulas de corpos de prova prismáticos de concreto armado, com relações água-cimento de 0,4 e 0,6, imersos em solução de NaCl a 5% por 18 meses. Os resultados dos potenciais mostraram uma boa correlação entre os dois eletrodos de referência, podendo avaliar a corrosão do sistema. Além disso, a técnica de ruído eletroquímico suporta o efeito dos íons cloreto. Portanto, sensores galvânicos podem ser considerados para implementação no monitoramento e avaliação do status de risco de corrosão em estruturas de concreto armado.

Palavras-chave: aço reforçado; concreto reforçado; potencial de corrosão; macrocélula; sensor galvánico.

Legal Information

Revista ALCONPAT is a quarterly publication by the Asociación Latinoamericana de Control de Calidad, Patología y Recuperación de la Construcción, Internacional, A.C., Km. 6 antigua carretera a Progreso, Mérida, Yucatán, 97310, Tel.5219997385893, alconpat.int@gmail.com, Website: www.alconpat.org

Reservation of rights for exclusive use No.04-2013-011717330300-203, and ISSN 2007-6835, both granted by the Instituto Nacional de Derecho de Autor. Responsible editor: Pedro Castro Borges, Ph.D. Responsible for the last update of this issue, Informatics Unit ALCONPAT, Elizabeth Sabido Maldonado.

The views of the authors do not necessarily reflect the position of the editor.

The total or partial reproduction of the contents and images of the publication is carried out in accordance with the COPE code and the CC BY 4.0 license of the Revista ALCONPAT.

1. INTRODUCTION

Corrosion of reinforcing steel due to the presence of chlorides in concrete generates deterioration of structures exposed to saline environments, putting their functionality and safety at risk, reducing the expected durability. In addition, this problem increases the inspection and maintenance cost or, in many cases, the risk of a collapse of the structure. Galvanic sensors have been used since 1990 as a preventive method against the attack of aggressive agents (Schiessl and Raupach, 1992). Mainly for a wide variety of marine structures, the performance of these sensors (galvanic pair) could detect the moment when the reinforcing steel is depassivated, and corrosion is activated by the presence of aggressive agents. Furthermore, corrosion macrocell sensors (Raupach, 1996) have been used to monitor the corrosion risk of reinforcing steel, strategically placed in the concrete cover zone and difficult access areas, improving service life prediction or expanding the study of durability (Raupach and Dauberschmidt, 2003) as a complement to other protection systems. However, more work needs to be done to obtain evaluations and results with practical applications using other materials, under different study conditions, and where relevant limit values can be determined (Raupach and Schießl, 2001; McCarter et al., 2001). Galvanic corrosion is known as corrosion macrocell; the potentials and currents are measured from the activity between a corroding anode and a passive cathode, where the reduction will be presented (Figure 1). The current recorded measures the corrosion caused by the cathode reduction process, without considering the anode corrosion itself (McCarter and Vennesland, 2004).

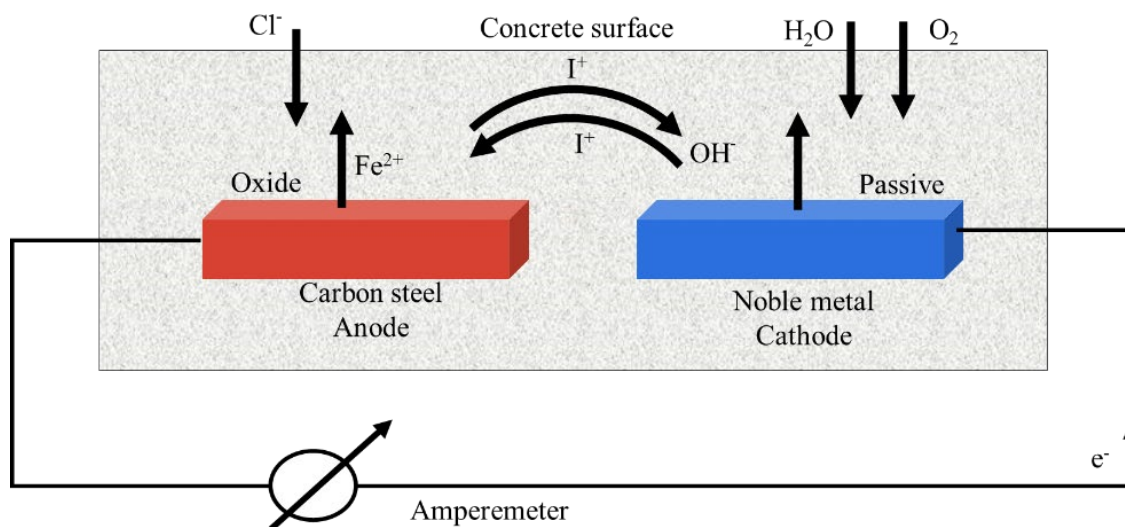


Figure 1. Corrosion Macrocell Scheme

Oxidation and reduction processes must occur in order for the electrochemical corrosion of steel to take place in concrete; where the main reactions (equations 1, 2) are as follows:



Corrosion process at the anode involves both reactions, but here the anodic current is higher than the cathodic current. At the cathode, the cathodic current is higher than the anodic current, which forms the corrosion macrocell.

Many factors influence the operation of a corrosion macrocell in concrete, such as the design in the geometric shape and sensors size, the position and placement within the concrete cover area, as well as the separation between the anodes and cathodes, which may cause an increase or decrease of the galvanic current values (Arya and Vassie, 1995). In this study, the influencing factors in the macrocell current signal were examined, such as the ratio of anode/cathode areas, the separation distances within the specimens, and the immersion level (vertical position of the specimens). In addition, variables such as concrete quality, the thickness of the concrete cover zone of reinforcing steel, the monitoring conditions of potentials, and the macrocell currents of sensor electrodes were considered to determine the corrosion mechanism of the system (Raupach and Dauberschmidt, 2003). In addition, we aim to evaluate whether the galvanic macrocell sensors based on 304 stainless-steel can be implemented as an alternative monitoring method to detect corrosion risk within concrete. 304 stainless steel was used because it represents an economical all-purpose material, resistant to corrosion, and with excellent strength and ductility. Also, this steel, embedded in concrete and placed next to the reinforcing steel, can work as an internal detection system in the concrete cover zone. Furthermore, it has the required characteristics of a resistant and easy-to-implement sensor (Llorens et al., 2019), although with another anode/cathode exposed area ratio (galvanic sensor: carbon steel/stainless steel) and with different test conditions (submerged environment). The concrete cover zone was also evaluated where the advantageous working conditions of the sensor are exposed to monitor its corrosion behavior in the presence of chloride ions, which will enter the concrete from the NaCl solution at 5% by water weight.

2. EXPERIMENTAL PROCEDURE

2.1 Materials for concrete mix

Two concrete mixtures made according to NMX C155 (2014) were used; ordinary Portland cement OPC 30R (NMX C414, 2004), crushed gravel with a maximum aggregate size of 19 mm (3/4"), fine aggregate with a fineness module of 2.71, drinking water, and water/cement ratio (a/c) of 0.60 and 0.40. The concrete specimens were cured under water for 28 days according to (NMX-C-159-ONNCCE-2004). Mixture proportion of concrete shown in Table 1 was obtained using the ACI-211.1 method (American Concrete Institute, 2002).

Table 1. Mixture proportion of concrete ((kg/m³ concrete) /proportion)

Mix ratio	Cement	Water	Gravel	Sand	Additive
w/c 0.60	324	209	1035	765	none
w/c 0.40	513	209	1035	606	none

2.2 Configuration of the prismatic specimens

Sixteen prismatic specimens with dimensions of 17 x 20 x 30 cm were made; the longitudinal steel of the steel truss (formed using longitudinal and transversal steel reinforcement) was separated 15 cm parallel to the side 1 and 10 cm perpendicular to side 1 (as indicated in Figure 2). was used with 9.5 mm (3/8") diameter carbon steel rods and 6.35 mm (1/4") stirrups fastened with tie wire. In each specimen, two sensors were placed next to the reinforcing steel, as shown in Figure 2. The anodes were placed on opposite side of the specimens: on side 1, the anode A1 and on side 2, the anode A2, at a depth of 8 cm and 22 cm in the longitudinal direction, concerning the water level (NA) or 5% NaCl solution (NS). An accessible area for the sensor of 3 cm was considered. The concrete cover for the steel reinforcement on the faces exposed to chloride penetration was 3.5 cm. The area of the faces exposed to chlorides was 20 x 30 cm. In comparison, the lateral sides of the specimens (17 x 20 cm and 17 x 30 cm) were covered with cement polish and solvent-based asphalt

waterproofing to restrict the penetration of chlorides (Figure 2). To identify the specimens, they were labeled with the acronym AP143, which corresponds to the number of specimen 1 exposed to tap water (AP1), water/cement ratio of 0.4 (number 4), and reinforcing steel of 9.5 mm (3/8 ") (number 3). For labels with the acronym SM563, refer to specimen number 5 exposed in brine (SM5), water/cement ratio of 0.6 (number 6), and reinforcing steel of 9.5 mm (3/8") (number 3).

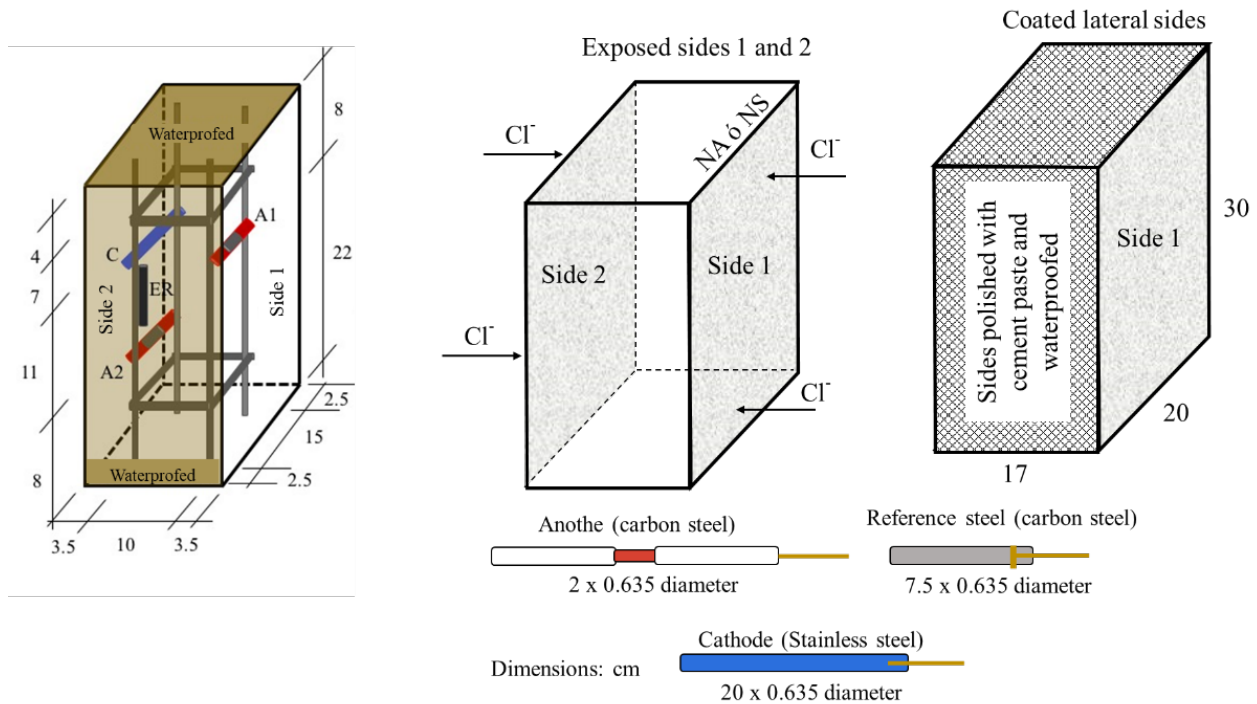


Figure 2. Scheme of the reinforced concrete specimens and embedded galvanic sensors.

2.3 Sensor system

Sensors were designed as a galvanic cell, consisting of carbon steel (anodes “A”) and stainless-steel electrodes (cathodes “C”), which were isolated from the steel truss using industrial hoses. The reference steel (AR) was left in electrical contact with the reinforcement. Copper wire was used to connect the electrodes (Figure 3), leaving extensions outside the specimen to close the electrical circuit and obtain the measurements through electrical signals. Due to the diameter of the copper wire to that of the electrodes, a representative effect on the values monitored during the test time was not considered. The sensor was fastened to the steel truss using plastic ties. The anode/cathode area ratio was 1:10, corresponding to 4 cm² for each anode and 40 cm² for the cathode. A cathode larger area than that of the anode was used to avoid low galvanic currents, especially for stainless steel electrodes, since a similar amount of space between the anode and cathode would have slight effectiveness in detecting corrosion damage of steel in concrete (Zinc-Taek et al., 2005).

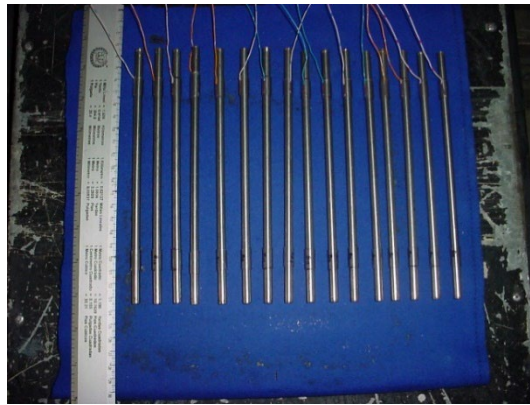


Figure 3. Type 304 Stainless Steel cathodes with copper wire connection, fastened with an industrial hose.

AISI-SAE 1020 (UNS G10200) steel was used as the anode, with the same composition as the steel truss; and type 304 austenitic stainless steel (UNS S30400) as the cathode (Table 2) (AISI-SAE, 1983; Hudok, 1990).

Sensor elemental chemical composition was analyzed with 3.0 g samples extracted from the anode and cathode material. Acid digestion was carried out in the microwave (CEM brand model MDS-200), applying the Still method 0.5 g of each sample was prepared with HCl, HNO₃, HF, and HBO₃. For elemental analysis, Plasma Emission Spectrometry (ICP-OES, IRIS-AP model), Atomic Absorption Spectrophotometry (FAA AVANTA SIGMA model), and Elemental Analyzer (EA-1110 model) (PROCEDURE LAQ03, 2005) techniques were used. The results of the analysis are shown in Table 2.

Table 2. Elemental chemical composition of the steel for the sensors and the reference electrode

Elements (% wt)	Cr	Ni	C	Mn	Si	S	P	Fe	Cu	Mo	Co
Carbon Steel 1020	0.041	0.027	0.198	0.429	----	0.021	0.02	bal	0.021	----	0.014
Stainless steel 304	17.864	7.719	0.072	2.003	0.484	0.032	0.045	bal	0.356	0.595	0.101

2.4 Exposure and monitoring with electrochemical techniques

Prismatic specimens were exposed for 18 months in immersion in two environments: tap water (AP) and NaCl solution at 5% by water weight ("SM" brine). During the exposure, it was supervised that the same liquid level was maintained, and the solution was changed every 3 months. The exact number of specimens with a w/c ratio of 0.6 and 0.4 were exposed in AP and SM. Monitoring the macrocell voltage and current in the specimens was carried out using a high impedance multimeter (FLUKE 87 III) through an external short circuit. The corrosion potentials were measured using an external reference electrode of Copper-Copper Sulfate (Cu/CuSO₄) or (CSC) (Figure 4).



Figure 4. Monitoring with multimeter and Cu/CuSO₄ reference electrode.

From the tenth month Electrochemical noise technique was used in the specimens immersed in SM for 9 months, due to the activation of the better quality or denser concrete specimens in months 7, 8, and 9 exposed in NaCl solution at 5% by weight of water. The above in order to know the effect of chlorides on the sensors (A1 and A2) and reinforcing steel, using a SOLARTRON 1285 Potentiostat/Galvanostat. This technique allows the detection and evaluation of the behavior of the general and localized corrosion (Dawson, 1996) through the random fluctuations of the potential or the current of the material subject to corrosion against time. The results were visually and statistically analyzed using MATLAB software. The circuit arrangement for monitoring is shown in Figure 5.

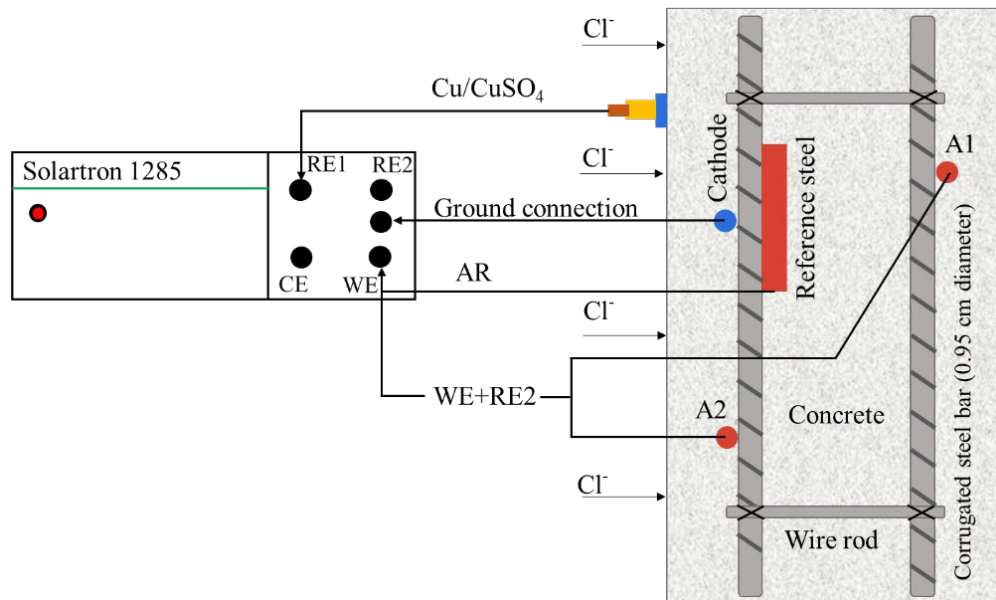
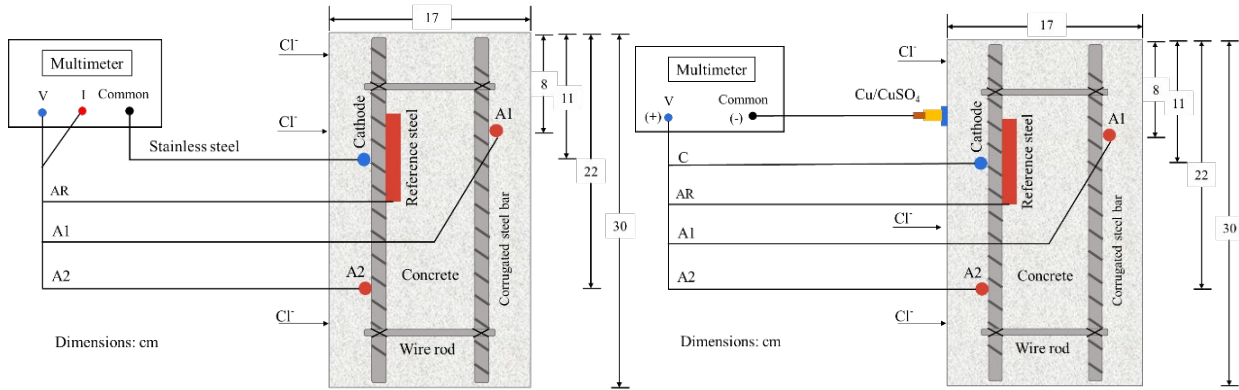


Figure 5. Diagram for monitoring Potential and Current in time

2.4.1 Monitoring potentials and currents

Voltages and currents were individually monitored for the anodes A1 and A2 and the reference steel (AR) against the cathode (Figure 6a). Thus, the corrosion potentials were also measured against the Cu/CuSO₂ reference electrode, using the reference steel (AR), the anodes (A1, A2), and the cathode (C) as the working electrode (Figure 6b).



Figures 6a and 6b. Diagrams for monitoring Macrocell Voltages and Currents and Corrosion Potentials.

Analysis of the macrocell voltages against the stainless steel and the corrosion potentials against the Cu/CuSO₄ electrode, was carried out following the reference values of the standard (ASTM C 876-91), establishing a reference equivalence of both electrodes (stainless steel and Cu/CuSO₄) against the standard hydrogen electrode (NHE) (Table 3). However, the analysis for the macrocell current was carried out according to the information available in the literature since there are no standardized values of the current levels that indicate the risk of corrosion for a reinforced concrete system and embedded sensors.

Table 3. Corrosion potentials vs. Cu/CuSO₄ and its equivalence for stainless steel, ASTM C 876-91.

Corrosion Potential (E _{corr}) (mV)	Macrocell voltage (V _{corr}) (mV)	Risk of damage (%)
More positive than -200	More positive than -95	10% corrosion probability
Values between -200 a -350	Values from -95 to -166	Uncertain corrosion
More negative than -350	More negative than -166	90% corrosion probability

2.5 Chloride tests

Free chloride content in the concrete specimens was obtained from the pulverized samples extracted from the areas near the anodes and the reinforcing steel 30 g of sample were used and followed the standard procedure (ASTM D 1411-99). The percentages of free chloride ions were calculated against the weight of concrete and cement for the concrete with a w/c ratio of 0.4 and 0.6.

2.6 Simple compression test

Simple compressive strength was determined after 28 days of curing (NMX C159, 2004) according to the ASTM C39-17 procedure (ASTM International, 2017). Three concrete cylinder specimens 15 cm in diameter by 30 cm in length were used for each w/c ratio. Sulfur mortar was used for leveling the cross sections of the cylinders. The simple compression test of the cylinders was carried out with a Universal Electric Hydraulic Press with a capacity of 120 Tons (Model ELVEC), equipped with a Model CT-715H pump. The load application speed was 5.3 kN/s, registering the maximum load until the collapse of the cylinders.

3. RESULTS AND DISCUSSION

3.1 Macrocell voltages

Macrocell voltages of the A1, A2, and AR anodes immersed in the specimens with a w/c ratio of 0.40, and exposed in AP, were higher than -95mV , representing a low risk of corrosion (Figure 7). For the A1, A2, and AR anodes of the specimens exposed in SM, the voltage values were more negative than -166 mV from month 7, representing a high probability of corrosion (Figure 7). In addition, anode A1 (located at a depth of 8 cm) presented more negative voltage values than anode A2 (located at a depth of 22 cm). Therefore, greater activation of the A1 anodes closer to the immersion surface than the A2 anodes was observed. Although access to oxygen is more restricted or low in wet and submerged concrete, the corrosion values are fundamental. They cannot necessarily be attributed only to the effect of oxygen (Alonso et al., 1998). Unusual behavior was observed in the SMA2 anode, which may be due to the concrete heterogeneity an isolated case not observed with the other electrodes in this work.

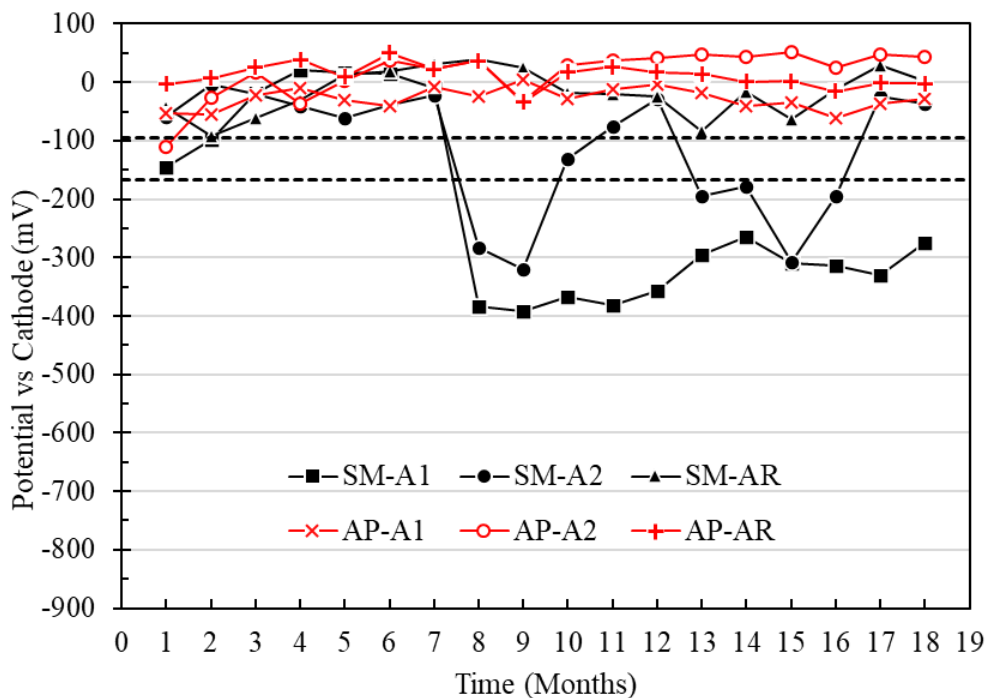


Figure 7. Potential vs. cathode of specimens with a w/c ratio of 0.4 exposed in tap water (AP) and 5% NaCl solution (SM).

For the specimens with a w/c ratio of 0.60 and exposed in AP, the macrocell voltages of the anodes A1, A2, and AR generally remained in the zone of low probability of corrosion, with values more positive than -95mV (Figure 8). At the same time, the anodes of the specimens immersed in SM presented voltage values more negative than -166 mV , with a trend towards values with a higher probability of corrosion from month 2 of exposure (Figure 8). It was observed that the A1 anode presented greater vulnerability to corrosion than the A2 anode, an effect like that of the beams with a w/c of 0.4 (Figure 7). Particularly for the case of reinforcing steel (SM-AR), a gradual decrease in potential or voltage was observed from the zone of low probability of corrosion to the area of high probability, reaching potentials of -300 mV for months 17 and 18, showing practically the same trend as anodes A1 and A2.

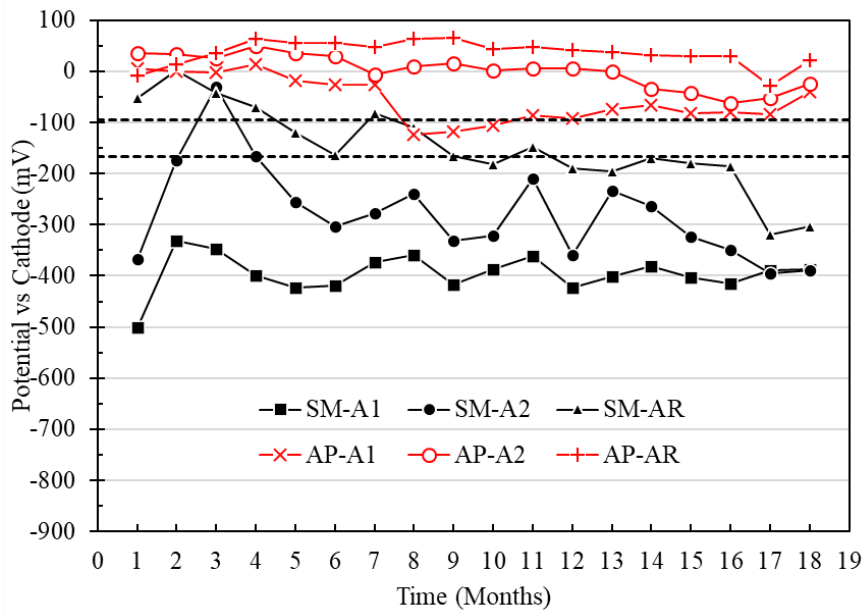


Figure 8. Potential vs. cathode specimens with a w/c ratio of 0.6 exposed in drinking water (AP) and 5% NaCl solution (SM).

3.2 Corrosion potentials vs CSC (Cu/CuSO₂)

Corrosion potentials of the A1, A2 and AR anodes with respect to the CSC electrode in the specimens with a w/c ratio of 0.40 and exposed in AP, were more positive than -200mV (low risk of corrosion) (Figure 9). Nevertheless, the anodes of the specimens exposed in SM reached potential values more negative than -200 mV, with indications of a high probability of corrosion after month 7. It was also observed that the A1 anode presented greater corrosion vulnerability than the A2 anode (Figure 9). This being consistent with the results obtained from the macrocell voltages (Figure 7 and 8). On the other hand, the potentials of the 304 steel used as cathode do not represent a probable risk of corrosion for the exposed specimens in AP and SM, indicating a good performance as a means of implementation for corrosion monitoring of reinforced concrete structures (Figure 8).

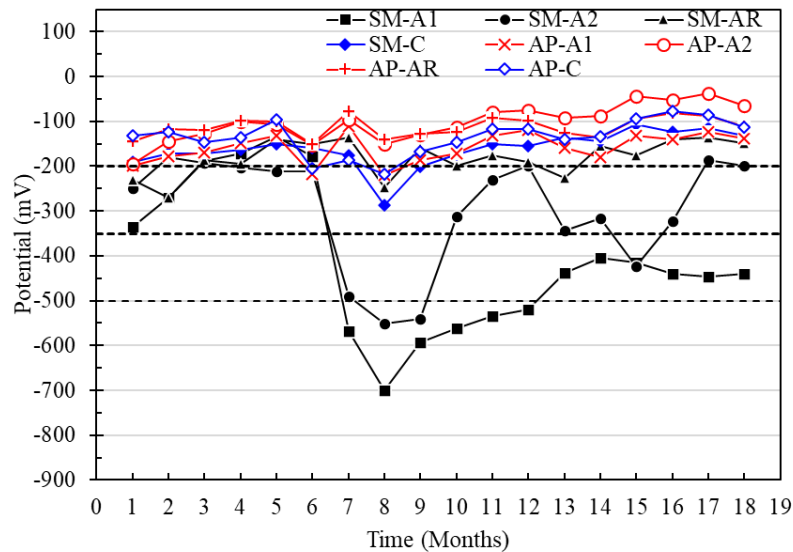


Figure 9. Potential vs. Cu/CuSO₄ from specimens with a w/c ratio of 0.4 exposed to drinking water (AP) and 5% NaCl solution (SM).

In the case of the specimens with a w/c ratio of 0.60 and exposed in AP, the corrosion potentials of A1, A2, and AR vs. CSC were greater than -200 mV, with a low probability of presenting corrosion. Meanwhile, the potentials of the anodes in the specimens immersed in SM showed trends from the high probability zone towards severe corrosion from month 2, with values from -300 mV to -700 mV approximately (Figure 10). This same effect was detected across the macrocell voltages (Figures 7 and 8). For the reinforcing steel potentials, a trend towards the high corrosion risk zone was observed, with potentials of up to -600mV for months 17 and 18. While the potential for the cathode in the specimens with a w/c ratio of 0.6 fluctuated in the range of -200 mV to -350 mV, being more evident between months 5 to 10, generally representing a low risk of corrosion.

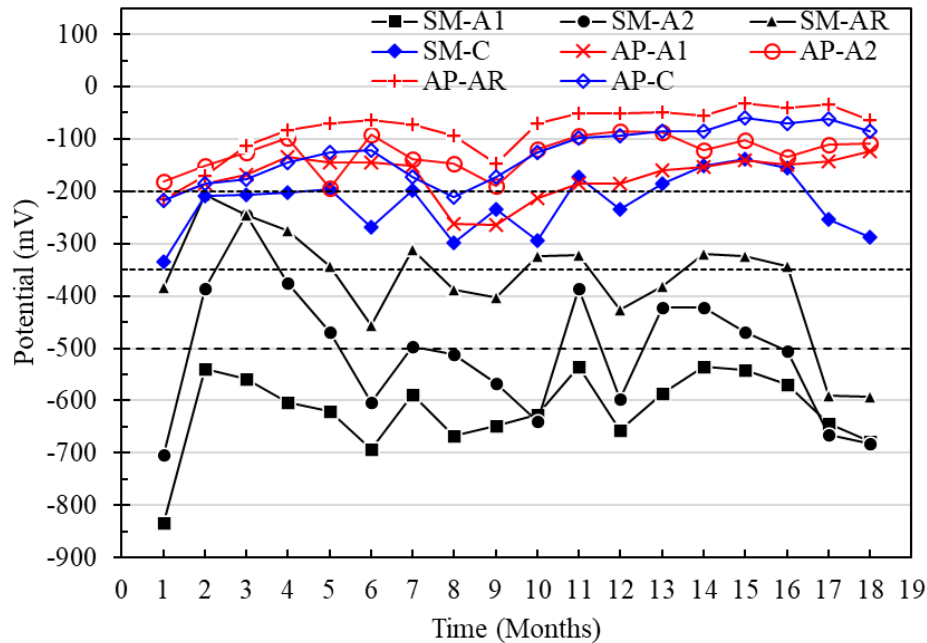


Figure 10. Potential vs. Cu/CuSO₄ from specimens with a w/c ratio of 0.6 exposed to drinking water (AP) and 5% NaCl solution (SM).

3.2.1 Comparison of potentials vs. cathode and vs. copper sulfate copper electrode (CSC)

Using the data of the potentials or voltages of the previous sections, the comparisons between the potentials vs. the cathode and the CSC is shown in Figure 11, corresponding to the anodes of the test tubes with a w/c ratio of 0.4 exposed in SM. A good correlation of the potentials obtained with different reference electrodes and during the monitoring time could be observed. Therefore, these galvanic sensors can be a viable option for the implementation and corrosion monitoring of reinforced concrete structures.

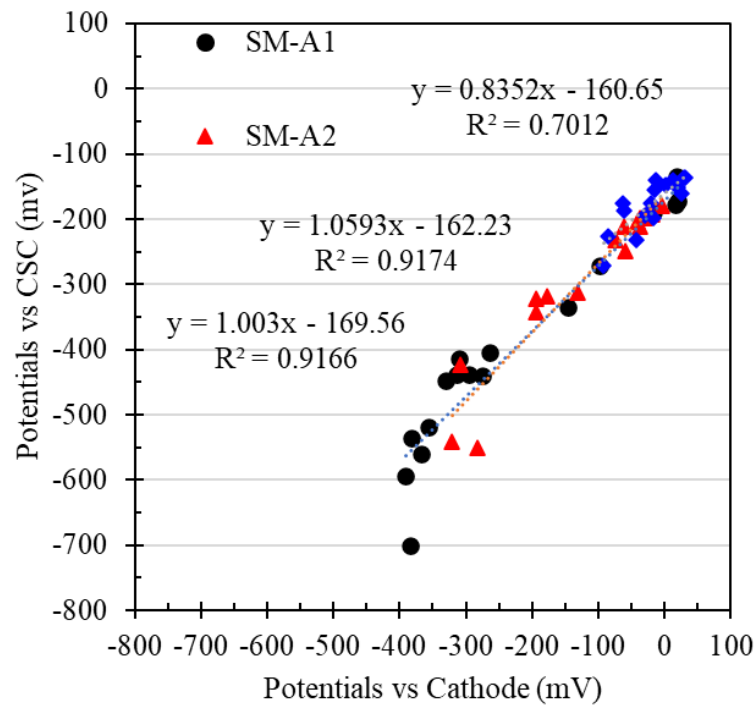


Figure 11. Comparison between the corrosion potentials vs. the cathode and the CSC electrode of the anodes of the test pieces with an a/c ratio of 0.4.

3.3 Macrocell current densities

In general, the macrocell current densities for the sensors placed in the specimens with a/c of 0.4 exposed to AP showed uniformity between the values within the region considered as negligible corrosion (Figure 12). However, the current densities of sensor A1 exposed to SM specimens were higher from month 6, reaching the values considered as moderate and high corrosion (greater than $0.1 \mu\text{A}/\text{cm}^2$), which also indicates active corrosion. (Figure 12). Although sensor A2 showed activation values from the sixth month, it was not maintained in the subsequent months, generating passivation from month 10. It was observed that sensor A1 of the specimens exposed to SM presented macrocell current values greater than A2, influenced by the depth at which the sensors were located and their oxygen availability. This difference was also observed by measurements of the macrocell voltages and the potentials respecting the CSC electrode.

Difference between the macrocell currents of the sensors A1 greater than A2, both exposed in AP and SM, may be due to the availability of oxygen. Observing that the oxygen diffusion is lower in a submerged environment, the corrosion activity decreases (Table 4). However, it has also been revealed in other studies (Alonso et al., 1998) that even under oxygen scarcity, reduction reactions can occur within the concrete.

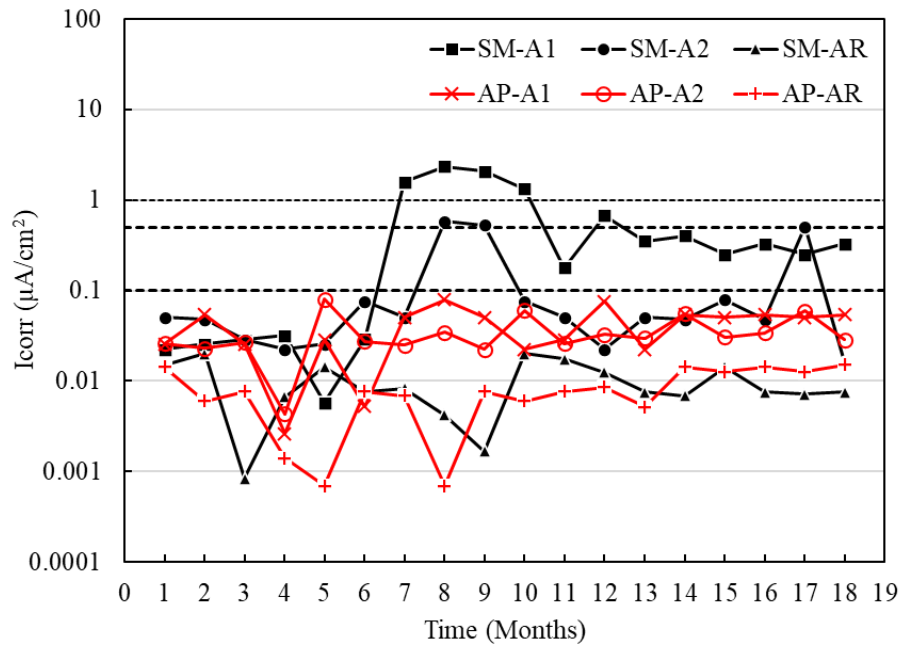


Figure 12. Macrocell current density of the specimens with w/c = 0.4 exposed to tap water (AP) and 5% NaCl solution (SM).

Figure 13 shows the results of the current densities of the sensors placed in the specimens with a w/c ratio of 0.6, exposed to AP and SM. The current values obtained in the anodes A1 and A2 exposed to AP generally indicate negligible corrosion (less than $0.1 \mu\text{A}/\text{cm}^2$), although sensor A1 (placed at 8 cm) showed signs of moderate corrosion from month 6. In the case of sensors A1 and A2 of the specimens exposed in SM, the current values initially led to high corrosion (greater than $1.0 \mu\text{A}/\text{cm}^2$) with a tendency towards moderate corrosion (less than $0.5 \mu\text{A}/\text{cm}^2$) after month 10. On the other hand, it was observed for the two types of mixtures with w/c ratios of 0.4 and 0.6 (Figures 12 and 13) that the current densities for the AR sensors exposed to AP and SM indicate stability and negligible corrosion.

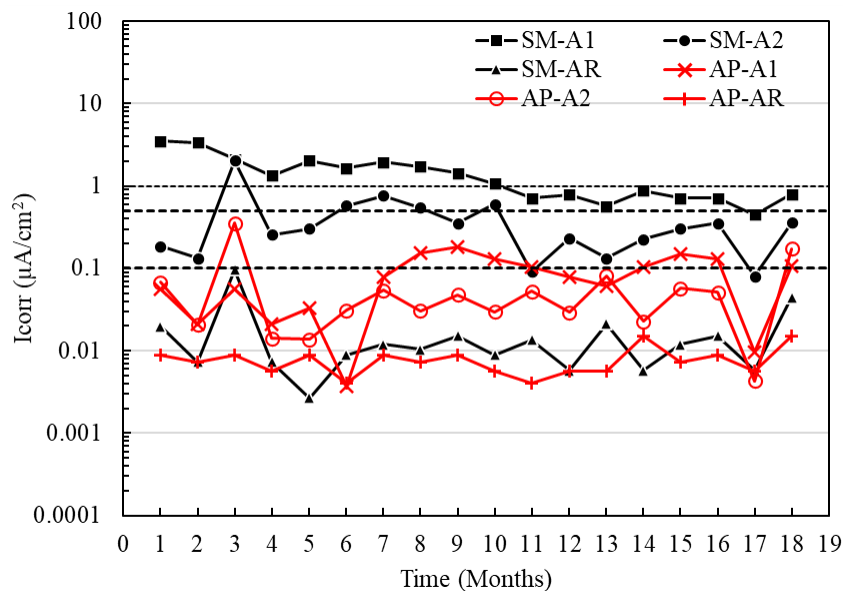
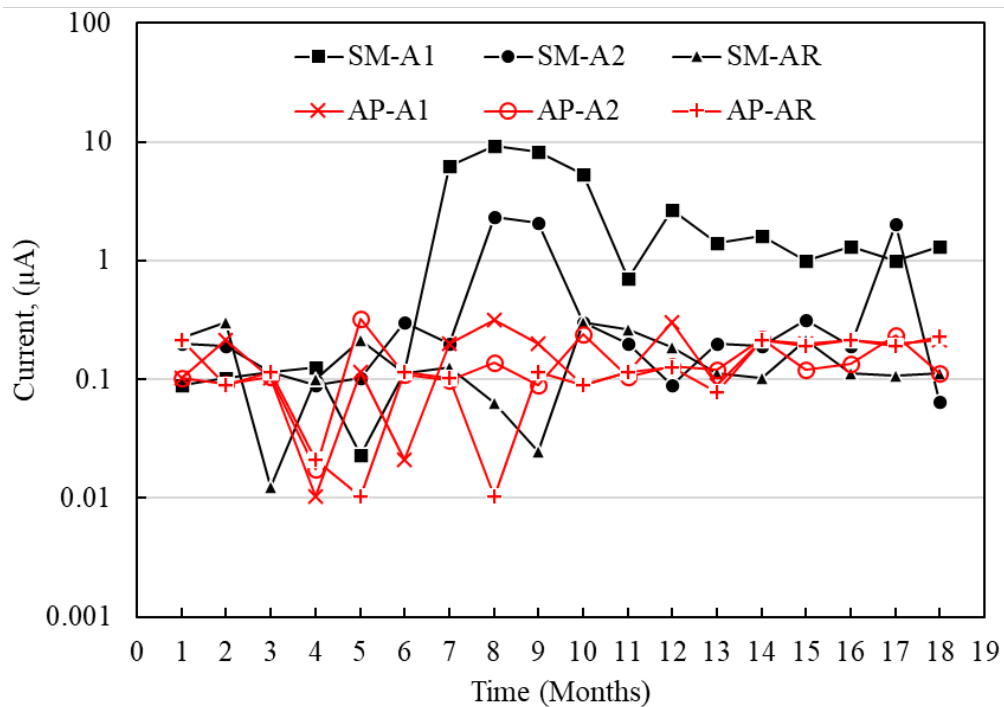


Figure 13. Macrocell current density of the specimens with w/c = 0.6 exposed to tap water (AP) and 5% NaCl solution (SM).

Table 4. Comparison of current density limit values

Sensor type	Test conditions	Rel. Area: Anode/Cathode	Limit Values	References
Steel/Stainless Steel 304	Submerged 5% NaCl	1:10	3.50 μ A/cm ²	Pérez et al., 2022
Steel/Copper Steel/Stainless Steel	Immersion-Gravity 3.5% NaCl	1:1	0.07 μ A/cm ² -0.02 μ A/cm ²	Zink Taek Park, 2005
Steel/Stainless Steel 1.4301	Mortar with 3% Cl ⁻ added to the water in the mix	1:5	5.00 μ A/cm ²	Elsener, 2002
Steel/Titanium-platinum	Humid and drying	1:8	3.00 μ A/cm ²	Raupach y Schiebl, 2001
Steel/Stainless Steel 316	95% RH and concrete with 3% Cl ⁻	1:30 1:33	3.85 μ A/cm ²	Arya y Vassie, 1995

In the analysis of the macrocell current intensity (Figure 14), it was possible to determine that the A1 sensors placed at a shallower depth in the specimens exposed to SM presented higher macrocell currents (9 μ A and 14 μ A for the concrete with a/c of 0.4 and 0.6, respectively) than the A2 sensors located deeper (2.40 μ A and 2.00 μ A for concrete with a/c of 0.4 and 0.6). According to the first microcell, current intensity values were like those reported in the literature, with galvanic current limit values of 15 μ A and 16 μ A. However, the difference may be due to the different test conditions, the sensor materials, the anode/cathode area ratios, and the geometric arrangements within the concrete (Raupach and Schiebl, 2001; Elsener, 2002), Table 5.



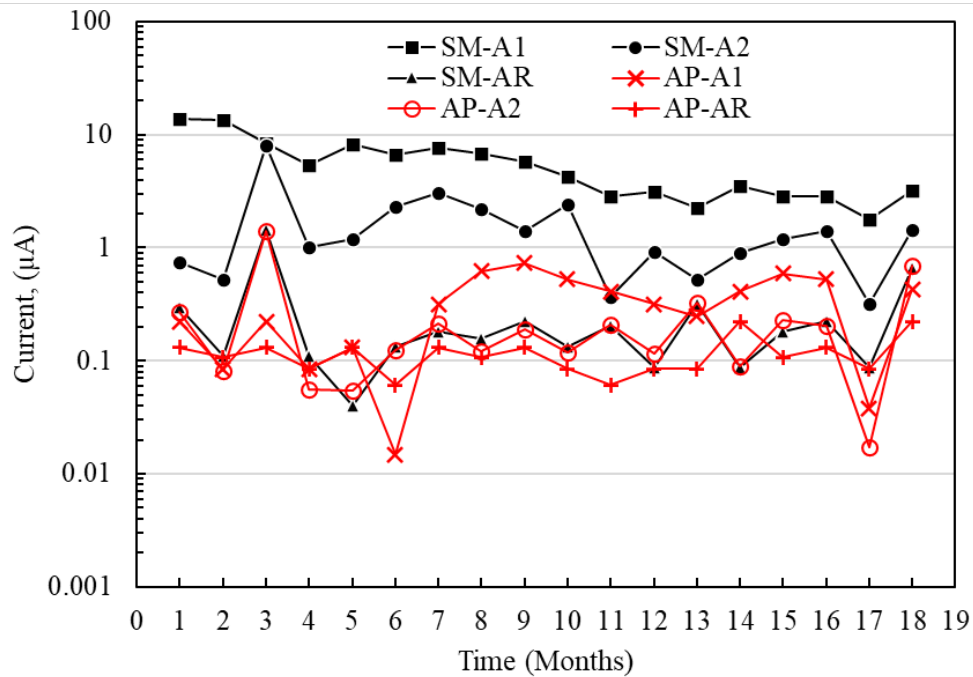


Figure 14. Macrocell current intensity of the specimens with a/c = 0.4 and 0.6 exposed to top water (AP) and 5% NaCl solution (SM).

Table 5. Comparison of current limit values

Sensor type	Test conditions	Rel. Area: Anode/Cathode	Limit Values	References
Steel/Stainless Steel 304	Submerged in 5% NaCl	1:10	14 µA	Pérez et al., 2022
Steel/Stainless Steel 1.4301	Mortar with 3% Cl ⁻ added to the mix	1:5	16 µA	Elsener, 2002
Steel/Titanium-platinum	Humid and drying	1:8	15 µA	Raupach y Schiebl, 2001

3.4 Electrochemical noise

Due to the null activation obtained from the sensors in AP, only the electrochemical noise results of the specimens exposed in SM are shown, and their analysis to determine the type of corrosion of the system. Potential (E) and current (I) data were recorded with 1024 pts at 1 pt/sec.

Figure 15 and Figure 16 show the example graphs of the potential and current density series over time for the A1 anodes immersed in concrete with a w/c ratio of 0.4 and 0.6, respectively. In both concrete mixtures, a behavior correspondence between the potential and current series could be observed, showing random oscillations of the signals with transients of 1.0 mV and 1.0 µA/cm² on the base signal of the potential and current. This type of behavior was associated with a kind of generalized corrosion.

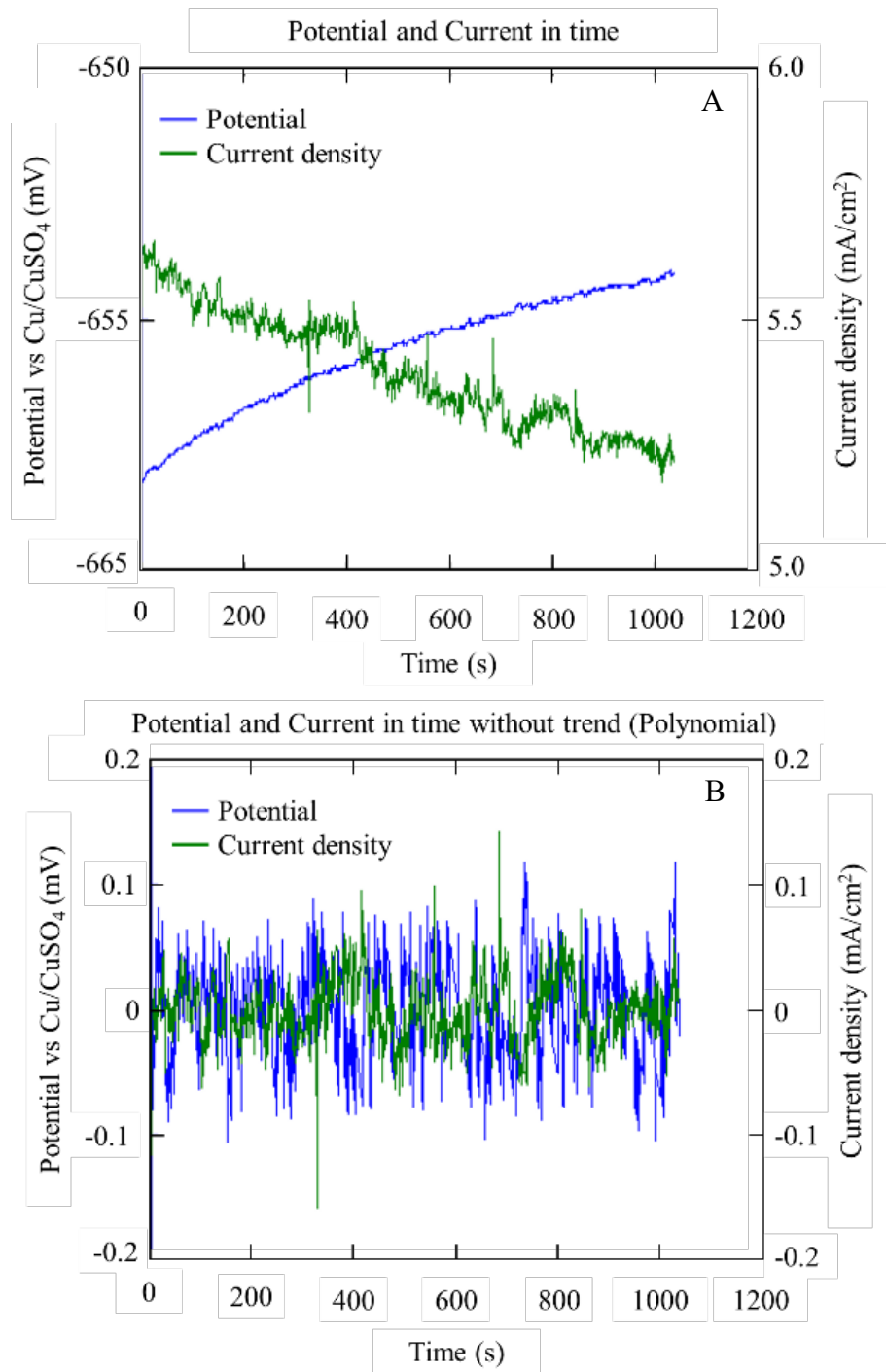


Figure 15. Series of potential and current over time obtained from anode A1 specifically with w/c 0.6, after 10 months in SM: with bias (A) and without bias (B).

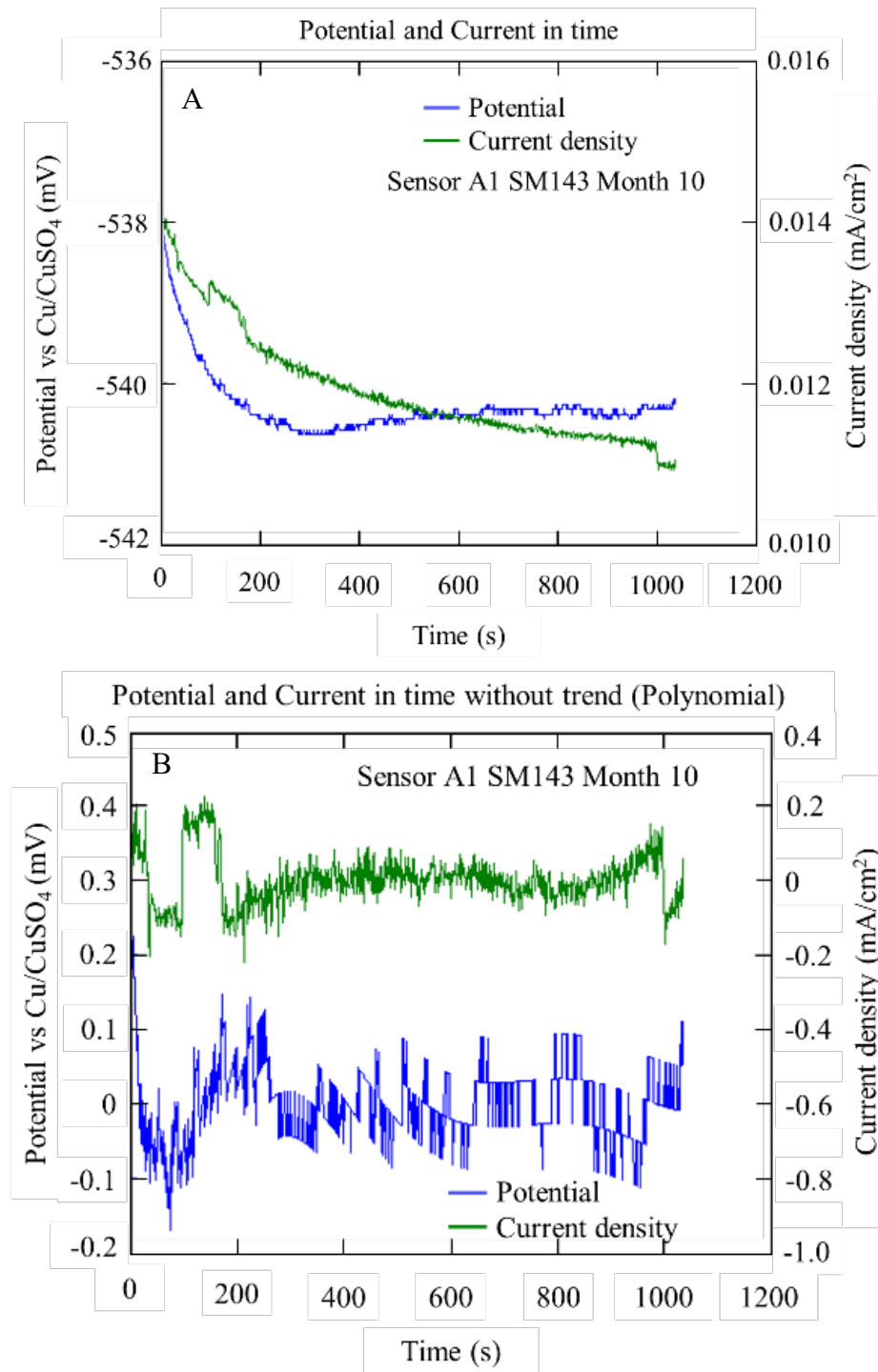


Figure 16. Potential and current series over time obtained from sensor A1 specifically with a/c 0.4, after 10 months in SM: with bias (A) and without bias (B)

Figures 17 and 18 show examples of the spectral densities of the potential and current density of the A1 anodes for concrete with a w/c ratio of 0.6 and 0.4 after 10 months of exposure. These graphs made it possible to determine the slopes with which the corrosion phenomenon in the anodes was evaluated. For this case, steeper slopes were indicative of some corrosion activity.

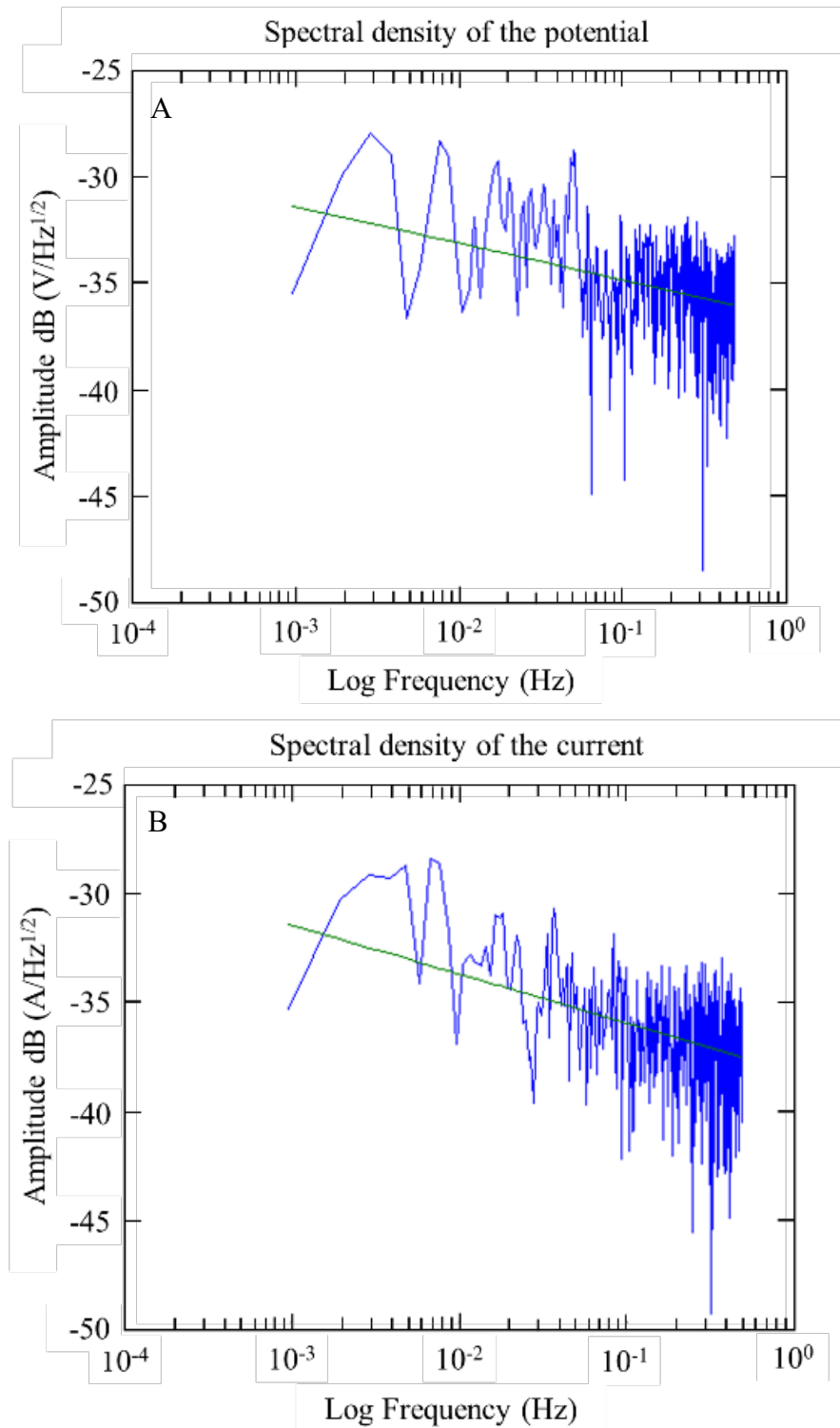


Figure 17. Spectral densities of potentials and currents over time were obtained from the A1 sensor, specifically at w/c 0.6 after 10 months of exposure.

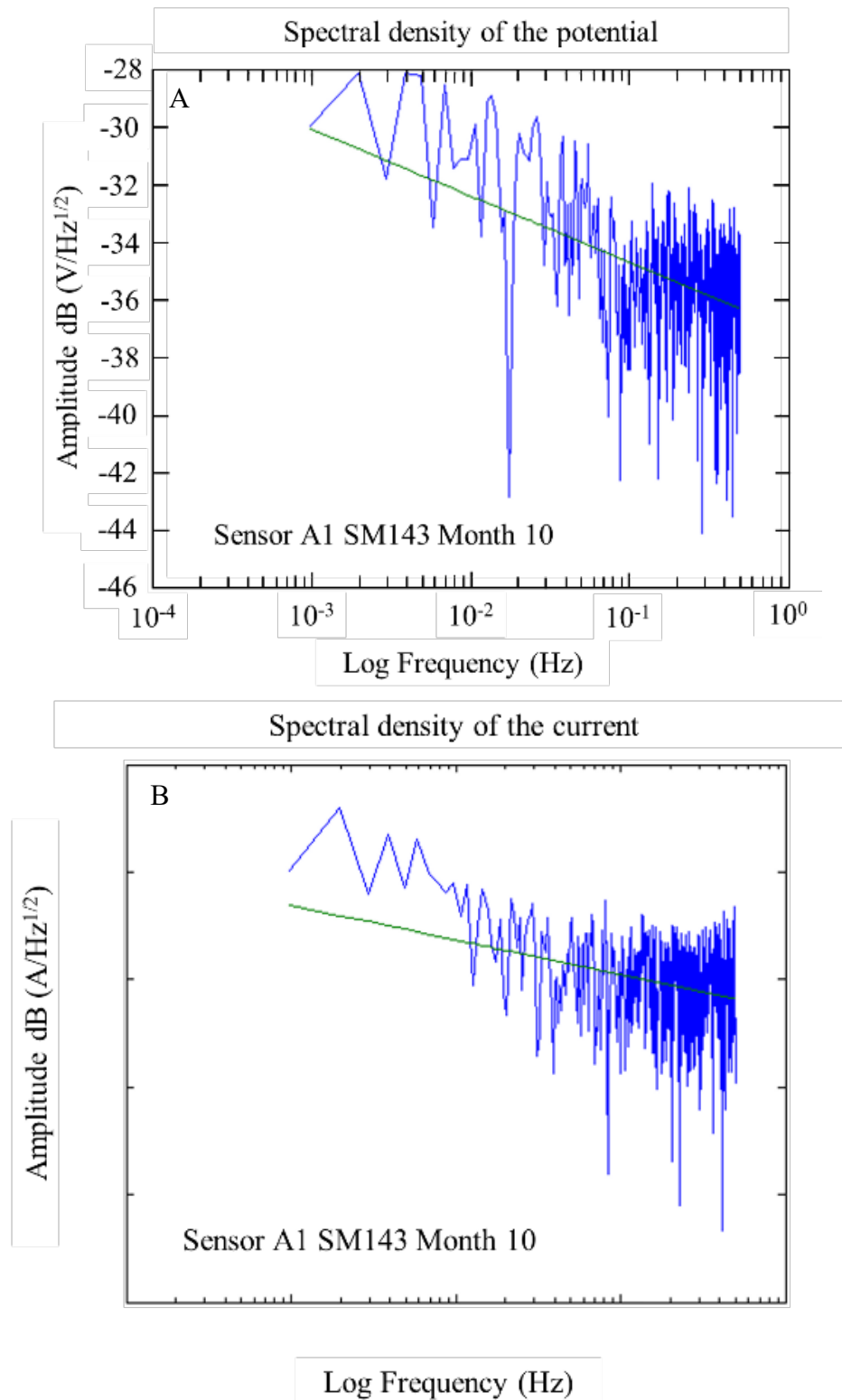


Figure 18. Spectral densities of potentials and currents over time were obtained from the A1 sensor, specifically at w/c 0.4 after 10 months of exposure.

During the 9 months of monitoring the sensors and the reinforcing steel of the 0.4 w/c specimens, the slopes obtained from the potential spectral densities were between -1.72 and -3.76; while for the specimens of w/c 0.6, they were between -2.06 and -3.48. The slopes of the spectral density records of the current of the 0.4 a/c specimens were -0.63 and -4.92, while for the specimens of

w/c 0.6, they were between -0.43 and -3.26. As a function of the slope of the frequency spectral densities, these values correspond to a type of uniform corrosion and passivation-uniform (Figures 17 and 18) (Legat and Dolecek, 1995).

With the electrochemical noise records of the test tubes with a w/c ratio of 0.6 and 0.4, a statistical analysis was carried out to determine the resistance, potential, and current data that allowed classifying the type of corrosion in the anodes, which are summarized in Table 6.

The values of the location index (I.L) (Kelly et al., 1996) obtained from the electrochemical noise records of the anodes for month 10 in both qualities of concrete indicate the types of generalized and mixed corrosion (Table 6). For month 18, mixed or hybrid corrosion was observed for both concrete types without exceeding a level greater than unity (>1), where there would be a pitting process in the sensors.

Table 6. Results of the statistical analysis of electrochemical noise and interpretation of the type of corrosion in the anodes of the concrete of w/c 0.6 and 0.4 for months 10 and 18.

W/C ratio	Electrode - Mes	Rn ($\Omega\text{-cm}^2$)	Location index, I.L.	Corrosion type	PSD potential (mV)	Corrosion type	PSD corrosion ($\mu\text{A/cm}^2$)	Corrosion type
0.40	A1-10	2.35E+04	0.0058	Generalized	-3.76	Uniform	-1.67	Uniform
0.40	A2-10	1.92E+04	0.0294	Mix	-3.24	Uniform	-0.63	Uniform Passivation
0.40	AR-10	1.26E+05	0.0878	Mix	-1.72	Uniform	-4.92	Uniform
0.60	A1-10	1.50E+04	0.0048	Generalized	-2.19	Uniform	-2.24	Uniform
0.60	A2-10	1.40E+04	0.0046	Generalized	-2.09	Uniform	-3.03	Uniform
0.60	AR-10	2.26E+05	0.0406	Mix	-2.06	Uniform	-0.43	Uniform Passivation
0.40	A1-18	1.30E+04	0.0325	Mix	-2.93	Uniform	-3.98	Uniform
0.40	A2-18	2.50E+04	0.0175	Mix	-2.00	Uniform	-1.39	Uniform
0.40	AR-18	1.26E+05	0.0878	Mix	-1.72	Uniform	-4.92	Uniform
0.60	A1-18	1.40E+04	0.0246	Mix	-3.48	Uniform	-3.26	Uniform
0.60	A2-18	1.60E+04	0.0469	Mix	-3.38	Uniform	-2.32	Uniform
0.60	AR-18	1.40E+04	0.0548	Mix	-2.27	Uniform	-0.68	Uniform Passivation

3.5 Content of free chlorides within the concrete by weight of the cement

Table 7 shows the results of the percentage of chloride ions soluble in water with respect to concrete and cement for the concrete specimens with a w/c ratio of 0.4 and 0.6. For both types of concrete exposed to AP, the amounts of chloride ions were negligible. In the case of the 0.4 w/c specimens exposed to 5% NaCl solution, the percentages of chloride ions were lower than in the 0.6 w/c beams, the latter reaching a value of 0.44% Cl⁻ with respect to cement. This value can be considered an eminent risk of corrosion, according to the values reported in the literature (Mohammed and Hamada, 2001; Alonso, 2001), Table 8; and by the values of macrocell voltages and currents that were monitored in this work, where at 10 months they show values of a high probability of corrosion.

Table 7. Water-soluble chloride ion content of both concrete mixtures

Mixture	% Cl ⁻ with respect to concrete		% Cl ⁻ with respect to cement	
	Tap water	NaCl solution	Tap water	NaCl solution
Ambient				
w/c: 0.40	0.0000	0.0470	0.00	0.21
w/c: 0.60	0.0035	0.0650	0.02	0.44

Table 8. Free chloride ions (Cl-) by weight of cement

References	% Cl ⁻ with respect to cement
ACI 318	< or = 0.15
ACI 222R	0.20
Brown,1980	0.40
Mohammed y Hamada 2001	
Others	0.10-0.60

3.6 Simple compression test

Table 9 shows the average compressive strength values of three cylindrical concrete specimens for each w/c ratio of 0.4 and 0.6. These stress values are relatively high, related to a slow corrosion process despite being in an aggressive environment in a 5% NaCl solution. These results corroborate that the concretes made with the standard specifications guarantee good quality and are less vulnerable to the entry of aggressive agents.

Table 9. Simple compression test results

W/C ratio	f'c = kg/cm ²
0.40	476
0.60	358

4. CONCLUSIONS

Using galvanic sensors, it is possible to monitor and evaluate the state of risk due to corrosion in reinforced concrete structures because the macrocell voltages of the internal galvanic sensor (carbon steel/stainless steel) presented a good correlation with respect to the corrosion potentials of the external Cu/CuSO₄ sensor, during the system test time.

Galvanic sensors can be considered for their implementation as a preventive method in correlation with existing electrochemical techniques because current limit values and current density, like other similar systems, were observed.

The behavior of the stainless-steel reference electrode (cathode "C"), embedded in reinforced concrete, generally maintained its stability against the risk of corrosion by chloride ions during the evaluation stage.

The value of free chlorides found near the sensor at 10 months reached a percentage of 0.44% with respect to the cement, which represents a risk with sufficient probability for the activation of corrosion in the reinforcing steel, this diagnosis being consistent with the macrocell voltage and current measurements, and by values close to those reported in the literature.

The information obtained with the electrochemical noise technique shows that the specimens have a uniform and mixed corrosion on the reinforcing steel and sensors due to the passivation of the system during the formation of the oxides in the exposure time; except for the lower quality specimen, which shows higher signs of corrosion in months 17 and 18, but still does not show localized corrosion.

5. REFERENCES

- AISI. (1983), *AISI – SAE Standard carbon steels. Steel products manual*, American Iron and Steel Institute.
- Alonso, C., Andrade, C., Castellote, M., Castro, P. (2001), *Reply to the discussion by T.U. Mohammed and H. Hamada of the paper: Chloride threshold values to depassivate reinforcing bars embedded in a standardized OPC mortar*. Cement and Concrete Research. 31(5):39-840. DOI: [https://doi.org/10.1016/s0008-8846\(01\)00486-0](https://doi.org/10.1016/s0008-8846(01)00486-0)
- Alonso, C., Andrade, C., García, A. M. (1990), *Oxygen availability in the corrosion of reinforcements*. Advances in Cement Research. 3(11):127-132. DOI: <https://doi.org/10.1680/adcr.1990.3.11.127>
- Alonso, C., Andrade, C., Nóvoa, X. R., Izquierdo, M., Pérez, M. C. (1998), *Effect of protective oxide scales in the macrogalvanic behaviour of concrete reinforcements*. Corrosion Science. 40(8):1379–1389. DOI: [https://doi.org/10.1016/S0010-938X\(98\)00040-7](https://doi.org/10.1016/S0010-938X(98)00040-7)
- American Concrete Institute (2002), *ACI 211.1: Recommended practice for selecting proportions for normal weight concrete*, p. 953. Retrieved from <https://doi.org/10.14359/7325>
- Arya, C., Vassie, O. (1995), *Influence of cathode-to-anode area ratio and separation distance on galvanic corrosion currents of steel in concrete containing chlorides*. Cement and Concrete Research. 25(5):989-998. DOI: [https://doi.org/10.1016/0008-8846\(95\)00094-s](https://doi.org/10.1016/0008-8846(95)00094-s)
- ASTM International. (2010). *ASTM D 1411-04 Standard Test Methods for Water-Soluble Chlorides Present as Admixtures in Graded Aggregate Road Mixes*. Retrieved from <https://doi.org/10.1520/d1411-04>
- ASTM International. (2016). *ASTM C 876-15 Standard Test Method for Corrosion Potentials of Uncoated Reinforcing Steel in Concrete*. Retrieved from <https://doi.org/10.1520/c0876>
- ASTM International. (2017). *ASTM C 39-17 Standard Test Method for Compressive Strength of Cylindrical Concrete Specimens*. Retrieved from https://doi.org/10.1520/c0039_c0039m-05e02
- Dawson, J. L. (1996). Electrochemical noise measurement. In: Kearns, J. R., Scull J. R. “*Electrochemical noise measurement for corrosion applications*”, ASTM STP 1277. Annual Book of ASTM Standards, Philadelphia, p. 3. DOI: <https://doi.org/10.1520/stp37949s>
- Elsener, B. (2002). *Macrocell corrosion of steel in concrete-implications for corrosion monitoring*. Cement and Concrete Composites. 24(1):65-72. DOI: [https://doi.org/10.1016/s0958-9465\(01\)00027-0](https://doi.org/10.1016/s0958-9465(01)00027-0)
- Hudok, D. (1990). *Properties and selection: irons, steels, and high-performance alloys*. In: “Metals handbook”, 1, E.U., pp. 200-211.
- Kelly R.G., Inman, M.E., Hudson, J.L. (1996), *Analysis of Electrochemical Noise for Type 410 Stainless Steel in Chloride Solutions*. In: Kearns, J. R., Scully, J. R. “*Electrochemical noise measurement for corrosion applications*”. Annual Book of ASTM Standards, Philadelphia, pp. 101-113. DOI: <https://doi.org/10.1520/stp37954s>
- Legat, A., Dolecek, V. (1995), *Corrosion Monitoring System Based on Measurement and Analysis of Electrochemical Noise*. Corrosion Science. 51(4): 295-300. DOI: <https://doi.org/10.5006/1.3293594>
- Llorens, M., Serrano, Á., Valcuende, M. (2019), *Sensors for Determining the Durability of Reinforced Concrete Constructions*. Revista Ingeniería de Construcción. 34(1): 81-98. DOI: <https://doi.org/10.4067/s0718-50732019000100081>
- McCarter, W. J., Chrisp, T. M., Butler, A., Basheer, P. A. M. (2001), *Near-Surface Sensors for Condition Monitoring of Cover-Zone Concrete*. Construction and Building Materials. 15(2-3): 115-124. DOI: [https://doi.org/10.1016/s0950-0618\(00\)00060-x](https://doi.org/10.1016/s0950-0618(00)00060-x)

- McCarter, W. J., Vennesland, Ø. (2004), *Sensor systems for use in reinforced concrete structures*. Construction and Building Materials. 18(6):51-358.
DOI: <https://doi.org/10.1016/j.conbuildmat.2004.03.008>
- Mohammed, T. U., Hamada, H. (2001), *A discussion of the paper: Chloride threshold values to depassivate reinforcing bars embedded in a standardized OPC mortar* by C. Alonso, C. Andrade, M. Castellote, and P. Castro. Cement and Concrete Research. 31(5): 835-838.
DOI: [https://doi.org/10.1016/s0008-8846\(01\)00485-9](https://doi.org/10.1016/s0008-8846(01)00485-9)
- NMX C155. (2014). *Industria de la construcción – Concreto hidráulico – Dosificado en masa – Especificaciones y métodos de ensayo*. Ciudad de México: ONNCCE.
- NMX C159. (2004). *Industria de la construcción -Concreto -Elaboración y curado de especímenes en el laboratorio*. Ciudad de México: ONNCCE.
- NMX C414. (2004). *Industria de la construcción -Cementos hidráulicos -Especificaciones y métodos de prueba*. Ciudad de México: ONNCCE
- PROCEDIMIENTO LAQ03. (2005), *Determinación del contenido de Al, C, Co, Cr, Cu, Mn, Mo, Ni, P, Pb, S, Si, Ti y Zn, de aceros al carbono y aceros inoxidables por ICP-AAE y CHNS-O*. CIMAV-EMA, BAJO NORMA ISO/IEC-17025-2005, México.
- Raupach, M. (1996), *Chloride-induced macrocell corrosion of steel in concrete-theoretical background and practical consequences*. Construction and Building Materials. 10(5): 329-338.
DOI: [https://doi.org/10.1016/0950-0618\(95\)00018-6](https://doi.org/10.1016/0950-0618(95)00018-6)
- Raupach, M., Dauberschmidt, C. (2003), “*Durability of marine structures made of high-performance concrete*”. In: RILEM Proceedings, PRO 32 International Conference on Advances in Concrete and Structures, 2, pp. 919-930. ISBN: 2-912143-41-1. e-ISBN: 2351580176
- Raupach, M., Schießl, P. (2001), *Macrocell sensor systems for monitoring of the corrosion risk of the reinforcement in concrete structures*. NDT & E International. 34(6):435-442.
DOI: [https://doi.org/10.1016/s0963-8695\(01\)00011-1](https://doi.org/10.1016/s0963-8695(01)00011-1)
- Schiessl, P., Raupach, M. (1992), *Monitoring system for the corrosion risk of steel in concrete structures*. Concrete International. 14(7):52-55.
- Zinc-Taek, P., Yoon-Seok, C., Jung-Gu, K., Lun, C. (2005), *Development of a galvanic sensor system for detecting the corrosion damage of steel embedded in concrete structure*. Cement and Concrete Research. 35(9): 1814-1819. DOI: <https://doi.org/10.1016/j.cemconres.2003.11.027>

Evaluation of the influence of corrosion on the global stability of reinforced concrete columns

M. F. dos Santos¹ , D. P. dos Santos^{2*} 

*Contact author: daniilo.pereira@engenharia.ufjf.br

DOI: <https://doi.org/10.21041/ra.v12i3.592>

Reception: 01/03/2022 | Acceptance: 08/07/2022 | Publication: 01/09/2022

ABSTRACT

This paper analyzes the impact of corrosion on the global stability of reinforced concrete columns, evaluating the effectiveness of the stiffness reduction criteria proposed by ABNT NBR 6118:2014. It was defined through finite element models that corrosion causes the intensification of the second-order effects. However, in critical situations, the failure in the transversal section led to structural collapse even before the stability loss. The study was conducted through nonlinear geometric analyses and applying the γ_z coefficient. It was concluded that the subsequent addition of rheological effects could exceed the limits proposed by the ABNT NBR 6118:2014.

Keywords: concrete; corrosion; global stability; second-order effects.

Cite as: dos Santos, M. F., dos Santos, D. P. (2022), “*Evaluation of the influence of corrosion on the global stability of reinforced concrete columns*”, Revista ALCONPAT, 12 (3), pp. 401 – 422, DOI: <https://doi.org/10.21041/ra.v12i3.592>

¹ Fundação Hermínio Ometto (FHO | Uniararas), Araras, Brasil.

² Universidade Federal Tecnológica do Paraná (UTFPR), Curitiba, Brasil.

Author contribution

In this paper, M. F. Santos contributed to the activities of developing the numerical model, results and discussion, writing and preparation of the original text; D. P. Santos contributed to the conceptualization activities, development of the numerical model, results and discussion, writing and preparation of the original text.

Creative Commons License

Copyright 2022 by the authors. This work is an Open-Access article published under the terms and conditions of an International Creative Commons Attribution 4.0 International License ([CC BY 4.0](https://creativecommons.org/licenses/by/4.0/)).

Discussions and subsequent corrections to the publication

Any dispute, including the replies of the authors, will be published in the third issue of 2023 provided that the information is received before the closing of the second issue of 2023.

Evaluación de la influencia de la corrosión en la estabilidad global de las columnas de hormigón armado

RESUMEN

Este trabajo analiza el impacto de la corrosión en la estabilidad global de las columnas de hormigón armado, evaluando la efectividad de los criterios de reducción de rigidez propuestos por la ABNT NBR 6118: 2014. Con los análisis, utilizando modelos de elementos finitos que reproducían el comportamiento de los materiales, se definió que la corrosión provoca la intensificación de los esfuerzos globales de segundo orden en la estructura. Sin embargo, en situaciones críticas, la pérdida de equilibrio en la sección transversal resultó en una falla estructural incluso antes de la pérdida de la estabilidad. El estudio se llevó a cabo tanto a través de un análisis geométrico no lineal como mediante la aplicación del coeficiente γ_z , donde se concluyó que la posterior adición de efectos reológicos puede conducir a una configuración que va más allá de los límites propuestos por la norma brasileña.

Palabras clave: hormigón; corrosión; estabilidad global; efectos de segundo orden.

Avaliação da influência da corrosão na estabilidade global de colunas em concreto armado

RESUMO

Este trabalho analisa o impacto da corrosão na estabilidade global de colunas em concreto armado, avaliando a eficácia dos critérios de redução de rigidez propostos pela ABNT NBR 6118:2014. A partir das análises, utilizando-se modelos em elementos finitos que reproduziram o comportamento dos materiais, definiu-se que a corrosão causa a intensificação dos esforços globais de segunda ordem na estrutura. Entretanto, em situações críticas, a perda de equilíbrio na seção transversal conduziu à falha estrutural antes mesmo da perda de estabilidade. O estudo foi realizado tanto por meio de uma análise não-linear geométrica, quanto pela aplicação do coeficiente γ_z , onde concluiu-se que a posterior adição de efeitos reológicos pode conduzir a uma configuração que ultrapasse os limites propostos pela norma brasileira.

Palavras-chave: concreto; corrosão; estabilidade global; efeitos de segunda ordem.

Legal Information

Revista ALCONPAT is a quarterly publication by the Asociación Latinoamericana de Control de Calidad, Patología y Recuperación de la Construcción, Internacional, A.C., Km. 6 antigua carretera a Progreso, Mérida, Yucatán, 97310, Tel.5219997385893, alconpat.int@gmail.com, Website: www.alconpat.org

Reservation of rights for exclusive use No.04-2013-011717330300-203, and ISSN 2007-6835, both granted by the Instituto Nacional de Derecho de Autor. Responsible editor: Pedro Castro Borges, Ph.D. Responsible for the last update of this issue, Informatics Unit ALCONPAT, Elizabeth Sabido Maldonado.

The views of the authors do not necessarily reflect the position of the editor.

The total or partial reproduction of the contents and images of the publication is carried out in accordance with the COPE code and the CC BY 4.0 license of the Revista ALCONPAT.

1. INTRODUCTION

Corrosion can be understood as the destructive interaction between steel and the environment. The corrosion is initiated by electrochemical, chemical, and physical actions or by their union. The process is usually aggravated by the activity of chlorides or by the development of cracks. The corrosion process in regions with tensile stresses is a severe problem since it can cause a brittle rupture without prior strain. (Helene, 1993; Schwartzman et al., 2010).

The steel in reinforced concretes (RCs) is protected by an iron oxide film that forms on the metal surface due to the alkalinity of the concrete, ensuring its passivation. However, the protection can be compromised with pH reduction to below nine due to the carbonation of the concrete. The carbonation process occurs due to the presence of chloride ions at critical rates of atmospheric pollution, which is intensified by the age of the construction (Maldonado-Bandala et al., 2018; Araujo et al., 2020; Silvestro et al., 2020).

The use of inadequate cover thicknesses due to design or execution errors can compromise the protection of the steel bars (Fusco, 2008; Malheiro et al., 2014; Felix e Carrazedo, 2021). Furthermore, the choice of cement, additives, and additions can mitigate or intensify the corrosive potential (Silva et al., 2015; Trevisol et al., 2017; Dietrich et al., 2017; Teixeira et al., 2021).

Steel corrosion results in a powdery hydroxide without adhesion or cohesion called rust, which increases in volume as it forms and can have eight to ten times the initial volume of steel. Thus, the rusted regions put pressure on the surrounding concrete, initiating the degradation of the structure. (Verçoza, 1991; Balestra et al., 2018).

Several studies aim to reproduce the deterioration conditions in the laboratory through accelerated tests (Meira e Ferreira, 2019). In addition, other authors intend to investigate the impact of different additions on the corrosive potential of RC (Amorim Júnior et al., 2021; Santos et al., 2020; Blanco et al., 2019; Figueiredo et al., 2014). Such studies are necessary as it is estimated that up to 3.5% of a developed country's Gross Domestic Product (GDP) is spent on repairs from corrosion degradation (Mackechnie e Alexander, 2001). Thus, research on mathematical models that can describe the structural degradation caused by corrosion is increasing.

Recent research has explored numerical simulation of chloride diffusion in concrete and reliability analyses based on probabilistic models (Ayinde et al., 2017; Souza and Leonel, 2021; Felix et al., 2020; Ramos and Carrazedo, 2021; Favretto et al., 2021). However, other applications use the finite element method, such as the one proposed by Ramos and Carrazedo (2020). They developed models capable of describing the different stages of damage propagation caused by the corrosive process on RC specimens.

Therefore, the present study aims to contribute to this area, adding to the corrosion problem the evaluation of global stability. For this purpose, the concrete behavior and the damage evolution were numerically reproduced. The numerical model was performed using the Finite Element Method (FEM), as discussed in this paper.

2. METHODOLOGY

Using numerical simulations to predict the behavior of reinforced concrete structures (in the presence of damage) requires a satisfactory stress-strain curve reproduction of the materials. This section will describe all the parameters used to simulate the mechanical behavior of concrete and steel. The validation of the constitutive models will be demonstrated through the comparison with the Model Code (2010).

2.1 Constitutive models

Materials settings that reproduce the behavior of steel and concrete have been added to finite element models. These settings contain characteristics such as density, Young's modulus, and Poisson's ratio.

In the case of concrete, due to the natural development of cracks, it is necessary to add more information so that the model can reproduce the behavior in tension, compression, inelastic strains, and damage.

The constitutive models used for the materials (concrete and steel) were extracted from the European code CEB-FIB (2010). Thus, this step aims to reproduce the mechanical behavior of reinforced concrete, its stress-strain curve, and the influence of applying a damage model.

2.1.1 Constitutive model of steel

The constitutive model used for steel describes its behavior in the presence of tensile (or compression) stresses, represented in the diagram in Figure 1. The first curve represents the linear response of the material until the yield strength (f_{yk}). After that, yield occurs until the characteristic strength (f_{tk}) and the maximum strain (ϵ_{uk}) are reached.

The stresses in the steel (σ_s) were obtained through Eq. (1), i.e., from the steel Young's modulus (E_s) and the steel strain (ϵ_s).

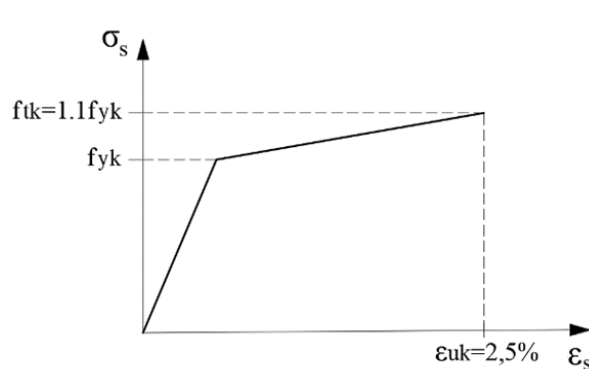


Figure 1. Stress-strain curve for the steel
(Adapted from CEB-FIB, 2010)

$$\sigma_s = E_s \cdot \epsilon_s$$

where: $E_s = 200\text{GPa}$, if $\epsilon_s \leq 0,207\%$ (1)
 $E_s = 2,2\text{GPa}$, if $\epsilon_s > 0,207\%$

2.1.2 Constitutive model of concrete

The constitutive model used in concrete reproduces its behavior in compression (Figure 2) and tension (Figures 3 and 4).

When compressed, the concrete presents an elastic behavior until reaching the average compressive strength (f_{cm}). After this point, microcracks development causes the *softening*, represented in the decreasing curve.

Tensile concrete presents a linear elastic behavior until reaching a deformation of 0.15‰ (ϵ_{ct}) in approximately 90% of the average tensile strength (f_{ctm}). At stresses close to the f_{ctm} , the microcracks intensify, and the material drastically reduces its stiffness.

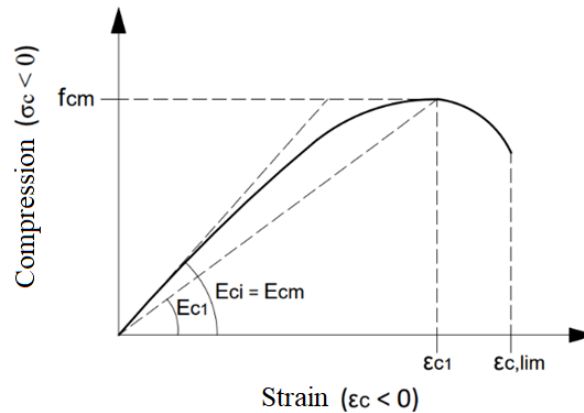


Figure 2. Stress-strain curve for the compressed concrete (Adapted from CEB-FIB, 2010)

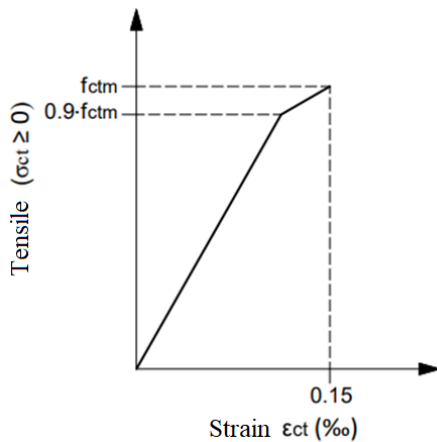


Figure 3. Stress-strain curve for tensile concrete (elastic behavior) (Adapted from CEB-FIB, 2010)

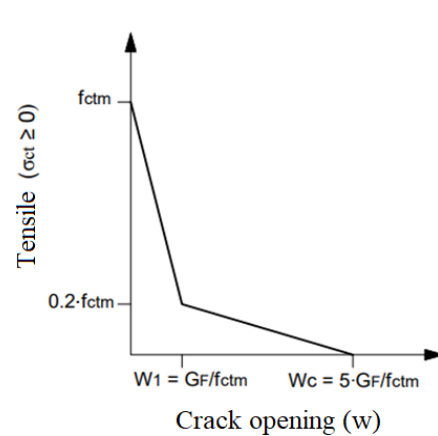


Figure 4. Stress-crack opening relation for tensile concrete (Adapted from CEB-FIB, 2010)

The f_{cm} was defined through Eq. (2) using the characteristic compressive strength (f_{ck}) and the difference between the average strength and the characteristic strength of concrete (Δf).

The secant module (E_{c1}) was defined from Eq. (3). In this equation, the maximum compression strain (ϵ_{c1}) is obtained through the tabulated values contained in the CEB-FIB (2010).

Eq. (4) was used to determine Young's modulus of the concrete at 28 days (E_{ci}), which depends on Young's modulus initial (E_{c0}), the nature of the aggregate (α_E), and the standardized value Δf , defined by consulting the CEB- FIB (2010).

The ratio between the strains (η) and the plasticity constant (k) was defined through Eqs. (5) and (6), respectively. Finally, Eq. (7) defined the stress-strain curve shown in Figure 2.

$$\begin{array}{l}
 f_{cm} = f_{ck} + \Delta f \quad (2) \\
 \eta = \frac{\varepsilon_c}{\varepsilon_{c1}} \quad (5)
 \end{array}
 \left| \begin{array}{l}
 E_{c1} = \frac{f_{cm}}{\varepsilon_{c1}} \quad (3) \\
 k = \frac{E_{ci}}{E_{c1}} \quad (6)
 \end{array} \right.
 \begin{array}{l}
 E_{ci} = E_{c0} \cdot \alpha_E \cdot \left(\frac{f_{ck} + \Delta f}{10} \right)^{1/3} \quad (4) \\
 \sigma_c = \left(\frac{k \cdot \eta - \eta^2}{1 + (k-2) \cdot \eta} \right) \cdot f_{cm} \quad (7)
 \end{array}$$

The tensile strength of concrete (f_{ctm}) was defined through Eqs. (8) and (9), which depends on its f_{ck} .

The stresses in the fracture zone (after f_{ctm}) are related to crack opening (w) through Eqs. (10) and Eq. (11). Finally, the fracture energy (G_F) was obtained from Eq. (12).

$G_F \times w$ alone is not enough for many applications. Therefore, Aitsin et al. (2008) define the characteristic length (l_{ch}), Eq. (13), as a useful value for evaluating crack opening in terms of strain.

$$\begin{array}{l}
 f_{ctm} = 0,3 \cdot (f_{ck})^{2/3}, \text{ if } f_{ck} \leq 50MPa \quad (8) \\
 f_{ctm} = 2,12 \cdot \ln(1 + 0,1 \cdot (f_{ck} + \Delta f)), \text{ if } f_{ck} > 50MPa \quad (10) \\
 w_1 = \frac{G_F}{f_{ctm}}, \text{ if } \sigma_t = 0, 20 \cdot f_{ctm} \quad (12)
 \end{array}
 \left| \begin{array}{l}
 w_c = 5 \cdot \frac{G_F}{f_{ctm}}, \text{ if } \sigma_t = 0 \quad (9) \\
 G_F = 73 \cdot f_{cm}^{0,18} \quad (11) \\
 l_{ch} = \frac{E_{ci} \cdot G_F}{f_{ctm}^2} \quad (13)
 \end{array} \right.$$

The strains ε_t had values ranging from zero to maximum cracks (w_c), defined from the ratio between w_c and l_{ch} . The tensile stress (σ_t) was defined up to a strain of 0.15‰ through Eqs. (14) and (15). In the fracture zone, the σ_t was determined using Eqs. (16) and (17), ranging from 0.15‰ to w_c .

$$\sigma_t = E_{ci} \cdot \varepsilon_t, \text{ if } \sigma_t \leq 0,9 \cdot f_{ctm} \quad (14)$$

$$\sigma_t = f_{ctm} \cdot \left(1 - 0,1 \cdot \frac{0,00015 - \varepsilon_t}{0,00015 - 0,9 \cdot f_{ctm} / E_{ci}} \right), \text{ if } 0,9 \cdot f_{ctm} < \sigma_t \leq f_{ctm} \quad (15)$$

$$\sigma_t = f_{ctm} \cdot \left(1 - 0.8 \cdot \frac{w}{w_1} \right), \text{ if } w \leq w_1 \quad (16)$$

$$\sigma_t = f_{ctm} \cdot \left(0,25 - 0,05 \cdot \frac{w}{w_1} \right), \text{ if } w_1 < w \leq w_c \quad (17)$$

The values of σ_c and σ_t were added to the damage model applied to concrete in the numerical simulations.

2.1.2.1 Damage model applied to the concrete model

The model adopted for concrete was the Concrete Damage Plasticity (CDP), developed by Lubliner et al. (1989) and improved by Lee and Felves (1998). This model is implemented and available in the Abaqus®.

The behavior in the presence of damage is represented in the diagrams in Figures 5 and 6. Eqs. (18) and (19) described the stress x strain relationship for compression and tensile, respectively (Hibbitt et al., 2011).

While intact, the concrete shows conservation in its initial Young's modulus (E_0). However, upon reaching the maximum stresses (σ_{tu} or σ_{cu}), the degeneration process begins as the damage variables d_t (traction) and d_c (compression) are increased. Finally, the plastic deformations in tension (ε_t^{pl}) and compression (ε_c^{pl}) add plasticity to the model.

The damage variables d_c and d_t were obtained through Eqs. (20) and (21), respectively, proposed by Yu et al. (2010), with the values of σ_c , σ_t , f_{cm} , and f_{ctm} already defined.

Thus, the calculated d_c and d_t damage variables were added to the concrete damage model.

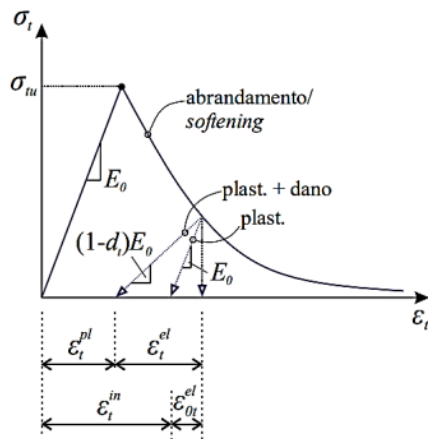


Figure 5. Stress-strain curve for the tensile concrete (Reginato, 2020)

$$\sigma_c = (1 - d_c) E_0 \cdot (\varepsilon_c - \varepsilon_c^{pl}) \quad (18)$$

$$\sigma_t = (1 - d_t) E_0 \cdot (\varepsilon_t - \varepsilon_t^{pl}) \quad (20)$$

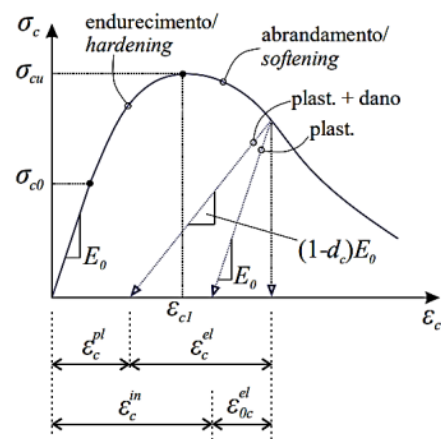


Figure 6. Stress-strain curve for the compressed concrete (Reginato, 2020)

$$d_c = 1 - \frac{\sigma_c}{f_{cm}} \text{ para } \varepsilon_c \geq \varepsilon_{c1} \quad (19)$$

$$d_t = 1 - \frac{\sigma_t}{f_{ctm}} \text{ para } \varepsilon_t \geq \varepsilon_{tu} \quad (21)$$

2.2 Validation of the constitutive models

Numerical simulations were performed in Abaqus® to analyze whether the constitutive models achieved the expected response.

In this first step, three analyzes were conducted, one to verify the behavior of the tensile steel (in 2D bar elements) and the other two to demonstrate the behavior of the tensioned and compressed concrete (in 2D linear solid elements with four nodes). The elastic properties of materials, such as Young's modulus (E) and Poisson's ratio (ν), were extracted from Álvares (1993). In addition, convergence tests were performed on the finite element meshes.

The results obtained with the numerical simulations were compared to the theoretical-analytical models proposed in CEB-FIB (2010). These comparisons are represented in Figures 7, 8, and 9.

From the analyses, it was possible to define that the constitutive model used in the steel guaranteed the expected behavior, presenting only a minor deviation at the beginning of the yield. Furthermore, Figures 8 and 9 also show adequate results for the modeled concrete.

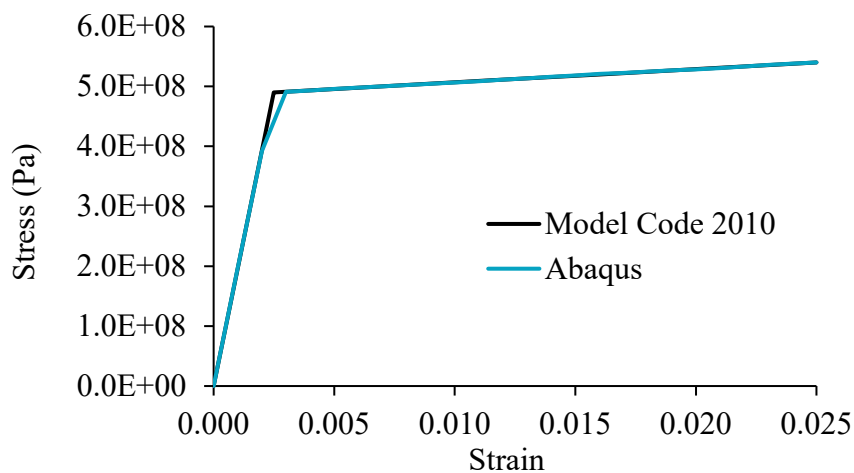


Figure 7. Comparison between the stress-strain curves: tensile steel

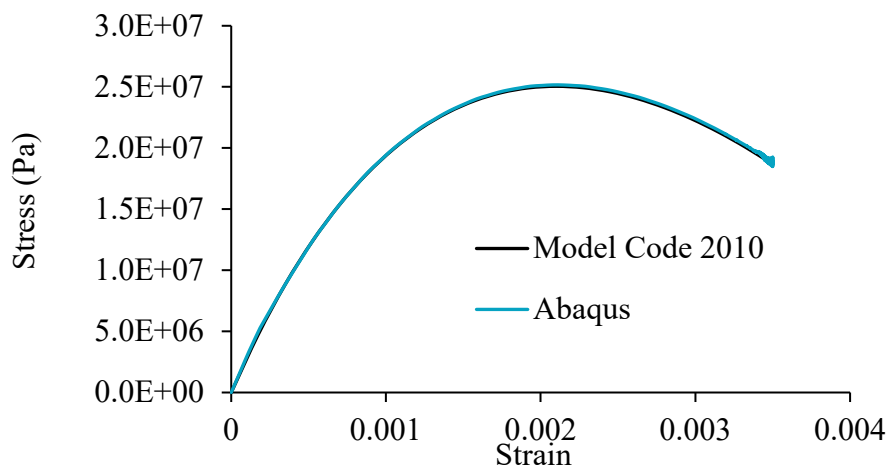


Figure 8. Comparison between the stress-strain curves: compressed concrete

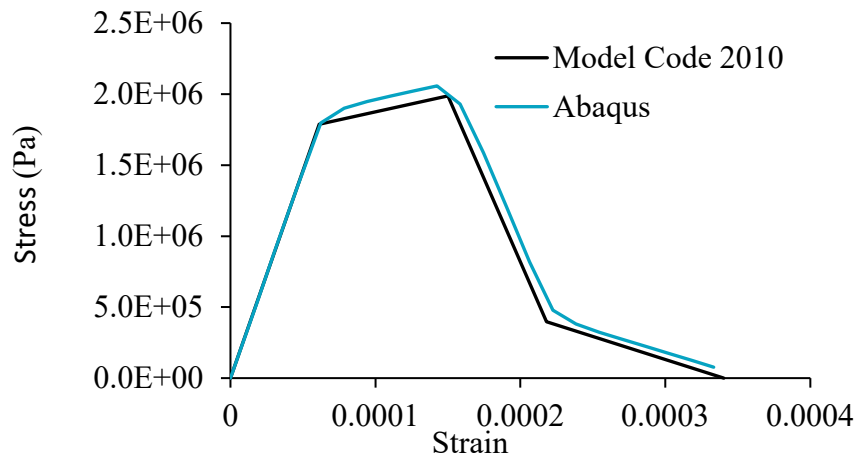


Figure 9. Comparison between the stress-strain curves: tensile concrete

The validated constitutive models were applied in a nonlinear numerical simulation of a reinforced concrete beam. For this, a 3D modeling was carried out in Abaqus®, using linear parallelepiped solid elements of 8 nodes (simulating concrete) and 3D bar elements (simulating steel bars and stirrups). Perfect adhesion between steel and concrete was considered.

The dimensions, reinforcement rate, load application, and elastic properties of the materials (Table 1) were extracted from Álvares (1993).

Convergence tests were performed on the structured finite element mesh. Thus, several linear analyzes were conducted, increasing the number of elements until the displacement at the center of the beam converged.

Table 1. Elastic properties of materials (Adapted from Álvares, 1993)

Material	Poisson's ratio	Young's modulus (MPa)
Concrete	0.2	29200
Steel	0.3	196000

The numerical analysis achieved a displacement of 8 mm in the center of the beam, corresponding to a load of approximately 47 kN.

Finally, the results were compared to those obtained in the experimental analysis by Álvares (1993) and to the theoretical model deduced by the authors, based on the cracking hypotheses proposed by Branson (1968) (Figure 10). Branson's model (1968) contemplates an *average inertia*, which considers the effects of cracking along the structural element, based on a semi-probabilistic analysis.

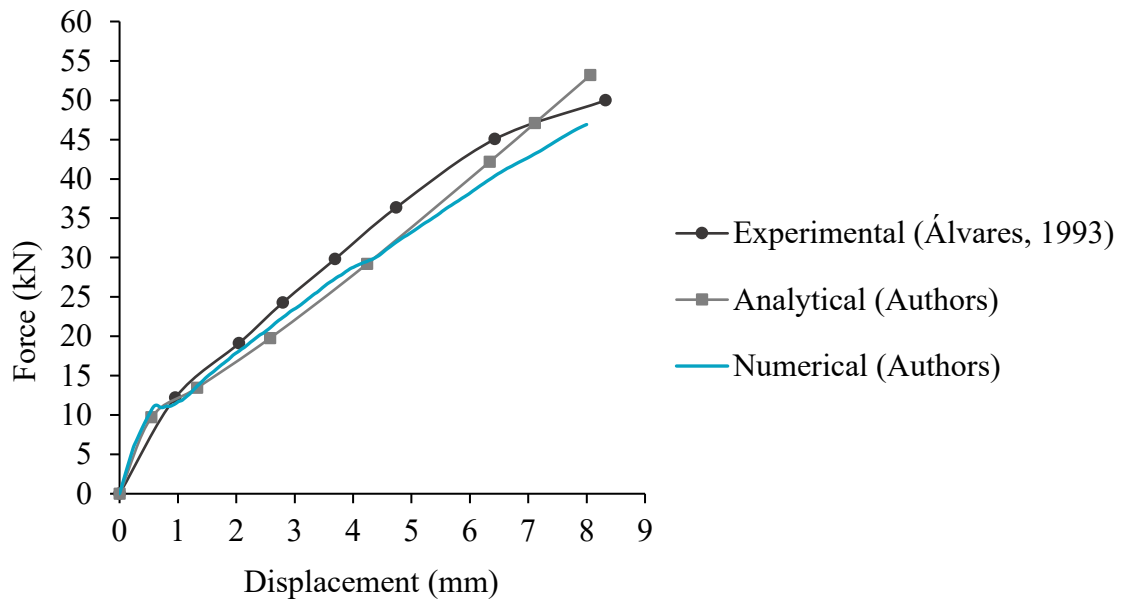


Figure 10. Comparison between the force-displacement curves

The numerical simulation presented similar results to the experimental analysis and the analytical model. However, slight divergences were observed, justified by the uncertainties associated with the concrete characterization parameters. Furthermore, there are significant differences between the boundary conditions adopted in the numerical model and those in the experimental test.

It was also possible to observe the evolution of the damage in the structure, represented in Figure 11. First, there was a development and propagation of cracks, until reaching a high state of degradation, in a very similar way to that observed by Álvares (1993) in his experimental analysis.

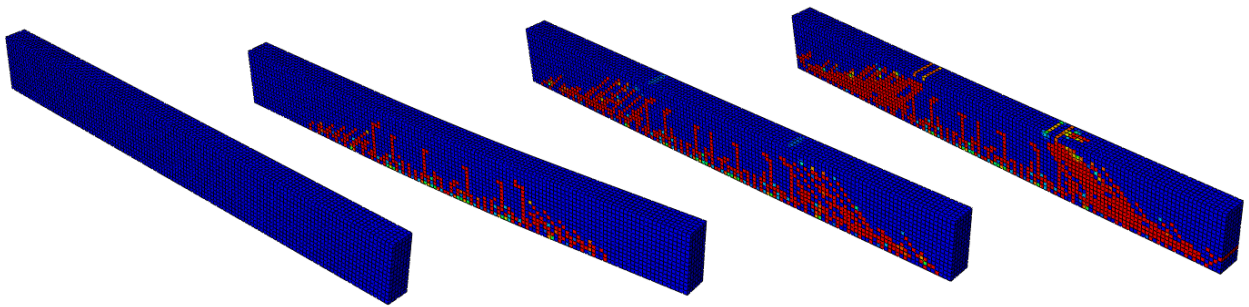


Figure 11. Evolution of cracks in the beam

After confirming the efficiency of the constitutive models applied and the damage model used to represent the degradation of concrete, a new structure was modeled in Abaqus[®]. Corrosion has now been added to the new structure, as discussed in the following sections.

2.3 Modeling of the structure

This section presents the idealization of the studied structure, the strategy for the numerical simulation of the degradation caused by the corrosion, and the methodology for evaluating global stability. Information about the modeling in finite elements will also be given.

2.3.1 Geometric characteristics of the structure

The proposed structure for the simulations is based on the one presented by Wahrhaftig (2008), Figure 12. It is a slender, hollow section structure in RC used to support a telephone transmission system. Although the dimensions reproduced in the numerical model are not the same as the real structure, the proportion of the slenderness was kept.

Thus, the structural element was modeled with a height of 14 m and is reinforced with 16 $\phi 25$ mm steel bars, arranged according to Figure 12.

The concrete and the steel bars were modeled with 8-node parallelepiped linear solid elements. The boundary conditions include a vertical load (5 kN) at the top, as a representation of the antennas, and a fixed set at the base.

Furthermore, the horizontal forces that characterize the wind load were added to the model in the form of forces every 1 m of the structure. Finally, the self-weight was considered ($g = 9.81 \text{ m/s}^2$), with the specific masses of concrete and steel equal to 2400 kg/m^3 and 7850 kg/m^3 , respectively (ABNT NBR 6120:2019).

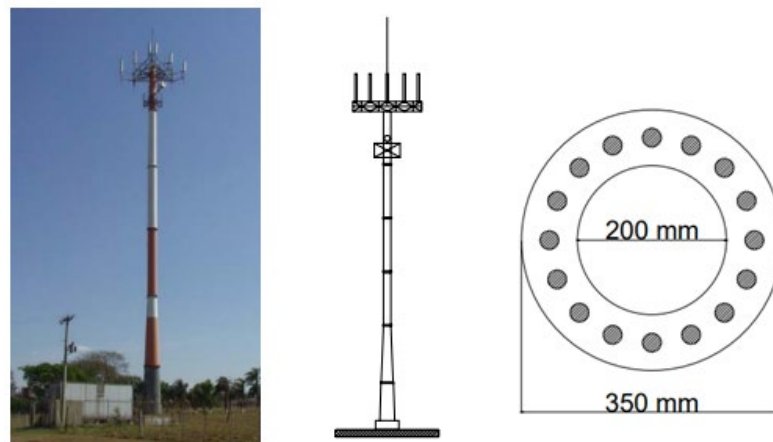


Figure 12. Real structure approximated by the numerical model (Adapted from Wahrhaftig, 2008)

2.3.2 Wind load considerations

The wind was estimated through equations extracted from ABNT NBR 6123:1988 and applied to the structure as horizontal forces every meter.

Initially, the factor S_2 was calculated. This factor considers the influence of ground roughness, dimensions, and height of the building (Eq. (22)). The topographic (S_1) and statistical (S_3) factors take into account the slopes of the land and the use of the building, their values must be directly consulted in the code. Another essential variable is the basic wind speed (V_0), defined by the location of the structure. The V_0 allied to the factors S_1 , S_2 and S_3 determine the characteristic wind speed, V_k (Eq. (23)).

Thus, after these definitions, the dynamic pressure (q) was calculated through Eq. (24); this value is useful for calculating horizontal forces.

Finally, the drag force (F_a), Eq. (25), took into account the drag coefficient (C_a), the reduction factor (K), the vertical distance between the forces (H), and the external diameter of section (D).

The F_a values, calculated for each meter, were the horizontal forces applied.

$$S_2 = b \cdot F_R \cdot Z^p \quad (22)$$

where
 $b = 1$; $F_R = 1$; $p = 0,085$
 Z : wind load altitude

$$V_k = S_1 \cdot S_2 \cdot S_3 \cdot V_0 \quad (24)$$

where
 $S_1 = 1$; $S_3 = 1,1$; $V_0 = 30 \text{ m/s}$

$$q = 0,613 \cdot V_k^2 \quad (23)$$

$$F_a = C_a \cdot q \cdot K \cdot H \cdot D$$

where
 $C_a = 0,60$; $K = 1$ (25)
 H : vertical distance between forces
 D : diameter of the section

2.3.3 Corrosion consideration

Corrosion was added in order to verify its influence on structural stability. The expansion generated by the corrosion products was represented through the application of radial displacements in pre-established extensions of the concrete in contact with the steel bars affected by corrosion. The corrosion points were chosen close to the maximum bending moment.

The method to define the values of the applied radial displacements was proposed by El-Maaddawy and Soudki (2007).

The hole flexibility constant (k) was obtained from Eq. (26). It is a constant that relates the radial displacement with the corrosion pressure, taking into account the porous zone present in the contact interface between the steel and the concrete. Physically, the porous region must initially be filled with corrosion products before the expansive stresses create pressure on the surrounding concrete. For Eq. (26), it is necessary to define: the Poisson's ratio (ν), Young's effective modulus (E_{ef}), steel bars diameter (D), porous zone thickness (δ_0), concrete cover (C), and factor (ψ) calculated with Eq. (27).

The radial pressure necessary to produce displacements in the concrete (P_{cor}) was calculated using Eq. (28), where the percentage of steel mass loss (m_l) varied according to the concrete strength. Finally, it was possible to define the displacement values in the concrete (δ_c) corresponding to the increase in volume generated by the rust (Eq. (29)).

The m_l can be related to the mass of steel consumed per unit of length (M_{loss}) through Eq. (30), using the diameter (D) and the density of the steel bars (ρ_s).

$$k = \frac{(1 + \nu + \psi) \cdot (D + 2\delta_0)}{2E_{ef}} \quad (26)$$

$$\psi = \frac{(D + 2\delta_0)^2}{2C \cdot (C + D + \delta_0)} \quad (28)$$

$$P_{cor} = \frac{m_l \cdot E_{ef} \cdot D}{90,9 \cdot (1 + \nu + \psi) \cdot (D + 2\delta_0)} - \frac{2\delta_0 \cdot E_{ef}}{(1 + \nu + \psi) \cdot (D + 2\delta_0)} \quad (30)$$

$$\delta_c = k \cdot P_{cor} \quad (27)$$

$$\left(\frac{M_{loss}}{\rho_s} \right) = \frac{m_l \cdot (\pi D^2)}{400} \quad (29)$$

2.4 Methodology for global stability assessment

Initially, three simulations were performed in Abaqus® to verify the stability of the structure with different concrete strengths (C20 to C50). The displacement at the top and the moment at the base were verified in each analysis.

The first step consisted of calculating the γ_z coefficient according to ABNT NBR 6118:2014, Eq. (31), using data from the first analysis (named AN1). Thus, AN1 consisted of an elastic and linear analysis with a reduction of Young's modulus (E) by 20%.

The γ_z coefficient depends on the moment at the base and the sum of the products between vertical forces and horizontal displacements obtained in the first-order analysis. This coefficient allows evaluating the importance of global second-order effects in the structure. Thus, if $\gamma_z < 1,1$, the second-order effects can be neglected.

Additional information about the γ_z coefficient, including its mathematical deduction, can be consulted in the paper of Franco and Vasconcelos (1991).

The geometrically nonlinear analysis (GNA) was added to the AN1 model, producing the second analysis (AN2), where the reduction of Young's modulus was maintained at 20%.

From the moment values at the base, obtained in the first and second analysis (AN1 and AN2), a new coefficient γ_z was calculated. The $\Delta M_{tot,d}$ used was the difference between the moment obtained in the AN2 and AN1, while the $M_{1,tot,d}$ was the moment of the first analysis (AN1). This calculation only confirmed the competence of the γ_z coefficient as an estimator of second-order effects.

Finally, in the third analysis (AN3), the E was kept intact and material nonlinearity (MNA) and GNA was added to the model. The coefficient γ_z , now renamed γ_{zcalc} , Eq. (32), was calculated and will be presented in the results of this paper.

Therefore, in AN3, the constitutive and damage models replaced the reduction of Young's modulus by 20%.

$$\gamma_z = \frac{1}{1 - \frac{\Delta M_{tot,d}}{M_{1,tot,d}}} \quad (31)$$

where

$\Delta M_{tot,d}$ is the sum of the products of the vertical forces by the horizontal displacements obtained in the 1st order analysis

$M_{1,tot,d}$ is the moment at the base (calculated from a linear analysis)

$$\gamma_{zcalc} = \frac{M_{2,tot,d}}{M_{1,tot,d}} \quad (32)$$

where

$M_{2,tot,d}$ is the total moment calculated from a 2nd order analysis

$M_{1,tot,d}$ is the moment at the base (calculated from a linear analysis)

Subsequently, corrosion was added to AN3, and eight more simulations were performed with each concrete class. Four analyses were performed on a model affected by corrosion in three steel bars in a 5 cm extension (AN4 to AN7). The other analyses were carried out in a model with corrosion action on five steel bars in a 10 cm extension (AN8 to AN11).

In both cases, corrosion was added at 30 cm from the base. In this step, the γ_{zcalc} coefficient was calculated as described in Eq. (32).

Furthermore, the adhesion between the steel and the concrete was considered perfect, except for the regions degraded by corrosion.

The summary of the analyzes can be found in Frame 1.

Frame 1. Summary of analyzes performed

Analysis	Description	
AN1	Linear analysis with a 20% reduction of Young's modulus	0.8E
AN2	Geometric nonlinear analysis with a 20% reduction of Young's modulus	GNA and 0.8E
AN3	Material and geometric nonlinear analysis without Young's modulus reduction	MNA, GNA, and E
AN4 a AN11	Material and geometric nonlinear analysis with corrosion	MNA, GNA, and corrosion

2.4.1 Finite element mesh

The finite element mesh comprised linear parallelepiped three-dimensional elements formed by six faces and eight nodes.

The mesh sizing applied to the model was performed through iterative simulations without nonlinearities. As a result, the number of finite elements was increased until the displacement at the top converged.

3. RESULTS AND DISCUSSIONS

Corrosion (m_I) was added to the model gradually, so the radial displacement was higher in each simulation with different concrete strength classes. The equivalence between the values of m_I , the radial displacement applied to the concrete (δ_c), and the mass of steel consumed (M_{loss}) are represented in Table 2.

Table 2. Parameters used in the simulations

Analysis	C20 e C30			C40 e C50			
	m_I [%]	Radial displacement δ_c [μm]	M_{loss} [g/m]	m_I [%]	Radial displacement δ_c [μm]	M_{loss} [g/m]	
3 bars	AN3	0.091	0.00	3.51	0.091	0.00	3.51
	AN4	0.150	8.13	5.79	0.300	28.75	11.57
	AN5	0.200	15.00	7.72	0.350	35.63	13.50
	AN6	0.250	21.88	9.65	0.400	42.51	15.43
	AN7	0.300	28.75	11.57	0.450	49.38	17.36
5 bars	AN3	0.091	0.00	3.51	0.091	0.00	3.51
	AN8	0.105	1.94	4.05	0.125	4.69	4.82
	AN9	0.110	2.63	4.24	0.138	6.41	5.31
	AN10	0.115	3.31	4.44	0.150	8.13	5.79
	AN11	0.120	4.00	4.63	0.163	9.85	6.27

After the simulations, it was possible to verify that the two parameters analyzed (displacement at the top and moment at the base) increased with the m_I , demonstrating that the evolution of corrosion generates a stiffness reduction, intensifying the second-order effects.

The moments at the base, obtained with the simulations, are represented in Figure 13.

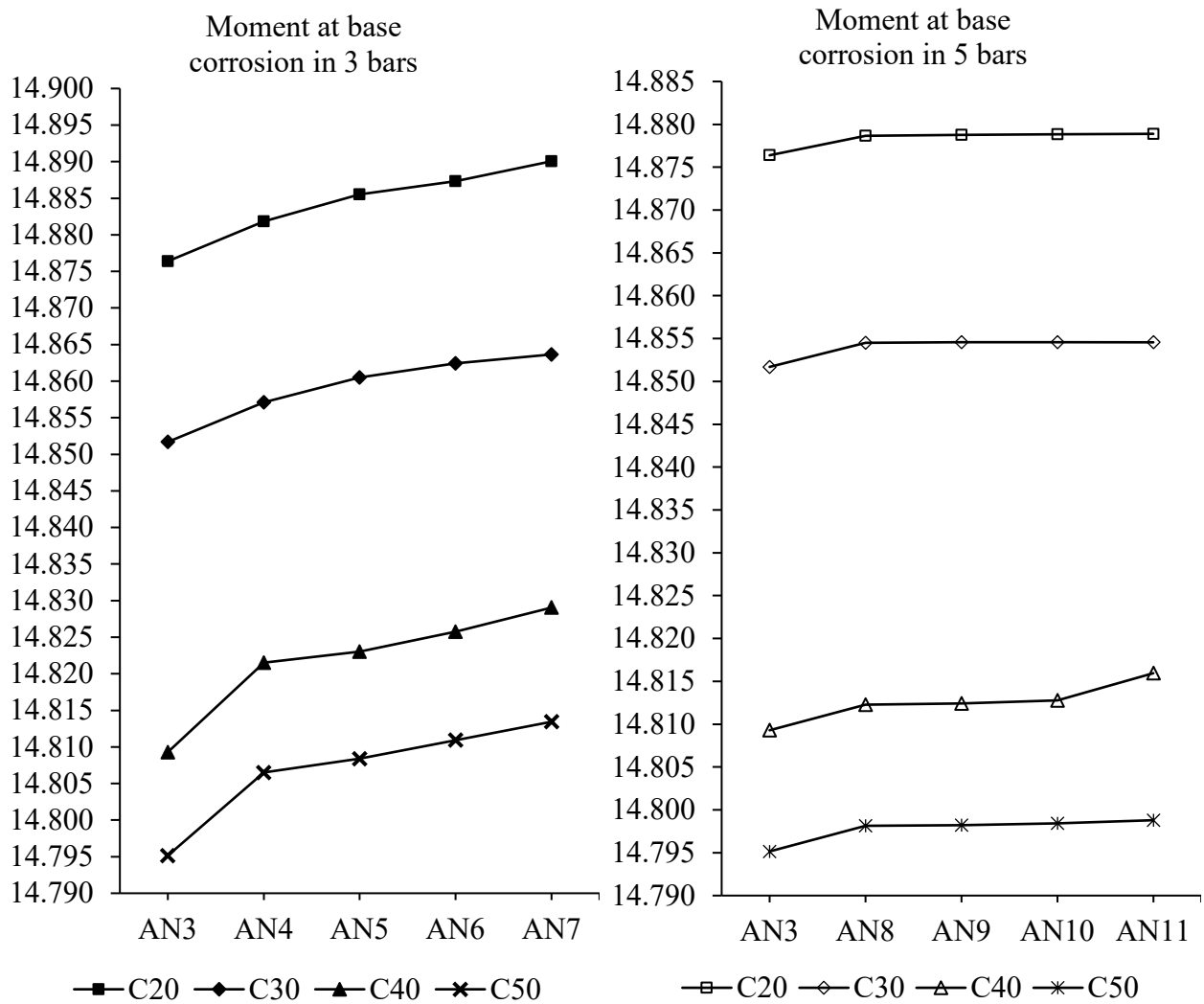


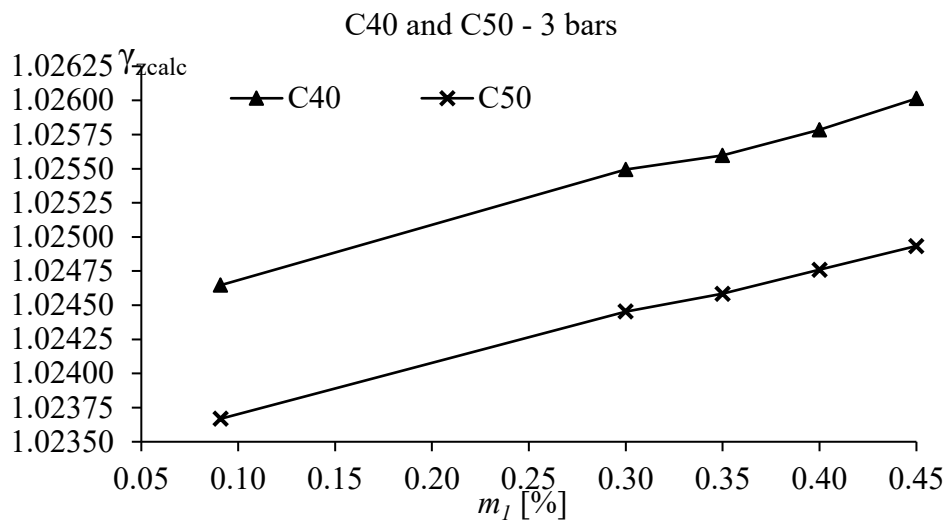
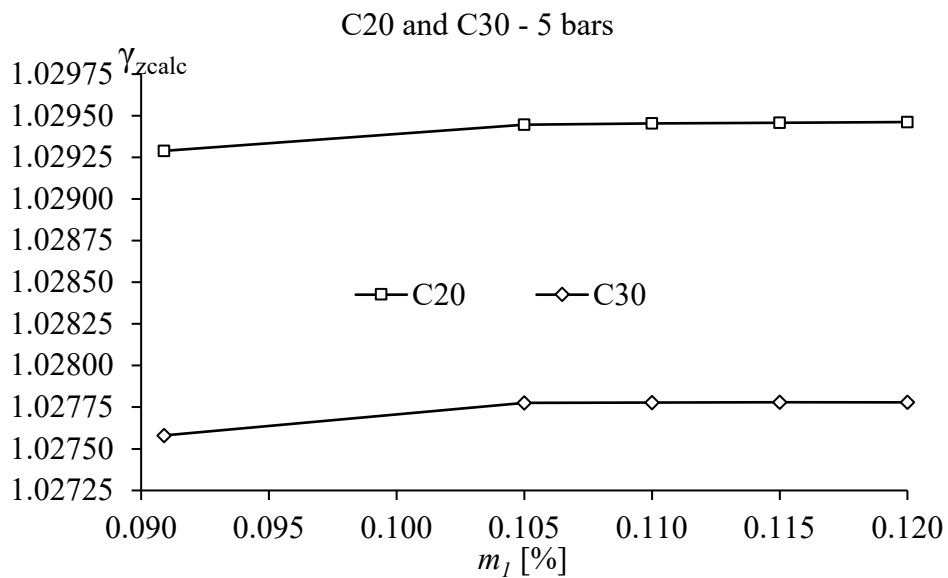
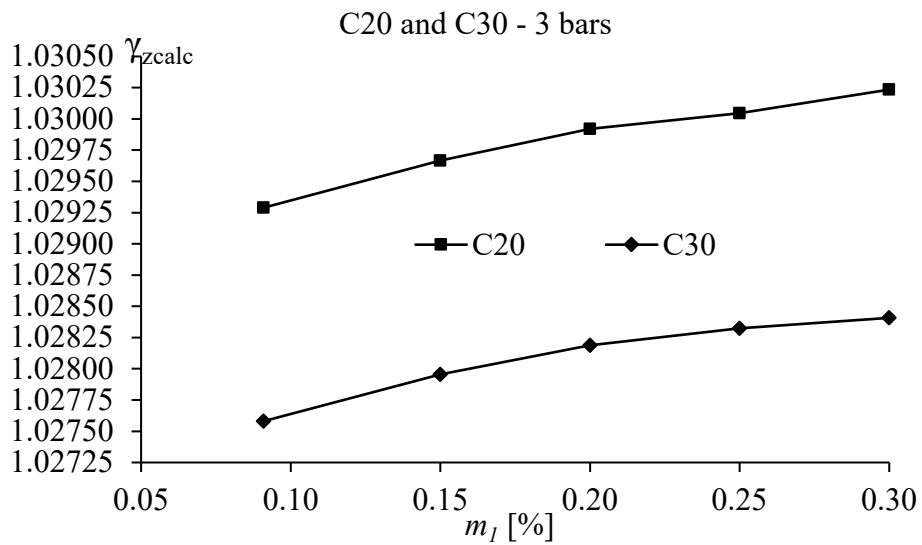
Figure 13. Moment at the base in the analyzed structures.

Table 3 presents the calculated values of γ_{zcalc} for the AN1, AN3, and AN7 simulations. The values shown for the corrosion simulations (AN7) were those obtained for degradation in 3 steel bars.

Table 3. Coefficient γ_{zcalc}

Concrete class	AN3	AN7	AN1 (NBR 6118:2014)	AN7 and AN1 ratio [%]
C20	1.0293	1.0302	1.0348	99.56
C30	1.0276	1.0284	1.0330	99.56
C40	1.0246	1.0260	1.0298	99.63
C50	1.0237	1.0249	1.0287	99.63

Figure 14 relates m_1 to the calculated values of γ_{zcalc} . It is possible to observe that in all concrete strength classes, γ_{zcalc} increases as m_1 increases.



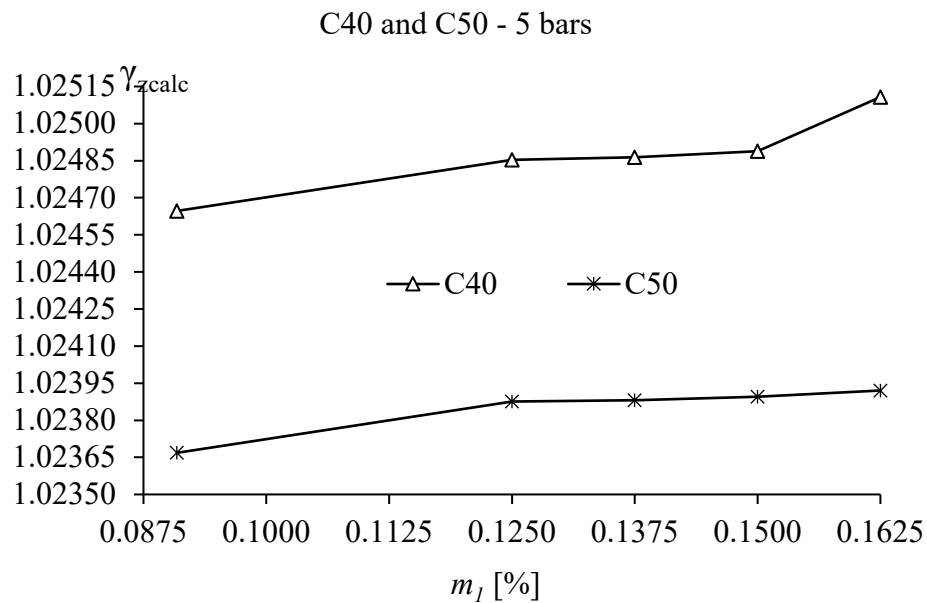


Figure 14. Relationship between m_1 and γ_{zcalc}

Table 3 and Figure 14 show that corrosion increased the γ_{zcalc} coefficient in all concrete strength classes. Thus, considering that γ_{zcalc} can be adapted to a coefficient of increase of first-order loads (NBR 6118:2014), it is possible to define that the addition of corrosion caused the intensification of second-order effects.

From the γ_{zcalc} values obtained in AN7 and AN1, it was possible to define that the second-order effects with the corrosion correspond to 99.6% of those determined by NBR 6118:2014. Thus, the values obtained based on the Brazilian code proved to be higher, demonstrating that the stiffness reduction proposed can accommodate the corrosion level evaluated in this paper.

In addition, it was observed that concretes with lower strength suffer more from corrosion. The concretes with a higher f_{ck} , even submitted to higher values of m_1 , presented lower γ_{zcalc} results, demonstrating greater resistance to external actions and degradation.

Figure 15 shows images of a cross-section of the model in the region where corrosion was added, in 3 and 5 steel bars, with C40 concrete, respectively. The cracks in Figure 15 are represented by the tensile damage variable (*damaget*).

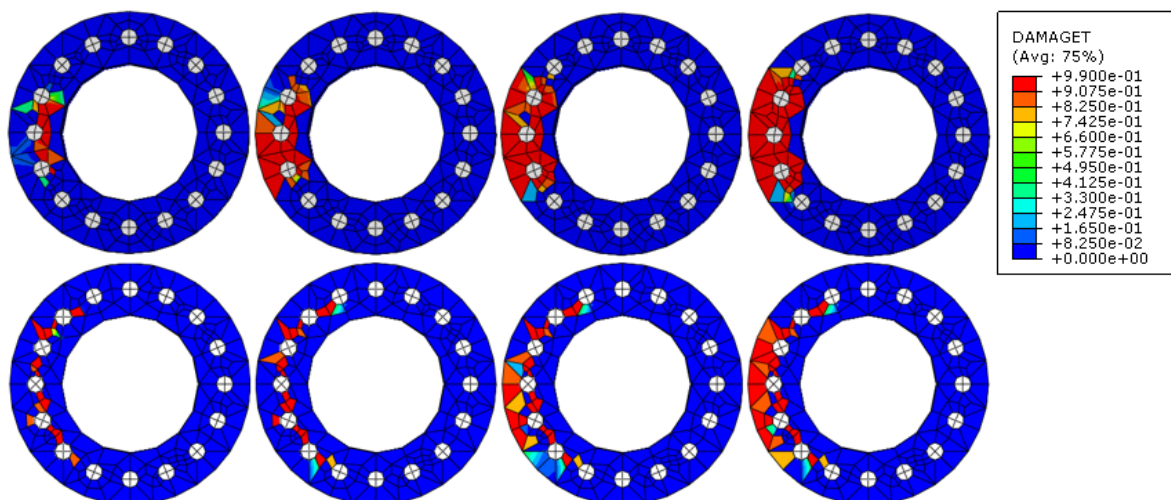


Figure 15. Evolution of damage in AN7 and AN11 models with C40 concrete.

With the evolution of the damage, the numerical convergence is difficult, delimiting the corrosion values possible to be analyzed. Thus, it is noted that collapse can occur due to cross-section failure before the instability problem for a certain level of corrosion.

As observed by Pereira Junior et al. (2016), the damage was concentrated in the tensioned regions. Furthermore, as the cracking increased, the meeting of the microcracks led to the fracture of the material. Finally, the connection of cracks developed around the bars increased the second-order effects on the structure.

4. CONCLUSIONS

Corrosion degrades the steel and initiates a process of concrete deterioration, as the opening of cracks leaves the element susceptible to attack by external agents.

This paper reproduced a methodology for simulating and validating the mechanical behavior of structural elements in reinforced concrete. In addition, this study included the effect of corrosion, that is, the intensification of the cracking process due to the expansive product of corrosion.

The study concluded that corrosion negatively influences the stability of reinforced concrete elements, as it intensifies the global second-order effects.

The comparison between the γ_z coefficient obtained with numerical simulations after corrosion and those calculated from NBR 6118:2014 indicated that the Brazilian code method is safe for the levels analyzed of corrosion.

However, numerical models also indicated that structural collapse could occur due to cross-section failure, even before the critical increase in second-order effects.

However, the stiffness reduction proposed by the Brazilian code must also consider the rheological effects of reinforced concrete. Therefore, the joint presence of these phenomena (corrosion + rheological effects) can lead the structure to a state not predicted by the numerical models presented. Consequently, it is recommended that future researchers analyze the rheological effects in the presence of intense levels of degradation to specify the level of security provided by the normative simplifications.

5. REFERENCES

Aitsin, A. C. et al. (2008), *Constitutive modelling of high strength/high performance concrete*. International Federation for Structural Concrete (FIB). Lausanne, Switzerland, p. 125.

Álvares, M. S. (1993), “*Estudo de um modelo de dano para o concreto: formulação, identificação paramétrica e aplicação com o emprego do método dos elementos finitos*”, Dissertação (Título de Mestre em Engenharia de Estruturas), Escola de Engenharia de São Carlos, Universidade de São Paulo, São Carlos, p. 123.

Amorim Júnior, N. S. A. et al. (2021), *Durability and service life analysis of metakaolin-based geopolymer concretes with respect to chloride penetration using chloride migration test and corrosion potential*. Construction and Building Materials, 287, 122970. <https://doi.org/10.1016/j.conbuildmat.2021.122970>

Araujo, A. D. et al. (2020), *Current condition of the exposed concrete façades reinforcement of the Vilanova Artigas building: modern architectural heritage*. Revista IBRACON de Estruturas e Materiais, 14. <https://doi.org/10.1590/S1983-41952021000100013>

Associação Brasileira de Normas Técnicas. (1988). *NBR 6123: Forças devidas ao vento em edificações*. Rio de Janeiro.

Associação Brasileira de Normas Técnicas. (2014). *NBR 6118: Projeto de estruturas de concreto – Procedimentos*. Rio de Janeiro.

- Associação Brasileira de Normas Técnicas. (2019). *NBR 6120: Ações para o cálculo de estruturas de edificações*. Rio de Janeiro
- Ayinde, O. O. et al. (2017), *Numerical simulation of concrete degradation due to chloride-induced reinforcement corrosion*. Proceedings of the 3rd international forum on energy, environment science and materials, v. 120.
- Balestra, C. E. T. et al. (2018), *Effect of corrosion degree on mechanical properties of reinforcements buried for 60 years*. Revista IBRACON de Estruturas e Materiais, 11, 474-498. <https://doi.org/10.1590/S1983-41952018000300003>
- Blanco, Y. D. et al. (2019), *Natural additive (nopal mucilage) on the electrochemical properties of concrete reinforcing steel*. Revista ALCONPAT, 9(3), 260-276. <https://doi.org/10.21041/ra.v9i3.429>
- Branson, D. E. (1968), *Procedures for computing deflections*. ACI Journal, New York, n. 65.
- Dietrich, Y. P. et al. (2017), *Desempenho mecânico e análise da corrosão das armaduras em concretos produzidos com adição de resíduos de rochas ornamentais*. Matéria (Rio de Janeiro), 22. <https://doi.org/10.1590/S1517-707620170004.0225>
- El-Maaddawy, T., Soudki, K. (2007), *A model for prediction of time from corrosion initiation to corrosion cracking*. Cement & Concrete Composites, v. 29, p. 168-175. <https://doi.org/10.1016/j.cemconcomp.2006.11.004>
- Favretto, F. et al. (2021), *Modelos de estimativa do grau de saturação do concreto a partir das variáveis ambientais aplicados à análise de confiabilidade de estruturas de concreto armado atacadas por íons cloreto*. Revista Matéria. 2021, 26(3): e13001. <https://doi.org/10.1590/S1517-707620210003.13001>
- Fédération Internationale du Béton/International Federation for Structural Concrete. (2010). *CEB-FIB MODEL CODE*.
- Felix, E. F. et al. (2020), *Development and analysis of a numerical model of the reinforced concrete expansion due to uniform corrosion*. Revista de la Asociación Latinoamericana de Control de Calidad, Patología y Recuperación de la Construcción, 10(3), 300-316. <https://doi.org/10.21041/ra.v10i3.395>
- Felix, E. F., Carrazedo, R. (2021), *Análise probabilística da vida útil de lajes de concreto armado sujeitas à corrosão por carbonatação via simulação de Monte Carlo*. Matéria (Rio de Janeiro), v. 26. <https://doi.org/10.1590/S1517-707620210003.13043>
- Figueiredo, C. P. et al. (2014), *O papel do metacaulim na proteção dos concretos contra a ação deletéria de cloretos*. Revista IBRACON de Estruturas e Materiais, 7, 685-708. <https://doi.org/10.1590/S1983-41952014000400008>
- Franco, M., Vasconcelos, A. C. (1991). *Practical assessment of second order effects in tall buildings*. Colloquium on the CEB-FIB MC 90, COPPE/UFRJ, Rio de Janeiro, RJ.
- Fusco, P. B. (2008), *Tecnologia do concreto estrutural: tópicos aplicados*. São Paulo: PINI.
- Helene, P. R. L. (1993), *“Contribuição ao estudo da corrosão em armaduras de concreto armado”*, Tese (Livre-docência junto ao Departamento de Engenharia de Construção civil). Escola Politécnica, Universidade de São Paulo, São Paulo, p. 231.
- Hibbitt, H. et al. (2011), *Abaqus analysis user’s manual version, 6.10*. Dassault Systèmes Simulia Corp.: providence, RI, USA.
- Lee, J., Fenves, G. L. (1998), *A plastic-damage model for cyclic loading of concrete structures*. Journal of Engineering Mechanics, ASCE, v. 124, p. 892- 900. [https://doi.org/10.1061/\(ASCE\)0733-9399\(1998\)124:8\(892\)](https://doi.org/10.1061/(ASCE)0733-9399(1998)124:8(892))
- Lubliner, J. et al. (1989), *A plastic-damage model for concrete*. International Journal of Solids and Structures, v. 25, n. 3, p. 299-326. [https://doi.org/10.1016/0020-7683\(89\)90050-4](https://doi.org/10.1016/0020-7683(89)90050-4)
- Mackechnie, J. R., Alexander, M. G. (2001), *Repair principles for corrosion-damaged reinforced concrete structures*. Research monograph, 5, 1-36.

- Maldonado-Bandala, E. E. et al. (2018), *Evaluation of pathological problems associated with carbonation and sulfates in a concrete tower with more than 50 years in service*. Revista ALCONPAT, 8(1), 94-107. <https://doi.org/10.21041/ra.v8i1.284>
- Malheiro, R. M. D. C. et al. (2014), *Influência da camada do revestimento de argamassa na penetração de cloretos em estruturas de concreto*. Ambiente Construído, 14, 41-55. <https://doi.org/10.1590/S1678-86212014000100005>
- Meira, G. R., Ferreira, P. R. R. (2019), *Revisão sobre ensaios acelerados para indução da corrosão desencadeada por cloretos em concreto armado*. Ambiente Construído, 19, 223-248. <https://doi.org/10.1590/s1678-86212019000400353>
- Pereira Junior, W. M. et al. (2016), *Análise numérica de vigas de concreto com fibras de aço utilizando mecânica do dano*. Revista IBRACON de estruturas e materiais, v. 9, n. 2, p. 153-191. <https://doi.org/10.1590/S1983-41952016000200002>
- Ramos, É. S., Carrazedo, R. (2020), *Cross-section modeling of the non-uniform corrosion due to chloride ingress using the positional finite element method*. Journal of the Brazilian Society of Mechanical Sciences and Engineering, 42(10), 1-18. <https://doi.org/10.1007/s40430-020-02627-5>
- Ramos, É. S., Carrazedo, R. (2021), *Numerical analysis of reinforced concrete beam subject to pitting corrosion*. Ambiente Construído, 22, 201-222. <https://doi.org/10.1590/s1678-86212022000100588>
- Reginato, L. (2020), “*Contribuição ao projeto de consolos de concreto com base em simulações numéricas*”. Dissertação (Título de Mestre em Engenharia de Estruturas), Escola de Engenharia de São Carlos, Universidade de São Paulo, São Carlos, p. 184.
- Santos, B. et al. (2020), *Effect of the addition of metakaolin on the carbonation of Portland cement concretes*. Revista IBRACON de Estruturas e Materiais, 13, 1-18. <https://doi.org/10.1590/S1983-41952020000100002>
- Schwartzman, M. M. A. M. et al. (2010), *Avaliação da corrosão sob tensão em aço inoxidável AISI 321 em ambiente de reator nuclear*. Matéria (Rio de Janeiro), 15, 40-49. <https://doi.org/10.1590/S1517-70762010000100006>
- Silva, S. H. et al. (2015), *Analytic Hierarchy Process to choose the cement type to protect reinforced concrete to corrosion caused by chloride ions attack*. Revista ALCONPAT, 5(3), 174-189. https://www.scielo.org.mx/scielo.php?pid=S2007-68352015000300174&script=sci_arttext&%20lng=en
- Silvestro, L. et al. (2020), *Penetração de cloretos em concretos expostos em zona de atmosfera marinha por um período de 9 anos*. Ambiente Construído, 21, 101-118. <https://doi.org/10.1590/s1678-86212021000100496>
- Souza, V. D. B., Leonel, E. D. (2021), *Probabilistic chloride diffusion modelling in cracked concrete structures by transient BEM formulation*. Revista IBRACON de Estruturas e Materiais, 15. <https://doi.org/10.1590/S1983-41952022000400002>
- Teixeira, F. R. et al. (2021), *Avaliação de propriedades relacionadas à penetração de cloretos em concretos produzidos com substituição parcial de cimento por resíduo de beneficiamento de rochas ornamentais*. Matéria (Rio de Janeiro), 26. <https://doi.org/10.1590/S1517-707620210003.13029>
- Trevisol, C. A. et al. (2017), *Avaliação de inibidores de corrosão para estruturas de concreto armado*. Matéria (Rio de Janeiro), 22. <https://doi.org/10.1590/S1517-707620170004.0238>
- Verçoza, E. J. (1991), “*Patologia das edificações*”. [S.I.]: Sagra.
- Wahrhaftig, A. M. (2008), “*Uma avaliação experimental e numérica do efeito da rigidez geométrica na resposta dinâmica de estruturas esbeltas sujeitas à excitação de vento*”. Tese (Título de Doutor em Engenharia), Escola Politécnica, Universidade de São Paulo, São Paulo, p. 209.

Yu, T. et al. (2010), *Finite element modeling of confined concrete-II: Plastic-damage model*. Engineering Structures, v. 32, n. 3, p. 680–691. <https://doi.org/10.1016/j.engstruct.2009.11.013>

Flexural behavior of reinforced concrete beams with electrochemical parameters associated with high level of corrosion

J. A. Moreno Herrera*¹, J. L. Varela Rivera¹, R. Visairo Méndez², P. Castro Borges²

*Contact author: joel.moreno@correo.uady.mx

DOI: <https://doi.org/10.21041/ra.v12i3.630>

Reception: 16/07/2022 | Acceptance: 17/08/2022 | Publication: 01/09/2022

ABSTRACT

In this work the change in the flexural behavior of reinforced concrete beams was evaluated. Beams without corrosion and beams with electrochemical parameters associated with high level of corrosion were considered. The electrochemical parameters considered were the corrosion rate, the electrical resistivity, and the concentration of chlorides. Beams were subjected to vertical incremental loads until failure. Cracking pattern, yielding load, maximum load, yielding stiffness, and displacement ductility of beams are presented. Based on the analysis of these structural parameters it is concluded that the flexural behavior of beams with and without corrosion was similar.

Keywords: reinforced concrete beams; corrosion; sustained loads; structural behavior; electrochemical behavior.

Cite as: Moreno Herrera, J. A., Varela Rivera, J. L., Visairo Méndez, R., Castro Borges, P. (2022), "Flexural behavior of reinforced concrete beams with electrochemical parameters associated with high level of corrosion", Revista ALCONPAT, 12 (3), pp. 422 – 432, DOI: <https://doi.org/10.21041/ra.v12i3.630>

¹ Facultad de Ingeniería, Universidad Autónoma de Yucatán, México.

² Centro de Investigación y de Estudios Avanzados, IPN, Unidad Mérida, México.

Contribution of each author

In this work, Joel Moreno Herrera contributed with the design of the test (100%), the analysis of the structural behavior of the beams (50%), as well as the writing of the article (100%); Jorge Luis Varela Rivera contributed with the analysis of the structural behavior of the beams (50%); Rebeca Visairo Méndez contributed with the measurement of the electrochemical parameters (100%), the testing of the beams during her master's studies (100%), and the analysis of the electrochemical behavior (50%); Pedro Castro Borges contributed with the analysis on the electrochemical behavior (50%).

Creative Commons License

Copyright 2022 by the authors. This work is an Open-Access article published under the terms and conditions of an International Creative Commons Attribution 4.0 International License ([CC BY 4.0](https://creativecommons.org/licenses/by/4.0/)).

Discussions and subsequent corrections to the publication

Any dispute, including the replies of the authors, will be published in the second issue of 2023 provided that the information is received before the closing of the third issue of 2023.

Comportamiento a flexión de vigas de concreto reforzado con parámetros electroquímicos asociados con un nivel de corrosión alto

RESUMEN

En este trabajo se evaluó el cambio en el comportamiento a flexión de vigas de concreto reforzado. Se consideraron vigas sin corrosión y vigas con parámetros electroquímicos asociados con un nivel de corrosión alto. Los parámetros electroquímicos considerados fueron la velocidad de corrosión, la resistividad eléctrica y la concentración de cloruros. Las vigas se ensayaron bajo cargas verticales incrementales hasta la falla. Se presentan los patrones de agrietamiento, las cargas de fluencia y máxima, la rigidez de fluencia y la ductilidad de desplazamiento de las vigas. Con base en el análisis de estos parámetros estructurales se concluye que el comportamiento a flexión de las vigas con y sin corrosión fue similar.

Palabras clave: vigas de concreto reforzado; corrosión; cargas sostenidas; comportamiento estructural; comportamiento electroquímico.

Comportamento à flexão de vigas de concreto armado com parâmetros eletroquímicos associados a um alto nível de corrosão

RESUMO

Neste trabalho, avaliou-se a mudança no comportamento de flexão de vigas de concreto armado. Foram consideradas vigas sem corrosão e vigas com parâmetros eletroquímicos associados a um alto nível de corrosão. Os parâmetros eletroquímicos considerados foram a taxa de corrosão, resistividade elétrica e concentração de cloretos. As vigas foram ensaiadas sob cargas verticais incrementais até a ruptura. São apresentados padrões de fissuração, cargas de escoamento, cargas máximas, rigidez de escoamento e ductilidade de deslocamento das vigas. Com base na análise desses parâmetros estruturais conclui-se que o comportamento de flexão das vigas com e sem corrosão foi semelhante.

Palavras chave: vigas de concreto armado; corrosão; cargas sustentadas; comportamento estrutural; comportamento eletroquímico.

Legal Information

Revista ALCONPAT is a quarterly publication by the Asociación Latinoamericana de Control de Calidad, Patología y Recuperación de la Construcción, Internacional, A.C., Km. 6 antigua carretera a Progreso, Mérida, Yucatán, 97310, Tel.5219997385893, alconpat.int@gmail.com, Website: www.alconpat.org

Reservation of rights for exclusive use No.04-2013-011717330300-203, and ISSN 2007-6835, both granted by the Instituto Nacional de Derecho de Autor. Responsible editor: Pedro Castro Borges, Ph.D. Responsible for the last update of this issue, Informatics Unit ALCONPAT, Elizabeth Sabido Maldonado.

The views of the authors do not necessarily reflect the position of the editor.

The total or partial reproduction of the contents and images of the publication is carried out in accordance with the COPE code and the CC BY 4.0 license of the Revista ALCONPAT.

1. INTRODUCTION

Reinforced concrete (RC) is one of the most used materials in the construction industry around the world. Concrete global production per year is about 11000 million cubic meters (Ceballos, 2016). Corrosion is one of the main problems that affects safety and durability of reinforced concrete structures (Rodríguez, 2014). Corrosion can initiate when different agents such as chlorides, sulfates and carbon dioxide penetrate into the concrete (Castro, 1988). Corrosion induces a degradation in the physical and mechanical properties of steel reinforcement. This degradation is associated with changes in the chemical composition related to the chemical reaction of steel with the corrosion agents in the surrounding environment (Maldonado-López, 1996). Corrosion can cause damage in RC elements such as cracking and loss of the concrete cover of the steel reinforcement. These damages are associated with losses in the strength and the deformation capacity of RC elements. These losses produce a reduction in the safety of RC structures. Damage in structures associated with corrosion generates expenses and economic losses in many countries (Vázquez-Castillo, 1998). The annual cost of repairs of RC structures in the UK it is approximately 755 million pounds (Rodríguez, 2014). The cost of maintenance and repairment of coastal infrastructure in the USA its around 600 million dollars (Xianming et al. 2012). Therefore, prevention, evaluation, and control of corrosion in RC structures are very important.

Current Mexican regulations on durability of reinforced concrete structures focus mainly in two aspects: prevention and evaluation. The specifications in the Mexican Complementary Technical Norms for the Design and Construction of Concrete Structures (NTCC-2017) focus on prevention of corrosion. In these technical norms, minimum requirements are specified for the compressive strengths of concrete and the thickness of the concrete cover as a function of different exposed environments. On the other side, there are some standards mainly based on the electrochemical behavior of reinforced concrete beams. For example, in the Mexican standard NMX-C-514-ONNCCE-2016, levels of corrosion are proposed as a function of the corrosion rate. In the same sense, in the Mexican standard NMX-C-523-ONNCCE-2015, corrosion risk levels are proposed as a function of the electrical resistivity of concrete. These standards are not explicitly related to the structural behavior of reinforced concrete elements.

There are some studies about the structural behavior of reinforced concrete elements with corrosion. The main variables studied were the level of corrosion (Gu et al., 2010; Ou et al., 2016; Ye et al., 2018), the diameter of the longitudinal steel reinforcement (Gu et al., 2010; Ou et al., 2016; Shaikh, 2018), and the magnitude of sustained loads (Tachibana et al., 1990; Castel et al., 2000; Vidal et al., 2007; Torres et al., 2007; Juárez et al., 2011; Ye et al., 2018). On the other side, there are studies about the electrochemical behavior of reinforced concrete beams with corrosion (Andrade and González, 1978; Andrade et al., 1993; Elsener et al., 2003). In the above studies, it was observed that, in general, the structural and electrochemical behavior of concrete elements are studied independently. Only one study was found where the relationship between the structural and electrochemical behavior was considered (Yu et al., 2015). However, in that study only two beams with corrosion were considered. The only variable studied was the corrosion rate. Therefore, it is observed that more experimental studies are still needed. In these studies, it is important to consider the relationship between the structural and electrochemical behavior of reinforced concrete beams. The main parameters used to define the structural behavior of RC beams are the strength, stiffness, and deformation capacity. The main parameters used to define the electrochemical behavior are the corrosion rate, electrical resistivity, and concentration of chlorides in concrete. The relationships between those parameters will allow a better evaluation of structures damaged by corrosion.

The objective of this work it is to evaluate the change in the flexural behavior of reinforced concrete beams. Beams without corrosion and beams with electrochemical parameters associated with high

level of corrosion were considered. The beams were obtained from the study carried out by Moreno-Herrera et al. (2022).

2. METHODOLOGY

2.1 Properties of existing beams

Eight existing reinforced concrete beams were considered, four control beams and four beams with corrosion (Moreno-Herrera et al., 2022). The dimensions of beams were 15 x 30 x 350 cm (width x height x length). Beams were design to induce flexural behavior. Longitudinal steel reinforcement of beams consisted of two #4 bars (13 mm diameter) in the tension zone and two #3 bars (9.5 mm diameter) in the compression zone. Deformed steel bars with nominal yield strength of 411.88 MPa (4200 kg/cm²) were used. Transverse steel reinforcement consisted of #2 hoops (6.4 mm diameter) at every 130 mm. Plain steel bars with nominal yield strength of 227.51 MPa (2320 kg/cm²) were used. Clear cover of the longitudinal reinforcement was 25 mm. The average compressive strength of concrete was 17.53 MPa (178.75 kg/cm²). Portland cement and calcareous aggregates with high absorption were used in the concrete mixture. The nominal maximum size of coarse aggregate was 19 mm. A water/cement ratio of 0.62 and a slump of 100 mm were considered. Beams were constructed by an experimented worker. The transverse steel reinforcement was painted with an anticorrosive alkyd enamel. This paint was used to induce the corrosion only in the longitudinal steel reinforcement. For the case of the control beams, the concrete was placed in a traditional way. For the case of the beams with corrosion, the concrete was placed in two layers of 150 mm heigh. The first layer with concrete contaminated with chlorides (1.5% of the cement weight) and the second layer with regular concrete. Beams were cured with drinking water for a period of 28 days.

Beams were subjected to incremental vertical loads until the target tensile stresses in the longitudinal steel reinforcement were reached (Table 1). Loads were applied using a traditional four-point load system (Figure 1). With this loading system, a constant bending moment with no shear force was induced in the central third of the beam length. In Table 1, VC refers to control beams, VCC to beams with corrosion, 0.4 and 0.8 refer to the target tensile stresses in the longitudinal steel reinforcement (40% and 80% of f_y). In Table 1, P_{cr} refers to the cracking load associated with flexural cracking strength and Δ_{cr} refers to the corresponding displacement, P_{m1} refers to the load associated with the target tensile stress and Δ_{m1} refers to the corresponding displacement. In that table, the initial stiffness (K_o) and the post-cracking stiffness (K_{cr}) of beams are included. The initial stiffness was calculated using P_{cr} and Δ_{cr} . The post-cracking stiffness was calculated using both P_{cr} and P_{m1} .

Table 1. Initial structural parameters of beams (Moreno-Herrera et al., 2022)

Beam	P_{cr} (kN)	Δ_{cr} (mm)	P_{m1} (kN)	Δ_{m1} (mm)	K_o (kN/mm)	K_{cr} (kN/mm)
VC1-0.4	7.69	0.83	18.17	4.32	10.30	3.00
VC2-0.4	5.20	0.45	18.29	4.25	12.90	3.44
VC1-0.8	8.03	0.80	35.80	10.63	11.18	2.82
VC2-0.8	5.40	0.68	35.31	11.77	8.86	2.70
VCC1-0.4	7.61	0.80	17.88	4.38	10.55	2.87
VCC2-0.4	9.74	0.98	18.37	4.09	11.21	2.78
VCC1-0.8	9.11	1.00	36.11	10.93	10.20	2.72
VCC2-0.8	7.93	0.92	36.37	11.17	9.56	2.78

2.2 Sustained loads and accelerated corrosion in existing beams

Beams were subjected to sustained loads for a period of 166 days (Moreno-Herrera et al., 2022). Sustained loads associated with target tensile stresses were considered (Table 1). Applied loads induced the same distribution of bending moments and shear forces in the beams as described before for the four-point load system. To induce the corrosion in the steel reinforcement, wetting and drying cycles were applied during this period. Beams were moistening every 12 hours, a first time with drinking water and a second time with a 3.5% saline solution. This concentration of chlorides is similar to the average concentration of chlorides of sea water. Table 2 shows the maximum values observed for the corrosion rate in the longitudinal steel reinforcement, electrical resistivity, and concentration of chlorides in concrete of beams. Corrosion rate and electrical resistivity of concrete were measured with a corrosimeter (James Instruments, 2010). Concentration of chlorides were determined according with the Mexican Standard NMX-C-523-ONNCCE-2015.

Table 2. Electrochemical parameter of beams (Moreno-Herrera et al., 2022)

Beam	Corrosion rate ($\mu\text{Amp}/\text{cm}^2$)	Electrical resistivity of concrete ($\text{k}\Omega \cdot \text{cm}$)	Concentration of chlorides (% per weight of cement)
VC1-0.4	0.45	11.97	0.3034
VC2-0.4			
VC1-0.8	0.65	11.08	0.3295
VC2-0.8			
VCC1-0.4	7.01	1.37	2.5853
VCC2-0.4			
VCC1-0.8	5.66	2.47	3.2038
VCC2-0.8			

Table 2 shows that the maximum corrosion rate of control beams (CV) was associated with a low to moderate level of corrosion (0.1 a $0.5 \mu\text{Amp}/\text{cm}^2$) (NMX-C-501-ONNCCE-2015). The electrical resistivity of concrete was associated with a low to moderate risk of corrosion (10 a $50 \text{k}\Omega \cdot \text{cm}$) (NMX-C-514-ONNCCE-2016). The concentration of chlorides was smaller than the threshold value of 0.52 proposed for concrete made of calcareous aggregates and a water/cement ratio of 0.6 (Castro et al., 1993). On the other side, Table 2 also shows that the corrosion rate of beams with corrosion (VCC) was associated with a high level of corrosion (larger than $1 \mu\text{Amp}/\text{cm}^2$). The electrical resistivity of concrete was associated with high risk of corrosion (less than $10 \text{k}\Omega \cdot \text{cm}$). The concentration of chlorides was at least five times larger than the proposed threshold value. Therefore, based on the electrochemical behavior, the VCC beams have parameters associated with a high level of corrosion.

For beams with the same target tensile stress, the cracking pattern was in general similar. For beams with target tensile stress of 0.8fy , larger and wider cracks were observed compared with beams with tensile stress of 0.4fy . This was related to the larger loads applied on beams with tensile stress of 0.8fy . After the corrosion technique was applied, the cracking pattern of beams was similar to that observed prior to the application of the corrosion technique.

2.3 Load system and instrumentation for testing of beams

Control beams and beams with corrosion were subjected to incremental vertical loads until failure. Beams were tested after the period of application of the corrosion technique. Loads were applied using the same four-point load system described before (Figure 1). Loads were applied using a hydraulic actuator and were measured with a load cell. Vertical displacements at the mid-length of beams were measured using two linear potentiometers. Strains of the longitudinal steel reinforcement were measured using strain-gages. The strain-gages were attached to the longitudinal steel reinforcement prior to pouring of concrete (Moreno-Herrera et al., 2022).

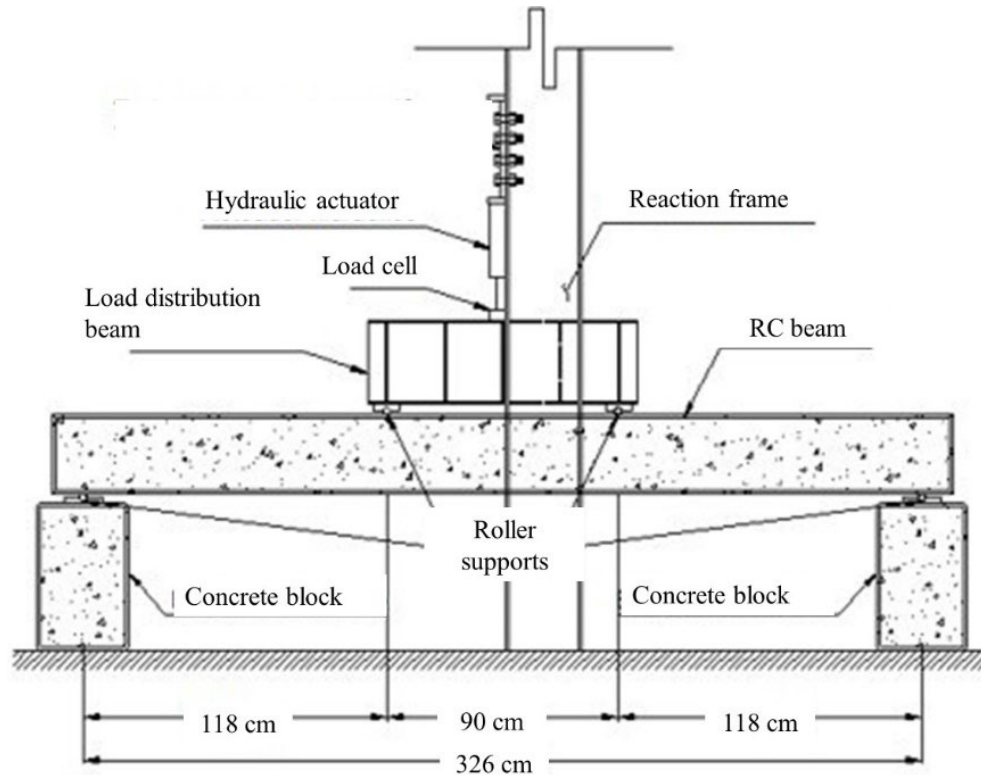


Figure 1. Four-point load system

3. RESULTS Y DISCUSION

The final cracking pattern of tested beams are presented in Figure 2. The final cracking pattern of control beams and beams with corrosion was similar. This cracking pattern was defined by the formation of vertical flexural cracks at the beam center and diagonal flexure-shear cracks at beams ends.

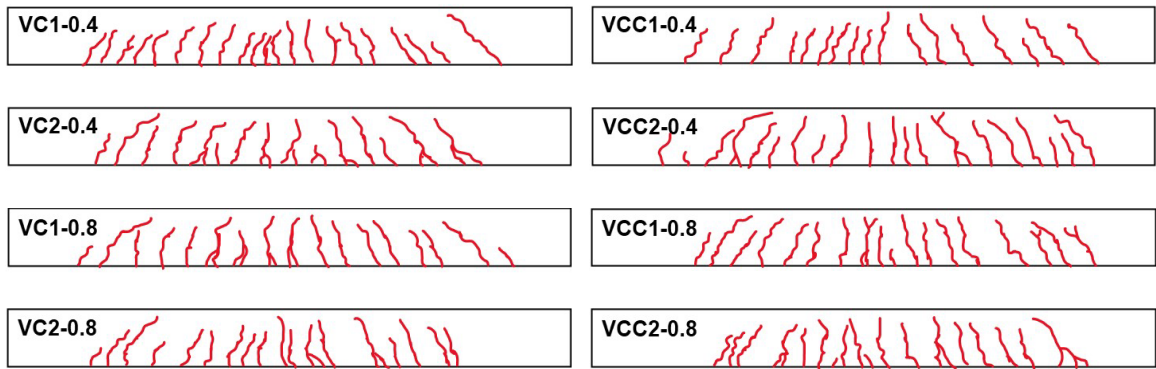


Figure 2. Final cracking pattern of beams

The load – displacement curves of beams are presented in Figure 3. Table 3 shows the yielding load (P_y) and corresponding yielding displacement (Δ_y), the maximum load (P_{m2}) and corresponding displacement (Δ_{m2}) of beams. Yielding loads were determined using the strains measured with the strain-gages. Initial yielding stiffness (K_y) and displacement ductilities (μ) of beam are presented in Table 3. Initial yielding stiffness was calculated using the yielding load. Displacement ductility was calculated as the ratio between the maximum displacement and the yielding displacement of corresponding beams. For beam VCC1-08, only the maximum load and corresponding displacement are presented because of problems with the measurements with the strain-gages.

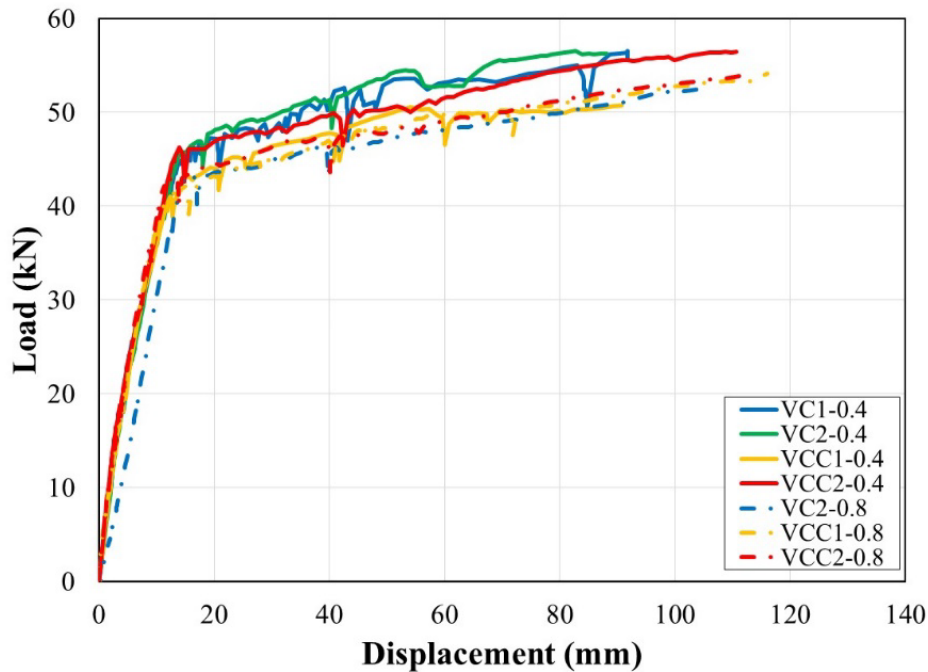


Figure 3. Load – displacement curves

Table 3. Structural parameters of beams tested until failure

Beam	P_y (kN)	Δ_y (mm)	P_{m2} (kN)	Δ_{m2} (mm)	K_y (kN/mm)	μ (Δ_{m2}/Δ_y)
VC1-0.4	43.47	13.08	56.54	91.79	3.32	7.02
VC2-0.4	44.09	13.24	54.45	88.18	3.33	6.66
VC1-0.8	--	--	52.93	119.30	--	--
VC2-0.8	42.52	14.35	52.56	105.87	2.96	7.38
Average	43.36	13.56	54.12	101.28	3.21	7.02
CV	0.02	0.05	0.03	0.14	0.07	0.05
VCC1-0.4	42.63	14.11	50.70	90.72	3.02	6.43
VCC2-0.4	46.13	15.59	56.48	110.66	2.96	7.10
VCC1-0.8	41.92	16.54	54.10	116.03	2.53	7.02
VCC2-0.8	42.93	14.44	53.92	112.79	2.97	7.81
Average	43.30	15.17	53.80	107.55	2.87	7.09
CV	0.04	0.07	0.04	0.11	0.08	0.08

Table 3 shows that the average yielding loads and the average maximum loads together with corresponding average displacements were similar for all beams, respectively. The ratio between the average yielding load of beams with corrosion and the average yielding load of control beams was 0.99. On the other hand, the ratio between the average maximum load of beams with corrosion and the average maximum load of control beams was 1.01.

In addition, Table 3 shows that the average initial yielding stiffness was similar for all beams. The ratio between the average initial yielding stiffness of beams with corrosion and the average initial yielding stiffness of control beams was 0.90. Table 3 also shows that the average displacement ductility of all the beams was similar. The ratio between the average displacement ductility of beams with corrosion and the average displacement ductility of control beams was 1.01.

Even though the electrochemical parameters of the beams with corrosion indicates a high level of corrosion, the flexural structural behavior of beams with corrosion compared with the behavior of control beams was similar. The difference between each behavior was not significant. Yielding load, maximum load, initial yielding stiffness and displacement ductility of beams were in general similar. Even though from a structural point of view the parameters observed are acceptable, the electrochemical parameters suggested a risk for the durability of the beams. Therefore, from the electrochemical point of view preventive actions should be taken for the beams with corrosion.

4. CONCLUSIONS Y RECOMENDATIONS

Eight reinforced concrete beams were subjected to incremental loads until failure. Beams had electrochemical parameters associated with high level of corrosion. Based on the experimental result of these beams the following conclusion and recommendations are presented:

- The final cracking pattern of control beams and beams with corrosion was similar. This cracking pattern was defined by the formation of vertical flexural cracks at the beam center and diagonal flexure-shear cracks at beams ends.

- Even though the electrochemical parameters of the beams with corrosion indicates a high level of corrosion, the flexural structural behavior of beams with corrosion compared with the behavior of control beams was similar. The difference between each behavior was not significant. Yielding load, maximum load, initial yielding stiffness and displacement ductility of beams were in general similar.
- Even though from a structural point of view the parameters observed are acceptable, the electrochemical parameters suggested a risk for the durability of the beams. Therefore, from the electrochemical point of view preventive actions should be taken for the beams with corrosion.
- It is recommended to study beams with electrochemical parameters associated with higher level of corrosion than that considered in this work. Physical parameter such as cracking of concrete and stains due to corrosion must be considered. These physical parameters were not observed in the beams studied. The parameters will help to establish a relationship between different levels of corrosion and corresponding structural damage in reinforced concrete beams. Levels of corrosion can be defined as a function of structural parameters such as loss of strength, stiffness, or deformation capacity. By the other side, physical parameters can be assessed as a function of the width and length of cracks developed parallel to the longitudinal steel reinforcement. This kind of cracks are typically observed in beams with high level of corrosion.

5. ACKNOWLEDGMENTS

R. Visairo Méndez thanks the National Council of Science and Technology for the master's scholarship received. Similarly, he thanks the Faculty of Engineering of UADY and Cinvestav Mérida for the facilities provided for structural and corrosion measurements.

6. REFERENCES

- Andrade F., y González J.A. (1978). Quantitative measurements of corrosion rate of reinforcing steels embedded in concrete using polarization resistance measurements. *Materials and Corrosion*. 29(8): 515-519.
- Andrade, C. (1993), Calculation of chloride diffusion-coefficients in concrete from ionic migration measurements. *Cement and Concrete Research*, 23 (3): 724-742. [https://doi.org/10.1016/0008-8846\(93\)90023-3](https://doi.org/10.1016/0008-8846(93)90023-3).
- Castro P. (1998). “*Corrosión en Estructuras de Concreto: teoría, inspección, diagnóstico, vida útil y reparaciones*”. 1ª Edición. Instituto Mexicano del Cemento y del Concreto A.C., México, DF.
- Castel A., François R., Arliguie G. (2000). *Mechanical behaviour of corroded reinforced concrete beams—Part I: Experimental study of corroded beams*. *Materials and Structures*, 33: 539-544, <https://doi.org/10.1007/BF02480533>
- Ceballos, M. (2016). “*El concreto, material fundamental para la infraestructura.*” Centro de Innovación Tecnológica para la Construcción. pp. 24-25.
- Elsener, B., Andrade, C. Gulikers, J., Polder, R y Raupach, M. (2003). *Half-cell potential measurements—Potential mapping on reinforced concrete structures*. *Materials and Structures*. 36: 461–471, <https://doi.org/10.1007/BF02481526>
- Gu X., Zhang W., Shang D., Wang X. (2010). “*Flexural Behavior of Corroded Reinforced Concrete Beams.*” *Earth and Space 2010: Engineering, Science, Construction, and Operations in Challenging Environments*, ASCE, 2, 3545–3552. [https://doi.org/10.1061/41096\(366\)339](https://doi.org/10.1061/41096(366)339)

- Juárez, C. A., Guevara, B., Fajardo, G., & Castro-Borges, P. (2011). *Ultimate and nominal shear strength in reinforced concrete beams deteriorated by corrosion*. *Engineering Structures*, 33(8): 3189-3196. <https://doi.org/10.1016/j.engstruct.2011.08.014>
- Maldonado López, L. (1996). "Corrosión del acero de refuerzo: revisión del estado del arte en México." En F. d. Yucatán (Ed.), VII Seminario de Investigación, (pág. 18). Mérida, Yucatán, México.
- Moreno-Herrera, J., Visairo-Méndez, R., Varela-Rivera, J., Balancan-Zapata, M., y Castro-Borges, P. (2022, enviado para su posible publicación). *Corrosion, The Journal of Science and Engineering*.
- NMX-C-501-ONNCCE-2015. (2015). "Industria de la Construcción - Durabilidad de Estructuras de Concreto Reforzado - Medición de Velocidad de Corrosión en Campo - Especificaciones y Método de Ensayo." Organismo Nacional de Normalización y Certificación de la Construcción y Edificación, S.C.
- NMX-C-514-ONNCCE-2016. (2016). "Industria de la Construcción - Resistividad Eléctrica del Concreto Hidráulico - Especificaciones y métodos de ensayo." Organismo Nacional de Normalización y Certificación de la Construcción y Edificación, S.C.
- NMX-C-523-ONNCCE-2016. (2016). "Industria de la construcción – Durabilidad de estructuras de concreto reforzado - Concentración de cloruros solubles en agua y ácido – determinación en concreto hidráulico - Método de extracción y método de determinación por ión selectivo." Organismo Nacional de Normalización y Certificación de la Construcción y Edificación, S.C.
- NTCC-2017 (2017). "Normas Técnicas Complementarias para Diseño y Construcción de Estructuras de Concreto." Órgano del Gobierno del Distrito Federal, Jefatura de Gobierno. México, D.F.: Administración Pública del Distrito Federal.
- Ou Y., Susanto Y., Roh H. (2016). *Tensile behavior of naturally and artificially corroded steel bars*. *Construction and Building Materials*, 103: 93–104, <https://doi.org/10.1016/j.conbuildmat.2015.10.075>
- Rodríguez-Rodríguez, A. (2014). *Las pérdidas económicas causadas por el fenómeno de la corrosión atmosférica del acero de refuerzo embebido en el hormigón armado*. CENIC: Ciencias Químicas, 45: 52-59.
- Shaikh, F.U.A. (2018). *Effect of Cracking on Corrosion of Steel in Concrete*. *International Journal of Concrete Structures and Materials*, 12(3), <https://doi.org/10.1186/s40069-018-0234-y>
- Tachibana Y., Maeda K., Kajikawa Y., Kawuamura M. (1990). *Mechanical behavior of RC beams damaged by corrosion of reinforcement*. *Corrosion of Reinforcement in Concrete Construction*, 178-187.
- Torres Acosta, A., Navarro Gutiérrez, S., & Terán, C. (2007). *Residual flexure capacity of corroded reinforced concrete beams*. *Engineering Structures*, 1145-1152. <https://doi.org/10.1016/j.engstruct.2006.07.018>.
- Vázquez Castillo, C. D. (1998). "Diagnóstico de la corrosión del puente de Celestún." Tesis. Mérida, Yucatán, México: Facultad de Ingeniería, Universidad Autónoma de Yucatán.
- Vidal T., Castel A., François R. (2007). *Corrosion process and structural performance of a 17 year old reinforced concrete beam stored in chloride environment*. *Cement and Concrete Research*, 37(11): 1551-1561, <https://doi.org/10.1016/j.cemconres.2007.08.004>
- Xianming, S., Ning, X., Keith, F., Jing, G. (2012) *Durability of steel reinforced concrete in chloride environments: An overview*. *Construction and Building Materials*, 37: 36-40, <https://doi.org/10.1016/j.conbuildmat.2011.12.038>
- Ye, H., Fu, C., Jin, N., Jin, X. (2018). *Performance of reinforced concrete beams corroded under sustained service loads: A comparative study of two accelerated corrosion techniques*. *Construction and Building Materials*, 162: 286–297, <https://doi.org/10.1016/j.conbuildmat.2017.10.108>

Yu, L., François, R., Hiep, V., L'Hostis, V., Gagné, R. (2015). *Development of chloride-induced corrosion in pre-cracked RC beams under sustained loading: Effect of load-induced cracks, concrete cover, and exposure conditions*. Cement and Concrete Research, 67: 246–258, <https://doi.org/10.1016/j.cemconres.2014.10.007>

Evaluation of the pathological manifestations of the Rio Negro Building in Anápolis-Goiás

G. H. Teixeira^{1*}  J. R. Silva¹  E. C. Alves² 

*Contact author: guilherme.henrique.eng@hotmail.com

DOI: <https://doi.org/10.21041/ra.v12i3.586>

Reception: 14/02/2022 | Acceptance: 08/07/2022 | Publication: 01/09/2022

ABSTRACT

This paper shows the application of the methodologies GDE (Degree of Structure Deterioration) and GUT (Severity, Urgency, and Tendency) quantifying the pathological manifestations and determining the points of greatest need for maintenance. Thus, a quantitative perspective was used with the application of the previously mentioned methodologies and after building inspections and visual analysis with a photographic record, notes and mappings the methodologies were applied and it was obtained that most of the pathological manifestations that occur in the structure of the building have humidity as origin, resulting in efflorescence, spots or infiltration. Thus, this work defined the points that need priority, directing measures that can later be taken. The methodologies proved to be efficient and important for decision-making.

Keywords: pathology; GUT; GDE; buildings

Cite as: Teixeira, G. H., Silva, J. R., Alves, E. C. (2022), “*Evaluation of the pathological manifestations of the Rio Negro Building in Anápolis-Goiás*”, Revista ALCONPAT, 12 (3), pp. 433 – 448, DOI: <https://doi.org/10.21041/ra.v12i3.586>

¹ Universidade Estadual de Goiás, Departamento de Engenharia Civil, Anápolis, Goiás, Brasil.

² Ministério Público do Estado de Goiás, Superintendência de Engenharia, Brasil.

Contribution of each author

In this work, Teixeira, G. H. contributed with original idea and the writing of the work (100%), experimentation (100%), data collection (100%) and discussion of results (50%). Silva, J.R. contributed with supervision (100%), discussion of results (25%) and text correction (100%). Alves, E.C., E. contributed with discussion of results (25%) and text correction (50%).

Creative Commons License

Copyright 2022 by the authors. This work is an Open-Access article published under the terms and conditions of an International Creative Commons Attribution 4.0 International License ([CC BY 4.0](https://creativecommons.org/licenses/by/4.0/)).

Discussions and subsequent corrections to the publication

Any dispute, including the replies of the authors, will be published in the second issue of 2023 provided that the information is received before the closing of the third issue of 2023.

Evaluación de las manifestaciones patológicas del edificio Río Negro en Anápolis-Goiás

RESUMEN

Este trabajo muestra la aplicación de las metodologías GDE (Grado de Deterioro de la Estructura) y GUT (Gravedad, Urgencia y Tendencia) cuantificando las manifestaciones patológicas y determinando los puntos de mayor necesidad de mantenimiento. Así, se aplicó una perspectiva cuantitativa con la aplicación de las metodologías citadas y tras las inspecciones del edificio y un análisis visual con registro fotográfico, anotaciones y mapeos se aplicaron las metodologías y se obtuvo que la mayoría de las manifestaciones patológicas que se producen en la estructura del edificio tiene como origen la humedad, dando lugar a eflorescencias, manchas o infiltraciones. De este modo, este trabajo definió los puntos que necesitan prioridad, orientando las medidas que pueden tomarse posteriormente. Las metodologías demostraron ser eficaces e importantes para la toma de decisiones.

Palabras clave: patología; GUT; GDE; edificios.

Avaliação das manifestações patológicas do Edifício Rio Negro em Anápolis-Goiás

RESUMO

Este trabalho mostra a aplicação das metodologias GDE (Grau de Deterioração da Estrutura) e GUT (Gravidade, Urgência e Tendência) quantificando as manifestações patológicas e determinando os pontos de maior necessidade de manutenção. Dessa forma, foi aplicado uma perspectiva quantitativa com a aplicação das metodologias citadas e após inspeções prediais e uma análise visual com registro fotográfico, anotações e mapeamentos, foram aplicadas as metodologias e obtido que parte das manifestações patológicas que ocorrem na estrutura do edifício tem como origem a umidade, resultando em eflorescências, manchas ou infiltrações. Dessa forma, esse trabalho definiu os pontos que necessitam de prioridade, direcionando medidas que posteriormente podem ser tomadas. As metodologias se mostraram eficientes e importantes para tomadas de decisões.

Palavras-chave: patologia; GUT; GDE; edifícios.

Legal Information

Revista ALCONPAT is a quarterly publication by the Asociación Latinoamericana de Control de Calidad, Patología y Recuperación de la Construcción, Internacional, A.C., Km. 6 antigua carretera a Progreso, Mérida, Yucatán, 97310, Tel.5219997385893, alconpat.int@gmail.com, Website: www.alconpat.org

Reservation of rights for exclusive use No.04-2013-011717330300-203, and ISSN 2007-6835, both granted by the Instituto Nacional de Derecho de Autor. Responsible editor: Pedro Castro Borges, Ph.D. Responsible for the last update of this issue, Informatics Unit ALCONPAT, Elizabeth Sabido Maldonado.

The views of the authors do not necessarily reflect the position of the editor.

The total or partial reproduction of the contents and images of the publication is carried out in accordance with the COPE code and the CC BY 4.0 license of the Revista ALCONPAT.

1. INTRODUCTION

The city of Anápolis, located in the Brazilian Central Plateau, in the state of Goiás - Brazil, is a centenary city, which was emancipated on July 31, 1907. As a result, there are old buildings, and more and more of these buildings are close to reaching the project life, because of this fact, it is important to highlight the need for investigations regarding the pathological manifestations and the performance of periodic inspections and maintenance as this makes it possible to prolong the useful life of the building and conserving buildings that are part of the history of the municipality.

The absence of preventive maintenance causes high costs in buildings over time, according to Sitter's law (1984) cited by Tutikian and Pacheco (2013) and also described by Souza and Ripper (2009), as the "law of fives", in which corrective interventions have a cost of 125 times the value of measures still in the design phase, while preventive maintenance has a cost of 25 times the same value.

Thus, as it is a more than 50-year-old building, besides its functional importance for the residents, it is an element that makes up the history of the city of Anápolis for being one of the first residential buildings in the city.

According to Souza and Ripper (2009), the pathology of structures is a branch of engineering that focuses on investigating the origins, forms, consequences, and mechanisms of the manifestations of failures in the structure. Similarly, Bolina, Tutikian, and Helene (2019) define that the "pathology of constructions" is a science, which through a systematic process seeks to investigate defects referring to the building as a whole, from materials to the elements that compose it, to know their origins and how they manifest themselves. The authors also differentiate the concept of pathology from constructions and from pathological manifestations, which are anomalies and defects present in the building that are characterized by being visible aspects indicative of possible problems.

Besides, according to NBR 16747 (ABNT, 2020), pathological manifestations are defined as the result of a degradation process that provides a reduction in the performance of the structure, which is manifested through symptoms.

During execution, other circumstances can lead to the emergence of pathological manifestations, whether in working conditions or related to the workforce, lack of quality control, and technical irresponsibility, a factor that is decisive, since an efficient inspection combined with qualified teams reduces the possibility of errors. Finally, no matter how correctly all the preceding steps are performed, it is possible that the emergence of pathological manifestations is related to improper use or lack of maintenance (Souza; Ripper, 2009). Authors such as Junior, Lima, and Balestra (2013), highlight the importance of periodic maintenance in order to prolong the useful life of the construction, providing better quality and performance of the building.

Furthermore, the concrete is subjected to the actions of the environment throughout the useful life of the building, so that reactions naturally occur that trigger the emergence of anomalies in the structure. In this way, care must be taken to ensure the conservation of the building so that it performs its function correctly over the time for which it was designed. With this in mind, it is essential to study the pathology in order to recognize the problems and their respective causes (Lopes, 2019).

In order to assist in this study, giving greater objectivity to the analysis and serving as a support for decision making, some techniques such as the GDE (Degree of Structure Deterioration) and GUT (Severity, Urgency, and Trend) methodologies can be applied, providing a quantification of the pathological manifestations obtained by the mathematical formulations proposed by the tools, which makes it possible to identify the state of a given structure and guarantee a more objective view for the analysis (Braga et al., 2019; Lima et al., 2019; Moura; Cavalheiros, 2019; Santana et al., 2019; Medeiros et al., 2020).

2. METHODOLOGY

The methodology applied in this work was the evaluation of pathological manifestations through the GDE (2007) and GUT (2014) methodologies. Data collection was carried out through building inspection through visual inspection, *in loco*, making photographic records of the identified pathological manifestations and mapping the anomalies in the plan of each inspected floor. The inspection was based on the descriptions of the National Building Inspection standard of the Brazilian Institute of Engineering Expert Assessments - IBAPE (2012), NBR 5674 (ABNT, 1999), NBR 16747 (ABNT, 2020) and the Technical Bulletin No. 1 of the Brazilian Association of Construction Pathology - ALCOPAT (2013). In addition, all information and documents regarding the building were collected.

Through the GUT methodology (2014) the pathological manifestations were quantified to posteriorly carry out a comparison and indicate the degree of priority for decision making. Through the methodology GDE/UnB (2007), also in order to quantify the pathological manifestations, the parameters of the degree of deterioration of elements, families, and structure were calculated, serving as a basis for the analysis and allowing the classification of the level of deterioration of elements and structure.

Subsequently, based on the literature and with the data obtained, comparison and analysis of the values obtained were carried out.

The tools used for the research were electronic spreadsheets for data organization, a smartphone for photographic records, a scalemeter, a fissurometer, and measuring tape.

2.1 GDE Methodology

Using the GDE methodology, the elements inspected were divided into groups of Pillars (P); Beams (V); Slabs (L); Stairs (E); Upper reservoir (R); Lower reservoir (R), and Expansion joints (J).

After this division, intensity factors (F_i) and weighting factors (F_p) were assigned for each manifestation present in the element, according to the tables present in the work by Fonseca (2007). Thus, it was possible to calculate the degree of damage, according to equations (1) and (2).

$$D = 0,8 \cdot F_p \cdot F_i \quad \text{To } F_i \leq 2,0 \quad (1)$$

$$D = (12 \cdot F_i - 28) F_p \quad \text{To } F_i \geq 3,0 \quad (2)$$

Where:

D - Degree of damage

F_i - Intensity factor

F_p - Weighting factor

With the degree of damage (D) of each manifestation, the degree of deterioration of the element (G_{de}) is calculated according to equation (3).

$$G_{de} = D_{m\acute{a}x} \left[1 + \frac{\left(\sum_{i=1}^n D_i \right) - D_{m\acute{a}x}}{\sum_{i=1}^n D_i} \right] \quad (3)$$

Where:

G_{de} - Degree of deterioration of the element;

D_i - Degree of damage “i”;

D_{max} - Highest degree of damage to the element;

n – Element damage numbers.

A level of deterioration is related to the value of the element's degree of deterioration and thus we obtain recommendations for actions to be taken. This relation can be seen in Table 1.

Table 1. Classification of the level of deterioration of the elements

Deterioration level	G_{de}	Recommended actions
Low	0-15	Acceptable state Preventive maintenance
Medium	15-50	Define deadline and nature of new inspection Plan long-term intervention (maximum 2 years).
High	50-80	Set deadline for specialized inspection Plan medium-term intervention (maximum 1 year)
Sufferable	80-100	Set deadline for rigorous expert inspection Plan short-term intervention (maximum 6 months)
Critical	>100	Immediate specialized intervention and emergency measures (load relief, shoring, etc). Plan immediate intervention.

Source: (Verly, 2015)

To determine the degree of deterioration of elements divided into similar groups, the degree of deterioration of the family (G_{df}) is calculated, which is a function of the degree of deterioration of the element (G_{de}) through equation (4).

$$G_{df} = G_{de,máx} \sqrt{1 + \frac{\left(\sum_{i=1}^n G_{de,i}\right) - G_{de,máx}}{\sum_{i=1}^n G_{de,i}}} \quad (4)$$

Where:

$G_{de,máx}$ – Highest degree of element deterioration

$G_{de,i}$ – Degree of element deterioration “i” (≥ 15)

m – Number of elements with $G_{de} \geq 15$

Finally, by obtaining the degree of deterioration of each family (G_{df}), the degree of deterioration of the structure (G_d) is calculated. The equation used for this calculation is expressed below, equation (5).

$$G_d = \frac{\sum_{i=1}^k F_{r,i} \cdot G_{df,i}}{\sum_{i=1}^k F_{r,i}} \quad (5)$$

Where:

k – Number of families in the structure;

$F_{r,i}$ – Structural relevance factor of the family “i”;

$G_{df,i}$ – Degree of family deterioration “i”.

Thus, for the degree of deterioration of the structure, similarly to the degree of deterioration of the element (G_{de}), an association can be made to a level of deterioration and consequently measures that can be taken in this situation can be obtained. The table applied for this analysis is Table 1, p. 05.

2.2 GUT Methodology

The GUT methodology originated in the 1980s through the work of Kepner and Tregoe with the aim of creating a strategic planning tool to assist in decision-making (Fáveri; Silva, 2016). In civil construction, the work of Verzola, Marchiori, and Aragon (2014) proposed changes in the methodology in order to allow its application in building inspections and reduce the possibility of errors through subjectivity. The methodology uses the variables Severity (G), Urgency (U), and Tendency (T), in which weights ranging from 1 to 10 are assigned, with 1 being assigned to the least severe and 10 to the most severe. Thus, through the product of the variables ($G \times U \times T$), a classification is made according to how critical each situation is (Verzola; Marchiori; Aragon, 2014).

Some researchers such as Santana et al. (2019), Moura and Cavalheiros (2019), and Braga et al. (2019) applied the GUT methodology in their research to carry out inspections and identify the most critical points of the building, proving it to be practical and making it possible to define priority for decision-making. According to Verzola, Marchiori, and Aragon (2014), tables 2, 3, and 4 determine the grades to be assigned for each grade according to the variable.

Table 2. Severity (G) classification.

SEVERITY		
Degree	Degree definition	Grade
TOTAL	Risk of death, risk of punctual or generalized collapse/collapse. Very high financial loss.	10
HIGH	Risk of injury to users, reversible damage to the environment or to the building. High financial loss.	8
AVERAGE	Risk to users' health, discomfort in the use of systems. Average financial loss.	6
LOW	No risk to the physical integrity of users, no risk to the environment, minor aesthetic or usage inconveniences. Small financial loss.	3
NONE	No risk to health, physical integrity of users, the environment or the building.	1

Source: (VERzola; Marchiori; Aragon, 2014)

Table 3. Trend (T) classification

TREND		
Degree	Degree definition	Grade
TOTAL	Immediate progression. It is going to get worse quickly, it can get worse.	10
HIGH	Short-term progression. It will get worse soon.	8
AVERAGE	Medium term progression. It will get worse in the medium term.	6
LOW	Probable long-term progression. It will take time to get worse.	3
NONE	It won't progress. It will not get worse, stabilized.	1

Fonte: (Verzola; Marchiori; Aragon, 2014)

Table 4. Classification for Urgency (U).

URGENCY		
Degree	Degree Definition	Grade
TOTAL	Incident in occurrence, immediate intervention subject to interdiction of the property. Intervention deadline: None	10
HIGH	Incident about to occur, urgent intervention. Deadline for intervention: Urgent	8
AVEREGE	Incident expected soon, short-term intervention. Deadline for intervention: As soon as possible	6
LOW	Indication of future incident, scheduled intervention. Deadline for intervention: You can wait a little	3
NONE	Unforeseen incident, indication of follow-up and scheduled maintenance. Deadline for intervention: No rush	1

Fonte: (Verzola; Marchiori; Aragon, 2014)

The grade corresponds to the value assigned to each pathological manifestation according to the associated degree, that is, in total degree, a grade of 10 is assigned, a high degree is grade 8, an average degree gets a grade of 6, a low degree is grade 3 and no degree gets a grade of 1. Thus, the grade is assigned for each variable of the manifestation, and using the product of these values, it is possible to list the problems that have higher priority. Those with greater value deserve special attention, as they are the most serious, and urgent and tend to get worse (Periard, 2011).

3. RESULTS AND DISCUSSIONS

3.1 Pathological manifestations

Mapping was carried out on each inspected floor to facilitate the identification of the elements. Furthermore, the evaluated elements were divided into families as proposed by the GDE methodology (2007). Then, the pathological manifestations identified were presented according to this division.

In the column family, only one element, P01, was identified, and it was possible to notice a great exposure of the reinforcements in the process of corrosion, identifying stains along the reinforcements and detachment of the concrete due to the expansion of the reinforcement, as can be seen in Figure 1.



Figure 1. Detachment of concrete and corrosion of reinforcement in element P01

In the slabs family, elements L01 to L08 were identified, as shown in Figure 2, in which stands out the constant presence of moisture, generating dark spots in element L01, detachment of the paint in element L02, formation of calcium carbonate stalactites, due to efflorescence in element L04, small stains and cracks in elements L05 and L08 and wear of waterproofing in element L03. There are also cracks in elements L06 and L07 due to additional loads applied by a telephone antenna over the roof.

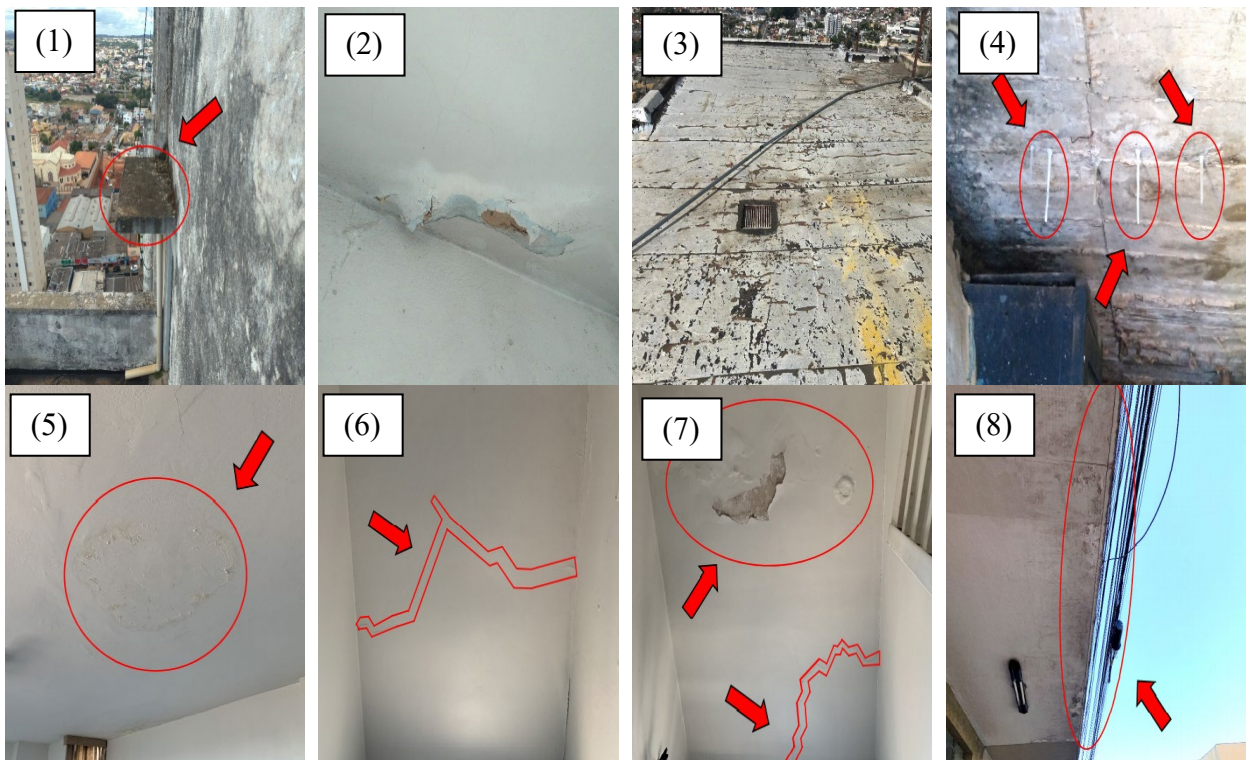


Figure 2. Pathological manifestations identified in the slabs. (1) Dark spots on element L01. (2) Detachment of the ping in element L02. (3) Wear of waterproofing on element L03. (4) Efflorescence with formation of stalactites in element L04. (5) Small moisture spots on the L05 element. (6) and (7) Cracks due to additional loading on the cover, on elements L06 and L07. (8) Dark spots of moisture on element L08.

The upper reservoir family and the lower reservoir family showed possible flaws in their waterproofing, identified by the characteristic appearance of light efflorescence stains on elements R01 and R02.

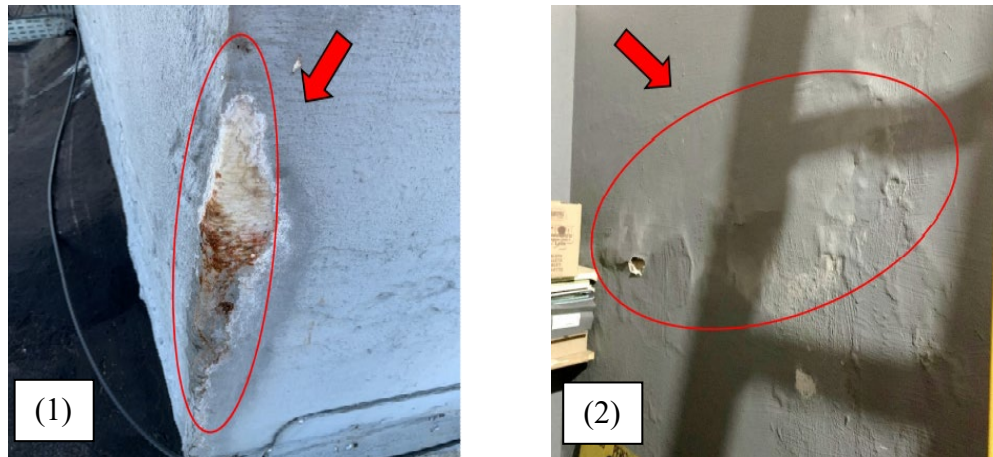


Figure 3. Efflorescence spots in the reservoir. (1) R01. (2) R02.

It is noted that the beam family did not present any element that demonstrated the development of pathological manifestations.

The elements of the family of stairs and expansion joints were E01 for the stairs and J01 and J02 for the expansion joints, as can be seen in Figure 4. In it, it is noted that the element E01 showed only wear on its steps due to the weather over the years and in elements J01 and J02, the constant presence of humidity resulted in the dark spots identified.

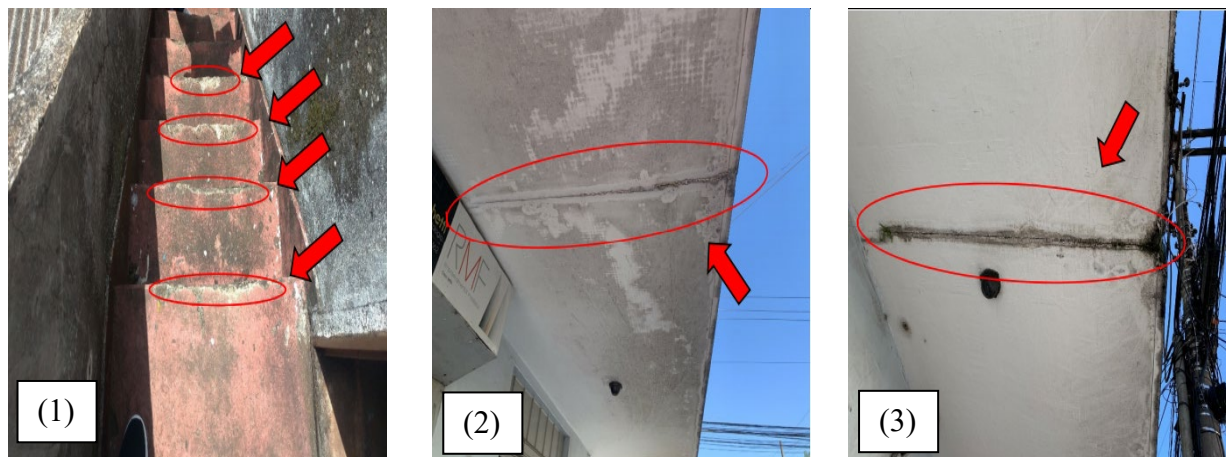


Figure 4. Efflorescence spots in the reservoir. (1) Wear of stair treads on element E01. (2) and (3) Stains due to humidity in elements J01 and J02.

3.2 Application of methodologies and analysis of results

First, it was observed that the family that has the largest number of elements that present pathological manifestations is the slab family, with 57.14% of the identified anomalies, as can be seen in Figure 5.

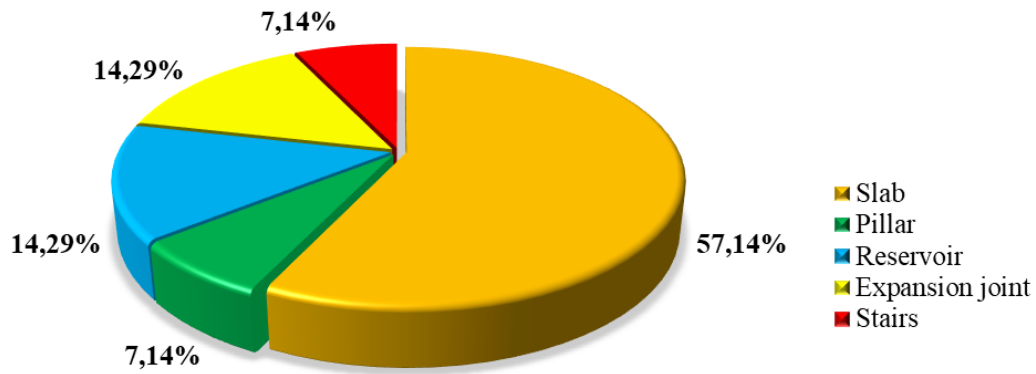


Figure 5. Graph of the frequency of pathological manifestations by family of elements.

Through the mapping of the pathological manifestations that affect the building, it was noticed that in the 14 structural elements inspected, 35.29% of the pathological manifestations are originated due to the infiltration of humidity as we can see in Figure 6. In addition, other pathological manifestations such as efflorescence (17.65%) and dark spots (11.76%) also have a similar cause.

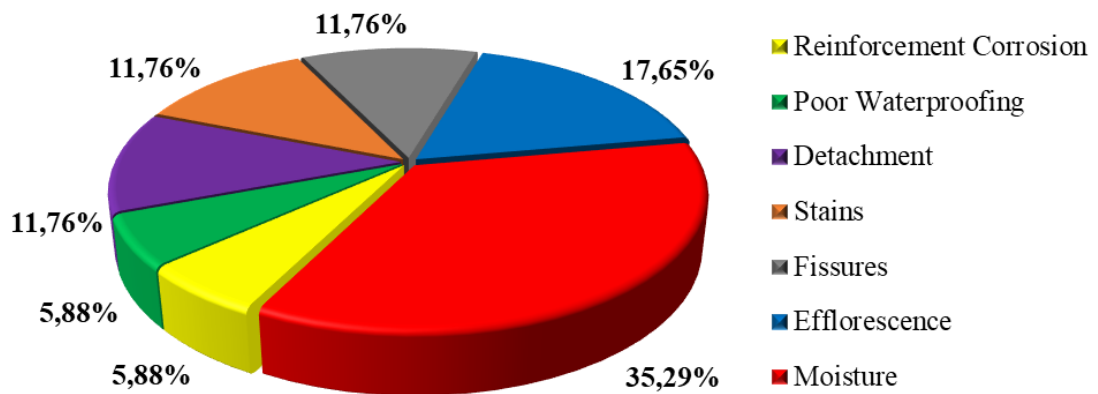


Figure 6. Graph of the frequency of pathological manifestations in the elements.

Regarding the GDE/UnB (2007) methodology, it is possible to raise some analysis based on the graphic model used by Medeiros et al. (2020). In the slab family, elements L06 and L07 are the ones that most influence the calculation of the degree of deterioration of the family, as can be seen in figure 7. In addition, it is worth noting that element L05 is not taken into account for the G_{df} calculation for presenting G_{de} less than 15.

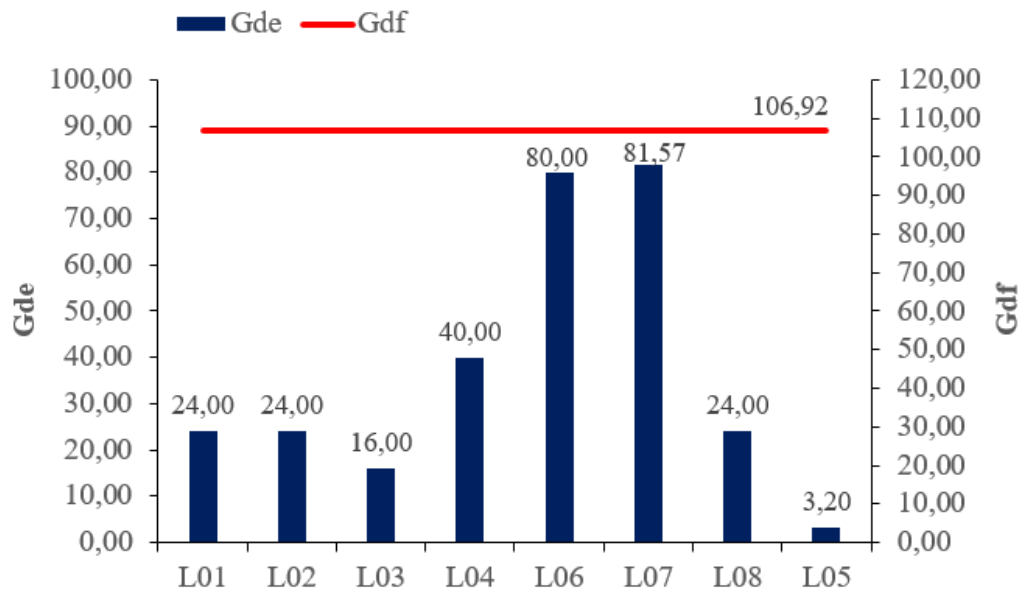


Figure 7. Degree of deterioration of the slabs.

The beam families have a null degree of deterioration, as no pathological manifestation was identified in the elements that compose them, in the family of stairs, the only identified element has G_{de} less than 15. Thus, for both, G_{df} equal to zero was calculated. As for the families of columns and upper and lower reservoirs, it is observed that they are composed of only one element, so the value of the degree of deterioration of the family corresponds to the value of the degree of deterioration of the element itself, this can be seen, respectively, in figures 8, 9 and 10.

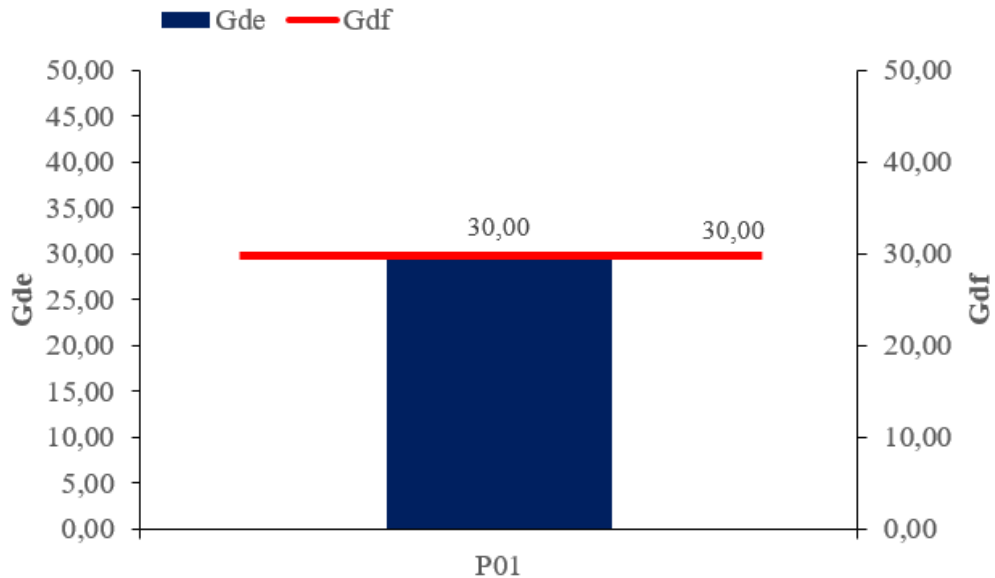


Figure 8. Degree of deterioration of the pillars.

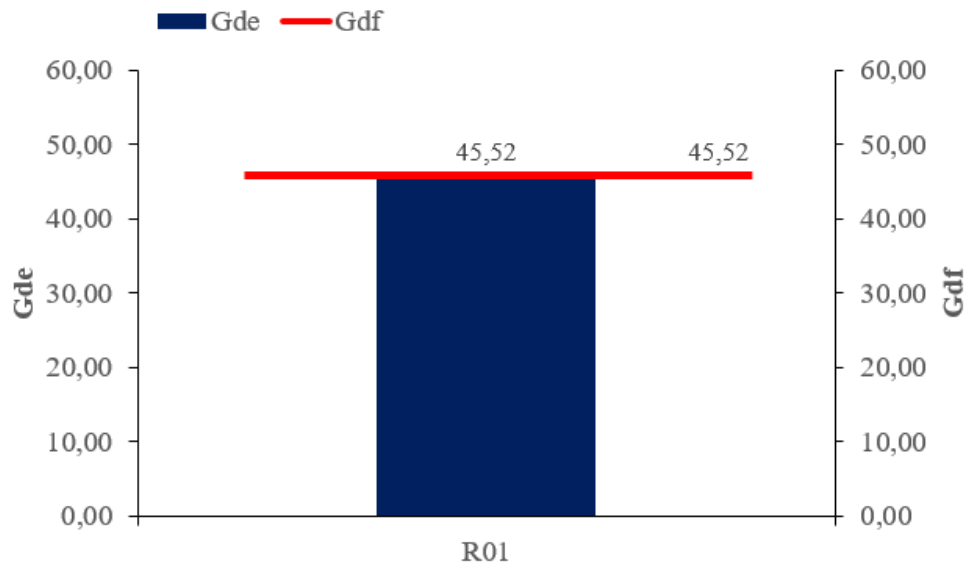


Figure 9. Degree of deterioration of the upper reservoir.

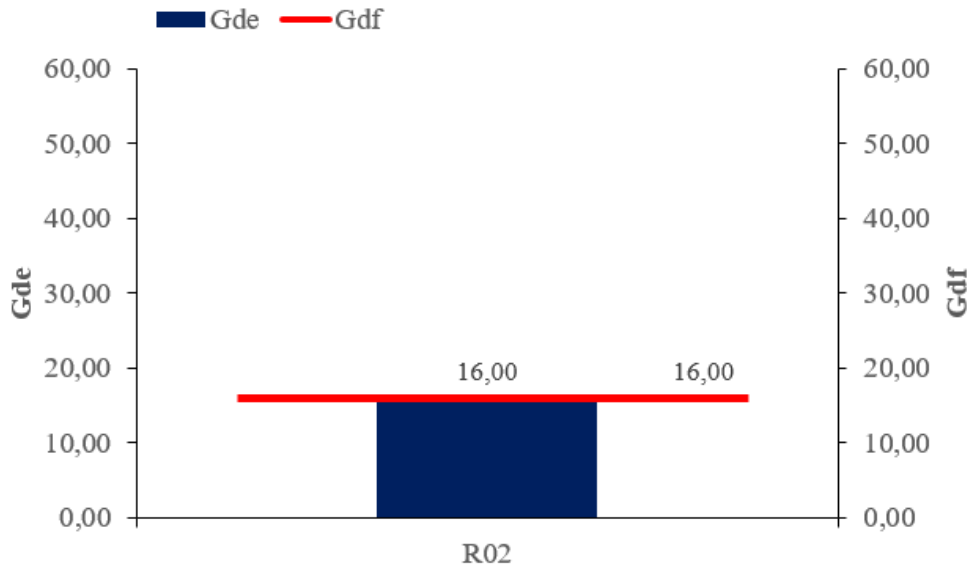


Figure 10. Degree of deterioration of the lower reservoir.

In addition, in the expansion joints, the presence of two elements that present the same degree of deterioration was found, but the degree of deterioration of the family is higher than the value obtained for the elements individually. Thus, by the mathematical formulations, it is possible to observe that the influence of the repetition of elements that have the same degree of deterioration does not represent such a significant increase since it has the maximum value as a reference, this value is multiplied by the result of the root that involves the sum and the maximum value. Figure 11 shows the value of G_{df} and the values of G_{de} for each element.

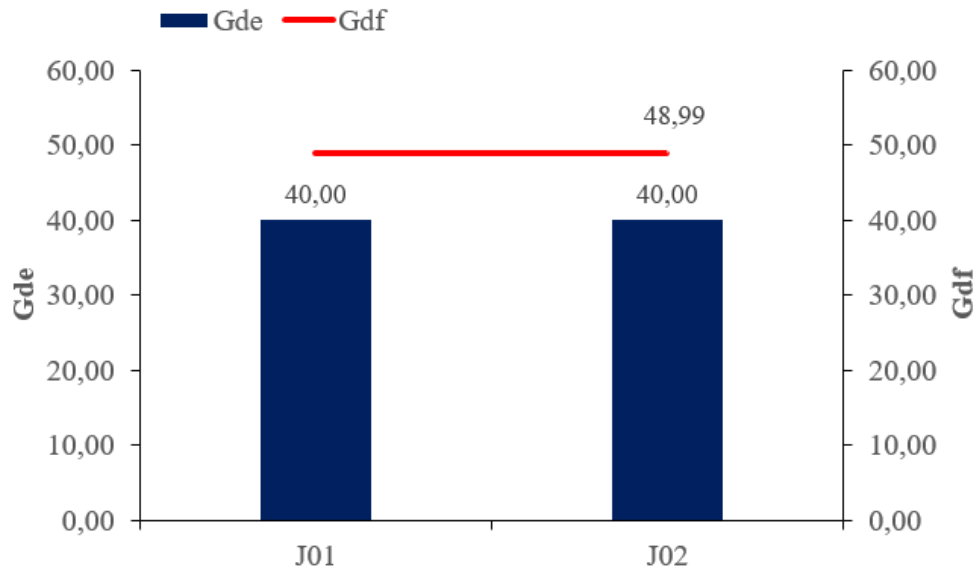


Figure 11. Degree of deterioration of expansion joints.

Thus, when evaluating the degree of deterioration of the families and the degree of deterioration of the structure, it is noted that the slabs are the ones that represent the greatest influence for the structure to be at an average deterioration level, 15 to 50, and therefore it needs intervention within a maximum period of 2 (two) years. Figure 12 shows the values of G_{df} of each family in comparison to the global value of the structure, G_d .

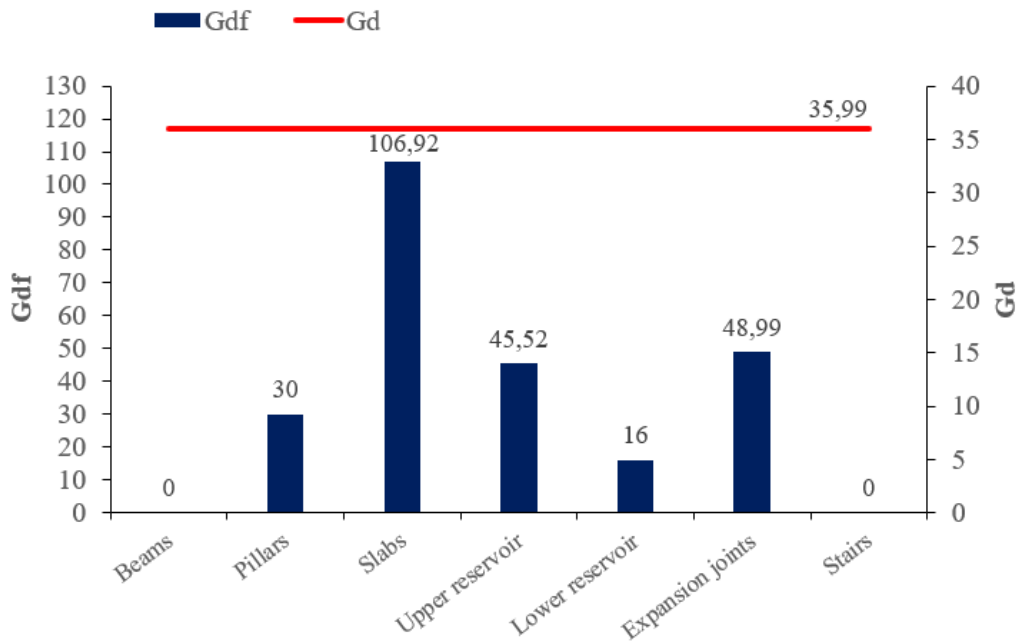


Figure 12. Degree of deterioration of the structure.

The application of the methodologies makes it possible to define which element or pathological manifestation needs priority within the global scenario, which can be decisive for assertive and efficient work. By the GDE methodology (2007) it is defined that the elements L07 and L06 need special attention, given that they present a poor and high level of deterioration, respectively, which implies a need for intervention within a maximum period of 6 (six) months for element L07 and 1

year for element L06. On the other hand, elements E02 and L05 have a low level of deterioration, requiring only preventive maintenance. The other elements are classified at a medium level of deterioration, with interventions being suggested within a maximum period of 2 (two) years. In addition, the structure has a G_d equal to 35.99, classifying it as an average level of deterioration, which requires a maximum intervention period of 2 (two) years. The list of maintenance priorities is presented in table 5(1).

Table 5. Table of maintenance priorities according to the GDE and GUT methodology
(1) GDE (2) GUT

(1) GDE				(2) GUT			
Element	G_{de}	Level of deterioration	Maximum intervention period	Element	Pathological Manifestation	Grade	Degree
L07	81,57	Suffering	6 months	P01	Corrosion	384	Medium
L06	80,00	High	1 year	L06	Cracks	384	Medium
R01	45,52	Medium	2 years	L07	Cracks	384	Medium
L04	40,00	Medium	2 years	P01	Concrete detachment	288	Low
J01	40,00	Medium	2 years	L04	Efflorescence	288	Low
J02	40,00	Medium	2 years	R01	Efflorescence	216	Low
P01	30,00	Medium	2 years	L02	Moisture	108	Low
L01	24,00	Medium	2 years	L07	Moisture	108	Low
L02	24,00	Medium	2 years	L08	Stains	108	Low
L08	24,00	Medium	2 years	R02	Efflorescence	108	Low
L03	16,00	Medium	2 years	L01	Dark spots	54	None
R02	16,00	Medium	2 years	L03	Moisture	54	None
E01	4,80	Low	Preventive maintenance	J01	Moisture	54	None
L05	3,20	Low	Preventive maintenance	J02	Moisture	54	None
				L05	Moisture	27	None
				R01	Poor waterproofing	27	None
				E01	Detachment	27	None

By the GUT methodology (2014), it is possible to evaluate only the pathological manifestations separately. Thus, based on the scale of values defined by the methodology, in tables 2, 3, and 4, where from 81% to 100% is defined as a total degree, it was considered that the attribution of grades 10 for the three parameters, or that is, grade 1000 represents 100% and consequently, the percentage of the other values can be easily obtained and thus assign a classification to the pathological manifestations. Having defined this, in table 5 (2) the pathological manifestations were listed in order of priority, that is, from the highest to the lowest score.

It is noted that by the GUT methodology (2014) there is a certain repetition of values, which makes it difficult to determine priority. In addition, most of the pathological manifestations are of a low or no degree, in terms of severity, urgency, and tendency, diverging from the GDE methodology (2007). However, for both methodologies, it is possible to define that elements L07 and L06 need maintenance priority.

4. CONCLUSIONS

From the analysis of the results, it was observed that most of the pathological manifestations that occur in the structure of the building are associated with humidity to a certain degree, either causing efflorescence, stains, or infiltrations. So, it is a recurring factor that must be solved because it can compromise the health and safety conditions of the owners.

Due to the age of the building, the projects do not meet with the administration of the condominium, so it was not possible to have access to the structural project, which made it difficult to identify some of the structural elements, such as the beams and pillars. Due to this fact, the analysis became limited only to what was inspected. The building underwent occasional maintenance as problems arose over time, which mitigates, to a certain extent, the effect of time on the building, with the upper part of the building being the one with the most degradation due to its exposure to the weather. Regarding the application of the methodologies, it was observed that the use of the two methodologies is complementary. However, as also performed by Santana et al. (2019), it was found that the use of the GUT methodology alone (2014) would be unfeasible due to repeated results, which makes it difficult to analyze the aspect of determining the maintenance priority. In addition, subjectivity is still present in the GUT methodology (2014), to a certain extent, when compared to the GDE methodology (2007), as the attribution of grades takes into account the evaluator's perception of concepts such as discomfort, annoyances, and others.

Using the GDE methodology (2007) it was possible to determine the degree of deterioration of each element and define the maintenance priority and its respective intervention period. In addition, it was determined that the degree of deterioration of the structure is equal to 35.99, which corresponds to an average level of deterioration and requires intervention within a maximum period of 2 (two) years. Comparing the values of the degree of deterioration of the family with the global value, it is noted that the family of slabs is decisive for defining the value obtained for the structure as a whole, from which it can be identified that the family of slabs needs priority.

By the GUT methodology (2014) it was possible to define the Severity, Urgency, and Tendency of each pathological manifestation present in the elements and not of each element itself, being possible only to define a maintenance priority, without defining a deadline for it to be carried out. In this way, the application of the methodologies, despite the difficulties pointed out, proves to be efficient and important for decision-making, as it allows an overview of the points that need more attention and facilitates the subsequent process of maintenance and recovery of these buildings.

So, in summary, the building's maintenance priorities are the L07 and L06 slabs, which need an in-depth investigation, to identify if there is a need for reinforcement to resist the additional loading and in addition to the recovery of their cracks in order not to the situation worsens.

5. ACKNOWLEDGMENTS

We thank the Universidade Estadual de Goiás for the support for the development of the research and the syndic Ilda Helena Nunes for the permission to carry out the study on the structure of the building.

6. REFERENCES

- Associação Brasileira de Normas Técnicas (2020), *NBR 16747 – Inspeção predial - Diretrizes, conceitos, terminologia e procedimento*. Rio de Janeiro, 14p.
- Associação Brasileira de Normas Técnicas (1999), *NBR 5674 - Edificações - Procedimento*. Rio de Janeiro, 6p.

- Bolina, F.; Tutikian, B.; Helene, P. (2019), *Patologia de Estruturas*. São Paulo: Oficina do texto.
- Braga, I. C., Brandão, F. da S., Ribeiro, F. R. C., Diógenes, A. G. (2019). *Application of GUT Matrix in the assessment of pathological manifestations in heritage constructions*. Revista ALCONPAT, 9(3), 320 - 335. <http://dx.doi.org/10.21041/ra.v9i3.400>
- Fáveri, R.; Silva, A. (2016), *Método GUT aplicado à gestão de risco de desastres: Uma ferramenta de auxílio para hierarquização de riscos*. Revista Ordem Pública, v. 9, n. 1, p. 93–107.
- Fonseca, R. A. (2007), *Estrutura do Instituto Central de Ciências: Aspectos históricos, científicos e tecnológicos de projeto, execução, intervenções e proposta de manutenção*. 231p. Dissertação (Mestrado em Estruturas e Construção Civil). Universidade de Brasília, Brasília, 2007.
- Ibape-instituto brasileiro de avaliações e perícias de engenharia (2012), *Norma de Inspeção Predial Nacional*. São Paulo. 18p.
- Junior, R.; Lima, M.; Balestra, C. (2013), *Identificação das principais manifestações patológicas em estruturas de concreto armado pertencentes ao DCTA*. In: Congresso internacional sobre patologia e reabilitação de estruturas, IX, 2013, João Pessoa. Anais..., João Pessoa, 9p.
- Lima, H. J. N., Ribeiro, R. da S., Melo, G. S. S. de A., & Palhares, R. de A. (2019). *Analysis of pathological manifestations of concrete in urban overpasses*. Revista ALCONPAT, 9(2), 247 - 259. <https://doi.org/10.21041/ra.v9i2.308>
- Souza Lopes, L. (2019). *Patologia da construção em concreto armado e as resoluções dos problemas de manutenção*. Revista Científica da Faculdade de Educação e meio ambiente, 10(1), 23–33. <https://doi.org/10.31072/ref.v10i1.804>
- Moura, L. G.; Cavalheiros, C. (2019), *Estudo para reabilitação de patologias nas fachadas de uma edificação*. In: congresso latinoamericano de patologia de construcción y congresso de control de calidad em la construcción, XV, XVII, v.2, Tuxtla Gutiérrez. Anais..., Tuxtla Gutiérrez, 2019, 15p.
- Periard, G. (2011), *Matriz GUT- Guia completo, Sobre Administração*, Disponível em: <http://www.sobreadministracao.com/matriz-gut-guia-completo/>. Acesso em: 15/07/2020.
- Santana, et al. (2019), *Manifestações Patológicas em Estruturas de Concreto Armado Submetidas a Ação de Incêndio : uma classificação prioritária para sua recuperação*. In: Congresso brasileiro do concreto, 61, 2019, Fortaleza. Anais..., Fortaleza: IBRACON, 17p.
- Medeiros, A. et al. (2020), *Aplicação de metodologias de inspeção em ponte de concreto armado*. Ambiente Construído, Porto Alegre, v. 20, n. 3, p. 687–702,
- Souza, V., Ripper, T. (2009), *Patologia, Recuperação e Reforço de Estruturas de Concreto*. 1. ed. São Paulo: Editora Pini Ltda.
- Tutikian, B., Pacheco, M. (2013), *Boletim Técnico nº 1 – Inspeção, Diagnóstico e Prognóstico na Construção Civil*. Mérida. 17p.
- Verzola, S.; Marchiori, F.; Aragon, J. (2014), *Proposta de lista de verificação para inspeção predial X urgência das manutenções*. In: Encontro nacional de tecnologia do ambiente construído, XV, Maceió. Anais..., Maceió, p. 1226-1235.